Some modeling and computational aspects of water waves action

Martin Parisot

▶ **To cite this version:**

Martin Parisot. Some modeling and computational aspects of water waves action. Numerical Analysis [math.NA]. Université de Bordeaux, 2024. tel-04814817

HAL Id: tel-04814817
https://hal.science/tel-04814817v1

Submitted on 2 Dec 2024

HAL is a multi-disciplinary open access archive for the deposit and dissemination of scientific research documents, whether they are published or not. The documents may come from teaching and research institutions in France or abroad, or from public or private research centers.

L'archive ouverte pluridisciplinaire **HAL**, est destinée au dépôt et à la diffusion de documents scientifiques de niveau recherche, publiés ou non, émanant des établissements d'enseignement et de recherche français ou étrangers, des laboratoires publics ou privés.

UNIVERSITY OF BORDEAUX

DOCTORAL SCHOOL EDMI

MATHEMATIQUES ET INFORMATIQUE

Habilitation à Diriger des Recherches

Specialty : MATHÉMATIQUES APPLIQUÉES

Defended by

Martin PARISOT

Some modeling and computational aspects of water waves action

prepared at INRIA Bordeaux, CARDAMOM Team

defended on November 29, 2024

Jury :

Reviewers :	Manuel Jesús CASTRO DÍAZ	-	Málaga University
	Michael DUMBSER	-	Trento University
	Jean-Luc GUERMOND	-	Texas A&M University
Examinators :	Christian BOURDARIAS	-	Savoie Mont Blanc University
	Sergey GAVRILYUK	-	Aix-Marseille University
	Frédéric LAGOUTIÈRE	-	Claude Bernard Lyon 1 University
	David LANNES	-	Bordeaux University
	Pascal NOBLE	-	INSA Toulouse
	Sebastian NOELLE	-	RWTH Aachen University
Invited :	Thierry GOUDON	-	Inria Sophia Antipolis
	Mario RICCHIUTO	-	Inria Bordeaux
	Jean-Paul VILA	-	INSA Toulouse

Acknowledgments

I would like to express my deepest gratitude to Manuel Jesus Castro Díaz, Michael Dumbser, and Jean-Luc Guermond for graciously accepting the role of reviewers for my work. Their exceptional expertise and generous investment of time have been invaluable in helping me refine my ideas and analyses. I am sincerely grateful for their efforts and dedication to fostering scientific excellence, and their constructive feedback has had a profound impact on the quality of this research. Thank you for your unwavering commitment.

I also extend my heartfelt thanks to the esteemed members of the jury for their time, expertise, and insightful feedback. It is a tremendous honor to have the opportunity to discuss and engage with you on these topics. I deeply appreciate the chance to benefit from your knowledge and experience, which have been instrumental in shaping my own contributions to this field. Indeed, it is through the foundation laid by your pioneering work that I have been able to pursue my own research.

I would like to acknowledge, with the greatest appreciation, Thierry Goudon, Nicole Goutal, Mario Ricchiuto, and Jean-Paul Vila. Your guidance, encouragement, and unwavering support have been fundamental to my career and intellectual growth. The wisdom you have shared so generously has not only enriched my understanding but also deeply influenced how I approach challenges and research as a whole. Your patience and kindness have been a continuous source of inspiration, and I am deeply thankful for the mentorship and leadership you have provided me throughout this journey.

Finally, I wish to extend my heartfelt gratitude to the members of the Egrin GdR, NumHyp, and more recently, the NumWave communities. It has been a privilege to collaborate with such talented and dedicated professionals. Your shared expertise, valuable ideas, and collaborative spirit have been incredibly stimulating and enriching for me, both personally and professionally. The opportunity to work alongside all of you is a source of great pride, and I look forward to continued collaboration in the future.

Contents

CHAPTER 1

Overview

"La contrainte est un instrument pour aller plus loin.
La création naît souvent de là."

Christian Lacroix

This manuscript outlines my approach to addressing issues related to waves propagation and their interaction with the surrounding environment. Some of the concepts discussed are common within the scientific community, where I exchange ideas and find inspiration. As a result, I am not the author of all the ideas presented here. However, my goal is to offer a personal perspective on certain mathematical and numerical modeling challenges. The descriptions provided are therefore selective and not exhaustive.

My research primarily focuses on the modeling and numerical resolution of free-surface flows over large time and spatial scales. Although the Navier-Stokes model is the cornerstone of fluid mechanics, at large scales, approximate models are often more appropriate. These models can deliver faster and sometimes more accurate results due to better-controlled numerical methods. In practice, numerous simulations are often required, either to account for uncertainties in the model or data, as in ensemble forecasting, or to optimize processes and devices. This makes it crucial to develop models that are both well-suited to their objectives and computationally efficient.

For free-surface flow applications, the shallow water model is the most widely used. It produces highly satisfactory results when estimating river current speeds or large-scale ocean currents. However, this model fails to describe correctly the waves propagation. To better capture the observed phenomena, additional processes like dispersion need to be considered. Similarly, secondary currents, which can arise from localized forces such as wind at the surface or friction at the bottom, require special treatment. My initial area of research focuses on enhancing approximate models based on vertical integration, like the shallow water model, to extend their validity across a broader range of flow conditions. The resulting models, often dispersive in nature, remain poorly understood. Key questions arise regarding their mathematical properties, particularly in relation to boundary conditions and long-term behavior, as well as challenges in their numerical resolution. In the first chapter of this manuscript, I will present these models as a hyperbolic system with a source term, maintaining a duality with a specific subset of functions in which the solution

will be sought. This formalism is commonly used for incompressible flows but is less frequently applied to dispersive equations derived from water waves model. Nonetheless, I believe it offers a promising framework for tackling several scientific challenges.

The second chapter focuses on some applications where approximate models for free-surface flows are particularly relevant.
In the first section, I explore the interactions with floating objects, primarily in the context of marine renewable energy. Mathematically, the presence of a structure above the flow introduces an inequality that restricts the solution to a subset of admissible functions, commonly referred to as a congestion constraint. In congested areas, free-surface flows, which are inherently hyperbolic (where information travels at finite speed), degenerate into an elliptic model (where information propagates infinitely fast). Furthermore, the interface between congested and free surface flows is typically unknown, as it shifts with the movement of the free surface. This necessitates the development of a robust numerical method to handle both regimes. The chapter also addresses coupling the flow with the dynamics of the floating object, as well as the behavior of potential air pockets trapped beneath the structure, with a focus on practical rather than theoretical solutions.
The second section delves into the modeling of continental water flows. In the context of climate change, managing water resources has become a critical societal challenge. Simulating continental waters is complex, not only because the surface equations are hyperbolic while the underground ones are parabolic, but also due to the difficulty of modeling mass exchanges between these domains. Typically, water emerges from the porous medium when it becomes fully (locally) saturated. This resurgence can be modeled through a constraint that limits the maximum volume within the porous medium. Unlike the congestion constraint, however, the excess water is transferred through exchange terms.

In general, these problems require the use of constraints to effectively model the phenomena involved. From a modeling perspective, constraints are a critical tool for incorporating complex physical processes. However, analyzing problems with constraints is inherently challenging. My focus has been on developing numerical solutions, primarily for hyperbolic problems, that involve various types of constraints. Special care has been taken to ensure these techniques are compatible with one another, allowing for example the simulations of waves interacting with a boat over a sandbank see as a porous medium. The Bassin of Arcachon is a very inspiring place.

1.1 About the geophysical context

The primary applications targeted by this work are free-surface flows over large time and spatial scales. Specifically, we focus on free-surface flows where the characteristic vertical length (typically the average water depth) is denoted by H and the characteristic horizontal length by L, as illustrated in Figure 1.1. Depending on the modeling objectives, the characteristic horizontal length can represent either the length of a boat or the distance between two waves. Given the large spatial scales, we assume the shallowness number, defined as

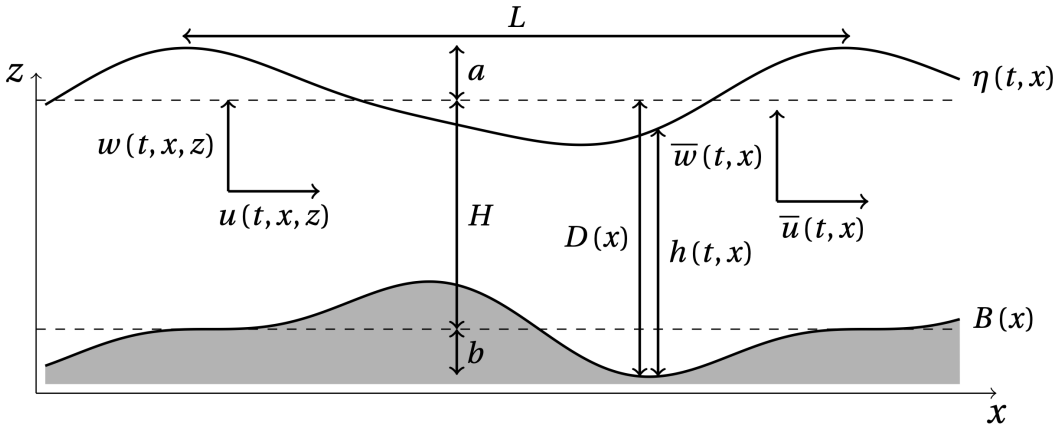

Figure 1.1: Characteristic values for free surface flows.

$\frac{H^2}{L^2}$, is small. The models discussed here can therefore be justified as asymptotic approximations of the water waves model, briefly outlined in §2.1.1, by neglecting terms of a certain order relative to the shallowness number, as detailed in [Lan13].

To complete the description of the dimensionless parameters characterizing the flows, we introduce the wave amplitude a and the amplitude of the bathymetry variations b, as shown in Figure 1.1. The nonlinearity number is defined as $\frac{a}{H}$, and the bathymetry number as $\frac{b}{H}$. Significant simplifications of the approximate models can be achieved when the nonlinearity number and/or the bathymetry number are small, as discussed in §2.2.2.3. However, these simplifications compromise the structure of the equations, particularly affecting energy conservation.

Energy conservation is one of the most fundamental principles in physics, asserting that the total energy of an isolated system remains constant over time, even as it transforms between different forms. When the energy can be divided into potential and kinetic components, the model exhibits an Hamiltonian structure. In mathematical terms, physical energy ats as the mathematical entropy in the models we study, serving as a critical tool for analyzing the qualitative behavior of solutions, including stability, existence, uniqueness, regularity, and asymptotic behavior. In numerical schemes, entropy dissipation is often a reliable indicator of solution stability, helping to prevent non-physical phenomena. By carefully controlling the dissipation of numerical energy, artificial dissipation introduced by the discretization, it becomes possible to develop higher-order schemes or refine the mesh in areas with high dissipation. Throughout my work, special attention has been paid to the conservation or controlled dissipation of mechanical energy, both in the formulation of models and their numerical resolution.

1.2 Description of the discrete notation

We recall discrete notations of finite volume method that will be used throughout this document. Consider a tessellation $\mathbb{T}$ of the domain $\Omega \subset \mathbb{R}^d$, consisting of $N = \text{card}(\mathbb{T})$ connexe

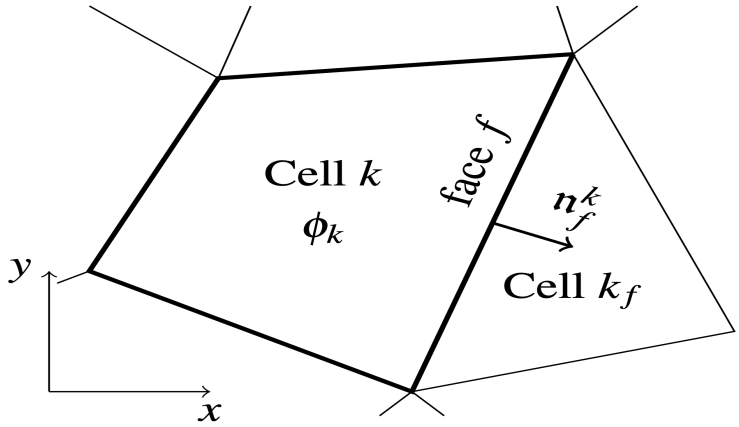

Figure 1.2: Illustration of the discrete notations.

control volumes. For free-surface flow applications, the computational domain is typically horizontal with $d = 2$. However, the proposed numerical strategies can be applied to other frameworks, as mentioned later, and are not restricted to 1D or 2D cases. For any element $k \in \mathbb{T}$ (referred to as a cell or control volume), let $\mathbb{F}_k$ represent the set of its faces, and $\mathfrak{m}_k$ its surface area (or length if $d = 1$, surface area if $d = 2$, volume if $d = 3$, etc.). For any face $f \in \mathbb{F} = \cup_{k\in\mathbb{T}}\mathbb{F}_k$, we denote by $\mathfrak{m}_f$ its length (with $\mathfrak{m}_f = 1$ by convention for $d = 1$). The neighbor of k across face f is denoted by k_f, such that $k \cup k_f = f$. The unit normal vector to the face f, pointing outward from cell k, is denoted by $\mathfrak{n}_f^k$, see Figure 1.2. For any $k \in \mathbb{T}$, ψ_k represents the approximation of the average value of a variable ψ (whether unknown or a parameter) within cell k. The set of these values across the tessellation is written as $\phi_\star = (\phi_k)_{k\in\mathbb{T}}$.

An adaptive time step δ_t^n is used, where the unknown ϕ^n approximates the value of ϕ at time $t^n = t^{n-1} + \delta_t^{n-1}$. This time step is computed to satisfy the CFL condition, which ensures the stability of the scheme by linking the maximum time step to the spatial step of the mesh. In multi-dimensional meshes, defining the spatial step can be challenging. To address this, we introduce the compactness, defined as the ratio of the cell surface area to its perimeter:, i.e. $\mathfrak{d}_k = \frac{\mathfrak{m}_k}{\sum_{\mathbb{F}_k}\mathfrak{m}_f}$. This length naturally appears in finit volume schemes and is often well-suited to characterize the spatial step of the mesh. Additionally, the distance between two cells, δ_f, is useful for constructing discrete differential operators or for variable reconstruction. This distance can be defined as the distance between the mass centers of the cells, or as an average based on their compactness.

CHAPTER 2

Free surface flows

"Si vague est la question,
approximative sera la réponse."
Jean Pierre Szymaniak

Contents

Contributions related to the chapter

[AAGP18] Some shallow water type models describing the vertical profile of the horizontal velocity with several degrees of freedom have been recently proposed. The question addressed in the current work is the hyperbolicity of a shallow water model with two velocities. The model is written in a nonconservative form and the analysis of its eigenstructure shows the possibility that two eigenvalues coincide. A definition of the nonconservative product is given which enables us to analyze the resonance and coalescence of waves. Eventually, we prove the well-posedness of the two dimensional Riemann problem with initial condition constant by half-plane.

[FNPPSM18] In geophysics, the shallow water model is a good approximation of the incompressible Navier-Stokes system with free surface and it is widely used for its mathematical structure and its computational efficiency. However, applications of this model are restricted by two approximations under which it was derived, namely the hydrostatic pressure and the vertical averaging. Each approximation has been addressed separately in the literature: the first one was overcome by taking into account the hydrodynamic pressure (e.g. the non-hydrostatic or the Green-Naghdi models); the second one by proposing a multilayer version of the shallow water model. In the present paper, a hierarchy of new models is derived with a layerwise approach incorporating non-hydrostatic effects to approximate the Euler equations. To assess these models, we use a rigorous derivation process based on a Galerkin-type approximation along the vertical axis of the velocity field and the pressure, it is also proven that all of them satisfy an energy equality. In addition, we analyse the linear dispersion relation of these models and prove that the latter relations converge to the dispersion relation for the Euler equations when the number of layers goes to infinity.

[Par19] This work is devoted to the numerical resolution in the multidimensional framework of a hierarchy of reduced models of the water wave equations, such as the Serre-Green-Naghdi model. A particular attention is paid to the dissipation of mechanical energy at the discrete level, which acts as a stability argument of the scheme,

even with source terms such space and time variation of the bathymetry. In addition, the analysis leads to a natural way to deal with dry areas without leakage of energy. To illustrate the accuracy and the robustness of the strategy, several numerical experiments are carried out. In particular, the strategy is capable of treating dry areas without special treatment.

[NPT22] This work is devoted to the structure of the time-discrete Green–Naghdi equations including bathymetry. We use the projection structure of the equations to characterize homogeneous and inhomogeneous boundary conditions for which the semi-discrete equations are well-posed. This structure allows us to propose efficient and robust numerical treatment of the boundary conditions that ensures entropy stability of the scheme by construction. Numerical evidence is provided to illustrate that our approach is suitable for situations of practical interest that are not covered by existing theory.

[Par24b] The primary focus of this work is the coupling of dispersive free-surface flow models through the utilization of a thick interface coupling technique. The initial step involves introducing a comprehensive framework applicable to various dispersive models, demonstrating that classical weakly dispersive models are encompassed within this framework. Next, a thick interface coupling technique, well-established in hyperbolic framework, is applied. This technique enables the formulation of unified models across different subdomains, each corresponding to a specific dispersive model. The unified model preserves the conservation of mechanical energy, provided it holds for each initial dispersive model. We propose a numerical scheme that preserve the projection structure at the discrete level and as a consequence is entropy-satisfying when the continuous model conserve the mechanical energy. We perform a deep numerical analysis of the waves reflected by the interface. Finally, we illustrate the usefulness of the method with two applications known to pose problems for dispersive models, namely the imposition of a time signal as a boundary condition or the imposition of a transparent boundary condition, and wave propagation over a discontinuous bathymetry.

[Par] Several dispersive models, such as the Benjamin-Bona-Mahony and Green-Naghdi models, can be formulated as hyperbolic systems with a source term. In recent decades, various numerical methods have been developed to construct schemes that maintain equilibrium between the hyperbolic flow and the source term, known as well-balanced schemes. The goal of this work is to adapt well-balanced hyperbolic schemes for dispersive models. A key characteristic of the dispersive source term is that it is not explicit but imposes a constraint on the velocity. Therefore, it is crucial to propose a suitable discretization of this constraint. We demonstrate that this discretization corresponds to a symplectic scheme of the Bernoulli equation associated with the dispersive model. Numerical experiments are conducted to illustrate the scheme's properties.

This chapter invites readers to consider dispersive models, especially those derived from simplifying the water wave model, as hyperbolic models whose solutions are sought within a linear subspace. In §2.1, we propose a strategy to approximate the water wave problem. Despite its crude formalism, this approach can recover several well-known models from the literature and ensures they share a consistent mathematical structure. §2.2 delves deeper into this mathematical structure and describe some tools that will be used later in the book. This structure, which closely resembles that of incompressible flow models, can be understood as a projection onto a linear subspace of the L^2 space. We establish the connection to the classical form of the models and highlight a remark on boundary conditions. In §2.3, we examine the discrete counterpart of the mathematical analysis discussed in the previous section. Specifically, preserving the structure helps ensure the stability of the numerical scheme according to certain criteria, such as entropy stability or the stability of steady solutions. The final section, §2.4, explores several strategies that utilize the projection structure to enhance the performance of numerical simulations.

2.1 Approximate models based on the projection structure

This section aims to present a modeling strategy for obtaining approximate models of the water wave problem. It is not intended to be an exhaustive review of models or methods. For a more comprehensive review of existing models, readers should refer to [Duc21]. The proposed strategy is based on a weak formulation of the water wave problem, tested on a space with a limited number of degrees of freedom. A rigorous derivation of most of the models described below can be found in [Lan13, Chapter 5] in the shallow water regime see §1.1.

2.1.1 Free surface incompressible Euler model

We will first outline the equations that will serve as a reference. These equations are established to describe the evolution of a fluid influenced by gravity. Motivated by the fact that gravity acts only along the vertical axis, we divide the frame between the horizontal coordinates $x \in \mathbb{R}^d$, with $d \in \{1,2\}$, and the vertical coordinate $z \in \mathbb{R}$. The differential operator ∇ refers to the horizontal spatial derivatives, i.e. $\nabla = (\partial_{x_i})^{\mathsf{T}}_{i\in[\![1,d]\!]}$. Due to gravity, we assume that the fluid remains at all times contained between two single-valued surfaces $B(t,x) \leq \eta(t,x)$, where the bottom $B(t,x)$ is given and the free surface $\eta(t,x)$ is an unknown. The velocity is also divided into its horizontal component $u(t,x,z) \in \mathbb{R}^d$ and its vertical component $w(t,x,z) \in \mathbb{R}$. The flow is governed by the Euler equation, i.e.

$$\begin{aligned} \partial_t u + u\cdot\nabla u + w\partial_z u &= -\nabla p \\ \partial_t w + u\cdot\nabla w + w\partial_z w &= -\partial_z p - \rho g \end{aligned} \tag{2.1}$$

where $\rho \in \mathbb{R}_+$ is the density of the fluid and $g \in \mathbb{R}_+$ is the gravity acceleration. The pressure inside the fluid $p(t,x,z) \in \mathbb{R}$ is a Lagrange multiplier associated with the incompressibility constraint

$$\nabla\cdot u + \partial_z w = 0. \tag{2.2}$$

At the bottom, we assume a non-penetration condition implying that the fluid cannot cross the bottom B, i.e.

$$u_{|_{z=B}} \cdot \nabla B - w_{|_{z=B}} = 0. \tag{2.3}$$

Similarly, the free surface is advected with the flow so that a kinematic condition is assumed at the free surface, i.e.

$$\partial_t \eta + u_{|_{z=\eta}} \cdot \nabla \eta - w_{|_{z=\eta}} = 0. \tag{2.4}$$

Finally, the pressure at the free surface $P_a \in \mathbb{R}_+$ is given and, for reasons of readability, it is assumed to be homogeneous. With the added curl free constraint, the (2.1), (2.2), (2.3) and (2.4) model is generally referred to as the water waves problem.

Proposition 2.1 *For sufficiently regular solutions of* (2.1), (2.2), (2.3) *and* (2.4), *the following mechanic energy conservation law holds*

$$\partial_t \left(\mathscr{P} + \mathscr{K}\right) + \nabla \cdot \left(\int_B^\eta \left(gz + p + \frac{|u|^2 + w^2}{2} \right) u \, \mathrm{d}z \right) = 0.$$

with $\mathscr{P} = g\left(\eta - B\right)\left(\frac{3B+\eta}{2}\right)$ *and* $\mathscr{K} = \int_B^\eta \frac{|u|^2+w^2}{2} \, \mathrm{d}z$.

In addition, it is well known that the phase velocity of the model is given by

$$c_p^{\text{AIRY}} = \sqrt{\frac{\tanh\left(kD\right)}{|kD|}} \sqrt{gD} \tag{2.5}$$

with D is the mean depth and k the wave number see [Air45]. The phase velocity is represented in Figure 2.5 with that of other models.

2.1.2 Hydrostatic models

2.1.2.1 The shallow water model

Unfortunately, the free-surface incompressible Euler model cannot be used for large-scale simulations, particularly for wave propagation, due to its complexity. One scientific challenge is to propose approximations of the free-surface incompressible Euler model that are applicable for geophysical purposes while preserving as many properties of the Euler model as possible. The most well-known approximate model derived from the free-surface incompressible Euler model is the shallow water model [dSV71], which is expressed as

$$\begin{aligned} \partial_t h + \nabla \cdot \left(h\overline{u}\right) &= 0 \\ \partial_t \left(h\overline{u}\right) + \nabla \cdot \left(h\overline{u} \otimes \overline{u}\right) &= -gh\nabla\left(B + h\right) \end{aligned} \tag{2.6}$$

where $h\left(t,x\right) = \eta\left(t,x\right) - B\left(x\right)$ represents the fluid depth, and $\overline{u}\left(t,x\right) = \frac{1}{h}\int_B^{B+h} u\left(t,x,z\right) \, \mathrm{d}z$ is the mean horizontal velocity. This model is based on two assumptions:

H_{yp}^p) Assume that the pressure is predominantly hydrostatic, i.e., $p = P_a + g\left(\eta - z\right)$.

H^u_{yp}) Assume that the horizontal velocity is nearly uniform throughout the water column, i.e., $\partial_z u = 0$.

It is noteworthy that these assumptions can be justified in the case of viscous flows [GP01] or by assuming a curl-free velocity field [Lan13] in the shallow water asymptotic regime, where the vertical length scale is much larger compared to the horizontal length scale. Additional source terms such as bottom friction, viscosity, and surface tension can also be incorporated [Mar07]. A mathematical analysis of the shallow water model (2.6) can be found for example in [GR96]. In one dimension, the model (2.6) is hyperbolic with eigenvalues $\overline{u} - \sqrt{gh}$, $\overline{u}$ and $\overline{u} + \sqrt{gh}$. We refer to [BN07] for a more complete analysis of the model.

Proposition 2.2 *For sufficiently regular solutions of* (2.6)*, the following mechanic energy conservation law holds*

$$\partial_t \left(\mathscr{P} + \mathscr{K}\right) + \nabla \cdot \left(\left(g\left(B+h\right) + \frac{|\overline{u}|^2}{2} \right) h\overline{u} \right) = 0.$$

with $\mathscr{P} = gh\left(B + \frac{h}{2}\right)$ *and* $\mathscr{K} = \frac{h}{2}|\overline{u}|^2$.

2.1.2.2 The depth averaged and moment equations

A natural way to eliminate the assumption H^u_{yp}) is to use a polynomial approximation in the vertical direction for the horizontal velocity. This approach is known as the Depth-Averaged and Moment Equations [SYC93]. In the simplest case, using a $\mathbb{P}_1[z]$-approximation, the shallow water model with linear velocity profil is given by

$$\begin{array}{ll} \partial_t h + \nabla \cdot (h\overline{u}) & = 0 \\ \partial_t (h\overline{u}) + \nabla \cdot (h(\overline{u} \otimes \overline{u} + \widetilde{u} \otimes \widetilde{u})) & = -gh\nabla(B+h) \\ \partial_t (h\widetilde{u}) + \nabla \cdot (h\widetilde{u} \otimes \overline{u}) + h\overline{u} \cdot \nabla \widetilde{u} & = 0 \end{array} \tag{2.7}$$

where the second component of the velocity can be interpreted as the oriented standard deviation, defined as $\widetilde{u}(t,x) = \frac{1}{h}\int_{-\frac{h}{2}}^{\frac{h}{2}} \theta_1\left(\frac{z}{h}\right) u\left(t,x,z+B+\frac{h}{2}\right) \mathrm{d}z$, with $\theta_1(z) = 2\sqrt{3}z$. This formulation recovers the bi-layer shallow water model (see §2.1.2.3) and in one dimension, the shallow water model with enstrophy (defined as $\frac{\widetilde{u}}{h}$) [Tes07, RG12]. A mathematical analysis of the Riemann problem for the shallow water model with two velocities (2.7) is presented in [AAGP18]. Specifically, (2.7) is hyperbolic with eigenvalues $\overline{u} - \sqrt{gh + 3\widetilde{u}^2}$, $\overline{u} - |\widetilde{u}|$, $\overline{u}$, $\overline{u} + |\widetilde{u}|$ and $\overline{u} + \sqrt{gh + 3\widetilde{u}^2}$.

Proposition 2.3 *For sufficiently regular solutions of* (2.7)*, the following mechanic energy conservation law holds*

$$\partial_t \left(\mathscr{P} + \mathscr{K}\right) + \nabla \cdot \left(\left(g\left(B+h\right) + \frac{|\overline{u}|^2 + |\widetilde{u}|^2}{2} \right) h\overline{u} \right) = 0.$$

with $\mathscr{P} = gh\left(B + \frac{h}{2}\right)$ *and* $\mathscr{K} = \frac{h}{2}\left(|\overline{u}|^2 + |\widetilde{u}|^2\right)$.

2.1.2.3 The layerwise shallow water model

Another approach is to assume a piecewise constant approximation of the horizontal velocity. Specifically, for a given number $L > 0$ of layers, we consider single-valued functions $\zeta_{i+1/2}(t,x)$ where $\zeta_{1/2}(t,x) = B(x)$, $\zeta_{L+1/2}(t,x) = \eta(t,x)$ and $\zeta_{1/2}(t,x) < \zeta_{L+1/2}(t,x)$. Using the Leibniz integral rule, we get

$$\begin{aligned} 0 = \int_{\zeta_{i-1/2}}^{\zeta_{i+1/2}} (\nabla \cdot u + \partial_z w)\,\mathrm{d}z = \partial_t\left(\zeta_{i+1/2} - \zeta_{i-1/2}\right) + \nabla\cdot\left(\int_{\zeta_{i-1/2}}^{\zeta_{i+1/2}} u\,\mathrm{d}z\right) \\ - \left(\partial_t \zeta_{i+1/2} + u_{|\zeta_{i+1/2}} \cdot \nabla\zeta_{i+1/2} - w_{|\zeta_{i+1/2}}\right) \\ + \left(\partial_t \zeta_{i-1/2} + u_{|\zeta_{i-1/2}} \cdot \nabla\zeta_{i-1/2} - w_{|\zeta_{i-1/2}}\right). \end{aligned}$$

Setting the unknowns $h_i(t,x) = \zeta_{i+1/2}(t,x) - \zeta_{i-1/2}(t,x)$, $u_i(t,x) = \frac{1}{h_i}\int_{\zeta_{i-1/2}}^{\zeta_{i+1/2}} u(t,x,z)\,\mathrm{d}z$ and $G_{i+1/2} = \partial_t\zeta_{i+1/2} + u_{|\zeta_{i+1/2}} \cdot \nabla\zeta_{i+1/2} - w_{|\zeta_{i+1/2}}$, we obtain the mass balance in each layer. That is, for $1 \le i \le L$

$$\partial_t h_i + \nabla\cdot(h_i u_i) = G_{i+1/2} - G_{i-1/2}. \tag{2.8}$$

The new unknowns $G_{i+1/2}$ can be interpreted as the flux of material passing through the interface $\zeta_{i+1/2}$. Using the non-penetration condition (2.3) and the kinematic condition (2.4), we have $G_{1/2} = 0$ and $G_{L+1/2} = 0$. However, the system has too many unknowns unless a specific definition of the interfaces is imposed. Several choices can be considered:

Imposing Interface Positions: In this case, all interfaces except the last one $\zeta_{L+\frac{1}{2}} = \eta$ are prescribed. This approach, proposed in [CC92, Ram11], resembles an Eulerian vertical discretization. It is limited to small variations in the free surface.

Following Material Interfaces: Here, the interfaces move with the material, leading to $G_{i+\frac{1}{2}} = 0$. This approach, proposed in [Aud05], resembles a Lagrangian vertical discretization. However, for homogeneous fluids, the resulting model is not hyperbolic. Even with variable density in well-stratified fluids, hyperbolicity is not guaranteed [Duc16, Mon14, Mon15].

Following Free Surface Dynamics: In this case, the interfaces follow the free surface such that the layer thickness $h_i = \ell_i h$, where $\ell_i > 0$ are weights satisfying $\sum_{i=1}^{L}\ell_i = 1$. This approach, introduced in [ABPSM11], can be viewed as an Arbitrary-Lagrangian-Eulerian (ALE) vertical discretization. It has been shown that the bilayer model is hyperbolic without additional conditions in [AAGP18]. However, extending this analysis to an arbitrary number of layers remains an open question.

Each approach has its advantages and limitations, depending on the specific characteristics of the fluid and the desired numerical properties of the model. We turn our attention to this last definition. By integrating the momentum equation across each layer, we derive the evolution of the velocity u_i, i.e.

$$\partial_t(\ell_i h u_i) + \nabla\cdot(\ell_i h u_i \otimes u_i) = -g\ell_i h\nabla(B+h) + u_{|\zeta_{i+1/2}} G_{i+1/2} - u_{|\zeta_{i-1/2}} G_{i-1/2}. \tag{2.9}$$

The system remains incomplete because the velocities at the interfaces $u_{|_{\zeta_{i-1/2}}}$ are not determined solely from the model's unknowns. In [ABPSM11], the authors propose a reconstruction method at the interfaces based on velocities from adjacent layers. This method can be understood as a Finite Volume scheme for vertical advection, specifically

$$u_{|_{\zeta_{i+1/2}}} = \frac{u_i + u_{i+1}}{2} + \lambda \frac{u_{i+1} - u_i}{2} \operatorname{sign}\left(G_{i+1/2}\right). \tag{2.10}$$

Proposition 2.4 *If $\lambda \geq 0$ and for sufficiently smooth solutions of the model (2.8)-(2.9), the following mechanic energy dissipation holds*

$$\partial_t \left(\mathscr{P} + \mathscr{K}\right) + \nabla \cdot \left(h \sum_{i=1}^{L} \left(\left(g\left(B+h\right) + \frac{|u_i|^2}{2} \right) \ell_i u_i \right) \right) \leq 0$$

with $\mathscr{P} = gh\left(B + \frac{h}{2}\right)$ and $\mathscr{K} = \frac{h}{2}\sum_{i=1}^{L}\left(\ell_i |u_i|^2\right)$. The equality holds when $\lambda = 0$.

One drawback of hydrostatic models is that the phase velocity of these models does not depend on the wave number. Specifically, the phase velocity of all the hydrostatic models presented here is

$$c_p^{\mathrm{SW}} = \sqrt{gD} \tag{2.11}$$

The phase velocity is represented in Figure 2.5 with that of other models.

2.1.3 Hydrodynamic models

One (very formal) method of deriving approximate models from the equations presented in §2.1.1 without assuming H_{yp}^p) is based on the weak formulation of the Euler equations. To proceed, we introduce the space of divergence-free functions that satisfy the non-penetration condition (2.3).

$$\mathbb{A}_\eta = \left\{ (\mathbf{u}, \mathbf{w}) \in \left(L^2\left(\mathbb{R}^d \times [B;\eta]\right)\right)^{d+1} \left| \begin{array}{c} \nabla \cdot \mathbf{u} + \partial_z \mathbf{w} = 0 \\ \mathbf{u}_{|_{z=B}} \cdot \nabla B - \mathbf{w}_{|_{z=B}} = 0 \end{array} \right. \right\}.$$

It is worth noting that the kinematic condition (2.4) is not a constraint for the flow but rather drives the dynamics of the free surface. We also introduce the hydrodynamic pressure q, defined as the difference between the fluid pressure and the hydrostatic pressure, i.e., $q = p - (P_a + \rho g(\eta - z))$. For any vector $(\mathbf{u}, \mathbf{w}) \in \mathbb{A}_\eta$ and any $q \in L^2\left(\mathbb{R}^d \times [B;\eta]\right)$ such that $q_{|_{z=\eta}} = 0$, we have $\langle (\mathbf{u},\mathbf{w})^\intercal, (\nabla q, \partial_z q)^\intercal \rangle = 0$. Then, the weak formulation of (2.1), (2.2), and (2.3) is to find $(u,w) \in \mathbb{A}_\eta$ such that for any $(\mathbf{u},\mathbf{w}) \in \mathbb{A}_\eta$, we have

$$\begin{aligned} \int_{\mathbb{R}^d} \int_B^{B+h} \big(& \mathbf{u}\left(\partial_t u + u \cdot \nabla u + w \partial_z u + g \nabla (B+h)\right) \\ & + \mathbf{w}\left(\partial_t w + u \cdot \nabla w + w \partial_z w\right) \big) \, \mathrm{d}z \, \mathrm{d}x = 0. \end{aligned} \tag{2.12}$$

Approximate models can be obtained by considering an "approximation" of the function space $\mathbb{A}_\eta$. It is important to note that this strategy does not guarantee that the approximation is accurate, meaning that the solution of the approximate model may not remain close to the solution of the equations in §2.1.1, even for a short period.

2.1.3.1 The Green-Naghdi model

Let us approximate the function space $\mathbb{A}_\eta$ by

$$\mathbb{A}_\eta^{\mathrm{GN}} = \left\{ (\mathbf{u},\mathbf{w}) \in \left(L^2\left(\mathbb{R}^d \times [B;\eta]\right)\right)^{d+1} \left| \begin{array}{c} \mathbf{u}(t,x,z) = \overline{u}(t,x) \\ \nabla\cdot\mathbf{u} + \partial_z \mathbf{w} = 0 \\ \mathbf{u}_{|_{z=B}} \cdot \nabla B - \mathbf{w}_{|_{z=B}} = 0 \end{array} \right. \right\}.$$

The first constraint in $\mathbb{A}_\eta^{\mathrm{GN}}$ still assumes that the horizontal velocity is constant along the water column and is equivalent to H_{yp}^u). However, we assume that the divergence-free condition is satisfied by the velocity fields, thereby removing the hydrostatic pressure assumption H_{yp}^p). Since $\mathbf{u} \in \mathbb{P}_0[z]$, the divergence free conclude that $\mathbf{w} \in \mathbb{P}_1[z]$, meaning it can be defined by two functions of time and horizontal space. We choose to define the vertical velocity from its mean horizontal value $\overline{\mathbf{w}}(t,x) = \frac{1}{h}\int_0^h \mathbf{w}(t,x,z+B)\,\mathrm{d}z$ and its oriented standard deviation $\widetilde{\mathbf{w}}(t,x) = \frac{1}{h}\int_{-\frac{h}{2}}^{\frac{h}{2}} \theta_1\left(\frac{z}{h}\right)\mathbf{w}\left(t,x,z+B+\frac{h}{2}\right)\mathrm{d}z$ with $\theta_1(z) = 2\sqrt{3}z$ with $\theta_1(z) = 2\sqrt{3}z$. This choice is motivated by the link between the this variables and the kinetic energy of the flow, i.e.

$$\int_B^{B+h} \mathbf{w}^2\,\mathrm{d}z = h\left(\overline{\mathbf{w}}^2 + \widetilde{\mathbf{w}}^2\right) \qquad \text{with} \qquad \mathbf{w}(t,x,z) = \overline{\mathbf{w}}(t,x) + \theta_1\left(\frac{z-B-\frac{h}{2}}{h}\right)\widetilde{\mathbf{w}}(t,x).$$

It is worth noting that there is an isomorphism between the function space $\mathbb{A}_\eta^{\mathrm{GN}}$ and

$$\widetilde{\mathbb{A}}_h^{\mathrm{GN}} = \left\{ (\overline{\mathbf{u}},\overline{\mathbf{w}},\widetilde{\mathbf{w}}) \in \left(L^2\left(\mathbb{R}^d,h\right)\right)^{d+2} \left| \begin{array}{c} \overline{\mathbf{w}} + \frac{h}{2}\nabla\cdot\overline{\mathbf{u}} - \overline{\mathbf{u}}\cdot\nabla B = 0 \\ \widetilde{\mathbf{w}} + \frac{h}{2\sqrt{3}}\nabla\cdot\overline{\mathbf{u}} = 0 \end{array} \right. \right\}.$$

Testing (2.12) with the function $(\mathbf{u},\mathbf{w}) = (1,0)$, $(\mathbf{u},\mathbf{w}) = (0,1)$ and $(\mathbf{u},\mathbf{w}) = \left(0,\theta_1\left(\frac{z-B-\frac{h}{2}}{h}\right)\right)$, we get the equations of $\overline{u}$, $\overline{w}$ and $\widetilde{w}$ respectively. However, when writing the strong formulation, it is important to include the elements of the dual space with respect to the inner product $\langle\bullet,\bullet\rangle_h$ associated with the weighted space $L^2\left(\mathbb{R}^d,h\right)$. We get

$$\begin{array}{ll} \partial_t(h\overline{u}) + \nabla\cdot(h\overline{u}\otimes\overline{u}) & = -gh\nabla(B+h) - h\psi_0 \\ \partial_t(h\overline{w}) + \nabla\cdot(h\overline{u}\,\overline{w}) & = -h\psi_1 \\ \partial_t(h\widetilde{w}) + \nabla\cdot(h\overline{u}\,\widetilde{w}) & = -h\psi_2 \end{array} \tag{2.13}$$

with the constraint

$$\overline{w} + \frac{h}{2}\nabla\cdot\overline{u} - \overline{u}\cdot\nabla B = 0 \qquad \text{and} \qquad \widetilde{w} + \frac{h}{2\sqrt{3}}\nabla\cdot\overline{u} = 0 \tag{2.14}$$

and $\left\langle(\mathbf{u},\mathbf{w},\widetilde{\mathbf{w}})^\intercal,(\psi_0,\psi_1,\psi_2)^\intercal\right\rangle_h = 0$ for any $(\mathbf{u},\mathbf{w},\widetilde{\mathbf{w}})^\intercal$ satisfying (2.14).

It is worth noting that for physical relevance, it is possible to link the dispersive source term Ψ to the hydrodynamic pressure q defined in §2.1.3. Specifically, by defining $\overline{q}(t,x) = \frac{h}{2}\left(\psi_1 + \frac{\psi_2}{\sqrt{3}}\right)$ and $q_B(t,x) = h\psi_1$, we express the dispersive source term as follows

$$h\psi_0 = \nabla(h\overline{q}) + q_B\nabla B\,, \quad h\psi_1 = q_B \quad \text{and} \quad h\psi_2 = \sqrt{3}(2\overline{q} - q_B).$$

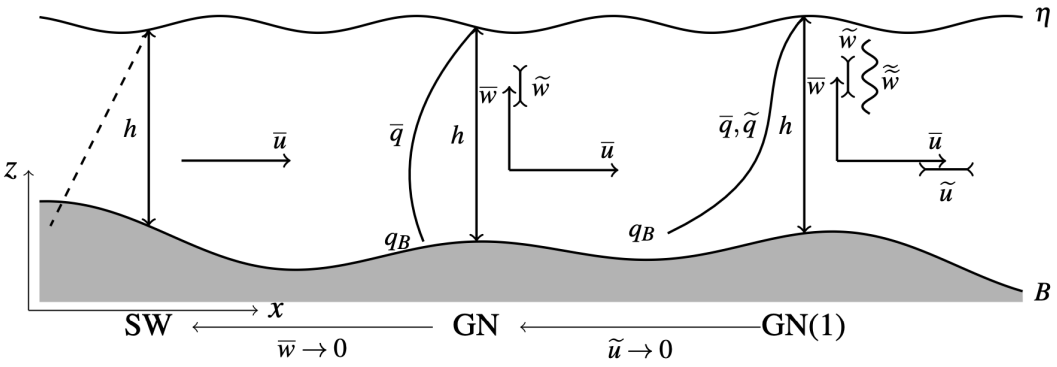

Figure 2.1: §2.1.3.2 | Illustration of the depth averaged semi-discretization §2.1.3.2 in the vertical plan. SW (2.6), GN (2.13) and GN(1) (2.16).

The unknown $\overline{q}$ is interpreted as the vertically averaged hydrodynamic pressure $\frac{1}{h}\int_B^{B+h} q\,\mathrm{d}z$ and q_B is interpreted as the hydrodynamic pressure at the bottom $q_{|_{z=B}}$. They act as the Lagrange multipliers associated with the constraint (2.14).

It can be shown that the model (2.13) and (2.14) is simply another formulation of the Green-Naghdi model [GN76]; see §2.2.2.2. A mathematical analysis of the Green-Naghdi model is provided in [Isr11] and [Lan13, chapter 6]. It is worth noting that the model (2.13) without the dispersive source term is hyperbolic, with eigenvalues $\overline{u}-\sqrt{gh}$, $\overline{u}$ (three times) and $\overline{u}+\sqrt{gh}$.

Proposition 2.5 *For sufficiently smooth solutions of the model (2.13), the following mechanic energy conservation law holds*

$$\partial_t\left(\mathscr{P}+\mathscr{K}\right)+\nabla\cdot\left(\left(g\left(B+h\right)+\overline{q}+\frac{|\overline{u}|^2+\overline{w}^2+\widetilde{w}^2}{2}\right)h\overline{u}\right)=0.$$

with $\mathscr{P}=gh\left(B+\frac{h}{2}\right)$ *and* $\mathscr{K}=\frac{h}{2}\left(|\overline{u}|^2+\overline{w}^2+\widetilde{w}^2\right)$.

In addition, the phase velocity of the Green-Naghdi model (2.13) reads

$$c_p^{\mathrm{GN}}=\sqrt{\frac{1}{1+\frac{1}{3}|gD|^2}}\sqrt{gD}. \tag{2.15}$$

The phase velocity is represented in Figure 2.5 with that of other models.

2.1.3.2 The depth averaged and moment dispersive model

To proceed further, we follow the strategy presented in §2.1.2.2 by approximating the function space $\mathbb{A}_\eta$ by

$$\mathbb{A}_\eta^{\mathrm{GN}(i)}=\left\{(\mathbf{u},\mathbf{w})\in\left(L^2\left(\mathbb{R}^d\times[B;\eta]\right)\right)^{d+1}\left|\begin{array}{r}\mathbf{u}\left(t,x,z\right)\in\mathbb{P}_i[z]\\ \nabla\cdot\mathbf{u}+\partial_z\mathbf{w}=0\\ \mathbf{u}_{|_{z=B}}\cdot\nabla B-\mathbf{w}_{|_{z=B}}=0\end{array}\right.\right\}.$$

The case of $\mathbb{A}_\eta^{\mathrm{GN}(0)}$ corresponds to the classical Green-Naghdi model (2.13). The case of $\mathbb{A}_\eta^{\mathrm{GN}(1)}$ corresponds to a hydrodynamic version of (2.7). More precisely, we utilize the Legendre normalized basis $\theta_i(z) \in \mathbb{P}_i(z)$, and the horizontal velocity is expressed as

$$u(t,x,z) = \overline{u}(t,x) + \theta_1\left(\frac{z-B-\frac{h}{2}}{h}\right)\widetilde{u}(t,x)$$

as in the hydrostatic case. Since $u \in \mathbb{P}_1[z]$, using the divergence-free condition, we conclude that $w \in \mathbb{P}_2[z]$. Therefore,

$$w(t,x,z) = \overline{w}(t,x) + \theta_1\left(\frac{z-B-\frac{h}{2}}{h}\right)\widetilde{w}(t,x) + \theta_2\left(\frac{z-B-\frac{h}{2}}{h}\right)\widetilde{\widetilde{w}}(t,x).$$

See Figure 2.1 for an illustration of the unknowns of the model (2.16). Now, testing (2.12) with $(\mathbf{u},\mathbf{w}) = (1,0)$ and $(\mathbf{u},\mathbf{w}) = (\theta_1,0)$, $(\mathbf{u},\mathbf{w}) = (0,1)$, $(\mathbf{u},\mathbf{w}) = (0,\theta_1)$ and $(\mathbf{u},\mathbf{w}) = (0,\theta_2)$, we obtain the equations to which we add the dispersive source term $(\psi_i)_{0\le i\le 4} \in \left(\mathbb{A}_\eta^{\mathrm{GN}(1)}\right)^\perp$. Thus, we have

$$\begin{aligned}
\partial_t h + \nabla\cdot(h\overline{u}) &= 0\\
\partial_t(h\overline{u}) + \nabla\cdot(h(\overline{u}\otimes\overline{u}+\widetilde{u}\otimes\widetilde{u})) + gh\nabla(B+h) &= -h\psi_0\\
\partial_t(h\widetilde{u}) + \nabla\cdot(h\widetilde{u}\otimes\overline{u}) + h\overline{u}\cdot\nabla\widetilde{u} &= -h\psi_1\\
\partial_t(h\overline{w}) + \nabla\cdot(h(\overline{u}\,\overline{w}+\widetilde{u}\widetilde{w})) &= -h\psi_2\\
\partial_t(h\widetilde{w}) + \nabla\cdot(h\widetilde{w}\,\overline{u}) + h\widetilde{u}\cdot\nabla\left(\overline{w}+\frac{2}{\sqrt{5}}\widetilde{\widetilde{w}}\right) + \frac{3}{\sqrt{5}}\widetilde{\widetilde{w}}\nabla\cdot(h\widetilde{u}) &= -h\psi_3\\
\partial_t\left(h\widetilde{\widetilde{w}}\right) + \nabla\cdot\left(h\left(\overline{u}\,\widetilde{\widetilde{w}}+\frac{2}{\sqrt{5}}\widetilde{u}\widetilde{w}\right)\right) - \frac{3}{\sqrt{5}}\widetilde{w}\nabla\cdot(h\widetilde{u}) &= -h\psi_4
\end{aligned} \tag{2.16}$$

with the constraint

$$\begin{aligned}
&\widetilde{\widetilde{w}} + \frac{h^2}{2\sqrt{15}}\nabla\cdot\left(\frac{\widetilde{u}}{h}\right) = 0\,, \qquad \widetilde{w} + \frac{h}{2\sqrt{3}}\nabla\cdot\overline{u} - \widetilde{u}\cdot\nabla\left(B+\frac{h}{2}\right) = 0\\
\text{and}\qquad &\overline{w} + \frac{h}{2}\nabla\cdot\overline{u} - \overline{u}\cdot\nabla B - \frac{h^2}{2\sqrt{3}}\nabla\cdot\left(\frac{\widetilde{u}}{h}\right) - \sqrt{3}\widetilde{u}\cdot\nabla\left(2B+\frac{h}{2}\right) = 0
\end{aligned} \tag{2.17}$$

and $\left\langle\left(\mathbf{u},\widetilde{\mathbf{u}},\mathbf{w},\widetilde{\mathbf{w}},\widetilde{\widetilde{\mathbf{w}}}\right)^{\mathsf{T}},(\psi_0,\psi_1,\psi_2,\psi_3,\psi_4)^{\mathsf{T}}\right\rangle_h = 0$ for any $\left(\mathbf{u},\widetilde{\mathbf{u}},\mathbf{w},\widetilde{\mathbf{w}},\widetilde{\widetilde{\mathbf{w}}}\right)^{\mathsf{T}}$ satisfying (2.17).

The model (2.16) was initially proposed in [EFNGD+23] in a slightly different formulation. The current formulation is intended to fit into the structure presented in §2.2. More precisely, without the dispersive source term, the model (2.16) is hyperbolic with the eigenvalues

$$\overline{u} - \sqrt{gh+3\widetilde{u}^2},\ \overline{u} - \frac{3}{\sqrt{5}}|\widetilde{u}|,\ \overline{u}-|\widetilde{u}|,\ \overline{u}\ \text{(twice)},\ \overline{u}+|\widetilde{u}|,\ \overline{u}+\frac{3}{\sqrt{5}}|\widetilde{u}|,\ \overline{u}+\sqrt{gh+3\widetilde{u}^2}.$$

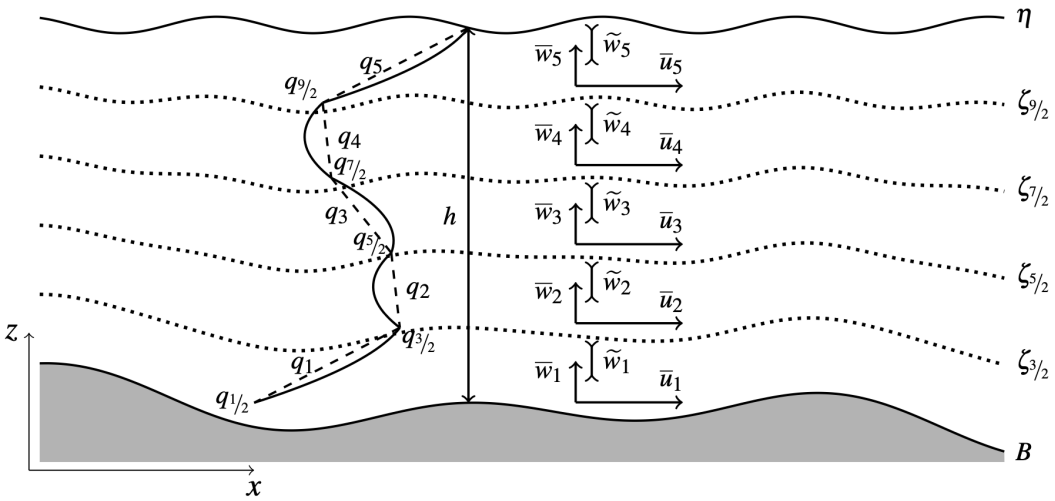

Figure 2.2: §2.1.3.3 | Illustration of the layerwise semi-discretization §2.1.3.3 in the vertical plan with $L = 5$.

Proposition 2.6 *For sufficiently smooth solutions of the model (2.16), the following mechanic energy conservation law holds*

$$\partial_t \left(\mathscr{P} + \mathscr{K}\right) + \nabla \cdot \left(\left(g\left(B+h\right) + \overline{q} + \frac{|\overline{u}|^2 + |\widetilde{u}|^2 + |\overline{w}|^2 + |\widetilde{w}|^2 + \left|\widetilde{\widetilde{w}}\right|^2}{2} \right) h\overline{u} + h\widetilde{q}\widetilde{u} \right) = 0.$$

with $\mathscr{P} = gh\left(B + \frac{h}{2}\right)$ *and* $\mathscr{K} = \frac{h}{2}\left(|\overline{u}|^2 + |\widetilde{u}|^2 + |\overline{w}|^2 + |\widetilde{w}|^2 + \left|\widetilde{\widetilde{w}}\right|^2\right)$.

In addition, the phase velocity of the model (2.16) reads

$$c_p^{\mathrm{GN}(1)} = \sqrt{\frac{1}{1 + \frac{|gD|^2}{12\left(1+\frac{|gD|^2}{60}\right)} + \frac{|gD|^2}{4\left(1+\frac{|gD|^2}{12\left(1+\frac{|gD|^2}{60}\right)}\right)}}} \sqrt{gD}. \tag{2.18}$$

The phase velocity is represented in Figure 2.5 with that of other models.

It is worth noting that a hydrodynamic version of the shallow water model with enstrophy is proposed in [KR19a]. The model (2.16) differs from the model proposed in [KR19a] in that it includes a dispersive source term ψ_1 in the equation for enstrophy. The model (2.16) could also be compared to the Green-Naghdi model with vorticity [CL14].

2.1.3.3 The layerwise Green-Naghdi model

We now examine the hydrodynamic version of the layerwise shallow water model (2.9), as detailed in [FNPPSM18, Cas99]. More specifically, we approximate the function space $\mathbb{A}_\eta$

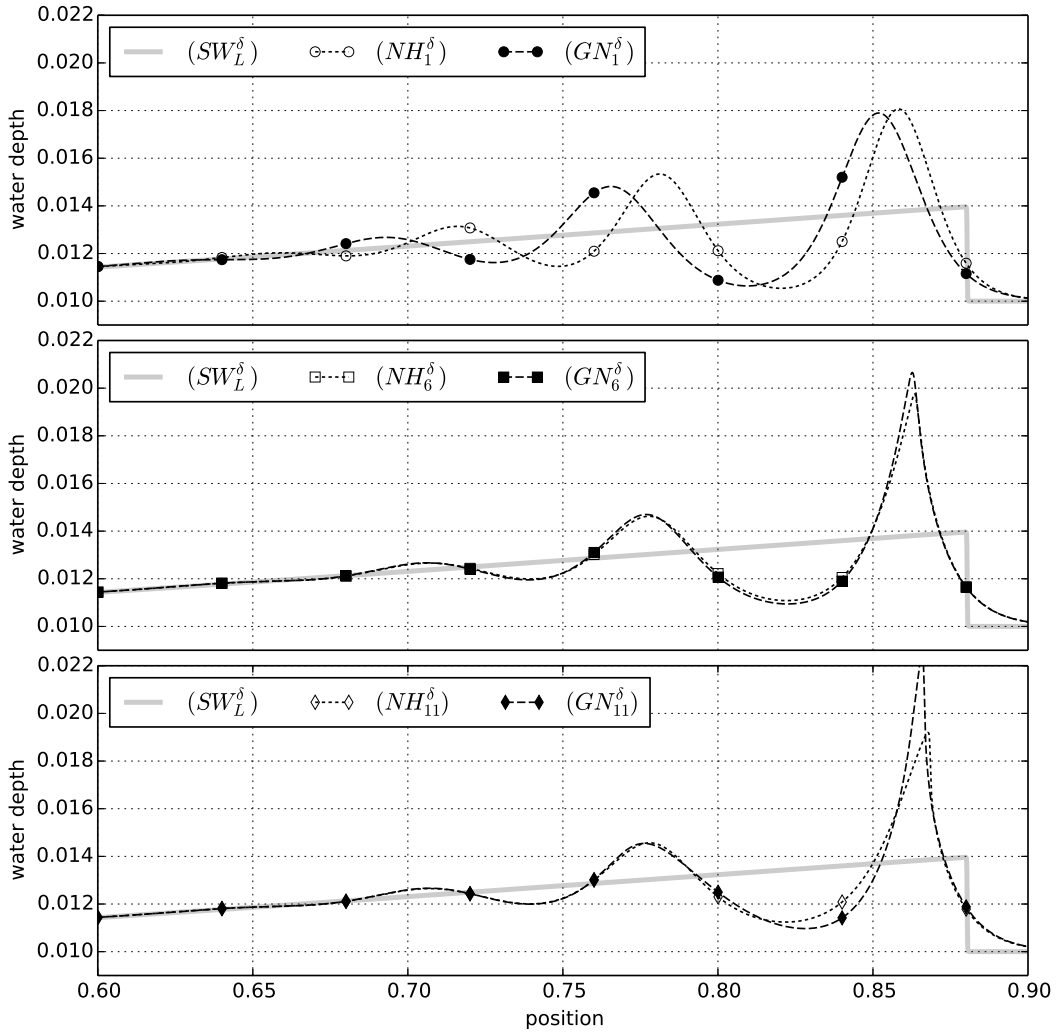

Figure 2.3: §2.1.3.3 | Simulations of the layerwise Green-Naghdi model (2.19) (dashed line) and the non-hydrostatic model [SM11] (dotted line) with one (top line), six (middle line) and eleven (bottom line) layers initialized by a Gaussian at rest.

by

$$\mathbb{A}^{\mathrm{GN}}_{\eta,L} = \left\{ (\mathbf{u},\mathbf{w}) \in \left(L^2\left(\mathbb{R}^d \times [B;\eta]\right)\right)^{d+1} \middle| \begin{array}{l} \mathbf{u}(t,x,z) = \sum_{i=1}^{L} u_i(t,x)\, \mathbb{1}_{\mathbb{L}_i}(z) \\ \nabla\cdot\mathbf{u} + \partial_z \mathbf{w} = 0 \\ \mathbf{u}_{|_{z=B}} \cdot \nabla B - \mathbf{w}_{|_{z=B}} = 0 \end{array} \right\}.$$

See Figure 2.2 for an illustration of the unknowns of the layerwise model. The case of $\mathbb{A}^{\mathrm{GN}}_{\eta,0}$ corresponds to the classical Green-Naghdi model (2.13). Testing (2.12) with the function $(\mathbf{u},\mathbf{w}) = (\mathbb{1}_{\mathbb{L}_i}(z),0)$ yields the equation for u_i, as in the case of (2.9), with an additional source term for the hydrodynamic pressure. Next, testing (2.12) with $(\mathbf{u},\mathbf{w}) = (0,\mathbb{1}_{\mathbb{L}_i}(z))$ and $(\mathbf{u},\mathbf{w}) = \left(0,\theta_1\left(\frac{z}{h} - \frac{\zeta_{i-1/2}+\zeta_{i+1/2}}{2h}\right)\mathbb{1}_{\mathbb{L}_i}(z)\right)$ gives us the equations for $\overline{w}_i$ and

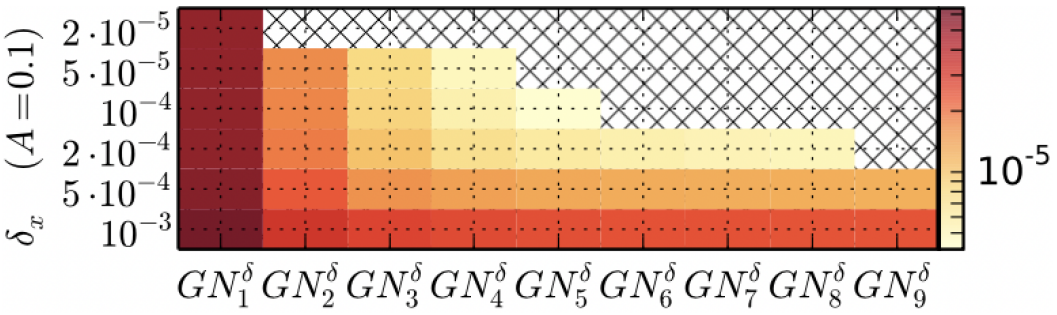

Figure 2.4: §2.1.3.3 | Comparison in L^2-norm of the simulated solution of the layerwise Green-Naghdi model (2.19) and the solitary wave of the Euler model (2.1) for several mesh sizes (lines) and number of layers (columns).

$\widetilde{w}_i$ respectively. More precisely, we write:

$$\begin{aligned}
\partial_t h + \nabla\cdot(hu_i) &= \frac{1}{\ell_i}[G_j]_{j=i-1/2}^{j=i+1/2} \\
\partial_t(hu_i) + \nabla\cdot(hu_i\otimes u_i) &= -gh\nabla(B+h) + \frac{1}{\ell_i}\left[u_{|\zeta_j}G_j\right]_{j=i-1/2}^{j=i+1/2} - h\psi_i^u \\
\partial_t(hw_i) + \nabla\cdot(hu_i\, w_i) &= \frac{1}{\ell_i}\left[w_{|\zeta_j}G_j\right]_{j=i-1/2}^{j=i+1/2} - h\psi_i^w \\
\partial_t(h\widetilde{w}_i) + \nabla\cdot(hu_i\,\widetilde{w}_i) &= \frac{1}{\ell_i}\left(\widetilde{w}_{i+1/2\ominus}G_{i+1/2} - \widetilde{w}_{i-1/2\oplus}G_{i-1/2}\right) - h\psi_i^{\widetilde{w}}
\end{aligned} \tag{2.19}$$

where the horizontal velocity at the interface is described by (2.10). Similarly, the vertical velocity at the interface is given by

$$\begin{aligned}
w_{|\zeta_{i+1/2}} &= \frac{w_i + w_{i+1} - \sqrt{3}(\widetilde{w}_{i+1} - \widetilde{w}_i)}{2} \\
&\quad + \lambda\frac{w_{i+1} - w_i - \sqrt{3}(\widetilde{w}_{i+1} + \widetilde{w}_i)}{2}\operatorname{sign}\left(G_{i+1/2}\right), \\
\widetilde{w}_{i+1/2\ominus} &= \sqrt{3}\left(w_{|\zeta_{i+1/2}} - w_i\right) - \widetilde{w}_i \\
\text{and}\qquad \widetilde{w}_{i+1/2\oplus} &= -\sqrt{3}\left(w_{|\zeta_{i+1/2}} - w_{i+1}\right) - \widetilde{w}_{i+1}.
\end{aligned} \tag{2.20}$$

The constraint of the linear subspace, expressed in terms of the new unknowns, reads

$$\begin{aligned}
w_i &= u_i\cdot\nabla\left(B + \sum_{j=1}^{i-1}\ell_j h\right) - \frac{\ell_i h}{2}\nabla\cdot u_i - \sum_{j=1}^{i-1}\ell_j\nabla\cdot(hu_j) \\
\text{and}\qquad \widetilde{w}_i &= -\frac{\ell_i h}{2\sqrt{3}}\nabla\cdot u_i.
\end{aligned} \tag{2.21}$$

The dispersive source term is an element of the dual space, defined by $\left\langle(\mathbf{u}_i,\mathbf{w}_i,\widetilde{\mathbf{w}}_i)_{1\le i\le L}^{\mathsf{T}}, (\psi_i^u,\psi_i^w,\psi_i^{\widetilde{w}})_{1\le i\le L}^{\mathsf{T}}\right\rangle_h = 0$ for any $(\mathbf{u}_i,\mathbf{w}_i,\widetilde{\mathbf{w}}_i)_{1\le i\le L}^{\mathsf{T}}$ that satisfies (2.21).

L	$P_L(x)$	$Q_L(x)$
1	1	$1+\frac{x}{3}$
2	$1+\frac{x}{12}$	$1+\frac{5x}{12}+\frac{7x^2}{576}$
3	$1+\frac{x}{9}+\frac{5x^2}{2916}$	$1+\frac{4x}{9}+\frac{19x^2}{972}+\frac{13x^3}{78732}$
4	$1+\frac{x}{8}+\frac{3x^2}{1024}+\frac{7x^3}{442368}$	$1+\frac{11x}{24}+\frac{37x^2}{1536}+\frac{71x^3}{221184}+\frac{97x^4}{84934656}$

Table 2.1: Phase velocity of (2.19) for a small number of layers

Proposition 2.7 *If $\lambda > 0$, for sufficiently regular solutions of the model (2.19), the following mechanic energy conservation law holds*

$$\partial_t(\mathscr{P}+\mathscr{K})+\nabla\cdot\left(h\sum_{i=1}^{L}\left(\left(g(B+h)+q_i+\frac{|u_i|^2+|w_i|^2+|\widetilde{w}_i|^2}{2}\right)\ell_i\overline{u}_i\right)\right)=0.$$

with $\mathscr{P}=gh\left(B+\frac{h}{2}\right)$ and $\mathscr{K}=\frac{h}{2}\sum_{i=1}^{L}\left(\ell_i\left(|u_i|^2+|w_i|^2+|\widetilde{w}_i|^2\right)\right)$. The equality holds when $\lambda=0$.

Additionally, the phase velocity (for any λ) of the model (2.19) is given by

$$c_p^{\mathrm{GN}_L}=\sqrt{\frac{P_L\left(|gD|^2\right)}{Q_L\left(|gD|^2\right)}}\sqrt{gD} \tag{2.22}$$

with $P_L(x)\in\mathbb{P}_{L-1}$ and $Q_L(x)\in\mathbb{P}_L$. Specifically, the polynomial for a small number of layers is provided in Table 2.1. We also demonstrate that the phase velocity (2.22) converges to the Airy phase velocity (2.5) as the number of layers tends to infinity. The phase velocity is represented in Figure 2.5 with that of other models. In [EFNGD+23], the authors propose a layerwise version of the model (2.16) with a linear approximation of the horizontal velocity in each layer. Figure 2.3 shows the results of the layerwise Green-Naghdi model (2.19) and the result of the non-hydrostatic model [SM11] using the numerical strategy presented in §2.3.1.1. In Figure 2.4, we compare the solution of the layerwise Green-Naghdi model (2.19) to the Euler model (2.1) initialized with the solitary wave of the Euler model given in [CD13].

2.2 The class of projected hyperbolic models

The dispersive models discussed in §2.1.3 all exhibit a common structure: they are hyperbolic models featuring a source term defined within the dual space of a linear subspace constrained by a specific conditions. In this section, we aim to delve into this structural similarity and establish connections with other established models.

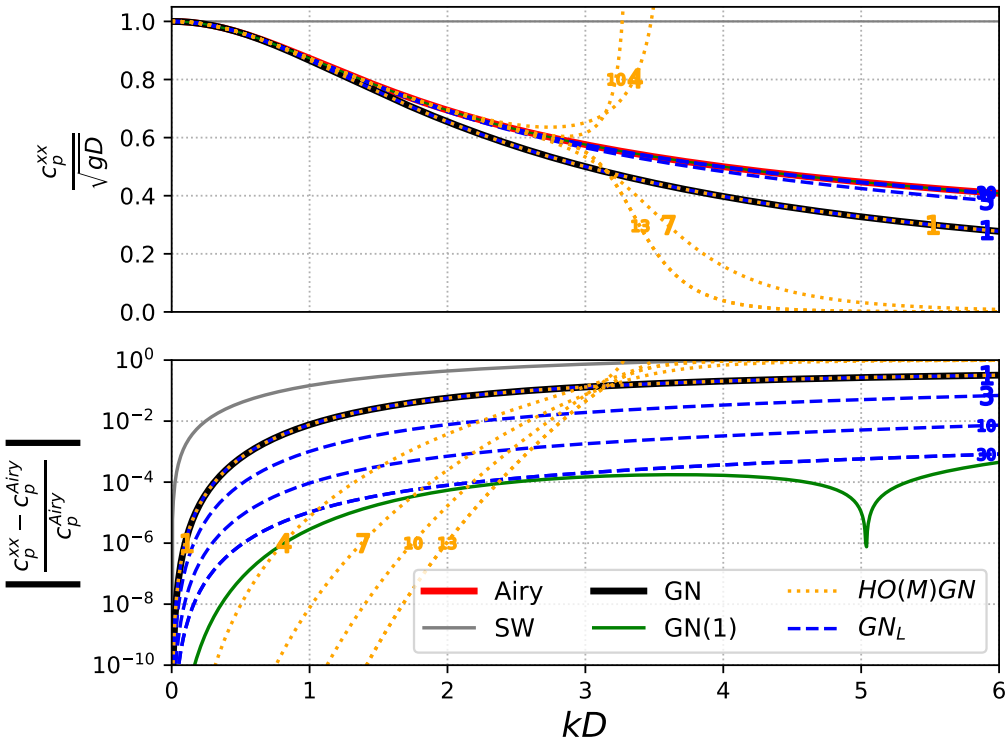

Figure 2.5: §2.1 | Comparison of phase velocity and relative error compared to the Airy phase velocity for different models:
- Red solid line: Airy model (2.5),
- Gray solid line: Hydrostatic models (2.11),
- Black solid line: Green-Naghdi model (2.15),
- Green solid line: Green-Naghdi model with linear velocity profile (2.18),
- Blue dashed line: Layerwise Green-Naghdi model (2.22), where the number on the curve corresponds to the number of layers L,
- Orange dashed line: Green-Naghdi model with linear velocity profile (2.50), where the number on the curve corresponds to the number of added velocities M.

2.2.1 Projected hyperbolic models of BBM-type

2.2.1.1 General description

We focus on models in the form, which we will later refer to as the projected hyperbolic model of BBM-type

$$\partial_t U + A(U)\,\partial_x U = -\Psi(Q) \tag{2.23}$$

where the state variable $U(t,x) : \mathbb{R}_+ \times \mathbb{R} \mapsto \mathbb{R}^{d_U}$ and $Q(t,x) : \mathbb{R}_+ \times \mathbb{R} \mapsto \mathbb{R}^{d_Q}$ with $d_Q < d_U$. The square matrix $A(U) : \mathbb{R}^{d_U} \mapsto M_{d_U}(\mathbb{R})$ is assumed to have real eigenvalues, ensuring that, when the dispersive source term Ψ is omitted, the model remains hyperbolic. Addi-

tionally, we assume there exists a flux $G(U) : \mathbb{R}^{d_U} \mapsto \mathbb{R}^{d_U}$ such that the relation

$$U^\intercal \cdot A(U) = (\nabla_U G)^\intercal \tag{2.24}$$

holds. This relation, known as the entropy-flux relation, is well-known in hyperbolic models for identifying an entropy for the system (see [Bou04]). In our case, the particularity lies in the fact that the entropy is the L^2-norm of the state variable U.

The right-hand side of (2.23), referred to as the dispersive source term $\Psi(Q)$, is not explicitly defined. However, it is constructed to ensure that the state variable satisfies the constraint

$$\mathscr{L}(U) = 0 \tag{2.25}$$

for a given linear application $\mathscr{L} : \left(L^2(\mathbb{R})\right)^{d_U} \mapsto \left(L^2(\mathbb{R})\right)^{d_Q}$. In other words, the dispersive source term Ψ ensures that the state variable U lies in the kernel of $\mathscr{L}$.

At this stage, the model is not yet fully defined since there are multiple ways to ensure that $U \in \ker(\mathscr{L})$. For example, setting $\Psi = -A\partial_x U$ reduces the model to $\partial_t U = 0$, which ensures that $U \in \ker(\mathscr{L})$ (assuming $U(t=0,x) \in \ker(\mathscr{L})$). However, this also implies that the model is irrelevant. To properly define the system, the dispersive source term is assumed to belong to the dual space $(\ker(\mathscr{L}))^\perp$ with respect to the L^2 inner product. This means that for any $V \in \ker(\mathscr{L})$ and any $\Phi \in (\ker(\mathscr{L}))^\perp$, we have

$$\langle V, \Phi \rangle = \int_{\mathbb{R}} V \cdot \Phi \, \mathrm{d}x = 0. \tag{2.26}$$

Eventually, to fully define the solution of the model, the unknown $Q(t,x)$ needs to be identified. This unknown acts as a Lagrange multiplier to ensure the constraint (2.25). To identify it, we need to ensure that the mapping $\Psi : \left(L^2(\mathbb{R})\right)^{d_Q} \mapsto (\ker(\mathscr{L}))^\perp$ is an isomorphism. In this case, we have

$$Q = \Psi^{-1}\left(\partial_t U + A(U)\,\partial_x U\right).$$

The orthogonality relation (2.26) allows us to extend the entropy conservation law identified by the relation (2.24) to the projected hyperbolic model (2.23).

Proposition 2.8 *For sufficiently regular solutions of* (2.23)*, the L^2-norm of the unknown is preserved, i.e.*

$$\partial_t \|U\|_2^2 = 0.$$

Some may wonder about a local formulation of entropy conservation Proposition 2.8. It is worth noting that the flux of entropy is not solely given by the hyperbolic part $G(U)$. There could also be a contribution from the dispersive source term $\mathscr{G}(U,Q)$, such that $\partial_x \mathscr{G}(U,Q) = U \cdot \Psi$. More precisely, for sufficiently regular solutions, we can write

$$\partial_t \left(\frac{1}{2} |U|^2 \right) + \partial_x \left(G(U) + \mathscr{G}(U,Q) \right) = 0 \tag{2.27}$$

with $|U|^2 = U \cdot U$.

Eventually, it is worth noting that the dual space $(\ker(\mathscr{L}))^{\perp}$ is, by definition, a linear subspace of $\left(L^2(\mathbb{R})\right)^{d_U}$. Hence, there exists a mapping $\mathscr{R} : \left(L^2(\mathbb{R})\right)^{d_U} \mapsto \left(L^2(\mathbb{R})\right)^{d_U - d_Q}$ such that $(\ker(\mathscr{L}))^{\perp} = \ker(\mathscr{R})$. By applying this operator to (2.23), the right-hand side vanishes, and we obtain an equation with only the state variable U as the unknown.

$$\partial_t \mathscr{R}(U) + \mathscr{R}(A(U)\,\partial_x U) = 0 \tag{2.28}$$

Using the constraint (2.25), the equation can be reduced to a small number of unknowns $d_U - d_Q$. It is often in this form that dispersive models are formulated and studied.

To summarize, the projected hyperbolic model is fully defined by the state variable U, the hyperbolic matrix $A(U)$ and the constraint $\mathscr{L}(U)$.

2.2.1.2 Link with the incompressible Euler model

The projection structure discussed in the previous section draws strong inspiration from the framework of incompressible flows. This observation allows us to leverage existing results from incompressible flow theory, such as those found in [Lio13], when studying the projected hyperbolic model (2.23). However, models like (2.13) have their own established theories and analyses, such as those detailed in [Lan13], which are likely more tailored to their specific characteristics. Despite this, numerical methods for solving dispersive models remain relatively underdeveloped. Therefore, it is pertinent to draw insights from the well-established methodologies within incompressible flow frameworks, as seen in works like [RT06, Cho68, Tem68].

To illustrate the connection between the projected hyperbolic model and incompressible flow, we can draw an analogy with the incompressible Euler equations discussed in §2.1.1. The projected hyperbolic model (2.23) resembles the time evolution of velocity (2.1), where the hyperbolic operator $A(U)$ plays a role akin to the advection operator $u \cdot \nabla u$ in (2.1), and the dispersive source term Ψ acts similarly to the pressure gradient ∇p in (2.1). The constraint (2.25) is analogous to the divergence-free condition (2.2). Furthermore, the L^2-orthogonal Helmholtz decomposition [Hel58] plays a crucial role in incompressible flows and shares similarities with the orthogonal constraint (2.26), which implies $L^2 = \ker(\mathscr{L}) \oplus \ker(\mathscr{R})$. Additionally, the operator $\mathscr{R}$ acts analogously to the curl operator, since $\mathscr{R}(\Psi) = 0$, much like $\operatorname{curl}(\nabla p) = 0$. Lastly, the reduced form of equation (2.28) can be likened to the vorticity equation of the incompressible fluid mechanics, see [Lio13, (4.6)].

The inherent similarity in projection structures between dispersive models and incompressible flows is not unexpected, given that many dispersive models approximate water wave models (discussed in §2.1.1), which inherently satisfy an incompressibility constraint. Maintaining this structural analogy during modeling can be viewed as advantageous.

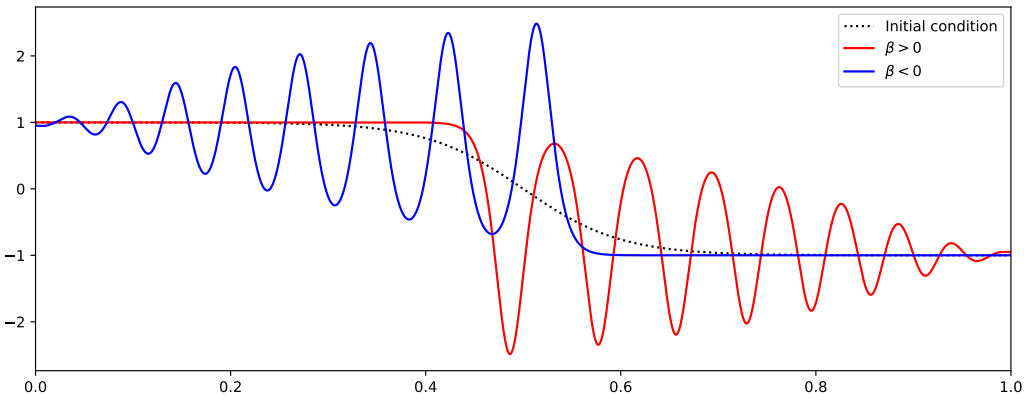

Figure 2.6: §2.2.1.3 | Simulations of the BBM model (2.33) with positive and negative transport velocity using the numerical strategy presented in §2.3.1.2.

2.2.1.3 The BBM model and its generalizations

To illustrate the presentation, we will provide some examples. Let's begin with a straightforward case where $U = (u, w)^\intercal$ and

$$\mathscr{L}(U) = w + \alpha \partial_x u \tag{2.29}$$

with $\alpha \in \mathbb{R}$. We will denote this constraint and the corresponding linear subspace in the context of the BBM model, since, as we will demonstrate later, it aligns well with the well-known Benjamin-Bona-Mahony (BBM) model [BBM97]. Let's begin by identifying the dual space $(\ker(\mathscr{L}))^\perp$, for any $V = (v_0, v_1)^\intercal \in \ker(\mathscr{L})$ and any $\Phi = (\phi_0, \phi_1) \in (\ker(\mathscr{L}))^\perp$, we have

$$0 = \langle V, \Phi \rangle = \int_{\mathbb{R}} (v_0\phi_0 + v_1\phi_1)\,\mathrm{d}x = \int_{\mathbb{R}} (v_0\phi_0 - \alpha\phi_1\partial_x v_0)\,\mathrm{d}x = \int_{\mathbb{R}} v_0\,(\phi_0 + \alpha\partial_x\phi_1)\,\mathrm{d}x.$$

This relation must be satisfied for any $v_0 \in L^2(\mathbb{R})$, hence, we conclude that $(\ker(\mathscr{L}))^\perp = \ker(\mathscr{R})$ with

$$\mathscr{R}(\mathbf{V}) = \mathbf{v}_0 + \alpha\partial_x \mathbf{v}_1 \qquad \text{for any} \qquad \mathbf{V} = (\mathbf{v}_0, \mathbf{v}_1)^\intercal \in \left(L^2(\mathbb{R})\right)^2. \tag{2.30}$$

Now, let us estimate the contribution of the dispersive operator to the flux of energy. We can express

$$V \cdot \Phi = v_0\,(\phi_0 + \alpha\partial_x\phi_1) - \partial_x\,(\alpha\phi_1 v_0)\,.$$

We conclude that $\mathscr{G}(U, Q) = \alpha\phi_1 v_0$.

Now, let us consider the following hyperbolic operator

$$A(U) = \begin{pmatrix} P_0(u) & 0 \\ 0 & P_1(w) \end{pmatrix} + \begin{pmatrix} wg(u,w) & -wf(u,w) \\ -ug(u,w) & uf(u,w) \end{pmatrix} \tag{2.31}$$

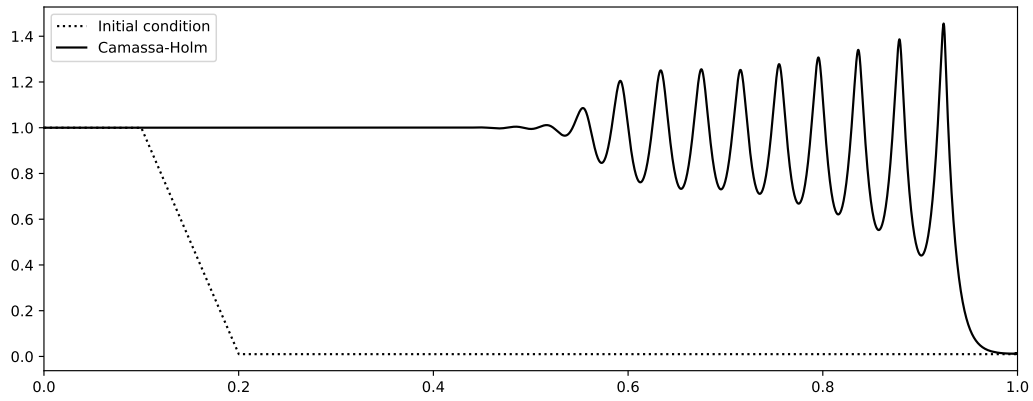

Figure 2.7: §2.2.1.3 | Simulation of the Camassa-Holm model (2.34) using the numerical strategy presented in §2.3.1.2 with non-conservative product §2.3.1.3.

where $P_0(x) = \sum_{i=0}^{n_0} a_{0,i} x^i$ and $P_1(x) = \sum_{i=0}^{n_1} a_{1,i} x^i$ are two polynomials with coefficients in $\mathbb{R}$ and $f : \mathbb{R}^2 \mapsto \mathbb{R}$ and $g : \mathbb{R}^2 \mapsto \mathbb{R}$ are arbitrary nonsingular functions. It is clear that the matrix satisfies the entropy-flux relation (2.24) with the flux $G(U) = \sum_{i=0}^{n_0} \frac{a_{0,i}}{i+1} u^{i+1} + \sum_{i=0}^{n_1} \frac{a_{1,i}}{i+1} w^{i+1}$. To ensure that the operator (2.31) is hyperbolic, we focus on the case $g(x,y) f(x,y) = 0$. In such a case, the matrix is triangular and trivially has real eigenvalues, which we assume to be distinct.

To obtain the reduced form of this model, we apply the operator $\mathscr{R}$ to (2.23), resulting in

$$\begin{aligned} 0 = \partial_t (u + \alpha \partial_x w) + (P_0(u) + w g(u,w)) \partial_x u - w f(u,w) \partial_x w \\ + \alpha \partial_x (-u g(u,w) \partial_x u + (P_1(w) + u f(u,w)) \partial_x w) \end{aligned}$$

then, using the constraint $\mathscr{L}(U) = 0$, we obtain

$$\begin{aligned} \left(\mathrm{I} - \alpha^2 \partial_x^2\right) \partial_t u + (P_0(u) - \alpha g(u, -\alpha \partial_x u) \partial_x u) \partial_x u \\ - \alpha \partial_x (u g(u, -\alpha \partial_x u) \partial_x u) \\ - \alpha^2 f(u, -\alpha \partial_x u) \partial_x u \partial_x^2 u \\ - \alpha^2 \partial_x \left((P_1(-\alpha \partial_x u) + u f(u, -\alpha \partial_x u)) \partial_x^2 u \right) = 0. \end{aligned} \tag{2.32}$$

Corollary 1 *For any polynomial functions $P_0(x)$ and $P_1(x)$, and any functions $f(x,y)$ and $g(x,y)$, the sufficiently regular solutions of (2.23) with the constraint (2.29) and the hyperbolic operator (2.31) preserve the L^2-norm of the unknown.*

Let us examine some specific parameter settings:

- Let $f = g = 0$, $P_0(x) = x$ and $P_1(x) = \frac{\beta}{\alpha^2}$. The model (2.32) reduces to the classical form of the Burgers-KdV-BBM model [BBM97]

$$\left(1 - \alpha^2 \partial_x^2\right) \partial_t u + u \partial_x u - \beta \partial_x^3 u = 0. \tag{2.33}$$

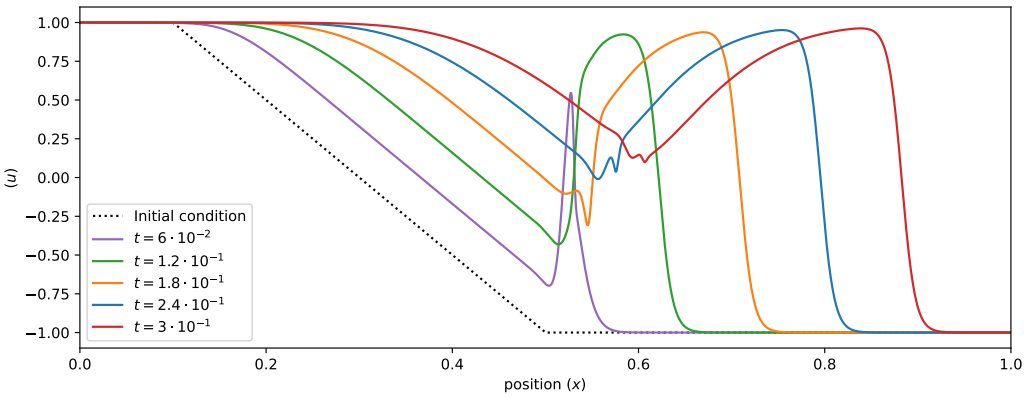

Figure 2.8: §2.2.1.3 | Simulation of the potential parabolic BBM model (2.35) using the numerical strategy presented in §2.3.1.2 with non-conservative product §2.3.1.3.

The traditional Burgers-BBM model is recovered when $P_1(x) = 0$. The KdV model lies outside the scope of the projected hyperbolic model (2.23), as setting $\alpha = 0$ only results in recovering the hyperbolic Burgers model. Figure 2.6 shows the results of the BBM model using the numerical strategy presented in §2.3.1.2. For explanations on the dispersive oscillations, see [EH16].

- With $P_0(x) = 3x + 2\kappa$ where $\kappa \in \mathbb{R}$, $P_1(x) = 0$, $f(x,y) = \frac{\gamma}{\alpha^2}$, and $g(x,y) = 0$, the model (2.32) reduces to the classical form of the Camassa-Holm model [CH93]

$$\left(1 - \alpha^2 \partial_x^2\right) \partial_t u + (3u + 2\kappa)\, \partial_x u - 2\gamma \partial_x u \partial_x^2 u - \gamma u \partial_x^3 u = 0. \tag{2.34}$$

  Figure 2.7 shows the results of the Camassa-Holm model.

- Let $P_0(x) = 1$, $P_1(x) = \frac{\beta}{\alpha^2}$, $f(x,y) = 0$ and $g(x,y) = \frac{\gamma}{\alpha}$. In this case, the model (2.32) reduces to the potential parabolic BBM model [AV18]

$$\left(1 - \alpha^2 \partial_x^2\right) \partial_t u + \partial_x u - 2\gamma |\partial_x u|^2 - \gamma u \partial_x^2 u - \beta \partial_x^3 u = 0. \tag{2.35}$$

  Figure 2.8 shows the results of the potential parabolic BBM.

2.2.1.4 The *abcd*-model and its modified version

Before concluding this section, let us introduce a slightly more complex model to illustrate the versatility of the projection structure. We will adjust the notation in this part to align with well-known models. Let us consider a system with four state variables $U = (\eta, u, \widetilde{\eta}, \widetilde{u})^\intercal$ with two constraints, i.e.

$$\mathscr{L}(U) = \begin{pmatrix} \widetilde{\eta} + \sqrt{b}\partial_x \eta \\ \widetilde{u} + \sqrt{d}\partial_x u \end{pmatrix} \tag{2.36}$$

with $b>0$ and $d>0$. We consider the following matrix

$$A(U)=\begin{pmatrix} u & 1+\alpha\eta & 0 & 0\\ 1 & u & 0 & 0\\ 0 & 0 & 0 & -\frac{a}{\sqrt{bd}}\\ 0 & 0 & -\frac{c}{\sqrt{bd}} & 0 \end{pmatrix} \tag{2.37}$$

where $(\alpha,a,c)\in\mathbb{R}^3$. Proceeding similarly to the BBM constraint (2.29), we find that $\ker(\mathscr{L})^{\perp}=\ker(\mathscr{R})$ with

$$\mathscr{R}(\mathbf{V})=\begin{pmatrix} \mathbf{v}_0+\sqrt{b}\partial_x\mathbf{v}_2\\ \mathbf{v}_1+\sqrt{d}\partial_x\mathbf{v}_3 \end{pmatrix}.$$

Applying this operator to (2.23) and using $\mathscr{L}(U)=0$, we obtain first

$$\begin{aligned} 0&=\partial_t\left(\eta+\sqrt{b}\partial_x\widetilde{\eta}\right)+u\partial_x\eta+(1+\alpha\eta)\partial_x u-\frac{a}{\sqrt{d}}\partial_x^2\widetilde{u}\\ &=\left(1-b\partial_x^2\right)\partial_t\eta+u\partial_x\eta+(1+\alpha\eta)\partial_x u+a\partial_x^3 u \end{aligned}$$

and secondly

$$\begin{aligned} 0&=\partial_t\left(u+\sqrt{d}\partial_x\widetilde{u}\right)+\partial_x\eta+u\partial_x u-\frac{c}{\sqrt{b}}\partial_x^2\widetilde{\eta}\\ &=\left(1-d\partial_x^2\right)\partial_t u+\partial_x\eta+u\partial_x u+c\partial_x^3\eta. \end{aligned}$$

This model with $\alpha=1$ is known as the *abcd*-model [BCS02]. However, this model does not fit exactly into the structure presented in Section 2. More precisely, assuming $\eta>-\frac{D}{\alpha}$ and $ac\geq 0$, the matrix $A(U)$ has four real eigenvalues

$$u-\sqrt{g(D+\alpha\eta)},\qquad -\sqrt{\frac{ac}{bd}},\qquad \sqrt{\frac{ac}{bd}},\qquad u+\sqrt{g(D+\alpha\eta)}.$$

Unfortunately, in general, it does not satisfy the entropy-flux condition (2.24), except in the particular case where $\alpha=\frac{1}{2}$ and $a=c$. We get

$$U^{\mathsf{T}}\cdot A(U)=\nabla_U\left(\left(\eta+\frac{\eta^2}{2}+\frac{u^2}{3}\right)u-\frac{a}{\sqrt{bd}}\widetilde{\eta}\widetilde{u}\right).$$

Corollary 2 *Let $\alpha=\frac{1}{2}$. For any $b>0$, $d>0$ and $a=c\in\mathbb{R}$, the sufficiently regular solutions of (2.23) with the constraint (2.36) and the hyperbolic operator (2.37) preserve the L^2-norm of the unknown. (2.27).*

2.2.2 Projected hyperbolic models of Boussinesq-type

2.2.2.1 General description

The main limitation of the framework described in §2.2.1.1 is that it restricts itself to L^2-stable equations with linear constraint. Although it can be extended easily to any Hilbert space, the models described in §2.1 do not fit into this framework. It is important to note that in these models, the dispersive operator acts only on unknowns representing velocity, not all unknowns, and the constraint is linear with respect to the velocity unknowns. Given

this observation, we divide the variables of the system into potential unknowns $H(t,x) : \mathbb{R}_+ \times \mathbb{R}^d \mapsto \mathbb{R}^{d_H}$ and kinetic unknowns $U(t,x) : \mathbb{R}_+ \times \mathbb{R}^d \mapsto \mathbb{R}^{d_U}$. The advantage of this separation is that the potential unknowns H are treated as parameters in the projection definition. In the subsequent sections, we expand the definition of projected hyperbolic models to incorporate the potential unknown H as a parameter. The class of models that we will refer to as the projected hyperbolic models of Boussinesq-type can be formulated as

$$\partial_t \begin{pmatrix} H \\ U \end{pmatrix} + \sum_{i=1}^{d} A_i(H,U)\, \partial_{x_i} \begin{pmatrix} H \\ U \end{pmatrix} = - \begin{pmatrix} 0 \\ \Psi_H(Q) \end{pmatrix} \tag{2.38}$$

$$\text{with} \quad A_i = \begin{pmatrix} A_i^{HH} & A_i^{HU} \\ A_i^{UH} & A_i^{UU} \end{pmatrix} \quad \text{and} \quad Q(t,x) : \mathbb{R}_+ \times \mathbb{R} \mapsto \mathbb{R}^{d_Q} \quad \text{with} \quad d_Q < d_U.$$

1 As in §2.2.1.1, the squared matrix $A_i(H,U) : \mathbb{R}^{d_H} \times \mathbb{R}^{d_U} \mapsto M_{d_H+d_U}(\mathbb{R})$ is assumed to have real eigenvalues, ensuring that, excluding the dispersive source term Ψ_H, the model remains hyperbolic. We assume the existence of an entropy $E(H,U) = \mathscr{P}(H) + \mathscr{K}_H(U)$, which can be decomposed into a potential part $\mathscr{P}(H)$, dependent only on the potential unknown H, and a kinetic part $\mathscr{K}_H(U) = \nu(H)\frac{|U|^2}{2}$, with the weight function of the potential unknown $\nu(H) : \mathbb{R}^{d_H} \mapsto \mathbb{R}_+$. Additionally, there exists a flux $G(H,U) : \mathbb{R}^{d_H} \times \mathbb{R}^{d_U} \mapsto \mathbb{R}^d$ that satisfies the entropy-flux relation

$$(\nabla_{H,U} E)^\intercal \cdot A_i = (\nabla_{H,U} G_i)^\intercal \tag{2.39}$$

where G_i are the component of G. This form of entropy is common in many problems, especially in physics. It can be directly linked to a Hamiltonian mechanics formalism by considering the Lagrangian $L(H,U) = \mathscr{K}_H(U) - \mathscr{P}(H)$. The dispersive source term $\Psi_H(Q)$ in (2.38) is not explicitly defined, but it is constructed to ensure that the state variable satisfies the constraint

$$\mathscr{L}_H(U) = 0 \tag{2.40}$$

with a given operator $\mathscr{L}_H : \left(L^2(\mathbb{R})\right)^{d_U} \mapsto \left(L^2(\mathbb{R})\right)^{d_Q}$, which is linear with respect to the kinetic unknown U and parameterized by the potential unknown H. In other words, the dispersive source term Ψ_H acts in such a way that the state variable U lies in the kernel of $\mathscr{L}_H$.

As for the projected hyperbolic models of BBM-type, the dispersive source term is assumed to belong to the dual space $(\ker(\mathscr{L}_H))^\perp$ with respect to $\langle \bullet, \bullet \rangle_H$, the $L^2(\widetilde{\nu}(H))$ inner product. That is, for any $V \in \ker(\mathscr{L}_H)$ and any $\Phi \in (\ker(\mathscr{L}_H))^\perp$, we have

$$\langle V, \Phi \rangle_H = \int_{\mathbb{R}} V \cdot \Phi\, \widetilde{\nu}(H)\, \mathrm{d}x = 0. \tag{2.41}$$

Note that, in order to recover certain models from the literature, see §2.2.2.3, we do not assume that the weight $\widetilde{\nu}$ used in the inner product is the same as the weight ν associated with the kinetic energy. However, the orthogonality relation (2.41) allows us to extend the entropy conservation law, as identified by relation (2.39), to the projected hyperbolic model (2.38) only when the weights are identical.

Proposition 2.9 *Assuming that the inner product $\widetilde{\nu}(H)$ is associated with the kinetic energy, i.e., $\widetilde{\nu}(H) = \nu(H)$, the sufficiently regular solutions of (2.38) satisfy the following energy conservation law*

$$\partial_t \int_{\mathbb{R}} E(H,U)\,\mathrm{d}x = 0.$$

It is worth noting that the flux of entropy is not solely the flux of the hyperbolic part, $G(H,U)$. There may also be a contribution from the dispersive source term $\mathscr{G}(H,U,Q)$ such that $\partial_x \mathscr{G}(H,U,Q) = \nu(H)U \cdot \Psi$. More precisely, for sufficiently regular solutions, we can express it as follows

$$\partial_t E(H,U) + \nabla \cdot (G(H,U) + \mathscr{G}(H,U,Q)) = 0.$$

Additionally, the Lagrange multiplier $Q(t,x)$ is selected so that the mapping $\Psi_H : \left(L^2(\mathbb{R})\right)^{d_Q} \mapsto (\ker(\mathscr{L}_H))^{\perp}$ is an isomorphism. This multiplier is defined by

$$Q = \Psi_H^{-1}\left(\partial_t U + \sum_{i=1}^{d}\left(A_i^{UH}\partial_{x_i}H + A_i^{UU}\partial_{x_i}U\right)\right).$$

Eventually, it is important to note that the dual space $(\ker(\mathscr{L}_H))^{\perp}$ is, by definition, a linear subspace of $\left(L^2(\mathbb{R})\right)^{d_U}$. Hence, there exists a mapping $\mathscr{R}_H : \left(L^2(\mathbb{R})\right)^{d_U} \mapsto \left(L^2(\mathbb{R})\right)^{d_U - d_Q}$ such that $\ker(\mathscr{R}_H) = (\ker(\mathscr{L}_H))^{\perp}$. Applying this operator to the equations of U in (2.38), the right-hand side vanishes, and we obtain an equation with only the state variable U as the unknown.

$$\mathscr{R}_H(\partial_t U) + \sum_{i=1}^{d}\left(\mathscr{R}_H\left(A_i^{UH}\partial_{x_i}H\right) + \mathscr{R}_H\left(A_i^{UU}\partial_{x_i}U\right)\right) = 0 \tag{2.42}$$

Utilizing the constraint (2.40), the equation can be reduced to a small number of unknowns, specifically $d_U - d_Q$. It is typically in this form that dispersive models are known.

In summary, the projected hyperbolic model of Boussinesq-type is fully characterized by the potential unknown H, the kinetic unknown U, the hyperbolic matrix A_i, and the constraint $\mathscr{L}_H(U)$ and the weight of the inner product $\widetilde{\nu}(H)$. A large class of dispersive models can be written in this way, in particular those that address the problem of water waves, see §2.1. However, it is clear that this structure is not common to all dispersive models. In particular, it is not satisfied by the Euler-Korteweg model [BGDD07, NV14], or by the Nwogu model [Oke93].

2.2.2.2 The Green-Naghdi model

In this section, we elaborate on the connection between the projected hyperbolic equations (2.13) and one of the classical forms of the Green-Naghdi model [GN76]. The potential unknown is represented as $H = (h,B)^{\mathsf{T}}$, the kinetic unknown is $U = \left((\overline{u}_i)_{1\le i\le d}, \overline{w}, \widetilde{w}\right)^{\mathsf{T}}$, and

the hyperbolic matrices are

$$A_1 = \begin{pmatrix} \overline{u}_1 & 0 & h & 0 & 0 & 0 \\ 0 & 0 & 0 & 0 & 0 & 0 \\ g & g & \overline{u}_1 & 0 & 0 & 0 \\ 0 & 0 & 0 & \overline{u}_1 & 0 & 0 \\ 0 & 0 & 0 & 0 & \overline{u}_1 & 0 \\ 0 & 0 & 0 & 0 & 0 & \overline{u}_1 \end{pmatrix} \quad \text{and} \quad A_2 = \begin{pmatrix} \overline{u}_2 & 0 & 0 & h & 0 & 0 \\ 0 & 0 & 0 & 0 & 0 & 0 \\ 0 & 0 & \overline{u}_2 & 0 & 0 & 0 \\ g & g & 0 & \overline{u}_2 & 0 & 0 \\ 0 & 0 & 0 & 0 & \overline{u}_2 & 0 \\ 0 & 0 & 0 & 0 & 0 & \overline{u}_2 \end{pmatrix}$$

which satisfies the entropy-flux relation (2.39) with the entropy given in Proposition 2.5. We deduce the weight $\nu(H) = h$, and we set $\widetilde{\nu}(H) = \nu(H)$. The constraint reads $\mathscr{L}_H(U) = \mathscr{L}[h,B](U)$, with

$$\mathscr{L}[\mathbf{h},\mathbf{B}](V) = \begin{pmatrix} v_1 - \sqrt{3}v_2 - \begin{pmatrix} v_0 \\ v_1 \end{pmatrix} \cdot \nabla \mathbf{B} \\ v_2 + \dfrac{\mathbf{h}}{2\sqrt{3}} \nabla \cdot \begin{pmatrix} v_0 \\ v_1 \end{pmatrix} \end{pmatrix}. \tag{2.43}$$

Using the orthogonality relation (2.41), we conclude that the dual space $\ker(\mathscr{R}_H)$ with $\mathscr{R}_H(\Phi) = \mathscr{R}[h,B](\Phi)$ and

$$\mathscr{R}[\mathbf{h},\mathbf{B}](\Phi) = \mathbf{h} \begin{pmatrix} \phi_0 \\ \phi_1 \end{pmatrix} + \nabla \left(\frac{\mathbf{h}^2}{2} \left(\phi_2 + \frac{\phi_3}{\sqrt{3}} \right) \right) + \mathbf{h}\phi_2 \nabla \mathbf{B}. \tag{2.44}$$

Applying this operator to the equation for U in (2.38), we obtain (2.42). Letting $\overline{u} = (\overline{u}_1, \overline{u}_2)^\mathsf{T}$ and using (2.40), we get

$$\begin{aligned} \mathscr{R}[\mathbf{h},\mathbf{B}](\partial_t U) &= \mathbf{h} \Big((1 + \mathscr{T}[\mathbf{h},\mathbf{B}]) \partial_t \overline{u} + \widetilde{Q}[\mathbf{h},\mathbf{B}](\partial_t \mathbf{h} \nabla \cdot \overline{u}) \Big) \\ \sum_{i=1}^{d} \mathscr{R}[\mathbf{h},\mathbf{B}] \left(A_i^{UH} \partial_{x_i} H \right) &= g\mathbf{h} \nabla (h + B) \\ \sum_{i=1}^{d} \mathscr{R}[\mathbf{h},\mathbf{B}] \left(A_i^{UU} \partial_{x_i} U \right) &= \mathbf{h} \Big(\overline{u} \cdot \nabla \overline{u} + \mathscr{Q}[\mathbf{h}](\overline{u}) + \mathscr{Q}_{\mathbf{B}}[\mathbf{h}](\overline{u}) + \widetilde{Q}[\mathbf{h},\mathbf{B}](\nabla \cdot (\mathbf{h}\overline{u}) \nabla \cdot \overline{u}) \Big) \end{aligned}$$

with the operators

$$\begin{aligned} \mathscr{T}[\mathbf{h},\mathbf{B}](V) &= \alpha_{\mathbf{B}} V + \frac{1}{\mathbf{h}} (\nabla(\gamma_{\mathbf{h},\mathbf{B}} \cdot V) - \gamma_{\mathbf{h},\mathbf{B}} \nabla \cdot V) - \frac{1}{\mathbf{h}} \nabla (\omega_{\mathbf{h}} \nabla \cdot V) \\ \mathscr{Q}[\mathbf{h}](V) &= -\frac{1}{\mathbf{h}} \nabla \left(\frac{\mathbf{h}^3}{3} \left(V \cdot \nabla (\nabla \cdot V) - |\nabla \cdot V|^2 \right) \right) \\ \mathscr{Q}_{\mathbf{B}}[\mathbf{h}](V) &= \frac{1}{\mathbf{h}} \left(\nabla \left(\frac{\mathbf{h}^2}{2} (V \cdot \nabla)^2 \mathbf{B} \right) - \frac{\mathbf{h}^2}{2} \left(V \cdot \nabla (\nabla \cdot V) - |\nabla \cdot V|^2 \right) \nabla \mathbf{B} \right) + \left((V \cdot \nabla)^2 \mathbf{B} \right) \nabla \mathbf{B} \\ \widetilde{Q}[\mathbf{h},\mathbf{B}](v) &= -\frac{1}{3\mathbf{h}} \nabla \left(\mathbf{h}^2 v \right) - \frac{v}{2} \nabla \mathbf{B}. \end{aligned}$$

$$\text{with} \quad \alpha_{\mathbf{B}} = \nabla \mathbf{B} \otimes \nabla \mathbf{B}, \quad \gamma_{\mathbf{h},\mathbf{B}} = \frac{\mathbf{h}^2}{2} \nabla \mathbf{B} \quad \text{and} \quad \omega_{\mathbf{h}} = \frac{\mathbf{h}^3}{3}. \tag{2.45}$$

Since $\widetilde{Q}[\mathbf{h},\mathbf{B}](v)$ is linear with respect to V, and using mass conservation, we conclude $\widetilde{Q}[\mathbf{h},\mathbf{B}](\partial_t h \nabla \cdot \overline{u}) + \widetilde{Q}[\mathbf{h},\mathbf{B}](\nabla \cdot (h\overline{u}) \nabla \cdot \overline{u}) = 0$. Assuming h is non-zero, we recover the form of the Green-Naghdi model [Lan13, (5.11)], i.e.

$$(1 + \mathscr{T}[h,B]) \partial_t \overline{u} + g \nabla (h + B) + \overline{u} \cdot \nabla \overline{u} + \mathscr{Q}[h](\overline{u}) + \mathscr{Q}_B[h](\overline{u}) = 0.$$

2.2.2.3 The Peregrine model

In the regime of weakly non-linear waves, where $h(t,x) = D(x) + O(\varepsilon)$ with $\varepsilon \ll 1$, it can be advantageous to replace the water depth $h(t,x)$ by the mean depth $D(x)$ during the projection step. This approach helps to reduce the computational cost of simulations. In the framework of projected hyperbolic models, this substitution is achieved by imposing the constraint $\mathscr{L}_H(U) = \mathscr{L}[D,B](U)$, with the definition (2.43), and setting the weight of the inner product $\widetilde{\nu}(H) = \nu(D)$. It is important to note that the inner product is no longer associated with kinetic energy. Consequently, Proposition 2.9 cannot be applied, and in practice, the model does not conserve energy. Nevertheless, the dual space of $\ker(\mathscr{L}_H)$ is $\ker(\mathscr{R}_H)$, where $\mathscr{R}_H(U) = \mathscr{R}[D,B](U)$, as defined by (2.44). From (2.42) and assuming D is non-zero, we obtain

$$\begin{aligned}(1+\mathscr{T}[D,B])\,\partial_t\overline{u} + g\nabla(h+B) + \overline{u}\cdot\nabla\overline{u} \\ + \mathscr{Q}[D](\overline{u}) + \mathscr{Q}_B[D](\overline{u}) + \widetilde{Q}[D,B](\nabla\cdot(D\overline{u})\nabla\cdot\overline{u}) = 0.\end{aligned} \tag{2.46}$$

It is not the classical Boussinesq-Peregrine model [Per67], which is given by

$$(1+\mathscr{T}[D,B])\,\partial_t\overline{u} + g\nabla(h+B) + \overline{u}\cdot\nabla\overline{u} = 0. \tag{2.47}$$

However, the Boussinesq-Peregrine model (2.47) can be reformulated in the projected hyperbolic form by omitting the advection of the vertical velocity, i.e., utilizing the hyperbolic operator

$$A_1 = \begin{pmatrix} \overline{u}_1 & 0 & h & 0 & 0 & 0 \\ 0 & 0 & 0 & 0 & 0 & 0 \\ g & g & \overline{u}_1 & 0 & 0 & 0 \\ 0 & 0 & 0 & \overline{u}_1 & 0 & 0 \\ 0 & 0 & 0 & 0 & 0 & 0 \\ 0 & 0 & 0 & 0 & 0 & 0 \end{pmatrix} \quad \text{and} \quad A_2 = \begin{pmatrix} \overline{u}_2 & 0 & 0 & h & 0 & 0 \\ 0 & 0 & 0 & 0 & 0 & 0 \\ 0 & 0 & \overline{u}_2 & 0 & 0 & 0 \\ g & g & 0 & \overline{u}_2 & 0 & 0 \\ 0 & 0 & 0 & 0 & 0 & 0 \\ 0 & 0 & 0 & 0 & 0 & 0 \end{pmatrix}. \tag{2.48}$$

This operator simply omits the advection terms involving the vertical velocities $\widetilde{w}$ and $\widetilde{\widetilde{w}}$, which renders the model non-Galilean invariant even over a flat bottom. The same simplification has been employed in fully nonlinear models like the Yamazaki model [YKC09], which can be formulated as a projected hyperbolic model using the hyperbolic operator (2.48), the constraint $\mathscr{L}_H(U) = \mathscr{L}[h,B](U)$ defined by (2.43) and the weight $\widetilde{\nu}(H) = \nu(H)$. It is important to note that both models (2.46) and (2.47) are not well-posed when the mean depth $D(x)$ becomes negative, thus they are unable to handle dry areas.

2.2.2.4 High order dispersive models

Now, we propose to extend the Green-Naghdi model by introducing additional unknowns and constraints to improve its dispersion relation. For simplicity, we focus on the 1D case with a flat bottom.

We define the projected hyperbolic model with the potential unknown $H = h$, and the kinetic unknown $U = \left(\overline{u}, (\overline{w}_i)_{1\leq i\leq M}\right)$ with $M \geq 1$. Here, $\overline{u}$ represents the horizontal velocity

and $(\overline{w}_i)_{1\leq i\leq M}$ denote additional velocities. The hyperbolic operator is derived from the shallow water model (2.6) with passive transport of these additional velocities. In other words,

$$\begin{pmatrix} \overline{u} & h & 0 \\ g & \overline{u} & 0 \\ 0 & 0 & \overline{u}\mathrm{I}_M \end{pmatrix}$$

and the constraint

$$\mathscr{L}_H(U) = \left(\overline{w}_i - \alpha_i (-h)^i \partial_x^i \overline{u}\right)_{1\leq i\leq M}. \tag{2.49}$$

As a consequence of Proposition 2.9, the model preserved an entropy.

Proposition 2.10 *For sufficiently smooth solutions of the high order dispersive model, the following mechanic energy conservation law holds*

$$\partial_t(\mathscr{P}+\mathscr{K}) + \partial_x\left(\left(g(B+h)+\overline{q}+\frac{|\overline{u}|^2+\sum_{i=1}^M \overline{w}_i^2}{2}\right)h\overline{u}\right) = 0.$$

with $\mathscr{P} = gh\left(B+\frac{h}{2}\right)$ *and* $\mathscr{K} = \frac{h}{2}\left(|\overline{u}|^2+\sum_{i=1}^M \overline{w}_i^2\right)$.

Now, computing the dispersion relation of the model (2.49), we obtain

$$v_p^{\mathrm{HO}(M)\mathrm{GN}} = \sqrt{\frac{1}{1+\sum_{i=1}^M \alpha_i^2 |kD|^{2i}}}\sqrt{gD} \tag{2.50}$$

By selecting the parameters α_i to match the Taylor expansion of $\frac{x}{\tanh(x)}$, we construct a high-order dispersive model. It is important to note that the Taylor expansion of $\frac{x}{\tanh(x)}$ has a finite radius of convergence, see Figure 2.5. In the case $M=2$, following similar calculations as those for the Green-Naghdi model in Section §2.2.2.2, we derive the high-order dispersive fully nonlinear model described in [Mat15, KZI18] or the high-order dispersive weakly nonlinear model described in [GK96, MS98] with the simplification presented in §2.2.2.3.

2.2.3 Boundary conditions of projected hyperbolic models

The current section addresses a remark on the boundary conditions for projected hyperbolic models. The issue of boundary conditions in dispersive models is complex and has been explored in only a few studies [Xue08, ADM09, Aud12, BELV16, BNS17, BMGN18, LM18, KN20, LW20] This remark stems from the necessity to maintain the projection structure onto a linear subspace when dealing with a bounded domain Ω. This requirement parallels the literature on boundary conditions for incompressible flow equations [AKM89, GHR12, KOS23]. We propose to focus on the auxiliary projection problem of the projected hyperbolic model of BBM-type. Specifically, for a function $U^* \in \left(L^2(\Omega)\right)^2$, we seek a function $U \in \ker(\mathscr{L})$ (defined in (2.29)) and $\Psi \in (\ker(\mathscr{L}))^\perp$ such that

$$U^* = U + \delta_t \Psi \tag{2.51}$$

For a given $\delta_t > 0$, the orthogonality relation (2.26) is modified for a bounded domain $\Omega = [0,1]$ to

$$0 = \int_0^1 V \cdot \Phi \, \mathrm{d}x = \int_0^1 v_0 \left(\phi_0 + \alpha \partial_x \phi_1\right) \mathrm{d}x - \alpha \left[v_0 \phi_1\right]_0^1$$

We conclude that, in addition to the duality between the kernel of $\mathscr{L}$ and the kernel of $\mathscr{R}$, the orthogonality property necessitates the condition for any $x \in \partial\Omega$

$$v_0(x)\,\phi_1(x) = 0. \tag{2.52}$$

We conclude that to ensure the orthogonality property on a bounded domain (which ensures control over the entropy), we need to decompose the boundary into two open sets (not necessarily connected), Γ_u and Γ_ψ , such that $\partial\Omega = \overline{\Gamma_u} \cup \overline{\Gamma_\psi}$ and $\Gamma_u \cap \Gamma_\psi = \varnothing$. Also we consider the functions $\mathring{u} : \Gamma_u \mapsto \mathbb{R}$ and $\mathring{\psi} : \Gamma_\psi \mapsto \mathbb{R}$, and we seek a solution to the projection problem (2.51) such that $u = \mathring{u}$ on Γ_u and $\psi = \mathring{\psi}$ on Γ_ψ. It is worth noting that for any $V \in \ker(\mathscr{L})$, we have $v_0 \in H^1$, and similarly, for any $\Phi \in \ker(\mathscr{R})$, we have $\phi_1 \in H^1$, ensuring their values at the boundary are well-defined.

2.2.3.1 Homogeneous boundary conditions

Let us first consider the homogeneous case where $\mathring{u} = 0$ and $\mathring{\psi} = 0$. We define the linear subspaces

$$\begin{aligned} \mathbb{A}^0_{\Gamma_u} &= \left\{ V \in \ker(\mathscr{L}) \mid v_{0|_{\Gamma_u}} = 0 \right\} \\ \left(\mathbb{A}^0_{\Gamma_\psi}\right)^\perp &= \left\{ \Phi \in \ker(\mathscr{L}) \mid \phi_{1|_{\Gamma_\psi}} = 0 \right\}. \end{aligned}$$

Thanks to the Hodge decomposition $\left(L^2(\Omega)\right)^2 = \mathbb{A}_{\Gamma_u} \oplus \left(\mathbb{A}_{\Gamma_\psi}\right)^\perp$, we conclude that the orthogonal projection $\Pi_{\mathbb{A}_{\Gamma_u}} : \left(L^2(\Omega)\right)^2 \mapsto \mathbb{A}_{\Gamma_u}$ is well-defined. This projection can be likened to the Leray-Hopf projector of the incompressible fluid mechanics.

2.2.3.2 Inhomogeneous boundary conditions

Now we consider the inhomogeneous boundary conditions. We define the set of admissible functions

$$\begin{aligned} \mathbb{A}_{\Gamma_u} &= \left\{ V \in \ker(\mathscr{L}) \mid v_{0|_{\Gamma_u}} = \mathring{u} \right\} \\ \left(\mathbb{A}_{\Gamma_\psi}\right)^\perp &= \left\{ \Phi \in \ker(\mathscr{L}) \mid \phi_{1|_{\Gamma_\psi}} = \mathring{\psi} \right\}. \end{aligned}$$

It is worth noting that the spaces $\mathbb{A}_{\Gamma_u}$ and $\left(\mathbb{A}_{\Gamma_\psi}\right)^\perp$ are not vector spaces, hence, the projection is not straightforward. However, if we take arbitrary functions $V_r \in \mathbb{A}_{\Gamma_u}$ and $\Phi_r \in \left(\mathbb{A}_{\Gamma_\psi}\right)^\perp$, called reference functions, the difference between the solution and the reference functions lies in the linear subspaces and can be defined by

$$U - V_r = \Pi_{\mathbb{A}_{\Gamma_u}}\left(U^* - V_r - \delta_t \Phi_r\right) \qquad \text{and} \qquad \Psi = \frac{U^* - U}{\delta_t}.$$

It remains to show that the solution U and Ψ is unique and does not depend on the reference functions. Consider two solutions defined from two different reference functions. By linearity, their difference is a solution of the projection problem (2.51) with $V = 0$ and homogeneous boundary conditions. Hence, we conclude that the two solutions agree. It follows that the auxiliary projection problem (2.51) is well-posed.

2.2.3.3 Boundary condition for Boussinesq-type projected models

In [NPT22], we apply the same strategy to the Green-Naghdi model (2.13). We would like to point out that in the case of projected models of the Boussinesq-type, the weight of the inner product $\nu(H)$ can vanish in parts of the computational domain, i.e. the dray areas. The domain where the projection is well-defined is only the support of the weight, $\Omega = \mathrm{supp}(\nu)$. For the Green-Naghdi model, the boundary condition for orthogonality (analogous to (2.52)) applied to the boundary of the wet area reads

$$h\overline{q}\,\overline{u}\cdot\mathfrak{n} = 0. \tag{2.53}$$

Hence, the boundary is decomposed into three open sets $\Gamma_h = \{\partial\Omega \mid h = 0\}$, $\Gamma_u \subset \partial\Omega - \Gamma_h$ and $\Gamma_\psi = \partial\Omega - \Gamma_h - \Gamma_u$. On Γ_h, no conditions can be imposed, on Γ_u the normal velocity $\overline{u}\cdot\mathfrak{n}$ is fixed, and on Γ_ψ the hydrodynamic pressure $h\overline{q}$ is fixed.

The main result, [NPT22, Theorem 6], states that assuming $B \in W^{1,\infty}(\Omega)$, for any $U^* \in \left(L^2(\Omega,h)\right)^{d+2}$, any $\mathring{u} \in H^{-1/2}(\partial\Omega)$, and any $\mathring{\psi} \in H^{1/2}\left(\Gamma_\psi\right)$, there exists a unique solution to the auxiliary projection problem (2.51) with the constraint (2.14).

Additionally, note that the condition (2.52) (BBM-type) or (2.53) (Boussinesq-type) is neither necessary nor sufficient to ensure that the projected hyperbolic model on a bounded domain is well-posed. It is not necessary because it is likely possible to define boundary conditions such that the projected hyperbolic model is well-posed without satisfying a projection structure. It is not sufficient because the condition alone does not ensure that the entire problem, particularly the hyperbolic operator, is well-defined without additional boundary conditions. Specifically, in the case of the Green-Naghdi model (2.13), it is clear that the vertical velocity $\widetilde{w}$ (and the standard deviation $\widetilde{\widetilde{w}}$, which are linked through the constraint) must be defined where the flow is incoming, i.e., $\overline{u}\cdot\mathfrak{n} < 0$. However, the condition (2.52) (or (2.53)) has allowed us to define stable boundary conditions, at least for the time-discrete problem. Boundary conditions used in practice are discussed in the fully discrete framework in §2.3.1.2.

2.3 Structure-preserving schemes for projected hyperbolic models

As presented in §2.2, the projected hyperbolic models have a structure similar to that of incompressible flows. In this section, we adapt numerical strategies initially developed for incompressible flow to our framework. It is conventional to classify numerical schemes for incompressible flows into three main categories. The first category is based on the finite-element method with elements satisfying a discrete counterpart of the Hodge decomposition, known as Raviart-Thomas elements [RT06], which ensures that the solution remains in the linear subspace of admissible functions. Adapting this strategy to our framework is not straightforward.

The second strategy, known as the projection scheme, involves splitting the process into a prediction step, driven by the hyperbolic operator, and a projection step onto the

linear subspace [Cho68]. This strategy is well-suited to our framework, as the numerical resolution of the hyperbolic operator is well established [GR96, LeV02, Bou04, Tor99], as is the projection at the discrete level.

The third strategy, called the pseudo-compressible scheme, also involves splitting the process into a prediction step and a projection step. However, in this case, the projection is approximated using a relaxation operator [Tem68]. Several authors have proposed numerical schemes based on a hyperbolization of the dispersive model [FG17, EDC19, BBBD20, BBD20a, BDE+21, GKPT22, DD22, TGM23, DR24], which can be considered an adaptation of the pseudo-compressible schemes to the dispersive framework.

Other discretisation techniques, still based on a splitting between the hydrostatic part and a hydrodynamic correction, exist in the literature [Bar04, MN08, CLM10, MRN16, BGL17, CFRB19, KR24] but their link with the projection structure is less obvious.

2.3.1 Entropy-satisfying scheme for projected hyperbolic models

2.3.1.1 General description of the projection scheme

We propose a projection scheme for the projected hyperbolic models. A review of projection schemes for incompressible flows can be found in [Gue94, GMS06, BBD+20b]. For simplicity, we consider a projected hyperbolic model (2.38) with a conservative form, i.e., there exists a flux $F(W)$ with $W=(H,U)^\intercal$ such that $\nabla_W F(W)=A(H,U)$. Note that several hyperbolic operators presented in this document cannot be written in a conservative form, such as (2.16), (2.19), and (2.31). These cases require particular attention, which will be considered in §2.3.1.3.

Prediction step: The first step of the scheme is to solve the hyperbolic operator at the discrete level. We use a classical finite volume discretization of the hyperbolic operator, as described in [GR96, LeV02, Bou04, Tor99]. We set

$$W_k^{n*}=W_k^n-\frac{\delta_t^n}{\mathfrak{m}_k}\sum_{f\in\mathbb{F}_k}\mathscr{F}\left(W_k^n,W_{k_f}^n\right)\cdot\mathfrak{n}_f^k\mathfrak{m}_f \tag{2.54}$$

where $\mathscr{F}(W_L,W_R)$ represents an approximate Riemann solver for the flux F, and $W_\star^{n*}$ denotes an approximation of the solution that disregards the dispersive source term. The explicit Godunov schemes exhibit stability subject to a CFL condition given by

$$\delta_t^n\leq\frac{\min\left(\mathfrak{d}_k,\mathfrak{d}_{k_f}\right)}{\lambda\left(W_k^n,W_{k_f}^n\right)} \tag{2.55}$$

where $\mathfrak{d}_k$ the compactness (see §1.2) and $\lambda(W_L,W_R)$ represents an approximation of the largest wave speeds which depends on the chosen Riemann solver. Assuming the hyperbolic scheme (2.54) satisfies the entropy condition implies the existence of a discretization of the integral operator $\langle\bullet\rangle^\delta$ such that

$$\langle E(H_\star^{n*},U_\star^{n*})\rangle^\delta\leq\langle E(H_\star^n,U_\star^n)\rangle^\delta$$

on an unbounded or periodic domain. Specifically, this approach results in a discretization of the inner product associated with the kinetic energy, namely

$$\langle \mathscr{K}_{H_\star}(U_\star)\rangle^\delta = \left\langle \frac{\nu(H_\star)}{2}|U_\star|^2 \right\rangle^\delta =: \langle U_\star, U_\star\rangle^\delta_{\nu(H_\star)}$$

For low-order schemes, the discretization of the integral operator typically takes the form

$$\langle f_\star\rangle^\delta = \sum_{k\in\mathbb{T}} f_k \mathfrak{m}_k \qquad \text{hence} \qquad \langle f_\star, g_\star\rangle^\delta_{\nu_\star} = \sum_{k\in\mathbb{T}} f_k g_k \nu_k \mathfrak{m}_k. \tag{2.56}$$

although other discretizations can be found. Several hyperbolic entropy-satisfying schemes can be found in the literature, such as those described in [God59, HLL83, Sul90, PS01].

Correction step: The next step involves solving the projection problem (2.51) at the discrete level. Firstly, it is important to note that since the dispersive operator does not affect the potential unknown, we have $H_\star^{n+1} = H_\star^{n*}$. We consider a discretization $\mathscr{L}^\delta_{k,H_\star}(V_\star)$ of the constraint $\mathscr{L}_H(V)$. Given that the discrete inner product is already determined by the advection step, we define the discrete operator $\mathscr{R}^\delta_{k,H_\star}(V_\star)$ to preserve the orthogonality property with respect to the discrete inner product $\langle\bullet,\bullet\rangle^\delta_{\nu_\star}$. The discrete projection problem aims to find $U_\star^{n+1} \in \mathbb{R}^{d_U\times N}$ and $\Psi_\star^{n+1} \in \mathbb{R}^{d_U\times N}$ such that

$$\begin{aligned} U_k^{n*} &= U_k^{n+1} + \delta_t^n \Psi_k^{n+1} \\ \text{with} \quad & \mathscr{L}^\delta_{k,H_\star^{n+1}}\left(U_\star^{n+1}\right) = 0 \\ \text{and} \quad & \mathscr{R}^\delta_{k,H_\star^{n+1}}\left(\Psi_\star^{n+1}\right) = 0. \end{aligned} \tag{2.57}$$

On an unbounded domain, the discrete projection problem is clearly well-posed because we construct the spaces $\ker\left(\mathscr{L}^\delta_{k,H_\star^{n+1}}\right)$ and $\ker\left(\mathscr{R}^\delta_{k,H_\star^{n+1}}\right)$ to satisfy a Hodge decomposition. Additionally, the projection problem remains linear, even if the initial problem is nonlinear. Specifically, all nonlinear terms are handled in the prediction step.

The system (2.57) is commonly referred to as the mixed formulation of the projection problem [GQ98, GS03]. It represents a sparse linear system with $2Nd_U$ unknowns. Importantly, the number of unknowns in the system can be effectively reduced. Applying the operator $\mathscr{R}^\delta_{k,H_\star^{n+1}}$ to the first equation of (2.57), the kinetic unknown satisfies

$$\mathscr{R}^\delta_{k,H_\star^{n+1}}\left(U_\star^{n+1}\right) = \mathscr{R}^\delta_{k,H_\star^{n+1}}\left(U_\star^{n*}\right) \tag{2.58}$$

and using the constraint $\mathscr{L}^\delta_{k,H_\star^{n+1}}\left(U_\star^{n+1}\right) = 0$, the system can be reduced to a sparse linear system with $N(d_U - d_Q)$ unknowns. This formulation is typically referred to as the velocity correction formulation. The dispersive source term $\Psi_\star^{n+1}$ can be computed using the first equation of (2.57), i.e.

$$\Psi_k^{n+1} = \frac{U_k^{n*} - U_k^{n+1}}{\delta_t^n}. \tag{2.59}$$

As an alternative, by applying the operator $\mathscr{L}^\delta_{k,H_\star^{n+1}}$ to the first equation of (2.57), the dispersive source term is found as the solution of

$$\delta_t^n \mathscr{L}^\delta_{k,H_\star^{n+1}}\left(\Psi_\star^{n+1}\right) = \mathscr{L}^\delta_{k,H_\star^{n+1}}\left(U_\star^{n*}\right) \tag{2.60}$$

and using the constraint $\mathscr{R}^{\delta}_{k,H^{n+1}_{\star}}\left(\Psi^{n+1}_{\star}\right)=0$, the system can be reduced to a sparse linear system with Nd_Q unknowns. This formulation is typically referred to as the pressure correction formulation. Then, the kinetic unknown is computed using the first equation of (2.57), i.e.,

$$U^{n+1}_k = U^{n*}_k - \delta^n_t \Psi^{n+1}_k. \tag{2.61}$$

For both formulations, the Lagrange multiplier $Q_\star$ can be chosen such that the discrete application $\Psi_{k,H_\star} : \mathbb{R}^{d_Q\times N} \mapsto \ker\left(\mathscr{R}^{\delta}_{k,H_\star}\right)$ is invertible, and we set

$$Q^{n+1}_k = \Psi^{-1}_{k,H^{n+1}_{\star}}\left(\Psi^{n+1}_{\star}\right). \tag{2.62}$$

For this scheme, neither the computation of the Lagrange multiplier nor the computation of the dispersive source term in the case of velocity correction using (2.59) are necessary.

Proposition 2.11 *Assuming the prediction scheme* (2.54) *is entropy-satisfying under the CFL condition* (2.55)*, then the full scheme, including the discrete projection problem* (2.54)-(2.57) *(or* (2.54)-(2.58) *or* (2.54)-(2.60)-(2.61)*), is also entropy-satisfying under the same CFL condition.*

A number of techniques now exist for constructing an entropy-satisfying scheme for hyperbolic equations [Bou03, BDS12, BLMP17, Abg18, BDF+19, AÖR22, BCDD+23, ABD23].

It may be advantageous to choose one formulation over the other depending on the sign of $\left(\frac{d_Q}{d_U}-\frac{1}{2}\right)$. However, the conditioning of the linear system is also an important consideration. Specifically, when $\delta^n_t \ll 1$, the pressure correction formulation tends to become badly conditioned.

2.3.1.2 Application to the BBM equation

This section is devoted to the application of the numerical strategy described in §2.3.1.1 to the case of the BBM equation (2.33) on $[0,1]$. The mesh is assumed to be Cartesian with a step size of $\mathfrak{m}_k=\delta_x$, and it is numbered from left to right, $\mathbb{T}=[1,N]\cap\mathbb{N}$. The conservative form of its hyperbolic operator is given by

$$F\begin{pmatrix}u\\w\end{pmatrix}=\begin{pmatrix}\frac{u^2}{2}\\cw\end{pmatrix}.$$

The hyperbolic scheme (2.54) provides the prediction $U^{n*}=(u^{n*},w^{n*})^\intercal$. It is worth noting that, using for example the HLL approximate Riemann solver [HLL83], the hyperbolic scheme (2.54) is entropy satisfying with the inner product (2.56) and the uniform weight $\nu=1$, i.e. there exists a numerical flux $\mathscr{G}_f$ such that

$$|u^{n*}_k|^2+|w^{n*}_k|^2 \le |u^n_k|^2+|w^n_k|^2 - \frac{\delta_t}{\mathfrak{m}_k}\sum_{f\in\mathbb{F}_k}\mathscr{G}_f\cdot\mathfrak{n}^k_f\mathfrak{m}_f$$

with *BC* being a term arising from the boundary conditions.

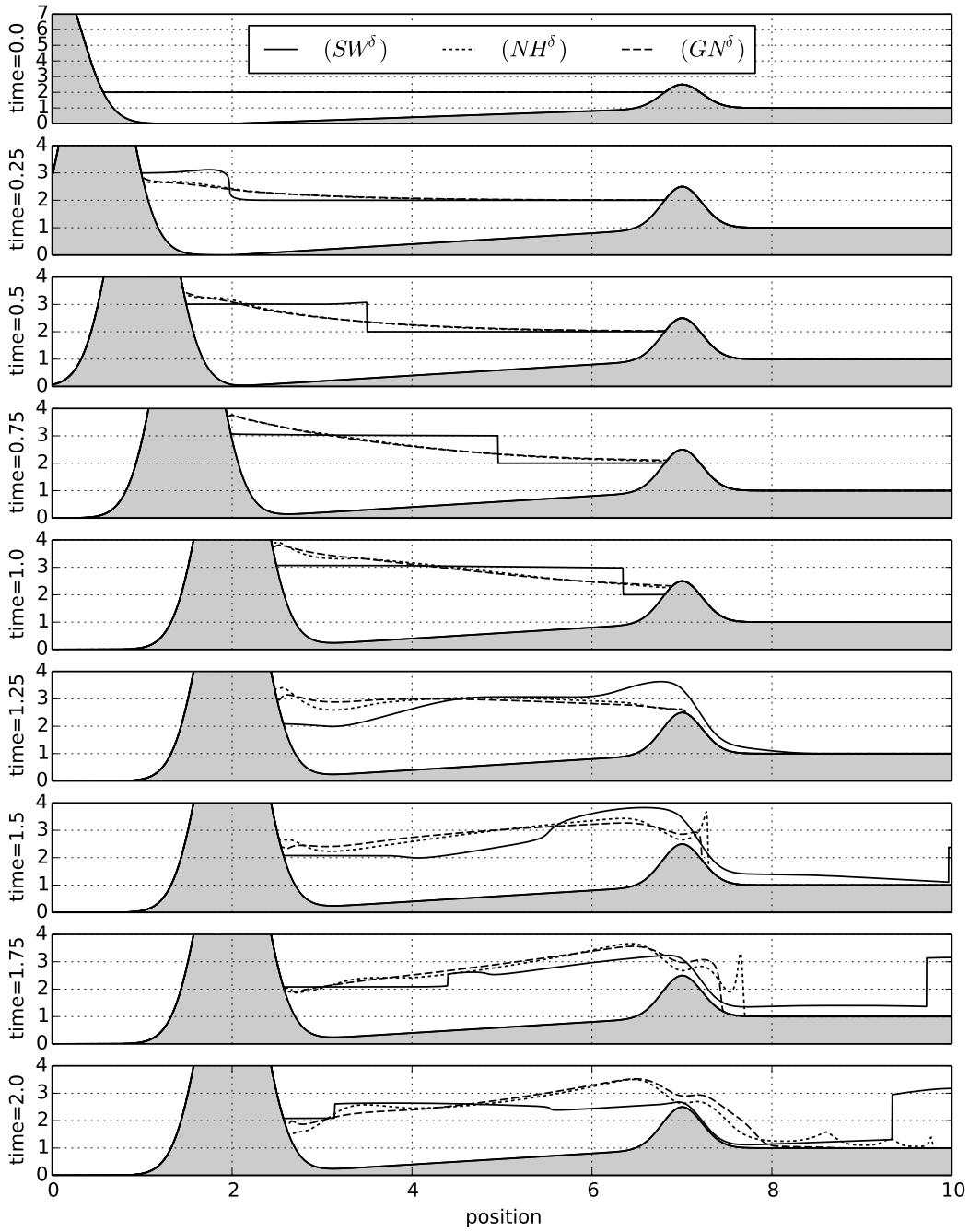

Figure 2.9: §2.2.3 | Simulations with **dry front** of a wave overtopping a dike using the shallow water model (2.6) (solid line), the non-hydrostatic model [SM11] (dotted line), and the Green-Naghdi model (2.13) (dashed line). Figure taken from [Par19].

Now, we turn our attention to the correction step. We propose to use a centered discretization approach. The discretization of the constraint (2.29) is given by

$$\mathscr{L}_k^\delta\left(V_\star\right) = v_{1,k} + \alpha\frac{v_{0,k+1} - v_{0,k-1}}{2\delta_x} \tag{2.63}$$

with $V_\star = \left(v_{0,k}, v_{1,k}\right)_{k\in\mathbb{T}}^\intercal$. Let $\Phi_\star = \left(\phi_{0,k}, \phi_{1,k}\right)_{k\in\mathbb{T}}^\intercal$ be in the dual space of $\ker\left(\mathscr{L}_\star^\delta\right)$. For any $V_\star \in \ker\left(\mathscr{L}_\star^\delta\right)$, we have

$$\begin{aligned}
0 &= \sum_{k=1}^{N}\left(v_{0,k}\phi_{0,k} + v_{1,k}\phi_{1,k}\right)\delta_x = \sum_{k=1}^{N}\left(v_{0,k}\phi_{0,k} - \alpha\frac{v_{0,k+1} - v_{0,k-1}}{2\delta_x}\phi_{1,k}\right)\delta_x \\
&= \sum_{k=1}^{N} v_{0,k}\left(\phi_{0,k} + \alpha\frac{\phi_{1,k+1} - \phi_{1,k-1}}{2\delta_x}\right)\delta_x \\
&\quad -\frac{\alpha}{2}\left[v_{0,f+1/2}\phi_{1,f-1/2} + v_{0,f-1/2}\phi_{1,f+1/2}\right]_{f=1/2}^{f=N+1/2}.
\end{aligned}$$

We conclude the discretization (2.30) of the operator $\mathscr{R}$ such that $\ker\left(\mathscr{R}_\star^\delta\right) = \left(\ker\left(\mathscr{L}_\star^\delta\right)\right)^\perp$ as follows

$$\mathscr{R}_k^\delta\left(\Phi_\star\right) = \phi_{0,k} + \alpha\frac{\phi_{1,k+1} - \phi_{1,k-1}}{2\delta_x}. \tag{2.64}$$

and the discrete counterpart of the boundary condition (2.52) is given by

$$v_{0,f+1/2}\phi_{1,f-1/2} + v_{0,f-1/2}\phi_{1,f+1/2} = 0. \tag{2.65}$$

It is worth noting that the discretization (2.64) and (2.65) strongly depend on the choice of the discretization (2.63). For instance, the dual of the left-upwind scheme in (2.63) corresponds to the right-upwind scheme in (2.64), and vice versa [CLR20].

Interior cells: The mixed formulation is given by (2.57).

The velocity correction is given by (2.58), and using the constraint (2.63), we have

$$u_k^{n+1} - \alpha^2\frac{u_{k+2}^{n+1} - 2u_k^{n+1} + u_{k-2}^{n+1}}{4\delta_x^2} = \mathscr{R}_k^\delta\left(U_\star^{n*}\right). \tag{2.66}$$

Then $w_\star^{n+1}$ is computed explicitly using (2.63), and optionally $\Psi_\star^{n+1}$ using (2.59).

The pressure correction is given by (2.60), and using the constraint (2.64), we have

$$\psi_{1,k} - \alpha^2\frac{\psi_{1,k+2} - 2\psi_{1,k} + \psi_{1,k-2}}{4\delta_x^2} = \frac{1}{\delta_t^n}\mathscr{L}_k^\delta\left(U_\star^{n*}\right). \tag{2.67}$$

Then $\psi_{0,\star}^{n+1}$ is computed explicitly using (2.64), and $U_\star^{n+1}$ using (2.61).

It is worth noting that both schemes (2.66) and (2.67) employ a discretization of the Laplacian where a cell is connected not to its immediate neighbor but to the neighbor of the neighbor. Such discretizations are known to have drawbacks, particularly the introduction of chessboard modes. In the context of projected hyperbolic models, these modes are not preserved by the prediction step (2.54) and thus are not a concern.

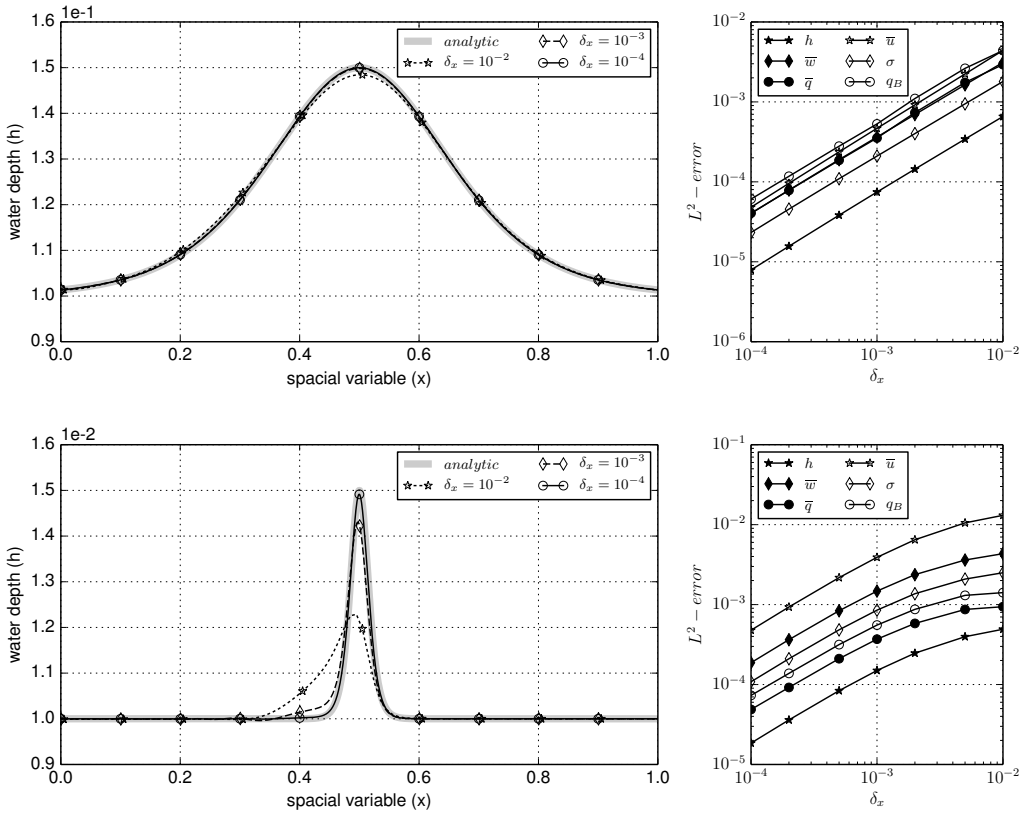

Figure 2.10: §2.2.3 | Exact and approximate solutions for the solitary wave of the Green-Naghdi model (2.13) incoming the computational domain **by fixing the water depth and velocity** using various mesh sizes.
- Top line: Low nonlinear soliton.
- Bottom line: Strong nonlinear soliton.
Figure taken from [NPT22].

Boundary cells: In the scheme (2.66) or (2.67), the two nearest cells to the boundary utilize ghost values. For example, at the left boundary, these values are u_0^{n+1} and $\psi_{1,0}^{n+1}$. For the velocity correction scheme (2.66), we have

$$u_1^{n+1} - \alpha \delta_t^n \frac{\psi_{1,2}^{n+1} - \psi_{1,0}^{n+1}}{2\delta_x} = u_1^{n*}$$
$$u_2^{n+1} - \alpha^2 \frac{u_4^{n+1} - 2u_2^{n+1} + u_0^{n+1}}{4\delta_x^2} = \mathscr{R}_2^{\delta}\left(U_\star^{n*}\right).$$

At the boundary conditions, we consider an inlet flow at the left and a fixed Lagrange multiplier at the right. Specifically:

- At the left boundary we fixe $u(t,0) = \mathring{u}(t) > 0$ and $w(t,0) = \mathring{w}(t)$. At the discrete level, we set $\frac{u_0^n + u_1^n}{2} = \mathring{u}(t^n)$. Then using (2.65), we have $\psi_{1,0}^n - \psi_{1,1}^n = 0$.

- At the right boundary we fixe $\psi_1(t,1) = \mathring{\psi}(t)$. At the discrete level, we set $\frac{\psi^n_{1,0}+\psi^n_{1,1}}{2} = \mathring{\psi}(t^n)$. Then using (2.65), we have $u^n_0 - u^n_1 = 0$.

To write the system focusing only on the velocity u for the velocity correction scheme (2.66) (or alternatively only on the Lagrange multiplier ψ_1 for the pressure correction scheme (2.67)), we use the constraints (2.63) and (2.64). Specifically,

$$\begin{aligned}\alpha\delta_t^n \frac{\psi^{n+1}_{1,2} - \psi^{n+1}_{1,0}}{2\delta_x} &= \alpha\delta_t^n \frac{\psi^{n+1}_{1,2} - \psi^{n+1}_{1,1}}{2\delta_x} \\ &= -\alpha\frac{w^{n+1}_2 - w^{n+1}_1}{2\delta_x} + \alpha\frac{w^{n*}_2 - w^{n*}_1}{2\delta_x} \\ &= \alpha^2\frac{u^{n+1}_3 - u^{n+1}_2 - u^{n+1}_1 + u^{n+1}_0}{4\delta_x^2} + \alpha\frac{w^{n*}_2 - w^{n*}_1}{2\delta_x}.\end{aligned}$$

Hence, the scheme in the first cell is given by

$$u^{n+1}_1 - \alpha^2\frac{u^{n+1}_3 - u^{n+1}_2 - 2u^{n+1}_1}{4\delta_x^2} = u^{n*}_1 + \alpha\frac{w^{n*}_2 - w^{n*}_1}{2\delta_x} + \alpha^2\frac{\mathring{u}\left(t^{n+1}\right)}{2\delta_x^2}$$

and we apply a similar approach at the right boundary. It is worth noting that with the discretization we used, imposing a Dirichlet condition on one variable leads to a Neumann condition on the other. This artificial coupling can impact the numerical solution, potentially causing it to be inconsistent with the continuous equations. However, this strategy ensures a robust numerical scheme.

In [Par19], we apply the same strategy to propose an entropy-satisfying scheme for the Green-Naghdi model (2.13). The boundary conditions are treated as discussed in [NPT22], where two out of the three unknowns h, $h\overline{u}$ and $h\overline{q}$ are fixed at the boundary. Additionally, the tangential horizontal velocity $\overline{u}\cdot\mathfrak{n}^\perp$ and the vertical velocities $\overline{w}$ and $\widetilde{w}$ are specified where the flow is incoming, i.e., $\overline{u}\cdot\mathfrak{n}_{|_{\partial\Omega}} \leq 0$ at the boundary of the wet domain, where $\mathfrak{n}$ represents the outward normal. In particular, the numerical strategy ensures the stability of the numerical resolution in the following cases, where the index $_g$ refers to the ghost cell and $_i$ to the interior cell closest to the boundary:

At dry fronts: where $h^{n+1}_k = 0$, see Figure 2.9.

With wall boundary conditions: setting $\partial_x h_{|_{\partial\Omega}} = 0$ and $\overline{u}_{|_{\partial\Omega}}\cdot\mathfrak{n} = \mathring{u}(t)$. At the discrete level, we set $h^{n+1}_g = h^{n+1}_i$ and $\overline{u}^{n+1}_g\cdot\mathfrak{n} = 2\mathring{u}\left(t^{n+1}\right) - \overline{u}^{n+1}_i\cdot\mathfrak{n}$. It follows that $h_g\overline{q}_g = h_i\overline{q}_i$.

By fixing the water depth and velocity: setting $h_{|_{\partial\Omega}} = \mathring{h}(t)$ and $\overline{u}_{|_{\partial\Omega}}\cdot\mathfrak{n} = \mathring{u}(t)$. At the discrete level, we set $h^{n+1}_g = 2\mathring{h}\left(t^{n+1}\right) - h^{n+1}_i$ and $\overline{u}^{n+1}_g\cdot\mathfrak{n} = 2\mathring{u}\left(t^{n+1}\right) - \overline{u}^{n+1}_i\cdot\mathfrak{n}$. It follows that $h_g\overline{q}_g = h_i\overline{q}_i$, see Figure 2.10. It is worth noting that the water depth or the horizontal velocity can be fixed using the Riemann invariant of the shallow water model, see [GR04], even if there is no mathematical reason other than coherence in the hyperbolic regime.

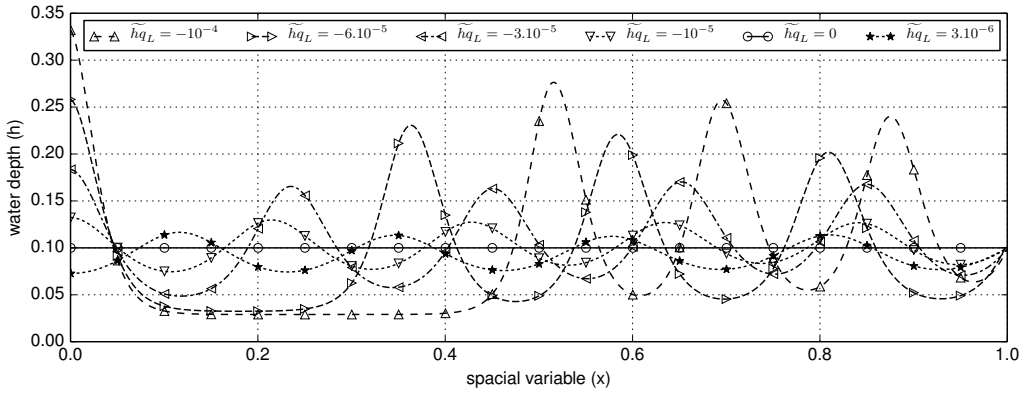

Figure 2.11: §2.2.3 | Simulations of the Green-Naghdi model (2.13) with incoming flows **by fixing the discharge and the pressure**. Figure taken from [NPT22].

By fixing the discharge and the pressure: setting $(h\overline{u}\cdot\mathfrak{n})_{|_{\partial\Omega}} = \mathring{m}(t)$ and $(h\overline{q})_{|_{\partial\Omega}} = \mathring{\psi}(t)$. At the discrete level, we set $h_g^{n+1}\overline{u}_g^{n+1}\cdot\mathfrak{n} = 2\mathring{m}\left(t^{n+1}\right) - h_i^{n+1}\overline{u}_i^{n+1}\cdot\mathfrak{n}$ and $h_g^{n+1}\overline{q}_g^{n+1} = 2\mathring{\psi}\left(t^{n+1}\right) - h_i^{n+1}\overline{q}_i^{n+1}$. It follows that $\overline{u}_g^{n+1} = \overline{u}_i^{n+1}$ and then $h_g^{n+1} = 2\frac{\mathring{m}\left(t^{n+1}\right)}{\overline{u}_i^{n+1}\cdot\mathfrak{n}} - h_i^{n+1}$, see Figure 2.11.

Open boundary conditions: at the discrete level, setting $h_g^{n+1} = h_i^{n+1}$ and $\overline{u}_g^{n+1}\cdot\mathfrak{n} = \overline{u}_i^{n*}\cdot\mathfrak{n}$. It follows that $h_g\overline{q}_g = h_i\overline{q}_i$, see Figure 2.12.

2.3.1.3 Non-conservative products

The correction step (2.57) is valid for any model using the constraint (2.29), i.e., all the models presented in §2.2.1.3. The difference between these models lies in the prediction step and, therefore, in the computation of $U_\star^{n*}$. Several dispersive models can be written under the projected hyperbolic form using non-conservative products, including the Camassa-Holm model (2.34), the Green-Naghdi model with linear velocity profile (2.16), and the layerwise Green-Naghdi model (2.19). The treatment of non-conservative products is complex from both theoretical and numerical perspectives. Although this question remains open, we can reference [DMLM95] for theoretical aspects and [CMP01, Par06, CDCRFNP07, AK10, HHMM10, CFMP13, CFMP13, Cha20, GCDM21] for numerical aspects. It is worth noting that, in the framework of projected hyperbolic models, the projection onto a linear subspace generally increases the regularity of the solution, which can aid in defining non-conservative products. For example, due to the energy conservation (2.8) in BBM-type models (with the constraint (2.29)), we conclude that the velocity $u \in H^1(\mathbb{R})$. Thus, the non-conservative products of the hyperbolic operator (2.31) in the Camassa-Holm setting (see (2.34)) are well defined. Additionally, in [AAGP18], we demonstrate that the non-conservative products of the shallow water model with two velocities (2.7) are well-defined for any monotonous path, which can be extended

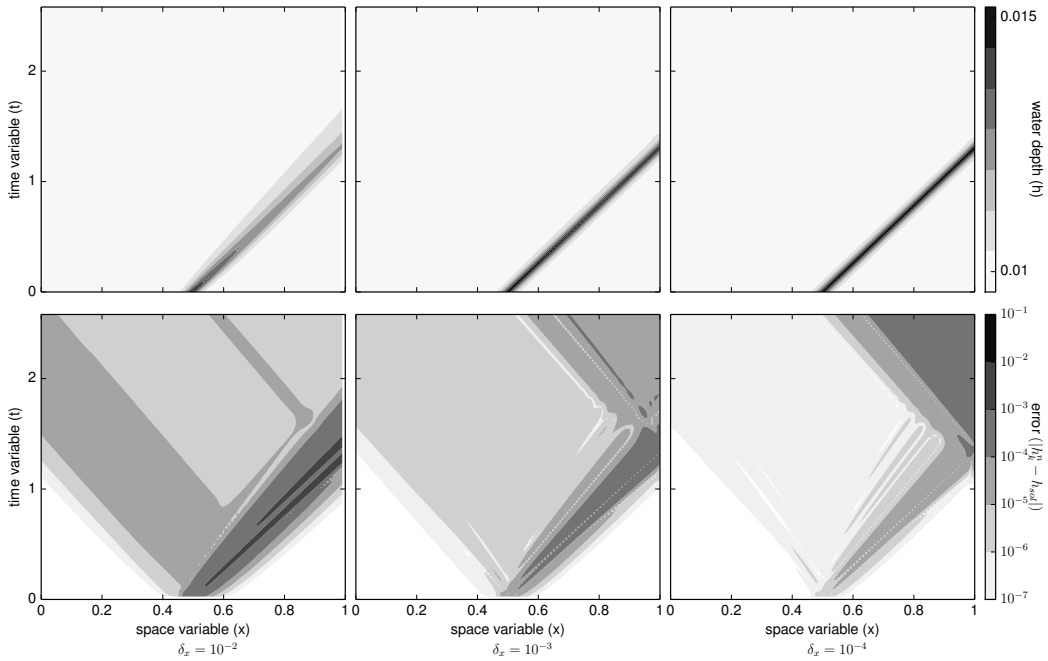

Figure 2.12: §2.2.3 | Simulations of solitary waves in the Green-Naghdi model (2.13) outcoming the computational domain with **open boundary conditions** using various mesh sizes.
- Top line: Water Depth.
- Bottom line: Difference from the Exact Solution.
Figure taken from [NPT22].

to the Green-Naghdi model with linear velocity profile (2.16).

Here, we highlight the specific case of exchanges between layers in the layerwise models (2.9) and (2.19). This approach can be compared to directional splitting. A similar strategy has been proposed for the kinetic solver in [ABD08], and is generalized here for any hyperbolic solver. Specifically, we start by considering the model without vertical exchanges or dispersive source terms. Essentially, this model is the shallow water equation with two passive transport models in each layer. Similar to the conservative case (2.54), the solution in each layer is approached using classical finite volume methods, i.e.

$$W_{i,k}^{n(1)} = W_{i,k}^{n} - \frac{\delta_t^n}{\mathfrak{m}_k} \sum_{f \in \mathbb{F}_k} \mathscr{F}\left(W_{i,k}^n, W_{i,k_f}^n\right) \cdot \mathfrak{n}_f^k \mathfrak{m}_f \tag{2.68}$$

where the state vector reads

$$W_{i,k}^n = \left(h_k^n, h_k^n \overline{u}_{i,k}^n\right)^\intercal \qquad \text{and} \qquad W_{i,k}^{n(1)} = \left(h_{i,k}^{n(1)}, h_{i,k}^{n(1)} \overline{u}_{i,k}^{n(1)}\right)^\intercal$$

for the layerwise shallow water model (2.9) and

$$W_{i,k}^n = \left(h_k^n, h_k^n \overline{u}_{i,k}^n, h_k^n \overline{w}_{i,k}^n, h_k^n \widetilde{w}_{i,k}^n\right)^\mathsf{T} \quad \text{and} \quad W_{i,k}^{n(1)} = \left(h_{i,k}^{n(1)}, h_{i,k}^{n(1)} \overline{u}_{i,k}^{n(1)}, h_{i,k}^{n(1)} \overline{w}_{i,k}^{n(1)}, h_{i,k}^{n*} \widetilde{w}_{i,k}^{n(1)}\right)^\mathsf{T}$$

for the layerwise Green-Naghdi model (2.19). In these last case, the two last unknown can be advected using a upwind scheme with the mass flux as a passive pollutant as presented in [Bou04, §2.7].

The total water depth at time t^n is given by h_k^n and $h_{i,k}^{n(1)}$ is an approximation of the total water depth at time t^{n+1} assuming the entire water column is moving at speed $\overline{u}_{i,k}^n$. In the second step of the scheme, vertical exchanges are taken into account, and the mass equation is given by

$$h_k^{n+1} = h_{i,k}^{n(1)} + \delta_t^n \frac{G_{i+1/2,k}^{n+1} - G_{i-1/2,k}^{n+1}}{\ell_i}.$$

It is a linear system by column of water with the unknowns $h_k^{n+1}, \left(G_{i+1/2,k}^{n+1}\right)_{1 \le i < L}$. The solution is straightforwardly given by

$$h_k^{n+1} = \sum_{i=1}^{L} \ell_i h_{i,k}^{n(1)} \qquad \text{and} \qquad G_{i+1/2,k}^{n+1} = \sum_{j=1}^{i} \ell_j \frac{h_k^{n+1} - h_{j,k}^{n(1)}}{\delta_t^n}. \tag{2.69}$$

Then, we use an upwind implicit scheme for the velocity, i.e.

$$\begin{aligned} h_k^{n+1} \overline{u}_{i,k}^{n*} = h_{i,k}^{n(1)} \overline{u}_{i,k}^{n(1)} + \frac{\delta_t^n}{\ell_i} \Big(& u_{i+1}^{n*} \left[G_{i+1/2}^{n+1}\right]_+ - u_i^{n*} \left[G_{i+1/2}^{n+1}\right]_- \\ & - \left(u_i^{n*} \left[G_{i-1/2}^{n+1}\right]_+ - u_{i-1}^{n*} \left[G_{i-1/2}^{n+1}\right]_- \right) \Big) \end{aligned} \tag{2.70}$$

with the positive and negative parts of the function defined by $[\phi]_\pm = \frac{|\phi| \pm \phi}{2} \ge 0$. Other advection schemes can be chosen, but this choice is motivated by the fact that the implicit upwind scheme is unconditionally entropy-stable [Bou04]. Additionally, the matrix of the system (2.70) is actually block triangular, allowing for explicit computation by processing the layers in the correct order. This means there exists an order to compute the layers such that either the flux is outward or the neighboring values are already known.

Proposition 2.12 *Assuming the scheme* (2.68) *for one layer shallow water model is entropy satisfying under a CFL condition* (2.55)*. Then the scheme* (2.68)-(2.69)-(2.70) *for the layerwise model* (2.9) *is entropy-satisfying under the same CFL condition.*

The treatment of the vertical velocities $\overline{w}_{i,k}^{n*}$ and $\widetilde{w}_{i,k}^{n*}$ is slightly more complex since they are coupled by the velocity at the interface (2.20). The unknowns of the vertical velocity in each layer are given by

$$A\left(h_{i,k}^{n+1}, G_{i-1/2,k}^{n+1}, G_{i+1/2,k}^{n+1}\right) \begin{pmatrix} \overline{w}_{i,k}^{n*} \\ \widetilde{w}_{i,k}^{n*} \end{pmatrix} = B_{i,k}^{n(1)}$$

with the matrix

$$A(H, G_d, G_u) = \begin{pmatrix} H + [G_d]_+ + [G_u]_- & \sqrt{3}\left([G_u]_- - [G_d]_+\right) \\ \sqrt{3}\left([G_u]_+ - [G_d]_-\right) & H + G_d + G_u + [G_d]_+ + [G_u]_- \end{pmatrix}$$

and the right-hand side can be computed explicitly by iterating through the layers in the correct order, similar to the horizontal velocity

$$B_{i,k}^{n(1)} = \begin{pmatrix} h_{i,k}^{n(1)} \overline{w}_{i,k}^{n(1)} \\ h_{i,k}^{n(1)} \widetilde{w}_{i,k}^{n(1)} \end{pmatrix} + \frac{\delta_t^n}{\ell_i} \left(\left(\overline{w}_{i+1}^{n*} - \sqrt{3} \widetilde{w}_{i+1}^{n*} \right) \left[G_{i+1/2}^{n+1} \right]_+ + \left(\overline{w}_{i-1}^{n*} + \sqrt{3} \widetilde{w}_{i-1}^{n*} \right) \left[G_{i-1/2}^{n+1} \right]_- \right) \begin{pmatrix} 1 \\ \sqrt{3} \end{pmatrix}.$$

Proposition 2.13 *Assuming the scheme* (2.68) *for one layer shallow water model is entropy satisfying under a CFL condition* (2.55)*. Then the scheme* (2.68)-(2.69)-(2.70) *with the correction step* (2.57) *for the layerwise model* (2.19) *is entropy-satisfying under the same CFL condition.*

It is worth noting that resolving the correction step involves coupling the velocities of all layers together, which can make the scheme computationally expensive as the number of layers increases.

2.3.2 Incremental scheme for projected hyperbolic models

2.3.2.1 First order incremental scheme

To address the drawback at small time steps, an incremental pressure method can be employed [God79, Gue99]. Specifically, we add to the prediction step with an explicit estimation of the dispersive source term. This explicit estimation could be its value from the previous time step, denoted as $\Psi_\star^n$, but this choice can influence the final solution even for larger time steps for the Boussinesq-type models. Another approach is to utilize the dispersive operator estimated with the Lagrange multiplier from the previous time step, denoted as $\Psi_{k,H_\star^{n+1}}(Q_\star^n)$. This choice is motivated by the fact that $\Psi_{k,H_\star^{n+1}} \in \ker\left(\mathscr{R}^\delta_{k,H_\star^{n+1}}\right)$, meaning that even if the estimation of the Lagrange multiplier is inaccurate, it does not significantly impact the final result. The fact that the dispersive operator is estimated with $H_\star^{n+1}$ poses no issue since the dispersive source term does not affect the potential unknown. During the first time step, the unknown nature of the Lagrange multiplier, since it is not provided by the initial condition, is not problematic. Any initial condition for the Lagrange multiplier can be chosen. (2.54) can be advantageously replaced by

$$W_k^{n*} = W_k^n - \frac{\delta_t^n}{\mathfrak{m}_k} \sum_{f \in \mathbb{F}_k} \mathscr{F}\left(W_k^n, W_{k_f}^n\right) \cdot \mathfrak{n}_f^k \mathfrak{m}_f - \delta_t^n \Psi_{k,H_\star^{n+1}}(Q_\star^n). \tag{2.71}$$

Then the projection step is carried out using one of the formulations (2.57), (2.58), or (2.60). However, in each case, the computed dispersive source term is adjusted based on the deviation from the explicitly estimated dispersive operator. For instance, in the case of velocity correction, (2.58) and (2.59) are replaced by

$$\mathscr{R}^\delta_{k,H_\star^{n+1}}\left(U_\star^{n+1}\right) = \mathscr{R}^\delta_{k,H_\star^{n+1}}(U_\star^{n*}) \qquad \text{and} \qquad \delta\Psi_k^{n+1} = \frac{U_k^{n*} - U_k^{n+1}}{\delta_t^n}. \tag{2.72}$$

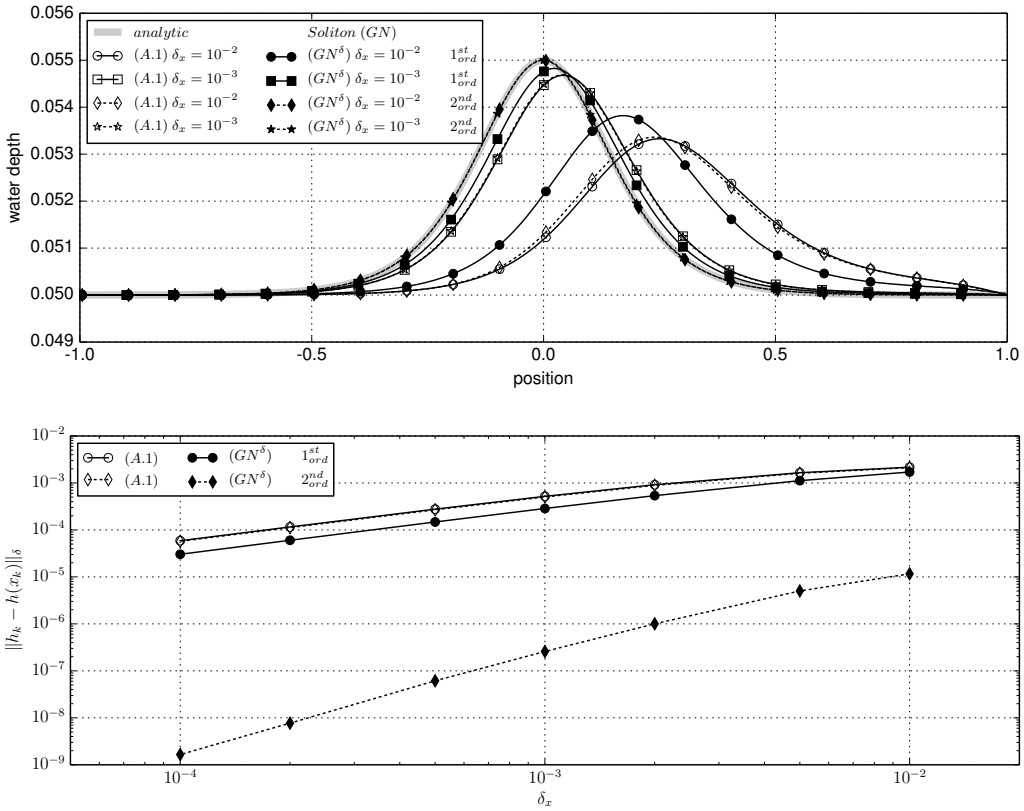

Figure 2.13: §2.3.2.2 | (Top line) Exact and approximate solutions of steady solitary wave of the Green-Naghdi model (2.13) with several mesh sizes. (Bottom line) Convergence curves.
$(A.1)$ Scheme witch does not satisfy the projection structure.
(GN^δ) Second order projection scheme §2.3.2.2.
Figure taken from [Par19].

Alternatively, in the case of pressure correction, (2.60) and (2.61) are replaced by

$$\delta_t^n \mathscr{L}^\delta_{k,H_\star^{n+1}}\left(\delta\Psi_\star^{n+1}\right) = \mathscr{L}^\delta_{k,H_\star^{n+1}}\left(U_\star^{n*}\right) \qquad \text{and} \qquad U_k^{n+1} = U_k^{n*} - \delta_t^n \delta\Psi_k^{n+1}. \tag{2.73}$$

Also, for the computation of the Lagrange multiplier, (2.62) is replaced by

$$Q_k^{n+1} = Q_k^n + \Psi^{-1}_{k,H_\star^{n+1}}\left(\delta\Psi_\star^{n+1}\right). \tag{2.74}$$

The entropy stability, as stated in Proposition 2.11, still holds with the incremental correction scheme (2.71)-(2.72)-(2.74) (or (2.71)-(2.73)-(2.74)).

2.3.2.2 High-order incremental scheme

The progressive system can be utilized cleverly to propose high-order schemes without the necessity of solving multiple linear systems. This strategy, well-established in the context

of incompressible flow [vK86], can be adapted to projected hyperbolic models. It can be employed with Backward Difference Formulas [CH52], although in the realm of hyperbolic models, explicit Runge-Kutta methods [Run95] are more commonly used. The following multi-step scheme for the prediction step is proposed

$$\begin{aligned} W^{n*} &= W^n + \delta_t^n \sum_{i=1}^{s} b_i K^{n(s)} \\ \text{with} \quad K^{n(i)} &= -A\left(W^n\right)\nabla W^n - \delta_t^n \Psi_{H^{n(i)}}\left(\widetilde{Q}^n\left(t^n + c_i\delta_t^n\right)\right) \\ W^{n(i)} &= W^n + \delta_t^n \sum_{j=1}^{i-1} a_{i,j} K^{n(j)} \end{aligned}$$

where $s \geq 1$ is the order of the scheme, and $a_{i,j}$, b_i and c_i are coefficients of the Butcher tableau [But21]. The reconstructed Lagrange multiplier $\widetilde{Q}^n(t)$ is a polynomial extrapolation of order $s-2$ of the Lagrange multiplier passing through the values at the previous time step. That is, if $s = 1$ we set $\widetilde{Q}^n = 0$ (non-incremental, see §2.3.1.1) or $\widetilde{Q}^n = Q^n$ (incremental §2.3.2.1). Otherwise

$$\widetilde{Q}^n(t) \in \mathbb{P}_{s-2}[t] \qquad \text{and for any } 0 \leq j \leq s-1, \qquad \widetilde{Q}^n\left(t^{n-j}\right) = Q^{n-j}.$$

Then a unique implicit correction step is performed (via (2.72) or (2.73)), and the Lagrange multiplier at time t^{n+1} is given by

$$Q^{n+1} = \widetilde{Q}^n\left(t^{n+1}\right) + \Psi_{H^{n+1}}^{-1}\left(\delta\Psi^{n+1}\right).$$

It remains to discuss the space discretization. Most high-order schemes are based on approximation of the solution on each control volume using several degree of freedom, as the continuous [Red93] or discontinuous [PE12] Galerkin methods. Similar to the first-order scheme discussed in §2.3.1.1, the prediction step consists of an entropy satisfying scheme for the associated hyperbolic models. Recently, a few entropy-satisfying high order schemes have been proposed in the context of hyperbolic models [GWK16, WWGK17, MÖR24]. These schemes involve high-order integration rules and inner products that replace the approximation (2.56). Following the construction of the first-order scheme, the next step is to propose a high-order discretization of the constraint $\mathscr{L}_H(V)$ to fully define the scheme. By ensuring the orthogonality property $\ker(\mathscr{R}_H) = (\ker(\mathscr{R}_H))^{\perp}$, Proposition 2.11 can be generalized to high-order schemes.

It is important to note that the inner product (2.56) and the centered discretization of the constraint ((2.63) for BBM) are already second-order accurate. Therefore, by employing a second-order MUSCL reconstruction for the prediction scheme, we can achieve a second-order scheme for projected hyperbolic models. This strategy has been advantageously used in the context of the Green-Naghdi equations to propose a second-order scheme, see Figure 2.13.

2.3.3 Well-balanced schemes for projected hyperbolic models

In recent decades, there has been considerable interest in developing numerical schemes capable of discretizing particular solutions of hyperbolic models. Although

not universally applicable, these solutions are typically characterized by a functional of the state variable that remains constant across the entire domain. One of the most classical examples is the preservation of the lake at rest equilibrium, characterized by $\nabla(B+h)=0$ and $\overline{u}=0$ for the shallow water model (2.6) [BV94, Gos00, Bou04, PC04, ABB+04, XS06, GPC07, NXS07, CGLGP08, BEKP11, DLGP13]. Numerous studies have extended this concept to more complex equilibria and models [XSN11, Xin14, DZBK16, BC16, MDBCF17, CN17, GdLP+18, BDF+19, CCH+19, Bar19, BBBBC21, GBCP21, BBF+22, CTR23, GM24, BMD24]. The projected hyperbolic form appears well-suited to extend this concept to dispersive models. Here, we outline a strategy for constructing a well-balanced numerical scheme for a one-dimensional steady solution based on piecewise steady solution approximations [GBCP21], although other strategies can likely be similarly extended.

Let us present the well-balanced scheme within the framework of projected hyperbolic models of BBM-types §2.2.1.1 in a conservative form on a homogeneous mesh $\mathfrak{m}_k=\delta_x$. Let $\widetilde{U}(x)$ denote a steady solution of the projected hyperbolic models. Similar to hyperbolic models, the steady states of the projected hyperbolic models satisfy the ODE

$$\partial_x F\left(\widetilde{U}\right)=-\widetilde{\Psi} \qquad \text{with} \qquad \mathscr{L}\left(\widetilde{U}\right)=0 \qquad \text{and} \qquad \mathscr{R}\left(\widetilde{\Psi}\right)=0 \tag{2.75}$$

where $\widetilde{\Psi}$ represents the dispersive source term at equilibrium. Let us focus on the time-discrete framework. The principle of the method is to handle the prediction step with the dispersive source term at equilibrium. That is, we set

$$U^{n*}=U^n-\delta_t^n\left(\partial_x F\left(U^n\right)+\widetilde{\Psi}^n\right)=U^n-\delta_t^n\partial_x\left(F\left(U^n\right)-F\left(\widetilde{U}^n\right)\right)$$

and the correction step is given by

$$U^{n*}=U^{n+1}+\delta_t^n\delta\Psi^{n+1} \qquad \text{with} \qquad \mathscr{L}\left(U^{n+1}\right)=0 \qquad \text{and} \qquad \mathscr{R}\left(\delta\Psi^{n+1}\right)=0$$

with $\delta\Psi^{n+1}=\Psi^{n+1}-\widetilde{\Psi}^n$. It is evident that $\widetilde{U}$ is a steady solution of the time-discrete scheme. At the continuous spatial level, the projection step remains unaffected by the scheme and is given by (2.72) or (2.73).

Now, consider the fully-discrete framework. We define

$$\begin{aligned}U_k^{n*}=U_k^n-\frac{\delta_t^n}{\delta_x}\Big(&\mathscr{F}\left(\widetilde{U}_{k\oplus}^n,\widetilde{U}_{k+1\ominus}^n\right)-\mathscr{F}\left(\widetilde{U}_{k-1\oplus}^n,\widetilde{U}_{k\ominus}^n\right)\\&-\left(F\left(\widetilde{U}_{k\oplus}^n\right)-F\left(\widetilde{U}_{k\ominus}^n\right)\right)\Big)\end{aligned} \tag{2.76}$$

where $\widetilde{U}_{k\oplus}^n=\widetilde{U}_k^n\left(\pm\frac{1}{2}\delta_x\right)$ and $\widetilde{U}_k^n(x)$ is the solution of the ODE (2.75) with the initial value $\widetilde{U}_k^n(0)=U_k^n$. Unfortunately, the solution of the ODE is typically not explicit. To estimate the values of the unknown at the faces within a control volume, an implicit Euler scheme for the ODE (2.75) is employed. This discretization of the ODE implies a specific discretization of the constraint $\mathscr{L}_k^{\mathrm{WB}}$ such that the discrete steady state $\widetilde{U}_\star^n(x)\in\ker\left(\mathscr{L}_k^{\mathrm{WB}}\right)$. The correction scheme is then implemented using the constraint $\mathscr{L}_k^{\mathrm{WB}}$.

Let us provide an example with the BBM model (2.33). The ODE (2.75) is given by

$$\begin{aligned}\partial_x\left(\frac{\widetilde{u}^3}{3}+\frac{\beta}{2\alpha^2}\widetilde{w}^2-\alpha\widetilde{u}\widetilde{q}\right)&=0\\ \widetilde{q}+\frac{\beta}{\alpha^2}\partial_x\widetilde{w}&=0\\ \widetilde{w}+\alpha\partial_x\widetilde{u}&=0.\end{aligned}$$

where the first equation has been replaced by the energy conservation equation (2.27), and we set $\widetilde{U}=(\widetilde{u},\widetilde{w})^\intercal$ and $\widetilde{q}=\psi_1$ as the Lagrange multiplier. Then, the implicit scheme for the ODE reads

$$\begin{aligned}\frac{\widetilde{u}_{k\oplus}^3}{3}+\frac{\beta}{2\alpha^2}\widetilde{w}_{k\oplus}^2-\alpha\widetilde{u}_{k\oplus}\widetilde{q}_{k\oplus}&=K_k\\ \widetilde{q}_{\oplus}\pm\frac{2\beta}{\alpha^2}\frac{\widetilde{w}_{k\oplus}-w_k}{\delta_x}&=0\\ \widetilde{w}_{k\oplus}\pm 2\alpha\frac{\widetilde{u}_{k\oplus}-u_k}{\delta_x}&=0.\end{aligned}\tag{2.77}$$

with $K_k=\frac{u_k^3}{3}+\frac{\beta}{2\alpha^2}w_k^2-\alpha u_k q_k$. It follows that the velocity $\widetilde{u}_{k\oplus}$ is a root of a following third-order polynomial. For sufficiently small δ_x, the polynomial has three real roots that approach $u_k,0$ and $\pm\infty$ as δ_x approaches zero. Due to the continuity of the steady state, the correctly reconstructed velocity corresponds to the root that is consistent with u_k. Then, $\widetilde{w}_{k\oplus}$ is obtained using the second equation of (2.77).

It is now necessary to establish the discretization of the constraint $\mathscr{L}_k^{\mathrm{WB}}$. The crucial point is that the steady state of the prediction step lies in the kernel of $\mathscr{L}_k^{\mathrm{WB}}$. At steady state, the reconstructed values are identical on both sides of an interface, i.e., $\widetilde{u}_{k\oplus}=\widetilde{u}_{k+1\ominus}$ and $\widetilde{w}_{k\oplus}=\widetilde{w}_{k+1\ominus}$. Using the third equation of (2.77), we deduce that

$$\mathscr{L}_k^{\mathrm{WB}}(U_\star)=\frac{w_k+w_{k+1}}{2}+\alpha\frac{u_{k+1}-u_k}{\delta_x}.\tag{2.78}$$

Unfortunately, the constraint (2.78) is not well-suited for the inner product (2.56) and leads to a non-sparse linear system when solving the correction step. To maintain the efficiency of the scheme, we utilize the following inner product

$$\langle f_\star,g_\star\rangle^{\mathrm{WB}}=\sum_{k\in\mathbb{T}}\left(f_{0,k}g_{0,k}+\frac{f_{1,k-1/2}g_{1,k-1/2}+f_{1,k+1/2}g_{1,k+1/2}}{2}\right)\delta_x.\tag{2.79}$$

The resulting correction scheme is given by

$$u_k^{n+1}-\alpha^2\frac{u_{k+1}^{n+1}-2u_k^{n+1}+u_{k-1}^{n+1}}{\delta_x^2}=u_k^{n*}+\alpha\frac{w_{k+1}^{n*}-w_{k-1}^{n*}}{2\delta_x}.\tag{2.80}$$

Proposition 2.14 *Let $K\in\mathbb{R}$. The numerical scheme (2.76)-(2.80) preserves solutions satisfying for any $k\in\mathbb{T}$,*

$$\frac{u_k^3}{3}+\frac{\beta}{2\alpha^2}w_k^2-\alpha u_k q_k=K.$$

It is important to note that since the prediction step is not inherently entropy-satisfying with the inner product (2.79), the well-balanced scheme is not entropy satisfying. Also it can be seen that the well-balanced scheme at steady state corresponds to a symplectic integrator for the EDO (2.75). In particular, it preserved the flux of momentum which acts as the energy for the EDO.

In Figure 2.14, we apply the previous strategy to the Green-Naghdi models (2.13) with a non-flat bottom. It is noteworthy that even with a coarse mesh (top line), the amplitude of the waves behind the bottom bump is well recovered.

2.4 A few steps further

We now consider the task of enhancing the projected hyperbolic models to increase their efficiency or improve their ability to replicate the underlying physics.

2.4.1 Coupling of projected hyperbolic models

It can be advantageous to employ different projected hyperbolic models in distinct regions of the computational domain. The primary goal here is to reduce computation time, as these models form a hierarchy where the most expensive in term of computational resources is needed only in a specific areas within the domain. For instance, it may be practical to utilize the Peregrine model (2.47) in regions sufficiently distant from the shore. However, as wave nonlinearity becomes more significant closer to shore, switching to the Green-Naghdi model (2.13) could be more appropriate. The Green-Naghdi model (2.13) remains stable up to the dry front, benefiting from boundary conditions proposed in §2.2.3.3. Nevertheless, it does not account for breaking waves. To address this, some propose implementing the shallow water model (2.6) in the surf zone to facilitate energy dissipation.

Another goal of the coupling is to enhance the robustness of the simulation. Specifically, dispersive models require a certain regularity in parameters to ensure well-posedness. To address this challenge, it is feasible to switch to a more robust model locally in regions where parameter regularity is insufficient. For example, it is well known that the Green-Naghdi model (2.13) is not well-posed on an irregular bottom (see [Lan13, §6.1.2]). Through coupling, the shallow water model (2.6) can be employed to solve locally around discontinuities in the bottom profile, ensuring stability and accuracy in these challenging areas, as illustrated in Figure 2.15. It is important to note that even the shallow water model (2.6) is not well-defined over a discontinuous bottom, see [And05, DLDP13].

Lastly, coupling can be employed to enforce well-known boundary conditions from a simpler model and then transfer the flow to a more complex model. For instance, at the boundary of the computational domain, a thin layer of the shallow water model can be utilized to apply established shallow water conditions [GR96] instead of the boundary conditions of the Green-Naghdi model (2.13), as illustrated in Figure 2.16. This approach can be likened to various studies where a boundary layer is employed, adjusting source terms within the equations to correctly impose the desired propagating signals [Ber94, WKS99, BGKN22].

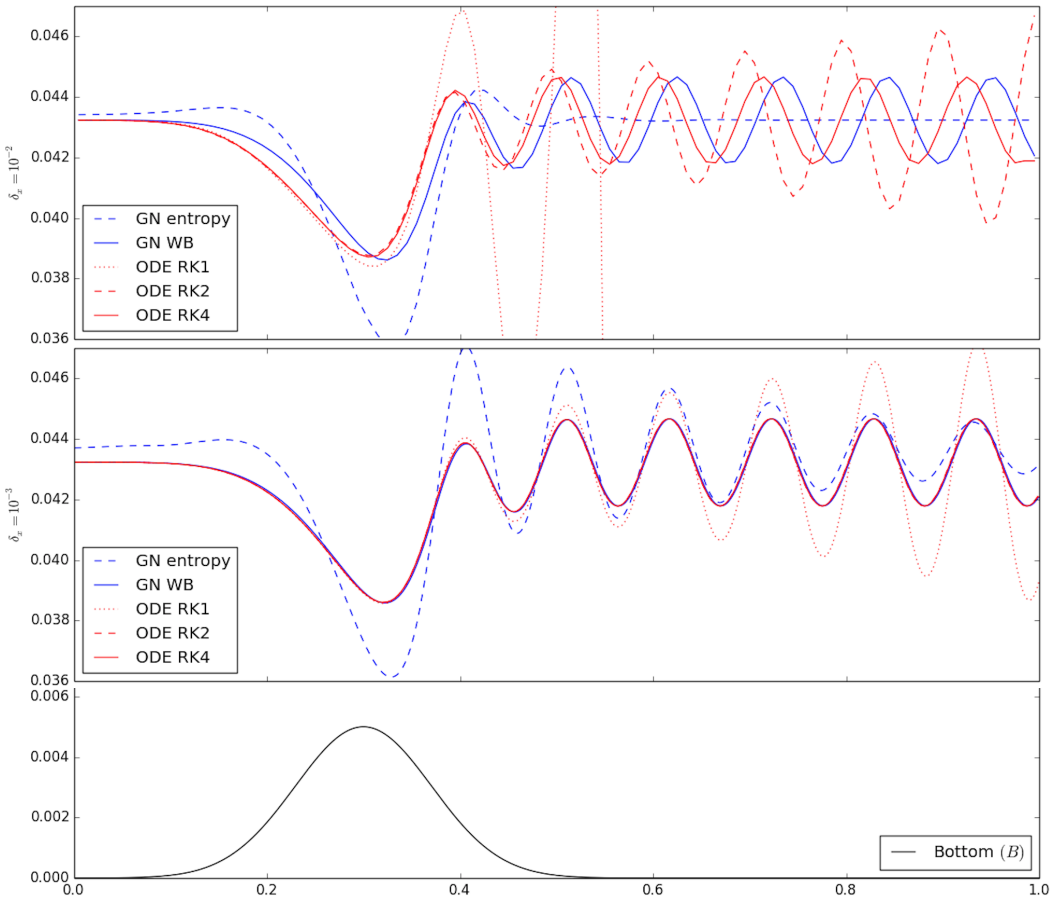

Figure 2.14: §2.3.3 | Simulations of the steady state of the Green-Naghdi model (2.13) are compared using different numerical schemes and resolutions:
- Dashed blue line: Green-Naghdi model (2.13) with entropy-satisfying scheme §2.3.1.
- Solid blue line: Green-Naghdi model (2.13) with well-balanced scheme §2.3.3.
- Dotted red line: Solution of the ODE steady state of the Green-Naghdi model (2.75) using Euler scheme.
- Dashed red line: Solution using second-order Runge-Kutta scheme.
- Solid red line: Solution using fourth-order Runge-Kutta scheme.
- Top line: Mesh size $\delta_x = 10^{-2}$.
- Middle line: Mesh size $\delta_x = 10^{-3}$.
- Bottom line: Bathymetry.

For simplicity, we focus on coupling two models with the same unknowns H and U and the same hyperbolic operator $A(H,U)$, but with different constraints $\mathscr{L}_H^0(U)$ and $\mathscr{L}_H^1(U)$. The coupling is achieved using a thick interface technique [GM98, GR04, GTR05]. We introduce a color function $\theta(t,x) \in [0,1]$, which serves as a parameter to switch between

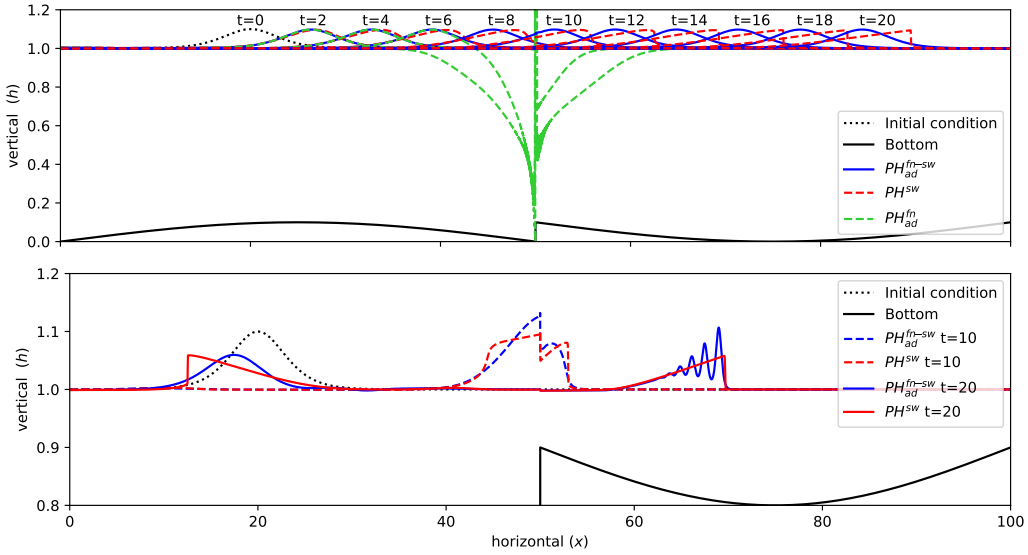

Figure 2.15: §2.4.1 | Simulations of a solitary wave over small discontinuity (top line) and large discontinuity (bottom line) in the bottom profile at various time steps are shown.
- Solid blue line: Coupled model (2.81).
- Dashed red line: Shallow water model (2.6).
- Dashed green line: Green-Naghdi model (2.13).
Figure taken from [Par24b].

these constraints. The constraint of the unified model is expressed as

$$\mathscr{L}_H^\theta(U) = (1-\theta)\,\mathscr{L}_H^0(U) + \theta\,\mathscr{L}_H^1(U). \tag{2.81}$$

Thus, each model is respectively recovered when $\theta = 0$ or $\theta = 1$. Moreover, to couple multiple models together, a similar strategy can be employed using a vector-valued color function. Consequently, the dispersive source term of the model is taken from the dual space of the set of functions that satisfy the constraint.

As an example, let us consider the coupling between the BBM equation (2.33) and the Burgers equation [Bur48]. We focus on the projected hyperbolic model of BBM-type (2.23) with $U = (u,w)$ and the hyperbolic operator (2.31) where $f = g = 0$, $P_0(x) = x$ and $P_1(x) = c$. It is noteworthy that the Burgers equation is recovered by using the constraint $\mathscr{L}^0(U) = w$, as this imposes no constraint on u, thereby causing the dispersive source term ψ_0 to vanish. Therefore, the constraint of the unified model (2.81) is expressed as

$$\mathscr{L}^\theta(U) = w + \theta\alpha\partial_x u.$$

Following the computations detailed in §2.2.1.3, the dispersive source term lies in the kernel of

$$\mathscr{R}^\theta(U) = \psi_0 + \alpha\partial_x(\theta\psi_1)$$

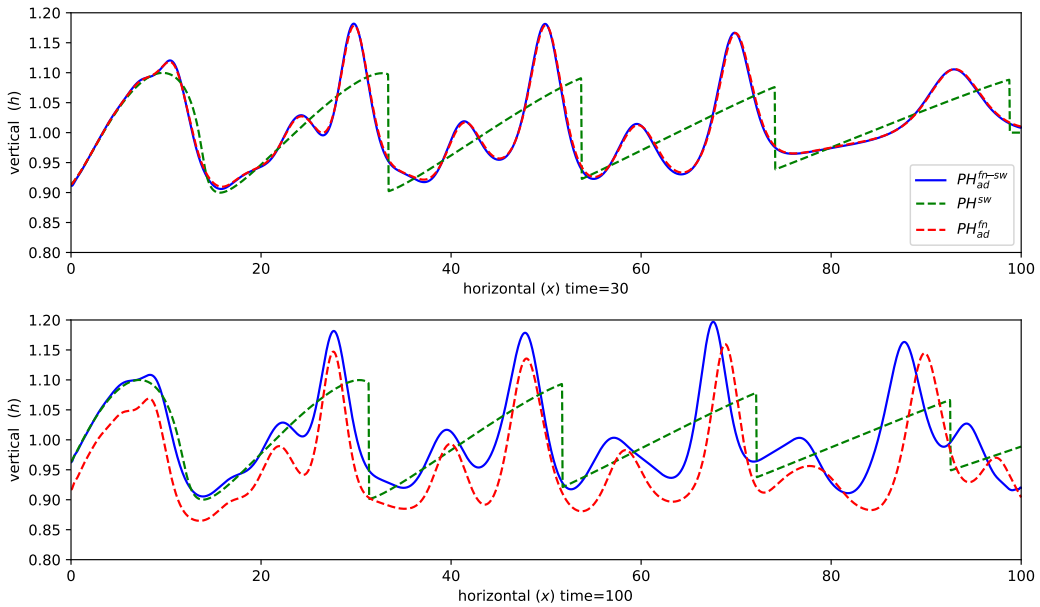

Figure 2.16: §2.4.1 | Simulations of a sinusoidal signal imposed at the left boundary with an open boundary condition at the right boundary are presented.
- Top line: Short time, depicting the behavior before the waves exit the computational domain.
- Bottom line: Long time, showing the behavior after several waves have exited the computational domain.
- Solid blue line: Coupled model (2.81).
- Dashed green line: Shallow water model (2.6).
- Dashed red line: Green-Naghdi model (2.13).
Figure taken from [Par24b].

and the reduced form of equation (2.28) reads

$$\left(1-\alpha^2\partial_x\left(\theta\partial_x\bullet\right)\right)\partial_t u+u\partial_x u-\alpha^2 c\partial_x\left(\theta\partial_x^2 u\right)=0. \tag{2.82}$$

One may wonder about the purpose of such coupling, rather than directly combining the two models linearly, i.e.,

$$\left(1-\theta\alpha^2\partial_x^2\right)\partial_t u+u\partial_x u-\theta\alpha^2 c\partial_x^3 u=0. \tag{2.83}$$

The advantage of maintaining the projection structure is that for sufficiently smooth solutions, the unified Burgers-BBM model (2.82) satisfies (by construction) the following energy conservation

$$\partial_t\left(\frac{u^2+w^2}{2}\right)+\partial_x\left(\frac{u^3}{3}+\frac{c}{2}w^2\right)=\partial_t\left(\frac{u^2+|\theta\partial_x u|^2}{2}\right)+\partial_x\left(\frac{u^3}{3}+\frac{c}{2}|\theta\partial_x u|^2\right)=0$$

unlike the averaged equation (2.83).

This coupling strategy is employed in [Par24b] for the coupling of the shallow water model (2.6), the Green-Naghdi model (2.13), the Boussinesq-type model (2.46), and the Peregrine model (2.47).

2.4.2 Adaptive projected hyperbolic models

The next step in the improvement process involves enhancing the ability of the numerical strategy to select the appropriate model for each region. For instance, breaking criteria [KDS14] are designed to identify when the shallow water model (2.6) should replace the Green-Naghdi model (2.13) to dissipate wave energy, hence improving physical relevance. Similarly, a criteria can be defined to reduce computation time by using the most efficient model that stays within the initially chosen error range. Consider two projected hyperbolic models: one fine model, for which we seek the solution with the constraint $\mathscr{L}_H^1$, and a coarse model, which approximates the first and is faster to compute, with its solution denoted as U^0. We propose to base the criterion on the estimator $\mathscr{L}_H^1\left(U^0\right)$. The coupling is achieved with the strategy presented in §2.4.1 by defining the color function as follows

$$\theta\left(t,x\right)=\max\left(0,\min\left(\frac{\left|\mathscr{L}_H^1\left(U^0\left(t,x\right)\right)\right|-\mathscr{L}_{min}}{\mathscr{L}_{max}-\mathscr{L}_{min}},1\right)\right)$$

with the two parameters $\mathscr{L}_{max}>\mathscr{L}_{min}\leq 0$. $\mathscr{L}_{min}$ is the tolerance within which the coarse model is considered acceptable. $\mathscr{L}_{max}$ is the distance from which the projection to the linear subspace of the fine model occurs. Setting $\mathscr{L}_{max}=\tau$ will result in the estimator creating two subdomains, each solved by its respective model. However, since the projection is not local, this setting will lead to a significant error at the interface. Using a larger $\mathscr{L}_{max}$ will create a thick interface where the error gradually decreases, see Figure 2.17.

It is worth noting that this strategy requires the computation of the coarse model throughout the entire domain. If the fully hyperbolic model, i.e., without projection, is used as the coarse model, its calculation is necessary regardless, see §2.3.1. Additionally, it may be beneficial to use an incremental pressure correction in the coarse model, see §2.3.2.1 to reduce the error before the correction step.

2.4.3 Fully dispersive model

The projected hyperbolic models presented in §2.2 are based on the principle that the constraint of these models must be a linear application of the kinetic unknown U, with parameters potentially dependent on space (see §2.4.1), and also non-linearly dependent on the potential unknown H. This insight allows us to modify the constraint of the model to improve certain relationships without compromising energy conservation. Here, we focus on adjusting the dispersion relation to be as close as desired to the Airy relation (2.5).

Consider the Green-Naghdi model (2.13) on a flat bottom (for simplicity) with the modified constraint

$$\mathscr{L}_H\left(U\right)=\begin{pmatrix}\overline{w}+\alpha\left(x,h\right)h\nabla\cdot\overline{u}\\ \widetilde{w}+\gamma\left(x,h\right)h\nabla\cdot\overline{u}\end{pmatrix}. \tag{2.84}$$

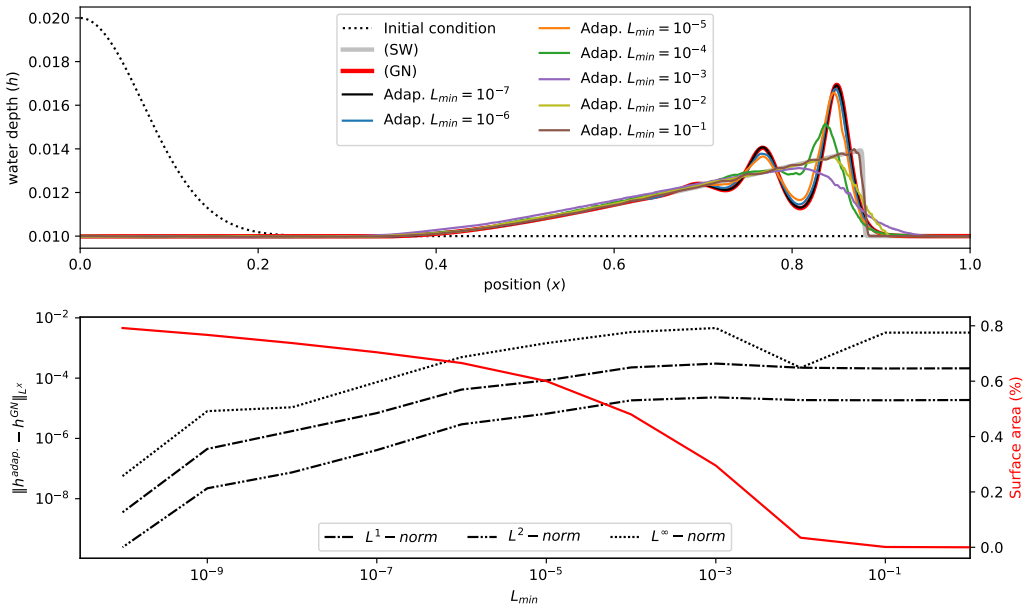

Figure 2.17: §2.4.2 | - Top line: Evolution of a Gaussian at rest with the Green-Naghdi model (2.13), the shallow water model (2.6) and the adaptive model with several value of $\mathscr{L}_{min}$ and $\mathscr{L}_{max} = 2\mathscr{L}_{min}$
- Bottom line: difference between the adaptive model and the Green-Naghdi model (2.13) in several norms (black line) and pourcentage of the surface area in the time-space plan of the domain where the projection occurs.

If $(\alpha,\gamma) = \left(\frac{1}{2}, \frac{1}{2\sqrt{3}}\right)$, we recover the constraint of the Green-Naghdi model (2.14). The parameters α and γ can be functions of the water depth h, which does not affect energy conservation Proposition 2.9, except through the definition of the energy. By computing the dispersion relation of the model with the constraint (2.84), we obtain:

$$v^{\mathrm{GN}}_{p,\alpha^2+\gamma^2} = \sqrt{\frac{1}{1+((\alpha(x,h))^2+(\gamma(x,h))^2)\,|kD|^2}}\sqrt{gD}. \tag{2.85}$$

It follows that we can exactly match the Airy phase velocity by setting

$$(\alpha(x,h))^2+(\gamma(x,h))^2 = \mathfrak{f}\left(\widehat{k}(x,h)\right) \qquad \text{with} \qquad \mathfrak{f}\left(\widehat{k}\right) = \frac{\widehat{k}-\tanh\left(\widehat{k}\right)}{\widehat{k}^2\tanh\left(\widehat{k}\right)}$$

where $\widehat{k} : \mathbb{R}^d \times L^2\left(\mathbb{R}^d\right) \mapsto \mathbb{R}$ is the local wavenumber of the water depth h. To define the parameters, we propose to maintain their ratio, i.e.

$$\alpha(x,h) = \sqrt{\frac{3}{4}}\sqrt{\mathfrak{f}\left(\widehat{k}(x,h)\right)} \qquad \text{and} \qquad \gamma(x,h) = \frac{1}{\sqrt{4}}\sqrt{\mathfrak{f}\left(\widehat{k}(x,h)\right)}$$

so that the model (2.84) corresponds to the Green-Naghdi model (2.14) in the small wavenumber limit. The local wavenumber corresponds to the wavenumber of the monochromatic signal that "*best*" fits the water depth h locally. Several definitions can be given, and the phase velocity (2.85) matches the Airy phase velocity (2.5) if and only if the local wavenumber corresponds to the wavenumber for a monochromatic input.

In practice, we propose to define the local wavenumber using a weighted Fourier transform as the smallest wavenumber with the largest energy, i.e.

$$\widehat{k}(x,h) = \min\left\{ \left| \arg\max_{k\in\mathbb{R}^d} \left| \int_{\mathbb{R}^d} (h(\widetilde{x}) - D(\widetilde{x}))\, e^{ik\widetilde{x}} \widehat{\nu}(|x-\widetilde{x}|)\, \mathrm{d}\widetilde{x} \right|^2 \right| \right\} \tag{2.86}$$

where $\widehat{\nu}(x) : \mathbb{R}^d \mapsto \mathbb{R}_+$ is a weight with compact support see Figure 2.18. In practice, we use a rectangular function or a truncated Gaussian. This strategy bears some similarity to the fully dispersive Green-Naghdi model proposed in [DIT16, Eme21, DK22], where a Fourier multiplier is used to obtain the Airy phase velocity (2.5). However, the strategy described above only requires the estimation of parameters using the Fourier transform, rather than employing a spectral method.

To test the fully dispersive model, we propose to compute numerically the phase velocity. In a long channel, we generate a wave using a sinusoidal water depth boundary condition, using the coupling strategy (2.4.1). After the signal has propagated, we record it once at a given instant in a spatial window, and again at a fixed position along a temporal window. Using a Fourier transform, the first signal allows us to obtain the wave number of the signal and the second the angular frequency. In Figure 2.19, the results has been plotted for the classical Green-Naghdi (2.13) (Red diamond points), the Green-Naghdi model where the vectorial space parameters are tune to correspond to the water depth boundary condition signal (Bleu circle points) and Green-Naghdi model where the vectorial space parameters are automatically estimated using the local water number (2.86). The results are in good agreement with the Airy phase velocity (2.5).

2.5 Perspectives

In this chapter, we present a general framework for the dispersive approximate models of water waves, focusing on their formulation and structure. While this framework advances our understanding, several significant questions remain open and, in my view, demand further investigation to achieve a more comprehensive understanding of these models and their practical utility.

First and foremost, establishing a clear and robust criterion for determining the well-posedness of models within the projected hyperbolic framework (2.38) is essential. In the literature, models such as the BBM model (2.33) and the Green-Naghdi model (2.13) have undergone extensive analysis, with their well-posedness conditions clearly defined. However, a generalization of this analysis, particularly one that leverages the projection structure of the model, could provide deeper insights. By following similar methods used for incompressible flow analysis, such as those found in the work of [Lio13], we might

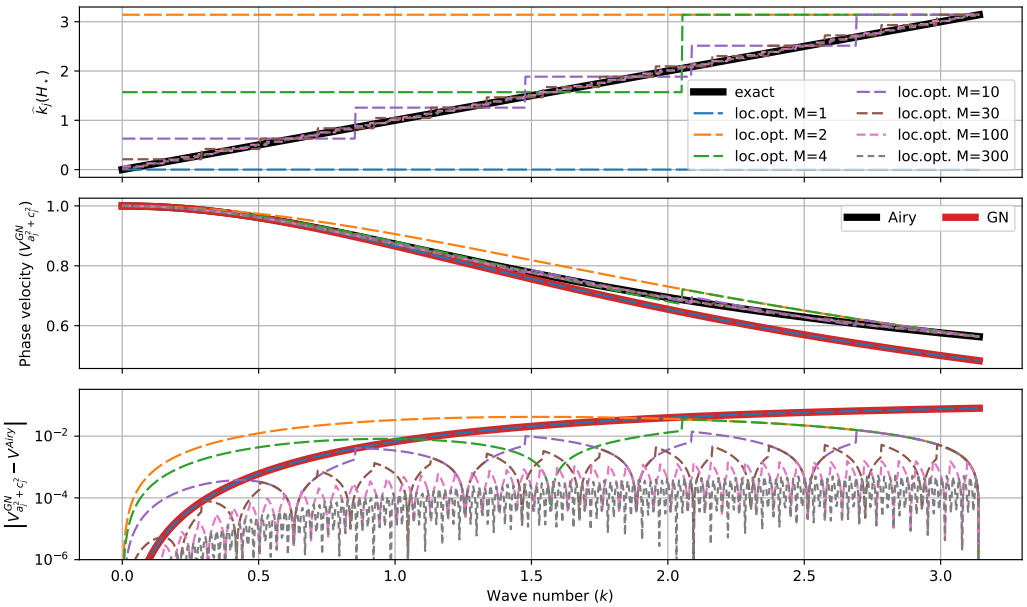

Figure 2.18: §2.4.3 | Wavenumber estimation (top line) depending on the size of the support of the weight $\widehat{\nu}$, corresponding phase velocity (middle line), and error compared to the Airy phase velocity (2.5) (bottom line).

extend these results to more complex models like the VAM model (2.16) or the layerwise Green-Naghdi model (2.19). These inquiries could be addressed in both unbounded and bounded domains by building on techniques developed for defining boundary conditions in the incompressible Euler equations and adapting them to the projected hyperbolic models.

Another important area of research concerns the characterization of weak solutions for dispersive models. In most cases, particularly with the Green-Naghdi model (2.13), well-posedness is guaranteed only within a finite time frame. As non-linearities come into play, the solutions tend to lose regularity over time, especially when the regularity is insufficient to define the mechanical energy flux. At this point, the solution exits the domain where all terms are well-defined, creating significant mathematical challenges. This issue is not unique to dispersive models; it also arises in hyperbolic systems. In conservative hyperbolic models, the Rankine-Hugoniot relation, combined with the Lax criterion, is commonly employed to define weak solutions. This raises the question: Is it possible to establish a similar criterion for dispersive models to characterize the solutions after they lose regularity? Some pioneering work in this area [Yin04, GS22]. This question, although theoretical, holds practical importance. Numerical simulations, especially those based on the projection strategy (2.3.1), often provide solutions beyond the theoretical time of existence, offering *"computed solutions"* even when regularity is lost. A key issue then becomes understanding the relationship between these numerically computed solutions and the actual solution of the model, and determining in what sense these computed solutions approximate the true solutions. Additionally, if these solutions exhibit energy

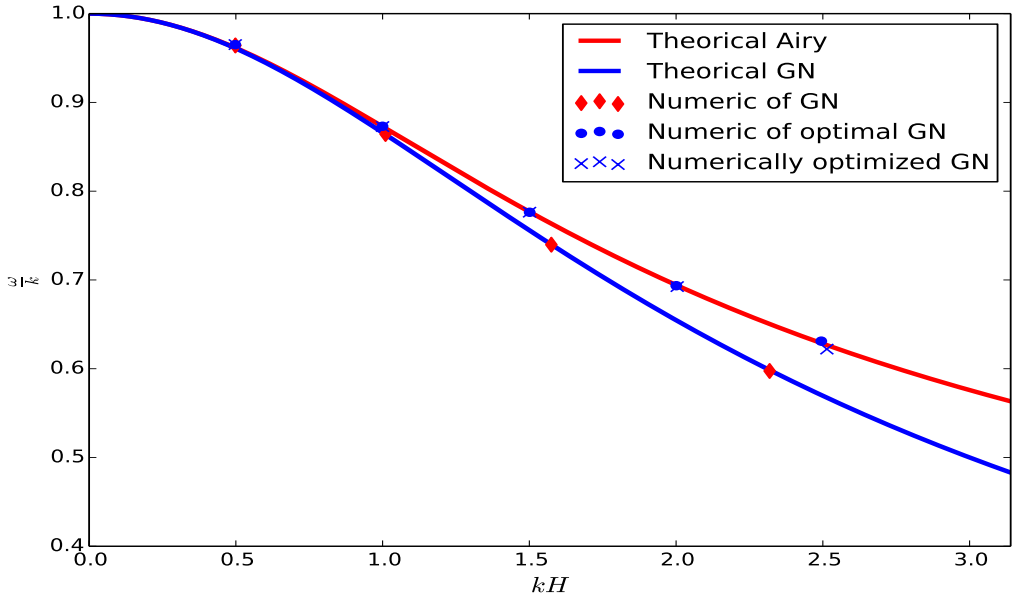

Figure 2.19: §2.4.3 | Theoretical and numerical estimation of the phase velocity.
- Solid red line: Airy phase velocity (2.5)
- Solid blue line: Green-Naghdi phase velocity (2.15)
- Red diamond points : Numerical estimation of the Green-Naghdi phase velocity
- Bleu circle points : Numerical estimation of the phase velocity with optimal vectorial space setting
- Bleu cross points : Numerical estimation of the phase velocity with computed vectorial space setting

dissipation, could they serve as a means of modeling wave breaking, as is sometimes the case with weak solutions in hydrostatic models? Energy dissipation processes in dispersive models are especially important in this context for accurately modeling wave breaking phenomena, as explored in works like [Zel91, KK92, MSS97b, MSS97a, SSM98, KCKD00, RCK10, CBB10, SKH+12, KDS14, RG15, RDF18, KR18, KR19b, Bon23].

From a practical perspective, one of the main obstacles limiting the widespread application of dispersive models is their computational expense. High-order numerical schemes and adaptive mesh refinement are crucial in addressing this challenge. These methods help ensure accuracy while reducing computational costs. Furthermore, model adaptation techniques can be developed to minimize unnecessary computations, and better a priori estimators than those presented in §2.4.2 could potentially be designed. Well-balanced schemes are also of particular interest, as they minimize numerical diffusion, especially around steady states. Yet, many real-world applications do not involve steady states or trivial rest states, but rather configurations that can be viewed as compositions of solitary

waves. Developing well-balanced schemes that preserve not just steady states, but also analytical solutions, those that can be computed using simple ODE solvers, could be particularly valuable, as they would ensure the local preservation of solitary waves in a wide range of applications.

Another interesting avenue for exploration involves the application of Thomas-Raviart-type discretization methods. These methods, where the degrees of freedom naturally satisfy the model constraints, could prove to be a powerful tool for improving the stability and efficiency of numerical schemes. Such discretization approaches have the potential to enhance both computational accuracy and stability by aligning the numerical degrees of freedom with the underlying physical constraints. However, when dealing with Boussinesq-type projected hyperbolic models (2.38), the challenge becomes more intricate. The Thomas-Raviart basis in these models depends on potential unknowns H, adding an additional layer of complexity and making the approach less straightforward. This dependency introduces new challenges in implementation and requires further investigation to develop effective numerical strategies.

In summary, while much progress has been made in the development and analysis of dispersive approximate models for water waves, a number of important questions remain. Addressing these open questions will be crucial for advancing both the theoretical understanding of these models and their practical application, especially in complex real scenarios involving wave breaking, stiff forcing terms and formation of shear.

CHAPTER 3

Water within its surroundings

"Détrompez-vous.
Un bateau n'est pas plus grand ou plus petit,
selon qu'il se trouve au creux ou au sommet de la vague."
Proverbe Breton

Contents

Contributions related to the chapter

[GPZ14] This work is dedicated to the modeling of exchanges between a river and its surrounding floodplains during floods overflowing its bed. Modeling flows in each subdomain, that of the river and that of the floodplain, has been the subject of numerous works for over 50 years and is now well understood. A coupling strategy is considered in order to preserve the advantages of 1D and 2D models in their respective subdomains. In comparison with other transverse coupling strategies already presented in the literature, we introduce a direct method, without overlapping the models or introducing numerical parameters. This strategy is based on the resolution of the Riemann 2D problem at the coupling interface (the bank) and requires the estimation of the transverse velocity close to the interface. We propose a model of transverse velocity using successive resolutions of Riemann problems. Then, we present a numerical resolution of the coupling system, based on a finite volume method for any Riemann solvers. Particular attention was given to the essential properties of the model (conservation of mass, positivity of water depth, and well-balanced scheme). Lastly, the precision and efficiency of the method are illustrated using examples of simulations.

[PV16] This paper is devoted to a centered ImEx scheme in a multidimensional framework for a wide class of multicomponent and isentropic flows. The proposed strategy is based on a regularized model where the advection velocity is modified by the gradient of the potential of the conservative forces in both mass and momentum equations. The stability of the scheme is ensured by the dissipation of mechanic energy, which stands for a mathematical entropy, under an advective CFL condition. The main physical properties, such as positivity, conservation of the total momentum, and conservation of the steady state at rest, are satisfied. In addition, asymptotic preserving properties in the regimes (“incompressible” and “acoustic”) are analyzed. Finally, several simulations are presented to illustrate our results in a simplified context of oceanic flows in one dimension.

[GPSMW18] We are interested in the modeling and the numerical approximation of flows in the presence of a roof, for example flows in sewers or under an ice floe. A shallow water model with a supplementary congestion constraint describing the roof is derived from the Navier-Stokes equations. The congestion constraint is a challenging problem for the numerical resolution of hyperbolic equations. To overcome this difficulty, we follow a pseudo-compressibility relaxation approach. Eventually, a numerical scheme based on a finite volume method is proposed. The well-balanced property and the dissipation of the mechanical energy, acting as a mathematical entropy, are ensured under a non-restrictive condition on the time step in spite of the large celerity of the potential waves in the congested areas. Simulations in one dimension for transcritical steady flow are carried out and numerical solutions are compared to several analytical (stationary and non-stationary) solutions for validation.

[GPSMW20] We consider the floating body problem in the vertical plane on a large space scale. More precisely, we are interested in the numerical modeling of a body floating

freely on the water such as icebergs or wave energy converters. The fluid-solid interaction is formulated using a congested shallow water model for the fluid and Newton's second law of motion for the solid. We make a particular focus on the energy transfer between the solid and the water since it is of major interest for energy production. A numerical approximation based on the coupling of a finite volume scheme for the fluid and a Newmark scheme for the solid is presented. An entropy correction based on an adapted choice of discretization for the coupling terms is made in order to ensure a dissipation law at the discrete level. Simulations are presented to verify the method and to show the feasibility of extending it to more complex cases.

[ABP21] The present paper deals with the modeling and numerical approximation of bed load transport under the action of water. A new shallow water type model is derived from the stratified two-fluid Navier–Stokes equations. Its novelty lies in the magnitude of a viscosity term that leads to a momentum equation of elliptic type. The full model, sediment and water, verifies a dissipative energy balance for smooth solutions. The numerical resolution of the sediment layer is not trivial since the viscosity introduces a non-local term in the model. Adding a transport threshold makes the resolution even more challenging. A scheme based on a staggered discretization is proposed for the full model, sediment and water.

[ACSE+21] In this paper, we analyze the relevance of the use of the shallow water model and the Boussinesq model to simulate tsunamis generated by a landslide. In a first part, we determine if the two models are able to reproduce waves generated by a landslide. Each model has drawbacks but it seems that it is possible to use them together to improve the simulations. In a second part we try to recover the landslide displacement from the generated wave. This problem is formulated as a minimization problem and we limit the number of parameters to determine assuming that the bottom can be well described by an empirical law.

[Par23] This work is concerned with the modeling and numerical resolution in a multidimensional framework of the interaction between the congested shallow water model and a polytropic air pocket dynamics. A weak coupling strategy is used, and the connectivity of the air pockets is obtained by comparing the horizontal support of the pockets. The relevance of the model and the robustness of the numerical strategy are illustrated by several numerical simulations in a one-dimensional framework. In particular, the method seems well suited to the numerical study of the hydraulics of underground rivers and coastal caves, such as the Cosquer Cave, and to the simulation of marine energy converters, such as the oscillating water column.

[Par24a] The current study is dedicated to the formal derivation of a hierarchic of asymptotic models that approximate the groundwater waves problem within the Dupuit-Forchheimer regime, over a regular, non-planar substratum. The derivation methodology employed bears resemblance to the techniques utilized in hierarchic of asymptotic models for approximating the water waves problem in the shallow water regime. Mathematically speaking, the asymptotic models manifest as nonlinear, non-local

diffusion equations. We identify an energy dissipation law inherent to these models, thereby bolstering the physical validity and confidence in the proposed framework. A numerical strategy is proposed that preserved at the discrete level the energy dissipation. Several simulations are conducted to discuss and validate the dynamic behavior of the solution.

[CP] This paper addresses the modeling and numerical approximation of exchanges between surface water and groundwater flow at the scale of a drainage basin. For large-scale simulations, approximate models are often employed for geophysical flows such as rivers, lakes, or coastal areas. The shallow water model is commonly used for surface flows, while the Dupuit-Forchheimer model is well-established for groundwater flows. Due to the differing mathematical characteristics and the fact that the flows overlap in the computational domain, coupling them is challenging. We propose a unified model that simultaneously treats surface water and groundwater. We demonstrate an energy dissipation law and present an entropy-satisfying numerical scheme. Several simulations are performed to analyze and validate the dynamic behavior of the solution.

[BBP] Wave energy is a promising and largely untapped source of clean energy. This paper examines a novel approach to study how wave energy converters (WECs) interact with ocean waves. Accurate models are needed to understand these interactions, but there's a balance between how detailed a model is and how much computing power it needs. This research uses both detailed Navier-Stokes equations and simpler Boussinesq models to create a combined approach. This method improves accuracy in studying local wave-structure interactions while remaining efficient for larger areas. The results can help improve the design and effectiveness of WECs, contributing to the use of wave energy in addressing climate change and energy resource challenges.

[KLP] This article presents the development of a second-order numerical method for the Shallow Water model specifically designed for the low-Froude regime. Numerical schemes that are well-suited for the low-Froude regime are typically implicit at least for some unknown and nonlinear, commonly referred to as ImEx schemes. High-order time integration methods, such as Runge-Kutta, necessitate solving an implicit nonlinear problem at each time sub iterations, which can limit their efficiency. In this work, we propose a second-order scheme that requires only a single implicit solve per time step. We demonstrate the method's efficiency by comparing it to explicit methods and other second-order ImEx schemes.

This chapter concentrate on fluid dynamics within its surrounding environment. By *surroundings*, we refer to structures that impose constraints, particularly on the flow regime. Our focus remains on geophysical applications, characterized by large time and space scales, which require approximated models of fluid dynamics, as presented in §2. The primary applications discussed will include marine energy §3.1 and water resources §3.2.

3.1 Fluid/structure interactions with vertical-averaged models

This section aims to propose models of wave/structure interactions to the simulation of marine energy converters. A well-established model for describing fluid/structure interactions is based on the Navier-Stokes equations, which govern fluid motion. This approach is extensively applied in areas such as blood flow, particularly in simulations of aortic flow [CPP13, QTV00]. Additionally, Navier-Stokes computational fluid dynamics simulations are used for modeling the flow around objects like yachts, fish, and wave energy converters [WT03, PQ05, AWvJ08, PEMPB13, YL13, BHI14, BI16]. At the interface between the fluid and the solid, two primary methods are employed: a moving grid with front-tracking techniques or a fixed mesh with a fictitious fluid domain. The moving grid method accurately captures the interface but requires a dynamic mesh, whereas the fixed mesh approach offers a stable mesh at the expense of precision in tracking the interface position. Despite their advantages, the Navier-Stokes equations are computationally intensive and impractical for large space and time scales, making them unsuitable for long-term simulations, such as assessing the operational efficiency of a marine energy converter farm over several days.

One of the first significant contributions to approximate models for Fluid/structure interactions was made by Fritz John, who introduced a mathematical formulation of the problem [Joh49, Joh50]. In this model, the fluid is represented by a linear potential flow, with the evolution of the free surface described by a linear model. The motion of the solid is assumed to be of small amplitude, allowing the interface between the water and the solid to remain constant over time. The surface pressure is then determined using the linearized Bernoulli equation. Although this model is relatively simplified, linear potential flow theory is still widely used in industrial applications due to its low computational cost [MBB$^+$12, BD15]. However, nonlinear terms play a significant role in wave propagation. Advances have been made to incorporate time-dependent interfaces [Kas00] and nonlinear effects using boundary element methods [HKP$^+$17], though these improvements require significantly higher computational resources.

Instead of relying on linear potential flow, it can be more appropriate to use a vertically-integrated model (see §2) as the foundation for fluid dynamics. However, the presence of a structure within the domain significantly alters the flow regime and the mathematical structure of the equations, necessitating specialized numerical techniques. Some of these techniques are described in the following sections.

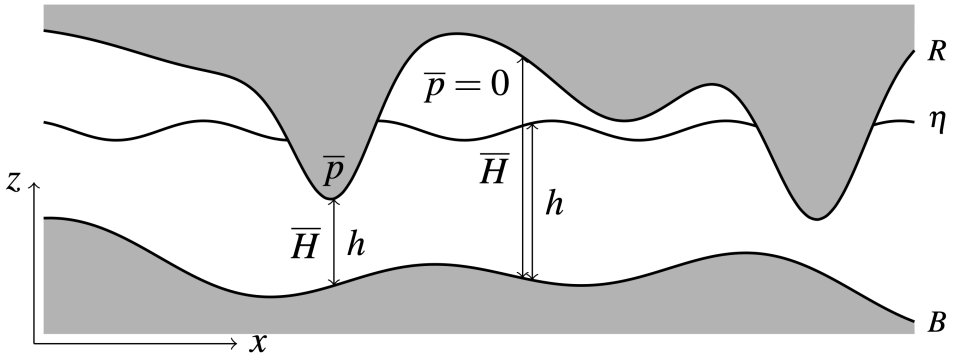

Figure 3.1: §3.1.1 | Illustration of the partially free surface problem and the unknown of the congested shallow water model in the vertical plane.

3.1.1 Roof modeling in free surface flow

3.1.1.1 Congested models

Before addressing the case of a freely floating body, the initial step is to consider a flow with a free surface constrained by an upper boundary, referred to as the roof, $R(t,x) \geq B(x)$ (see Figure 3.1 for an illustration of the problem). This type of flow is typically observed in scenarios such as water movement in underground rivers or partially filled pipes. Specifically, we consider the incompressible free surface Euler model (2.1)-(2.2)-(2.3)-(2.4), with the additional unilateral non-penetration condition at the roof, defined as

$$\partial_t R + u_{|_{z=R}} \cdot \nabla R - w_{|_{z=R}} \geq 0.$$

This condition is similar to the no-penetration condition (2.3) and serves to prevent the flow from penetrating the roof. However, unlike the standard no-penetration condition (2.3), this condition allows for the possibility of flow detachment from the roof, which is why it is expressed as an inequality. In the specific case of a horizontal steady roof, the vertical velocity at the roof cannot be positive, as this would imply penetration through the roof, but it may be negative. This type of constraint is known as a unilateral condition and has been previously proposed, particularly in the context of gas dynamics [BBCR00, Ber02, BB03, PZ15].

To develop approximate models in the spirit of those described in §2.1, two approaches can be considered. The first approach can be categorized as a coupling strategy between the free surface and the pressurized regions [Kas00, Lan17]. The primary advantage of this method lies in the ability to compute the surface pressure induced by the roof using an elliptic equation. Additionally, this approach allows each sub-domain to be solved using the most appropriate numerical techniques. However, it requires the assumption of a sufficiently smooth flow to establish transmission conditions at the coupling interface, an assumption that is not always met (see Figure 3.6). Moreover, this strategy necessitates the precise description of the interface position, which is a significant challenge since the interface is closely tied to the flow dynamics. In most cases, this strategy is applied in

scenarios where the interface between the free surface region and the pressurized region is vertical, thereby fixing the position of the interface [BEKER19, Boc19, Boc20].

The second strategy involves the development of a unified model across the entire domain [TD90, Fua02, BG07, BG08, BEG12, BEG14, GPSMW18]. By applying the method described in §2.1 to obtain approximate models for water waves, we derive approximate models in the shallow water regime with an additional unknown variable, $\overline{p}(t,x)$, representing the pressure exerted by the roof, along with a congestion constraint. In the case of the shallow water model with a roof, the equations can be expressed as

$$\begin{aligned} \partial_t h + \nabla\cdot(h\overline{u}) &= 0 \\ \partial_t(h\overline{u}) + \nabla\cdot(h\overline{u}\otimes\overline{u}) &= -gh\nabla(B+h) - h\nabla\overline{p} \end{aligned} \tag{3.1}$$

with the congestion constraint

$$\min\left(\overline{H}-h,\overline{p}\right) = 0 \tag{3.2}$$

where $\overline{H}(t,x) = R(t,x) - B(x)$ is referred to as the opening. This strategy is advantageous because it eliminates the need to describe the interface position or impose transmission conditions at the interface. We also highlight the conservation of energy demonstrated in [GPSMW18].

Proposition 3.1 *The sufficiently regular solutions of* (3.1) *satisfy the following energy conservation law*

$$\partial_t(\mathscr{P}+\mathscr{K}) + \nabla\cdot\left(\left(gh(B+h) + \overline{p} + \frac{|\overline{u}|^2}{2}\right)h\overline{u}\right) = -\overline{p}\partial_t R$$

with $\mathscr{P} = gh\left(B+\frac{h}{2}\right)$ *and* $\mathscr{K} = \frac{h}{2}|\overline{u}|^2$.

The congestion constraint (3.2) ensures three conditions simultaneously: the water depth remains less than or equal to the opening $h \le \overline{H}$, the roof reaction is positive $\overline{p} \ge 0$, and the support of the roof reaction is confined to the region where the water reaches the roof, i.e., where $\overline{p}(t,x) > 0$ we have $h(t,x) = \overline{H}(t,x)$. This implies that there is effectively only one unknown in addition to the velocity, which is either the water depth in the free surface region or the pressure in the congested region. For practical purposes, it is useful to combine these into a single variable. The potential of conservative forces, $\phi(t,x) = g(B(x)+h(t,x)) + \overline{p}(t,x)$, can serve this role. The model (3.1) can be rewritten as:

$$\begin{aligned} \partial_t\left(\mathscr{H}\left[\overline{H},B\right](\phi)\right) + \nabla\cdot\left(\mathscr{H}\left[\overline{H},B\right](\phi)\overline{u}\right) &= 0 \\ \partial_t\left(\mathscr{H}\left[\overline{H},B\right](\phi)\overline{u}\right) + \nabla\cdot\left(\mathscr{H}\left[\overline{H},B\right](\phi)\overline{u}\otimes\overline{u}\right) &= -\mathscr{H}\left[\overline{H},B\right](\phi)\nabla\phi \end{aligned} \tag{3.3}$$

where $\mathscr{H}\left[\overline{H}(t,x),B(x)\right](\phi(t,x))$ represents the mapping that gives the water depth as a function of the potential, i.e. $h(t,x) = \mathscr{H}\left[\overline{H}(t,x),B(x)\right](\phi(t,x))$ with $\mathscr{H}\left[\overline{H},B\right](\phi) = \min\left(\frac{\phi}{g}-B,\overline{H}\right)$ see Figure 3.2. The pressure can then be determined as $\overline{p}(t,x) = P\left[\overline{H}(t,x),B(x)\right](\phi(t,x))$ with $P\left[\overline{H},B\right](\phi) = \phi - \mathscr{H}\left[\overline{H},B\right](\phi)$. It is important to note that the constraint (3.2) is inherently included in the definition of

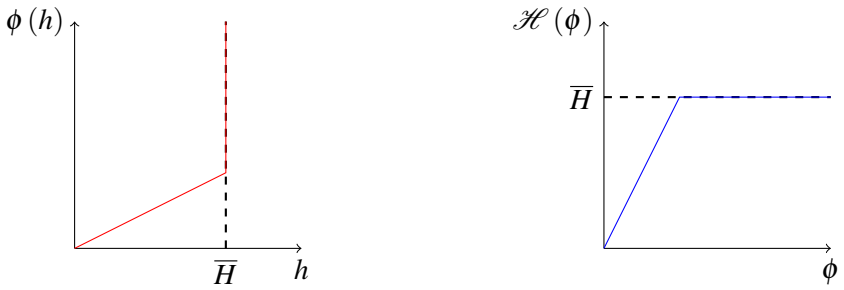

Figure 3.2: §3.1.1.1 | Illustration of the change of variables. (Left) Original variables and multivalued potential. (Right) New variables.

the water depth function $\mathscr{H}\left[\overline{H},B\right](\phi)$. Thus, the model (3.3) no longer requires an explicit constraint but an additional non-linearity has been introduce through the function $\mathscr{H}$.

The shallow water model with a roof is not the only model that incorporates a congestion constraint. Several other models also address congestion in different contexts:

- A congested gas dynamics [BBCR00, Ber02, BB03, PZ15] is used in several context for complexe rheology to flow in porous media [BC17] and §3.2. For a mathematical analysis of the model in the viscous case, see [PZ15, Per18].
- In [DNBS10, MRCS10], a model of crowd motion with congestion is considered.
- Some bio-mathematical models use a congestion constraint for chemotaxis dynamics [Per04] or tumor growth [DMC20].
- Various models of traffic flow incorporate congestion constraints, including those discussed in [AR00, BGC03, CP05, BDLB$^+$08, BDDR08, BB12].

A simplest congested model reads

$$\begin{aligned}\partial_t\rho+\nabla\cdot(\rho u) &= S(t,x,\rho)\\ u &= U(t,x,\rho)-\kappa\nabla(p(\rho)+\overline{p})\\ \min\left(\overline{R}-\rho,p\right) &= 0\end{aligned}$$

with S is a growth rate, used for tumor growth, $U(t,x)$ is the wanted velocity, used for crowd motion and $p(\rho)$ is a pressure used for porous media (Darcy law). Assuming $p(\rho)$ strictly increasing hence invertible, the density can be see as a function of the potential $\phi=p(\rho)+\overline{p}$ as in the shallow water case. In the case without internal pressure $p(\rho)=0$, an auxiliary variable is required. We use $\sigma=\rho+\overline{p}$ as unknown, and we set $\rho(t,x)=R(\sigma(t,x))$ with $R(\sigma)=\min\left(\overline{R},\sigma\right)$ and $\overline{p}(t,x)=P(\sigma(t,x))$ with $P(\sigma)=\sigma-R(\sigma)$. This auxiliary variable can be see as the curvilinear coordinates of the curve ϕ as function of ρ. The simplest congested model reads

$$\begin{aligned}\partial_t(R(\sigma))+\nabla\cdot((R(\sigma))u) &= S(t,x,R(\sigma))\\ u &= U(t,x,R(\sigma))-\kappa\nabla(p(R(\sigma))+\sigma-R(\sigma)).\end{aligned}$$

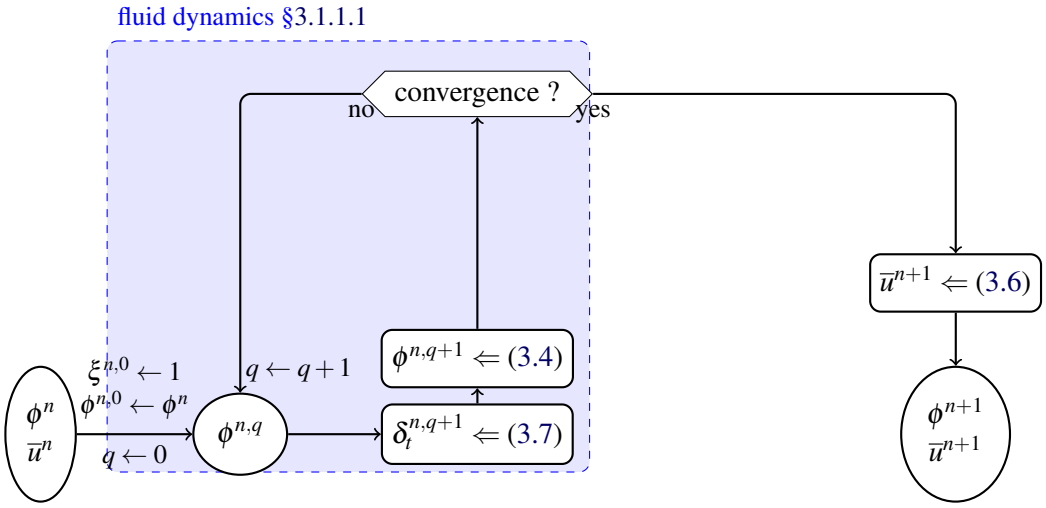

Figure 3.3: §3.1.1.2 | Flowchart of a time steps of scheme (3.4)-(3.6).

3.1.1.2 Entropy-satisfying numerical scheme

Due to its unilateral nature, the space generated by the constraint (3.2) is not a linear subspace [MRCS10]. While prediction/correction methods, such as the projection strategy employed in §2, can be used (see [MP17]), this approach is not straightforward. After its reformulation in (3.3), the model becomes a nonlinear PDE system. However, in congested areas, i.e. under structures, the flow behaves in an incompressible regime, analogous to gas dynamics, while in free surface regions, the flow is compressible. In the specific regime of incompressible flow, numerical schemes are designed as low-Mach schemes in the literature, drawing further parallels with gas dynamics, and is well-documented, see [CC92, Cas99, RM00, LG08, Del10, Rie11, HJL12, CDK12, GVV13, LG13, CGK13, Cas14, PV14, HKL14, PV16, DJOR16, BEK+17, DLV17, CKS19, GLM20, BRMVCD21, Bar21, BD22, BHL24]. In [GPSMW18], we propose a numerical scheme for floating body simulations based on the low-Mach scheme developed in [PV16]. A similar strategy is also employed in [BD23].

To avoid a restrictive CFL condition, we will implement an implicit scheme for the potential unknown and an explicit scheme for the kinetic unknown. This type of scheme is commonly known as an ImEx (Implicit-Explicit) scheme in the literature. There is also a fully explicit version of the scheme, as described in [CDV17], which shares the same stability properties, such as being entropy-satisfying and asymptotic-preserving in low-Mach regimes, but operates under a more restrictive CFL condition. To further generalize the scheme for arbitrary potential forces, the flow is decomposed into advection and potential force components. This approach is often referred to as the AUMS (Advection Upstream Splitting Method) scheme in the literature [LSJ93].

Let us first focus on the mass conservation equation, which is discretized using a three-point scheme. This scheme is implicit for the potential ϕ and explicit for the velocity $\overline{u}$,

and is represented as follows

$$\mathscr{H}_k^{n+1}\left(\phi_k^{n+1}\right) = h_k^n - \frac{\delta_t^{n+1}}{\mathfrak{m}_k}\sum_{f\in\mathbb{F}_k}\mathscr{F}_f^{n+1}\cdot\mathfrak{n}_f^k\mathfrak{m}_f \tag{3.4}$$

where $\mathscr{H}_k^n(\phi) = \mathscr{H}\left[\overline{H}_k^n, B_k\right](\phi)$ and $h_k^n = \mathscr{H}_k^n\left(\phi_k^n\right)$. The numerical mass flux

$$\mathscr{F}_f^{n+1} = \mathscr{F}_{CPR}\left(\delta_t^{n+1}, \begin{pmatrix}\mathfrak{d}_k\\ \mathscr{H}_k^{n+1}\left(\phi_k^{n+1}\right)\\ \phi_k^{n+1}\\ \overline{u}_k^n\end{pmatrix}, \begin{pmatrix}\mathfrak{d}_{k_f}\\ \mathscr{H}_{k_f}^{n+1}\left(\phi_{k_f}^{n+1}\right)\\ \phi_{k_f}^{n+1}\\ \overline{u}_{k_f}^n\end{pmatrix}\right)$$

is defined as

$$\mathscr{F}_{CPR}\left(\delta_t, \begin{pmatrix}\mathfrak{d}_L\\ \mathscr{H}_L\\ \phi_L\\ \overline{u}_L\end{pmatrix}, \begin{pmatrix}\mathfrak{d}_R\\ \mathscr{H}_R\\ \phi_R\\ \overline{u}_R\end{pmatrix}\right) = \frac{1}{2}\left(\mathscr{H}_L\overline{u}_L + \mathscr{H}_R\overline{u}_R - \gamma\delta_t\left(\frac{\mathscr{H}_L}{\mathfrak{d}_L} + \frac{\mathscr{H}_R}{\mathfrak{d}_R}\right)\frac{\phi_R - \phi_L}{2}\mathfrak{n}_f^L\right). \tag{3.5}$$

Here, $\mathfrak{d}_k$ represents the compactness of the cell, see §1.2. Next, the velocity is computed explicitly using an upwind scheme for the advection term and a centered scheme for the gradient of potential forces, as recommended in [Del10] for consistency with low-Mach regimes

$$\begin{aligned} h_k^{n+1}\overline{u}_k^{n+1} = h_k^n\overline{u}_k^n &- \frac{\delta_t^{n+1}h_k^{n+1}}{\mathfrak{m}_k}\sum_{f\in\mathbb{F}_k}\frac{\phi_k^{n+1}+\phi_{k_f}^{n+1}}{2}\mathfrak{n}_f^k\mathfrak{m}_f \\ &- \frac{\delta_t^{n+1}}{\mathfrak{m}_k}\sum_{f\in\mathbb{F}_k}\left(\overline{u}_k^n\left[\mathscr{F}_f^{n+1}\cdot\mathfrak{n}_f^k\right]_+ - \overline{u}_{k_f}^n\left[\mathscr{F}_f^{n+1}\cdot\mathfrak{n}_f^k\right]_-\right)\mathfrak{m}_f \end{aligned} \tag{3.6}$$

with the positive and negative parts of the function defined by $[\phi]_\pm = \frac{|\phi|\pm\phi}{2} \geq 0$.

In [PV16], it is demonstrated that the numerical scheme (3.4)-(3.6) satisfies entropy conditions under certain technical assumptions. The entropy-satisfying property is particularly noteworthy because it does not depend on the specific form of the potential of conservative forces, $\phi(x,h)$, allowing the scheme to be applied to a wide variety of models. The key requirement for this property is the existence of a convex potential energy function, $\mathscr{P}(x,h)$, such that $\partial_h\mathscr{P} = \phi$ and $\partial_h\phi \geq 0$.

Proposition 3.2 *Assume that the time step satisfies the following implicit CFL condition*

$$\delta_t^{n+1} \leq \frac{\min\left(\mathfrak{d}_k, \mathfrak{d}_{k_f}\right)}{2\nu_f} \text{ with } \nu_f = \frac{\left|\frac{h_k^{n+1}\overline{u}_k^n + h_{k_f}^{n+1}\overline{u}_{k_f}^n}{2}\cdot\mathfrak{n}_f^k\right| + \frac{h_k^{n+1}+h_{k_f}^{n+1}}{2}\sqrt{\frac{\gamma}{4}\left|\phi_{k_f}^{n+1} - \phi_k^{n+1}\right|}}{\min\left(h_k^{n+1}, h_{k_f}^{n+1}\right)}. \tag{3.7}$$

Hence for any $\gamma \geq 1$, the numerical scheme (3.4)-(3.6) is entropy-satisfying, i.e. there exists a numerical flux $\mathscr{G}_f$ (details in [PV16]) such that

$$\mathscr{P}_k^{n+1} + \mathscr{K}_k^{n+1} + \frac{\delta_t}{\mathfrak{m}_k}\sum_{f\in\mathbb{F}_k}\mathscr{G}_f\cdot\mathfrak{n}_f^k\mathfrak{m}_f \leq \mathscr{P}_k^n + \mathscr{K}_k^n$$

where $\mathscr{P}_k^n = \mathscr{P}\left(x_k, h_k^n\right)$ *and* $\mathscr{K}_k^n = \frac{h_k^n}{2}\left|\overline{u}_k^n\right|^2$. *Also, the numerical scheme is well-balanced for steady state at rest, i.e. If there exist* $\Phi \in \mathbb{R}$ *such that* $\phi_k^n = \Phi$ *and* $\overline{u}_k^n = 0$, *then the numerical scheme is steady, i.e. we have* $\phi_k^{n+1} = \Phi$ *and* $\overline{u}_k^{n+1} = 0$.

The method does not require complex computations, such as the estimation of eigenvalues, and it can be adapted to a wide range of physical models. The only requirement is the implementation of the water depth function $\mathscr{H}$ and its derivative, used in the fixed-point method, which varies depending on the physical context. Since the CFL condition in Proposition 3.2 is implicit, it must be verified after the computation. Additionally, because the first step of the scheme in (3.4) is non-linear and implicit, an iterative fixed-point method is required for computation. Using a quasi-Newton fixed-point method, quadratic convergence is typically observed in simulations without a roof. The numerical scheme (3.4)-(3.6) is illustrated in Figure 3.3.

This scheme is employed in [PV16] for simulations of the multi-layer shallow water model without exchanges (see §2.1.2.3 Following Material Interfaces), using five layers, as shown in Figure 3.4. For large time steps, the scheme (3.4)-(3.6) exhibits significant numerical diffusion at high frequencies, though the low frequencies are well-preserved. For small time steps, the wave amplitudes are well-maintained, although a shift in the wave position can be observed.

With the presence of a roof, the water depth function $\mathscr{H}$ is not differentiable, but hopefully only in a single point $\phi = g\left(B + \overline{H}\right)$. This is not a significant issue, and the numerical method can still be applied; however, the convergence of the fixed-point method becomes linear in this case. In Figure 3.5, the simulation of a flow transitioning to a supercritical regime due to the roof is compared, in the steady state, with the analytical solution derived from Bernoulli's principle. The results show good agreement for both the water depth h and velocity $\overline{u}$. However, the original scheme struggles to accurately capture the pressure $\overline{p}$ (Figure 3.5, curve $\lambda = 0$). There is an overestimation of the roof reaction $\overline{p}$ at the inlet the flow, followed by an underestimation further downstream. For applications where pressure is crucial, such as in the case of floating objects (see §3.1.2), this inaccurate pressure estimation makes the scheme unsuitable. To address this issue, a regularization of the water depth function $\mathscr{H}$ is introduced. We define

$$\mathscr{H}\left[\overline{H}, B\right](\phi) = \min\left(\widetilde{h}[B](\phi), \frac{\overline{H} + \lambda^2 \widetilde{h}[B](\phi)}{1+\lambda^2}\right) \quad \text{with} \quad \widetilde{h}[B](\phi) = \frac{\phi}{g} - B. \tag{3.8}$$

Other regularization methods can also be applied. The parameter $\lambda \geq 0$ can be interpreted as the extent of water penetration into the roof. Numerical experiments suggest setting $\lambda^2 = \mathfrak{d}_k$. With this adjustment, the pressure $\overline{p}$ is well-recovered, as shown in Figure 3.5.

In Figure 3.6, the simulation of a hydraulic jump interacting with the roof is shown. This simulation highlights the robustness of the scheme, as at the hydraulic jump, the water depth, roof reaction, and energy are all discontinuous. The reference solution plotted in Figure 3.6 corresponds to the steady-state solution without a roof, for both the water depth and velocity. The reference pressure is determined to ensure the correct hydraulic head under the roof. However, the exact location of the jump, is out of the reach of the classical

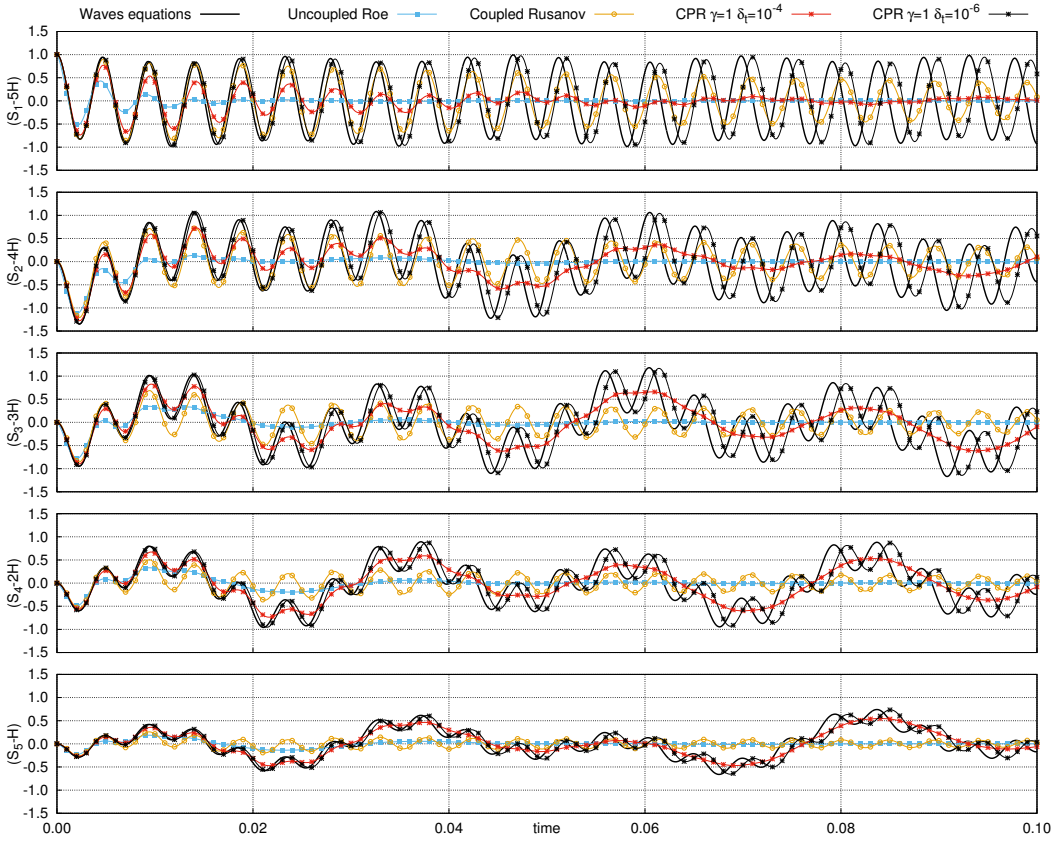

Figure 3.4: §3.1.1.2 | Simulation of oscillating surfaces: Comparison between the scheme (3.4)-(3.6) (CPR), classical Godunov schemes, and the asymptotic exacte solution of the asymptotic regime of waves equations. Figure taken from [PV16].

theory, which is based on the Rankine-Hugoniot relation, due to the non-conservative term $h\nabla\overline{p}$. Nevertheless, we observe good agreement in both the water depth h and velocity $\overline{u}$, and the regularization method ensures a reliable estimation of the pressure $\overline{p}$ as well.

Lastly, it is important to note that the congestion constraint can be incorporated into a more sophisticated fluid dynamics model. Specifically, the congested Green-Naghdi model, i.e. (2.13) with the addition of the roof reaction term as in (3.1) and the congestion constraint (3.2), can be effectively approximated using the numerical scheme (3.4)-(3.6) with the two addition unknowns $\overline{w}$ and $\widetilde{w}$ simply advected using the upwind scheme, and finally projected using the scheme (2.72).

3.1.1.3 Second order numerical scheme for congested models

The scheme (3.4)-(3.6) can be easily enhanced to second order in space by employing a MUSCL reconstruction in the upwind advection step [vL79]. However, improving the time discretization is more complex due to the implicit-explicit (ImEx) strategy used. High-order methods can be developed using two interconnected Butcher tableaux [DLMDV18,

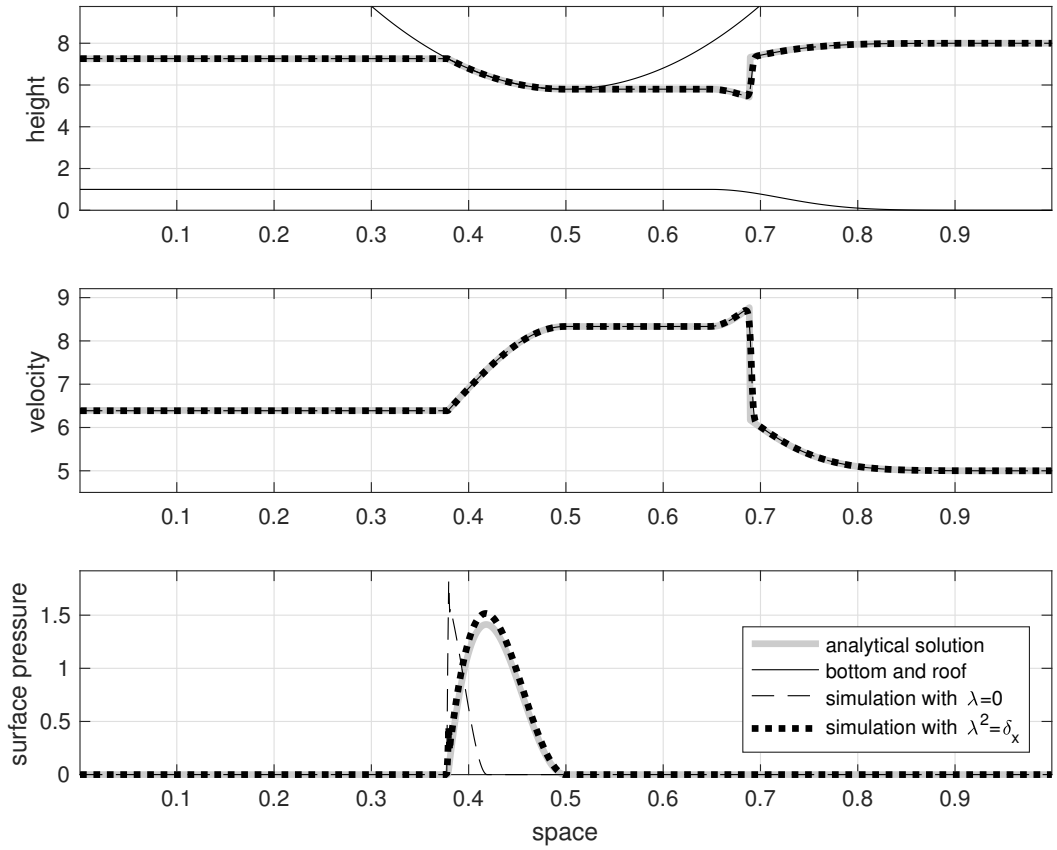

Figure 3.5: §3.1.1.2 | Steady flow passing into supercritical regime because of the roof. Figure taken from [GPSMW18].

BDL+20, MDT21]. While this approach theoretically allows for arbitrary order accuracy, it requires solving nonlinear systems like (3.4) multiple times per time step. For geophysical applications, it is often more practical to use a scheme that achieves second-order accuracy while minimizing the number of nonlinear systems that need to be solved. Our approach relies on a Crank-Nicolson scheme with a time extrapolation of the velocity to balance accuracy and computational efficiency. The implicit mass scheme reads

$$\mathscr{H}_k^{n+1} = h_k^n - \frac{\delta_t^{n+1}}{\mathfrak{m}_k} \sum_{f \in \mathbb{F}_k} \mathscr{F}\left(\delta_t^{n+1}, \frac{h_k^n \overline{u}_k^n + h_{k_f}^n \overline{u}_{k_f}^n}{2}, \begin{pmatrix} \mathfrak{d}_k \\ \mathscr{H}_k^{n+1/2} \\ \phi_k^{n+1/2} \end{pmatrix}, \begin{pmatrix} \mathfrak{d}_{k_f} \\ \mathscr{H}_{k_f}^{n+1/2} \\ \phi_{k_f}^{n+1/2} \end{pmatrix} \right) \cdot \mathfrak{n}_f^k \mathfrak{m}_f \tag{3.9}$$

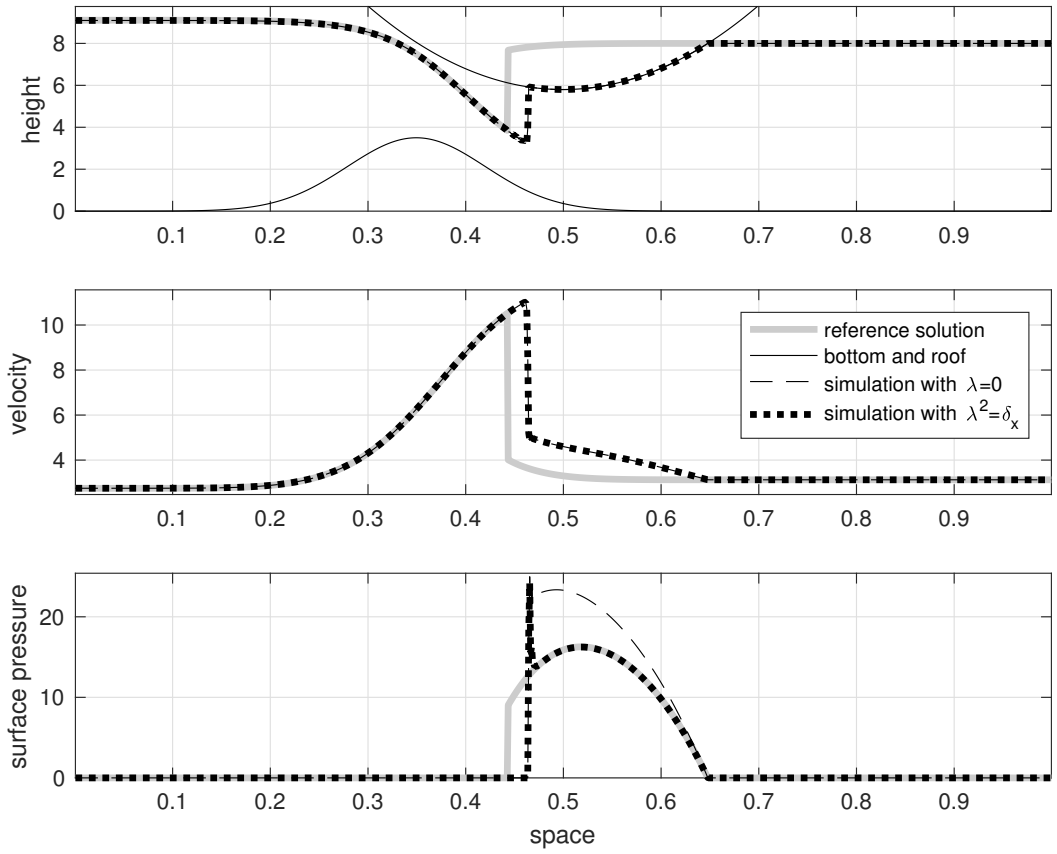

Figure 3.6: §3.1.1.2 | Steady flow with hydraulic jump hitting the roof. Figure taken from [GPSMW18].

with $\mathscr{H}_k^{n+1/2} = \mathscr{H}\left[\overline{H}_k^{n+1/2}, B_k\right]\left(\phi_k^{n+1/2}\right)$ and $\phi_k^{n+1/2} = \frac{\phi_k^n + \phi_k^{n+1}}{2}$. The numerical flux reads

$$\mathscr{F}\left(\delta_t, Q, \begin{pmatrix}\mathfrak{d}_L\\ \mathscr{H}_L\\ \phi_L\\ \overline{u}_L\end{pmatrix}, \begin{pmatrix}\mathfrak{d}_R\\ \mathscr{H}_R\\ \phi_R\\ \overline{u}_R\end{pmatrix}\right) = Q - \gamma\frac{\delta_t}{2}\left(\frac{\mathscr{H}_L}{2\mathfrak{d}_L} + \frac{\mathscr{H}_R}{2\mathfrak{d}_R}\right)\frac{\phi_R - \phi_L}{2} - \frac{\delta_t}{\mathfrak{d}_L + \mathfrak{d}_R}\left(\overline{u}_L \max\left(0, Q\cdot\mathfrak{n}_f^k\right) + \overline{u}_R \min\left(0, Q\cdot\mathfrak{n}_f^k\right)\right).$$

Once the new potential and water depth is known, the velocity is computed with the same type of scheme than (3.6), i.e.

$$\begin{aligned} h_k^{n+1}\overline{u}_k^{n+1} = {} & h_k^n\overline{u}_k^n - \frac{\delta_t^{n+1}h_k^{n+1/2}}{\mathfrak{m}_k}\sum_{f\in\mathbb{F}_k}\frac{\phi_k^{n+1/2} + \phi_{k_f}^{n+1/2}}{2}\mathfrak{m}_f \\ & - \frac{\delta_t^{n+1}}{\mathfrak{m}_k}\sum_{f\in\mathbb{F}_k}\left(\underline{\widetilde{\overline{u}_k^{n+1/2}}}_f \max\left(0, \mathscr{F}_f^{n+1/2}\cdot\mathfrak{n}_f^k\right) + \underline{\widetilde{\overline{u}_{k_f}^{n+1/2}}}_f \min\left(0, \mathscr{F}_f^{n+1/2}\cdot\mathfrak{n}_f^k\right)\right)\mathfrak{m}_f \end{aligned} \tag{3.10}$$

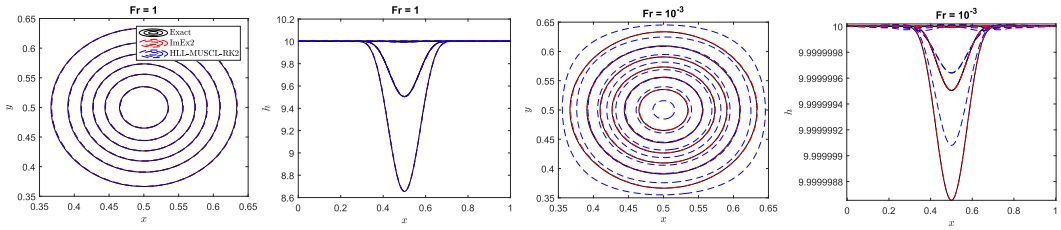

Figure 3.7: §3.1.1.3 | Simulation of the traveling vortex with the second order schemes (3.9)-(3.10) (in red) and the explicit HLL-MUSCL-RK2 (in blue) compare to the analytical solution (in black) for $F_r = 1$ and $F_r = 10^{-3}$.

with $\mathscr{F}_f^{n+1/2} = \mathscr{F}\left(\delta_t^{n+1}, \frac{h_k^n \overline{u}_k^n + h_{k_f}^n \overline{u}_{k_f}^n}{2}, \begin{pmatrix} \mathfrak{d}_k \\ \mathscr{H}_k^{n+1/2} \\ \phi_k^{n+1/2} \\ \overline{u}_k^n \end{pmatrix}, \begin{pmatrix} \mathfrak{d}_{k_f} \\ \mathscr{H}_{k_f}^{n+1/2} \\ \phi_{k_f}^{n+1/2} \\ \overline{u}_{k_f}^n \end{pmatrix}\right)$ and the velocity $\underline{\widetilde{u_k^{n+1/2}}}_f$ is the MUSCL reconstruction at the face of the time extrapolation at the half time step, i.e.

$$\underline{\widetilde{u_k^{n+1/2}}}_f = \widetilde{u_k^{n+1/2}} + D_k^f \Delta_k\left(\widetilde{u_\star^{n+1/2}}\right) \qquad \text{with} \qquad \widetilde{u_k^{n+1/2}} = \overline{u}_k^n + \delta_t^{n+1} \frac{\overline{u}_k^n - \overline{u}_k^{n-1}}{\delta_t^n}$$

D_k^f the distance between the cell center and the face center and $\Delta_k(U_\star)$ is the approximation of the slope of U in the cell k see [EGH00].

To demonstrate the efficiency of the scheme, we simulate the test case of a traveling vortex, with the analytical solution provided in [RB09]. For comparison, we also plot results for the classical Runge-Kutta 2 (RK2) time scheme combined with the MUSCL reconstruction and the HLL scheme. The results are illustrated in Figure 3.7, and the L^1-errors for h are shown in Figure 3.8. For a Froude number $F_r = 1$, both schemes produce results that are in good agreement with the analytical solution. However, the scheme (3.9)-(3.10) is noticeably less efficient. Specifically, the HLL-MUSCL-RK2 scheme is approximately 20 times faster on a 200x200 grid mesh. This efficiency gap arises from the implicit nonlinear components of the scheme, which make (3.9)-(3.10) (and similarly (3.4)-(3.6)) less effective for large Froude numbers. Conversely, for a Froude number $F_r = 10^{-3}$, despite its second-order accuracy, the HLL-MUSCL-RK2 scheme is highly diffusive. In contrast, the scheme (3.9)-(3.10) remains well-aligned with the analytical solution. Additionally, at this low Froude number, the CPR scheme is approximately 20 times faster than the HLL scheme on a 200x200 grid mesh. This efficiency difference is due to the CFL condition (3.7), which is independent of the Froude number, unlike the CFL condition for Godunov-type solvers (2.55).

3.1.2 On floating body

Floating structures are used in the marine environment for various purposes, including addressing stability issues for bridges or platforms, studying drift dynamics for icebergs or

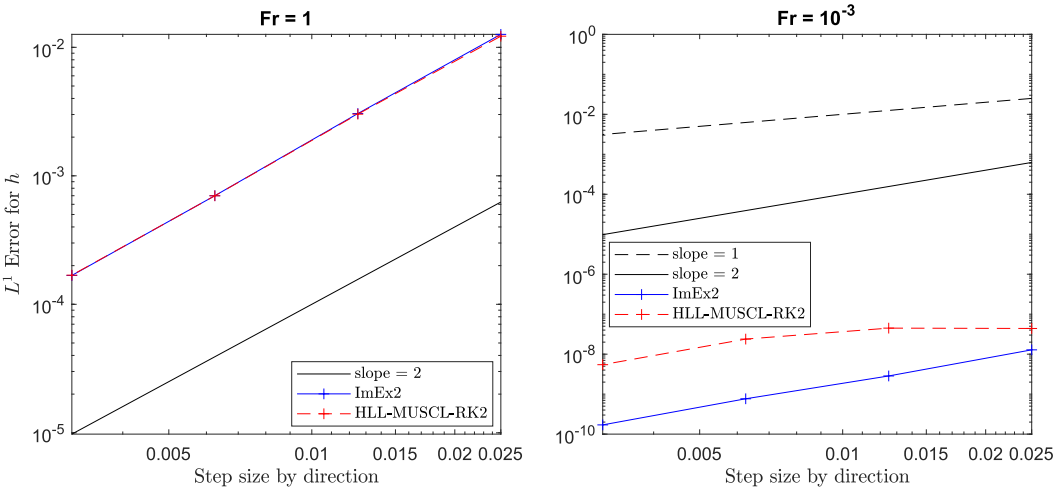

Figure 3.8: §3.1.1.3 | L^1-errors for h of the explicit HLL-MUSCL-RK2 scheme and the second order schemes (3.9)-(3.10) for traveling vortex for $F_r = 1$ and $F_r = 10^{-3}$.

debris, and optimizing the movement of marine energy converters. These considerations are essential for enhancing the performance and safety of floating structures in diverse applications. For large-scale applications, the congested shallow water model (3.1), when coupled with body dynamics, provides an effective model for floating bodies. The numerical coupling is explored in the 2D vertical plane in [GPSMW20]. While this approach simplifies the body dynamics, it still necessitates careful attention to the challenges associated with such coupling.

3.1.2.1 Dynamics of floating body over shallow water flow

In the 2D vertical plane, the body's position is described by three degrees of freedom $\Lambda = (\chi, \zeta, \theta)^\intercal$, where $\chi(t) \in \mathbb{R}$ represents the horizontal coordinate, $\zeta(t) \in \mathbb{R}$ denotes the vertical coordinate of the body's center of mass, and $\theta(t) \in]\pi, \pi]$ is its orientation in the plane relative to a reference position, see Figure 3.9. The complete dynamics of the body can thus be characterized by six degrees of freedom: Λ (position) and $\dot{\Lambda}$ (speed). For a given orientation θ, let $\mathbb{B}(\theta)$ represent the set of coordinates (x,z) within the body, and define the lower surface as $\underline{S}(x,\theta) = \min\{z \mid (x,z) \in \mathbb{B}(\theta)\}$. In practice, the body is described by its function $\underline{S}(x,\theta)$ given. The lower surface for a body positioned at $\Lambda = (\chi, \zeta, \theta)^\intercal$ is given by

$$R(x,\chi,\zeta,\theta) = \begin{cases} \underline{S}(x-\chi,\theta) + \zeta\,, & \text{if} \quad x - \chi \in \operatorname{supp}(\underline{S}(\bullet,\theta)) \\ \Pi & , \quad \text{else} \end{cases} \tag{3.11}$$

where Π is set sufficiently large to ensure it is never reached by the flow, typically $\Pi = 10^{40}$. We assume that this lower surface acts as a roof for the fluid dynamics, see §3.1.1.1. This assumption implies that the flow does not pass over the surface, making this approach suitable for relatively lightweight floating objects.

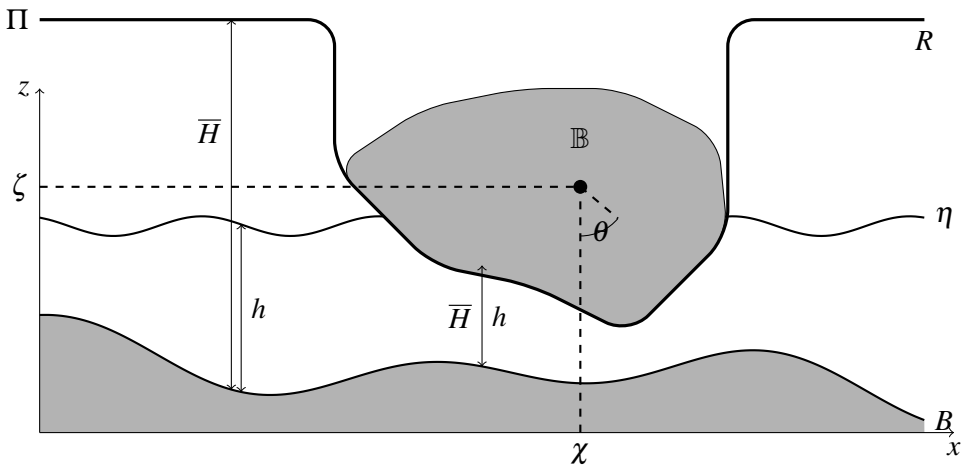

Figure 3.9: §3.1.2.1 | Illustration of the unknowns of the floating body dynamics.

According to Newton's laws of motion, the dynamics of a body with mass $M = \int_{X\in\mathbb{B}} \rho(X)\,\mathrm{d}x\mathrm{d}z$ and moment of inertia $J = \int_{X\in\mathbb{B}} |XO|^2 \rho(X)\,\mathrm{d}x\mathrm{d}z$, subjected to a pressure $\overline{p}$ on its lower surface and gravitational force, are given by

$$\begin{aligned} M\ddot{\chi} &= \int_{\mathbb{R}} \overline{p}\partial_\chi R\,\mathrm{d}x \\ M\ddot{\zeta} &= \int_{\mathbb{R}} \overline{p}\,\mathrm{d}x - Mg \\ J\ddot{\theta} &= \int_{\mathbb{R}} \overline{p}\partial_\theta R\,\mathrm{d}x. \end{aligned} \tag{3.12}$$

The first two equations directly apply Newton's laws. The third equation arises from the fact that, for a rigid body, the motion of points on the body in its reference frame describes concentric circles. It follows the relation of the point of a rigid body, see [KH12]

$$(x-\chi) + (R-\zeta)\,\partial_x R + \partial_\theta R = 0. \tag{3.13}$$

With this formulation, the conservation of energy can be readily established.

Proposition 3.3 *On an infinite, periodic or closed domain, the regular enough solutions of the coupled system* (3.1)-(3.12) *satisfies the following conservation of energy*

$$\partial_t \left(\int_{\mathbb{R}} \left(\mathscr{P}(x,h(t,x)) + \mathscr{K}(h(t,x),\overline{u}(t,x)) \right) \mathrm{d}x + E\left(\Lambda(t),\dot{\Lambda}(t)\right) \right) = 0.$$

with $\mathscr{P}(x,h) = gh\left(B(x)+\frac{h}{2}\right)$, $\mathscr{K}(h,\overline{u}) = \frac{h}{2}|\overline{u}|^2$ *and the energy in the solid* $E\left(\Lambda,\dot{\Lambda}\right) = Mg\zeta + \frac{M}{2}\left(\dot{\chi}^2+\dot{\zeta}^2\right) + \frac{J}{2}\dot{\theta}^2$.

3.1.2.2 Entropy-satisfying numerical scheme

We now focus on the numerical resolution of the model (3.1)-(3.12), ensuring that the discrete scheme preserves the stability of energy as described in Proposition 3.3. In §3.1.1.2,

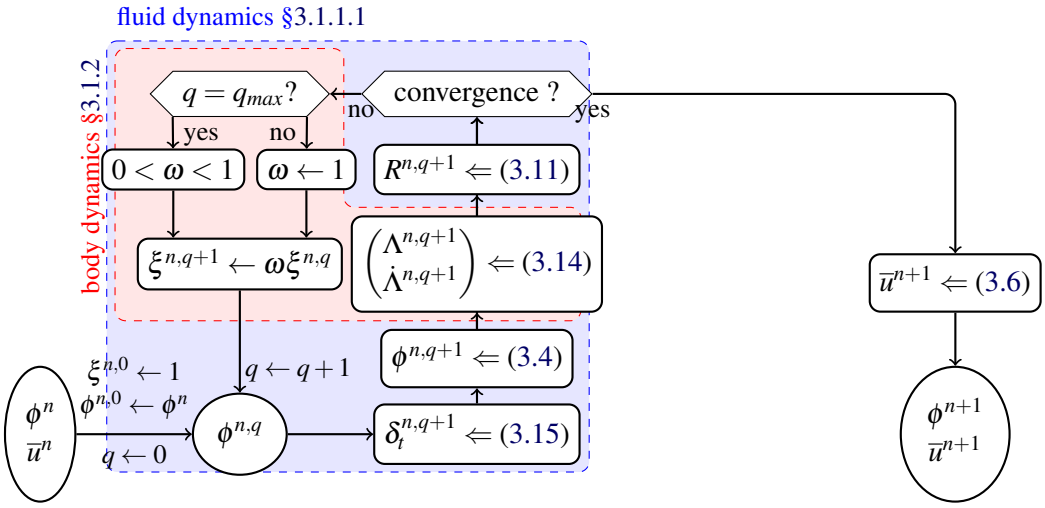

Figure 3.10: §3.1.2.2 | Flowchart of a time steps of scheme (3.4)-(3.6)-(3.14).

we previously proposed an entropy-satisfying scheme for the congested shallow water model (3.1) see Proposition 3.2. Similarly, several entropy-satisfying schemes for body dynamics are available in the literature. Our coupling approach utilizes a Newmark scheme, which is defined as follows:

$$\begin{aligned}
\Lambda^{n+1} &= \Lambda^n + \delta_t^{n+1}\dot{\Lambda}^n + \frac{\delta_t^{n+1}}{2}\left(\alpha_0\ddot{\Lambda}^{n+1} + (1-\alpha_0)\ddot{\Lambda}^n\right) \\
\dot{\Lambda}^{n+1} &= \dot{\Lambda}^n + \delta_t^{n+1}\left(\alpha_1\dot{\Lambda}^{n+1} + (1-\alpha_1)\dot{\Lambda}^n\right) \\
M\ddot{\chi}^{n+1} &= \int_{\mathbb{R}} \left(\alpha_2\overline{p}^{n+1} + (1-\alpha_2)\overline{p}^n\right)\partial_\chi^k\left(R_\star^{n+1}\right)\mathrm{d}x \\
M\ddot{\zeta}^{n+1} &= \int_{\mathbb{R}} \left(\alpha_2\overline{p}^{n+1} + (1-\alpha_2)\overline{p}^n\right)\mathrm{d}x - Mg \\
J\ddot{\theta}^{n+1} &= \int_{\mathbb{R}} \left(\alpha_2\overline{p}^{n+1} + (1-\alpha_2)\overline{p}^n\right)\partial_\theta^k\left(R_\star^{n+1}\right)\mathrm{d}x
\end{aligned} \tag{3.14}$$

where $R_k^{n+1} = R\left(x_k, \chi^{n+1}, \zeta^{n+1}, \theta^{n+1}\right)$ and the discrete operators $\partial_\chi^k\left(R_\star^{n+1}\right)$ and $\partial_\theta^k\left(R_\star^{n+1}\right)$ are respectively the discrete counterparts of the spatial and orientation derivatives ∂_χ and ∂_θ in cell k between times t^n and t^{n+1}. Before defining the discrete derivatives, we highlight the following property

Proposition 3.4 *On an infinite, periodic, or closed domain, with the parameters* $(\alpha_0, \alpha_1, \alpha_2) = (1,1,1)$ *and assuming that the CFL condition* (3.7) *is satisfied, if the discrete derivatives satisfy the following relation*

$$\left(\chi^{n+1} - \chi^n\right)\partial_\chi^k\left(R_\star^{n+1}\right) + \left(\zeta^{n+1} - \zeta^n\right) + \left(\theta^{n+1} - \theta^n\right)\partial_\theta^k\left(R_\star^{n+1}\right) = R_k^{n+1} - R_k^n,$$

then the scheme (3.4)-(3.6)-(3.14) *is entropy satisfying, i.e. we have*

$$\begin{aligned}
\sum_{k\in\mathbb{T}} &\left(\mathscr{P}\left(x_k, h_k^{n+1}\right) + \mathscr{K}\left(h_k^{n+1}, \overline{u}_k^{n+1}\right)\right)\delta_k + E\left(\Lambda^{n+1}, \dot{\Lambda}^{n+1}\right) \\
&\leq \sum_{k\in\mathbb{T}} \left(\mathscr{P}\left(x_k, h_k^n\right) + \mathscr{K}\left(h_k^n, \overline{u}_k^n\right)\right)\delta_k + E\left(\Lambda^n, \dot{\Lambda}^n\right).
\end{aligned}$$

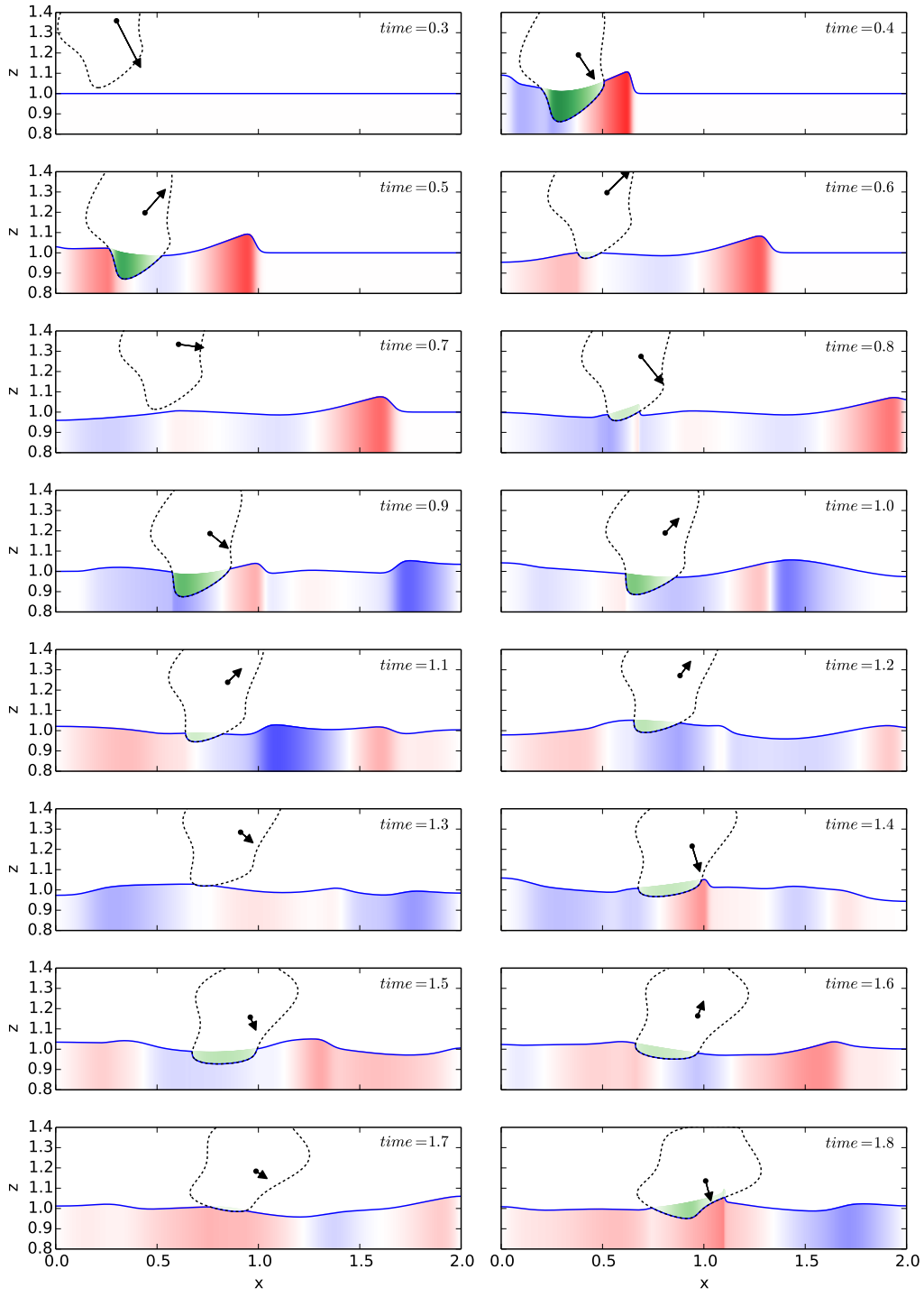

Figure 3.11: §3.1.2.2 | Buoy (black dotted line), water height (blue solid line), velocity (filled surface in the water – blue$<0<$red) and surface pressure (green filled surface in the buoy) at several times.

To satisfy the assumptions of Proposition 3.4, we propose the following discrete operators

$$\partial_\chi^k\left(R_\star^{n+1}\right) = \begin{cases} \dfrac{R\left(x_k,\chi^{n+1},\zeta^{n+1},\theta^{n+1}\right)-R\left(x_k,\chi^{n},\zeta^{n+1},\theta^{n+1}\right)}{\chi^{n+1}-\chi^n} & , \quad \text{if} \quad \chi^{n+1}\neq\chi^n \\ -\dfrac{R_{k+1}^n-R_{k-1}^n}{2\delta_k} & , \quad \text{else} \end{cases}$$

$$\text{and} \quad \partial_\theta^k\left(R_\star\right) = \begin{cases} \dfrac{R\left(x_k,\chi^{n},\zeta^{n},\theta^{n+1}\right)-R\left(x_k,\chi^{n},\zeta^{n},\theta^{n}\right)}{\theta^{n+1}-\theta^n} & , \quad \text{if} \quad \theta^{n+1}\neq\theta^n \\ -\left(x_k-\chi^n\right)-\left(R_k^n-\zeta^n\right)\dfrac{R_{k+1}^n-R_{k-1}^n}{2\delta_x} & , \quad \text{else.} \end{cases}$$

The first case of the two derivatives uses secant approximation, which is consistent with the continuous derivative as δ_t^{n+1} approaches zero. However, when the degrees of freedom remain unchanged, this formula can become ill-defined. For the horizontal derivative, we employ a centered spatial discretization, noting that $\partial_\chi R = -\partial_x R$. For the orientation derivative, we use the relationship for points on a rigid body as described in (3.13).

The scheme (3.4)-(3.6)-(3.14) is non-linear and implicit with the unknowns $\phi, \Lambda, \dot{\Lambda}$. Treating all the unknowns simultaneously would result in a system with a large stencil, because all the cells where water interacts with the body are connected through the body dynamics. To simplify the implementation and avoid a full matrix, we use a weak coupling within the iterative process. Specifically, we first compute the free surface assuming the roof is steady, as detailed in §3.1.1.1, and then update the dynamics of the body. Convergence issues can arise when the body moves through the water at high velocity, and if the scheme does not converge after several iterations, we address this by reducing the time step. This is done by employing an adaptive CFL parameter. The time step is defined as

$$\delta_t^{n,q+1} = \min\left(\delta_t^{n,q}, \frac{\xi^{n,q}\min\left(\mathfrak{d}_k,\mathfrak{d}_{k_f}\right)}{2\nu_f}\right) \tag{3.15}$$

with ν_f defined in (3.7) and $\xi^{n,q} > 0$ is decreasing while q increase with $\xi^{n,0} = 1$. The flowchart of the scheme (3.4)-(3.6)-(3.14) is presented in Figure 3.10.

One of the advantages of the scheme (3.4)-(3.6)-(3.14) is that it does not require estimating the subdomains as congested or free surface. This capability allows for simulations where the topology of these subdomains changes dynamically, as illustrated by the buoy throw example in Figure 3.11. Additionally, to demonstrate the consistency of the scheme, we compare the computed solution to the analytical solution for return to equilibrium established in [Lan17, Corollary 1]. This solution corresponds to the vertical movement of a rectangular buoy, floating freely above initially still water with a flat bottom $B = 0$. The comparison with the simulation results is shown in Figure 3.12. A similar analytical solution within an axisymmetric framework is presented in [Boc19].

To conclude this section, we note that with the parameters $(\alpha_0,\alpha_1,\alpha_2) = \left(\frac{1}{2},\frac{1}{2},\frac{1}{2}\right)$, the Newmark scheme (3.14) achieves second-order accuracy. When coupled with the second-order scheme (3.9)-(3.10), this setup is expected to yield a second-order accurate scheme for floating bodies.

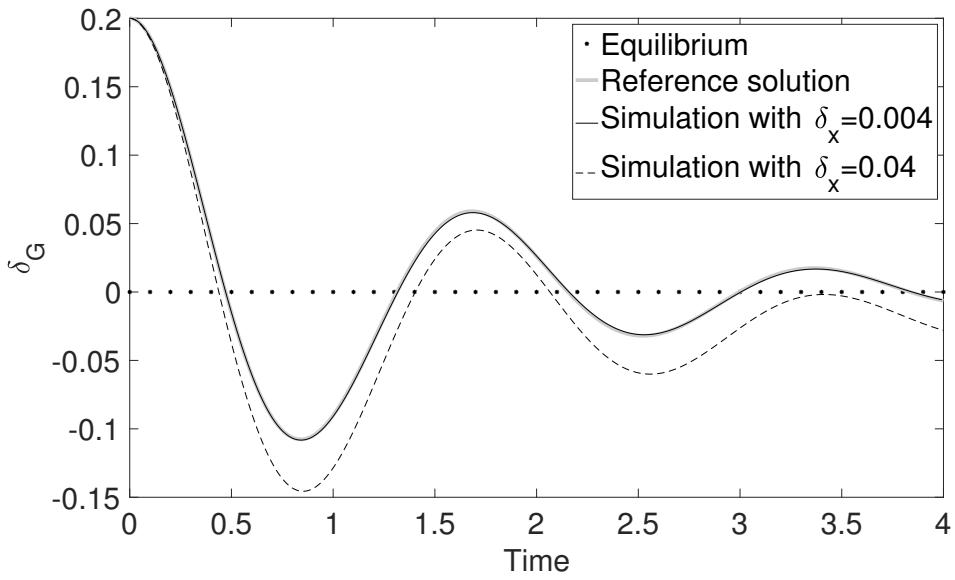

Figure 3.12: §3.1.2.2 | Time evolution of the distance to the equilibrium position $\delta_G = \zeta - \zeta_0$ for the analytical solution [Lan17, Corollary 1] and the numerical solutions.

3.1.3 Trapped air pockets modeling

The presence of a roof not only restricts water flow but also blocks air circulation. This can lead to air pockets being trapped between the roof and the water surface, which can affect the water level and potentially impact discharge rates in pipes. Such phenomena occur in environments like underground rivers, submerged coastal caves [CBCC92], under ice sheets, in sewers during floods [CSZ97], and in certain marine energy converter devices, such as oscillating water columns [dOF10, §6]. Modeling air pockets above a free-surface flow introduces a two-phase liquid-gas problem [CRT08, LZ07], which has been extensively studied in both modeling and numerical simulation contexts [SMM13], particularly in pipe flows. Paradoxically, air pocket modeling is essential to prevent the formation of unrealistic "vacuum" pockets [GMCC13], especially when simulating pumping in deep aquifers (see §3.2).

Depending on the application, two types of models are commonly used for air-water interaction: the incompressible two-phase model [BHI14, Boy02, CPT01] and the compressible two-phase model [CGHS02, KKKP04]. Due to the complexity of these models, numerical simulations at large scales (several km^3) become unfeasible. In geophysical flows, simplified models like shallow water equations are typically employed [LB09]. Vertical integrated models for incompressible flows have been explored in [AK09], but in our case, the air phase cannot be treated as incompressible due to its variable domain. An integrated incompressible/compressible model for liquid-gas interaction was proposed in [BEG13], though it is well-posed only for small relative velocities between the phases, limiting its robustness for broader applications. In [DH17, DBdM+19], a vertically integrated

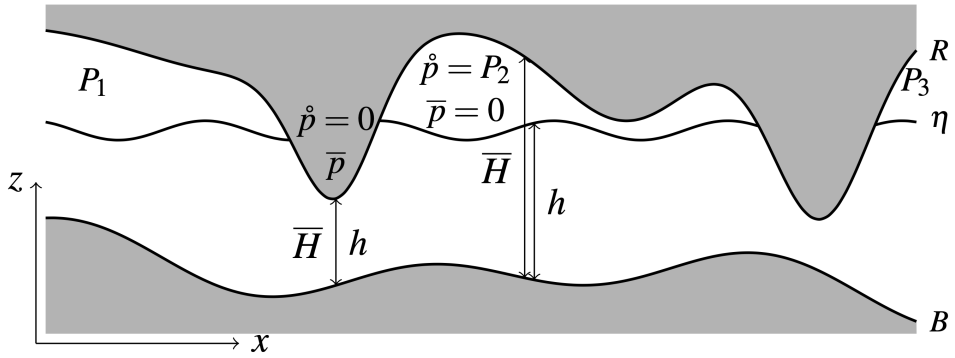

Figure 3.13: §3.1.3 | Illustration of the partially free surface problem and the unknown of the congested shallow water with air pockets model (3.16)-(3.2)-(3.18)-(3.19)-(3.20) in the vertical plane.

model with two fluids and two pressures is developed, highlighting the disparity in sound speed between the air and water phases, which leads to time-scale issues. However, as our focus is on the fluid dynamics, we assume the air pressure relaxation time is small enough to treat the air dynamics as quasi-stationary. In [Par23], we proposed a polytropic model for air pocket dynamics [PCC88], incorporating the merging and splitting of air pockets for simulations that align with practical applications, thus improving the method's robustness.

3.1.3.1 A quasi-steady pressure dynamics

Let us focus on the experiment conducted by Torricelli in 1643 and examine what the congested shallow water model (3.1)-(3.2) lacks in order to replicate this phenomenon. Torricelli immersed a glass tube, sealed at one end, into a container of mercury, filling it completely. He then lifted the closed end of the tube, keeping the open end submerged in the mercury. Initially, the mercury filled the tube above the mercury level in the container. However, the mercury stopped rising after reaching a height of approximately 73 cm, leaving a vacuum at the top of the tube.

In the congested shallow water model (3.1)-(3.2), the roof reaction force, denoted as $\overline{p}$, is assumed to be positive. One could attempt to relax this assumption by considering $\overline{p}$ as surface pressure, allowing it to become negative and causing the mercury level to rise. However, this approach renders the model ill-posed, as it leads to two possible outcomes: one where the fluid remains attached to the roof under negative pressure, and another where the fluid detaches from the roof with zero pressure. Moreover, this method fails to capture a key feature observed in Torricelli's experiment, the presence of two distinct fluid levels in separate regions at equilibrium.

As Giovanni Battista Baliani explained in 1630, the liquid doesn't adhere to the roof but is instead pushed upward by the external air pressure. This insight introduces an additional unknown into the model: the air pressure, $\mathring{p}(t,x) \geq 0$. The congested shallow water model

with air pockets can be expressed as follows

$$\begin{aligned} \partial_t h + \nabla \cdot (h\overline{u}) &= 0 \\ \partial_t (h\overline{u}) + \nabla \cdot (h\overline{u} \otimes \overline{u}) &= -gh\nabla (B+h) - h\nabla (\overline{p} + \mathring{p}) \end{aligned} \tag{3.16}$$

with the congestion constraint (3.2). The air pressure term, $\mathring{p}(t,x)$, still needs to be properly defined.

Assuming that the relaxation time of air pressure is much shorter than the characteristic time of fluid dynamics, the air pressure $\mathring{p}$ can be treated as uniform within each air pocket. By "pocket," we refer to a spatial region bounded by the contact between the fluid and the roof. Thus, the air pressure $\mathring{p}$ is modeled as a piecewise constant function

$$\overline{p}(t,x) = \sum_{i=1}^{N_p\left(\mathring{h}\right)} P_i(t)\, \mathbb{1}_{\Omega_i\left(\mathring{h}\right)}(x) \qquad \text{with} \qquad \mathring{h}(t,x) = \overline{H}(t,x) - h(t,x) \tag{3.17}$$

where $N_p\left(\mathring{h}\right) \in \mathbb{N}$ is the number of pockets, $\Omega_i\left(\mathring{h}\right) \subset \Omega$ represents the horizontal support occupied by the i^{th} pocket, and $P_i(t)$ is the pressure inside the i^{th} pocket, see Figure 3.13.

As long as pockets remain isolated and do not interact, the pressure changes only in response to pocket deformation, particularly due to changes in volume. This follows a polytropic relation

$$\partial_t \left(P_i V_i^d\right) = 0 \tag{3.18}$$

where $V_i\left(\mathring{h}\right) = \int_{\Omega_i\left(\mathring{h}\right)} \mathring{h}\,\mathrm{d}x$ is the volume of the i^{th} pocket and d is the polytropic coefficient of deformation. For slow enough deformations, due to thermal exchange with the fluid, the process can be considered isothermal, leading to $d = 1$.

To advance the modeling, we must consider changes in the topology of the air support, specifically the merging and splitting of air pockets. Let us begin with the case where a pocket splits into several smaller pockets at a specific time τ. Since this process is instantaneous, the splitting is isochoric, meaning the total volume remains constant. Let $\mathbb{W}_i(\tau)$ denote the set of indices of the pockets that result from the splitting of pocket i. This implies

$$\sum_{j \in \mathbb{W}_i(\tau)} \Omega_j(\tau_+) = \Omega_i(\tau_-) \qquad \text{with} \qquad \tau_\pm = \lim_{\substack{\varepsilon \to 0 \\ \varepsilon > 0}} \tau \pm \varepsilon.$$

We assume that the splitting process follows a polytropic relation, described as

$$\sum_{j \in \mathbb{W}_i(\tau)} P_j(\tau_+) \left|V_j(\tau_+)\right|^s = P_i(\tau_-) \left|V_i(\tau_-)\right|^s \qquad \text{and} \qquad \sum_{j \in \mathbb{W}_i(\tau)} V_j(\tau_+) = V_i(\tau_-). \tag{3.19}$$

In most cases, the splitting process is considered isobaric, which simplifies the model by setting $s = 0$.

Now, let us focus on the case where multiple pockets merge to form a new pocket at a specific time τ. As with the splitting process, merging is considered instantaneous, making

it isochoric, the total volume remains unchanged. Let $\mathbb{V}_j(\tau)$ represent the set of indices of the pockets that merge to create the new pocket j. This relationship can be written as

$$\Omega_j(\tau_+) = \sum_{i\in\mathbb{V}_j(\tau)} \Omega_i(\tau_-).$$

We assume that, similar to splitting, the merging process follows a polytropic relation described by

$$\left|P_j(\tau_+)\right|^{\frac{1}{m}} V_j(\tau_+) = \sum_{i\in\mathbb{V}_j(\tau)} \left|P_i(\tau_-)\right|^{\frac{1}{m}} V_i(\tau_-) \qquad \text{and} \qquad V_j(\tau_+) = \sum_{i\in\mathbb{V}_j(\tau)} V_i(\tau_-). \quad (3.20)$$

Typically, the merging process is considered adiabatic, resulting in $m = \gamma$, where γ is the adiabatic index, approximately 1.4 for air.

Lastly, we consider the formation of a vacuum pocket, a case that is physically relevant, as demonstrated by Torricelli. If a new pocket forms in a region where no pocket previously existed, the pressure inside this new pocket is set to zero.

The quasi-steady pressure model discussed in this section can be integrated with other congested models. For instance, it can be applied to the congested Navier-Stokes model with air pockets to serve as a simplified two-fluid model for phenomena such as bubble rise in magmatic chambers. This approach allows for the simulation of complex fluid dynamics involving both the liquid and gas phases, providing insights into behaviors such as bubble dynamics and fluid interactions in various geological and industrial contexts.

3.1.3.2 Numerical resolution of quasi-steady pressure dynamics

We now address the numerical solution of the congested shallow water model with air pockets, described by equations (3.16)-(3.2)-(3.18)-(3.19)-(3.20). The fluid dynamics are approached using the numerical scheme outlined in §3.1.1.2, considering the air pressure at the previous time step, and acting as the bathymetry see [Bou04, §4.12]. Specifically, the scheme (3.4) is applied with the updated bathymetry function $\mathscr{H}_k^{n+1}(\phi) = \mathscr{H}\left[\overline{H}_k^{n+1}, B_k + \frac{\hat{p}_k^n}{g}\right](\phi)$, utilizing the definition provided in (3.8).

Once the new water surface is determined, we can deduce the connexe supports Ω_i^{n+1}, the number of pockets $N_p^{n+1} = \text{card}\left(\Omega_i^{n+1}\right)$, and the volume $V_i^{n+1} = \sum_{i\in\Omega_i^{n+1}} \mathring{h}\mathfrak{m}_k$ of the new pockets. With the support of the pockets at the previous iteration known, the next step is to establish the connectivity between the pockets, i.e. identifying which pockets have split or merged to form new pockets. This task is a classical problem in optimal transport, as discussed in [PC18]. However, given that the time step δ_t^{n+1} is relatively small compared to the motion of the pockets, we can infer the connectivity based on the overlap of the pocket supports. Specifically, if an old pocket at time t^n shares part of its support with a new pocket at time t^{n+1}, they are considered to be connected, see Figure 3.15. Using this approach, we construct $\mathbb{W}_i^{n+1}$, the set of new pockets connected to the old pocket i, and $\mathbb{V}_j^{n+1}$, the set of old pockets connected to the new pocket j. At each time step, this process generates a bipartite graph representing the connections between the old and new pockets

$$\left(\left[1, N_p^n\right]\cap\mathbb{N}, \left[1, N_p^{n+1}\right]\cap\mathbb{N}, \mathbb{W}_{1\le i\le N_p^n}^{n+1}, \mathbb{V}_{1\le j\le N_p^{n+1}}^{n+1}\right).$$

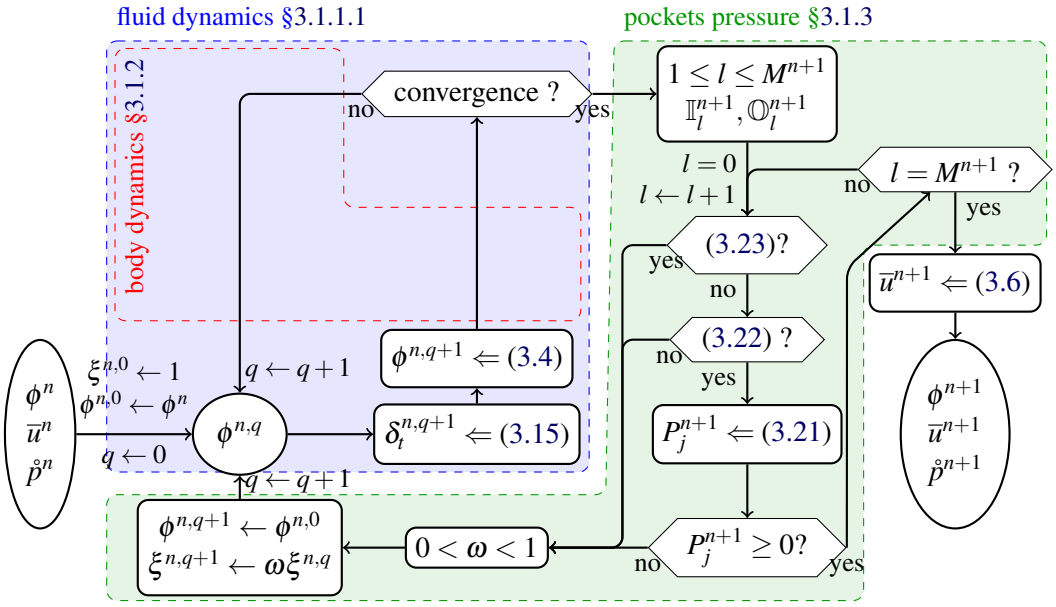

Figure 3.14: §3.1.3.2 | Flowchart of a time steps of scheme (3.4)-(3.6)-(3.21).

To simplify the problem, we can analyze the connected subgraphs (or components) independently. This results in a set of components

$$\left(\mathbb{I}_l^{n+1}, \mathbb{O}_l^{n+1}, \mathbb{W}_{\mathbb{I}_l^{n+1}}^{n+1}, \mathbb{V}_{\mathbb{O}_l^{n+1}}^{n+1}\right).$$

Even if the total number of pockets in the domain is large, the number of pockets involved in each connected subgraph is generally small (typically between 1 and 4) due to the small time step.

The problem of pressure dynamics can be formulated as

Given the connected and bipartite graph of interactions $(\mathbb{I}, \mathbb{O}, \mathbb{W}_{\mathbb{I}}, \mathbb{V}_{\mathbb{O}})$*, and the following quantities: the volume* $V_{i\in\mathbb{I}}^n$ *and pressure* $P_{i\in\mathbb{I}}^n$ *of the old pockets, and the volumes* $V_{j\in\mathbb{O}}^{n+1}$ *of the new pockets, determine the pressures* $P_{j\in\mathbb{O}}^{n+1}$ *in the new pockets based on the physical processes described by equations* (3.18)*,* (3.20)*, and* (3.19)*.*

This problem is evidently ill-posed without additional assumptions. First, although it's possible for a pocket to split, deform, and re-merge without leaving any evidence, we assume that such cases do not occur. Additionally, since the timing of splitting and merging is unknown, we assume the dynamics of pockets at each time step can be divided into three distinct steps, as illustrated in Figure 3.15

S1 **Splitting Step:** Splitting occurs only at the beginning of the time step and follows (3.19) with $\tau = t^n$. Therefore, for any $i \in \mathbb{I}$, we have

$$\sum_{j\in\mathbb{W}_i} V_{ij}^{n,1} = V_i^n \qquad \text{and for any } j \in \mathbb{W}_i, \quad P_{ij}^{n,1}\left(V_{ij}^{n,1}\right)^s = P_i^n\left(V_i^n\right)^s$$

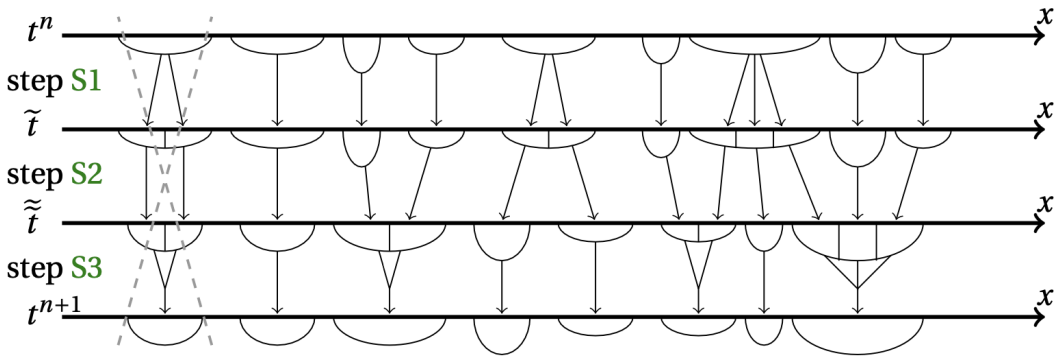

Figure 3.15: §3.1.3.2 | Illustration of the connectivity between the pockets and the substeps of the pressure dynamics scheme. From left to right: Unaccepted splitting/merging, typical deformation case, typical merging case, typical splitting case and general case with splitting and merging.

where $V_{ij}^{n,1}$ and $P_{ij}^{n,1}$ are the volume and pressure in the pocket after the splitting step and before the deformation step.

S2 **Deformation Step:** Deformation occurs throughout the time step. Integrating (3.18) over the time step gives us for any $i \in \mathbb{I}$ and $j \in \mathbb{W}_i$

$$P_{ij}^{n,2}\left(V_{ij}^{n,2}\right)^d = P_{ij}^{n,1}\left(V_{ij}^{n,1}\right)^d$$

where $V_{ij}^{n,2}$ and $P_{ij}^{n,2}$ are the volume and pressure in the pocket after the deformation step and before the merging step.

S3 **Merging Step:** Merging occurs only at the end of the time step and follows (3.20) with $\tau = t^{n+1}$. Therefore, for any $j \in \mathbb{O}$, we have

$$\left(P_j^{n+1}\right)^{\frac{1}{m}} V_j^{n+1} = \sum_{i \in \mathbb{V}_j} \left(P_{ij}^{n,2}\right)^{\frac{1}{m}} V_{ij}^{n,2} \qquad \text{and} \qquad V_j^{n+1} = \sum_{i \in \mathbb{V}_j} V_{ij}^{n,2}.$$

The model remains ill-posed because we lack information about the volume of pockets after splitting and before merging. To address this issue, we propose the assumption that all pockets within a connected subgraph grow at the same rate. Specifically, there exists a constant Γ such that for all $(i,j) \in \mathbb{I} \times \mathbb{O}$, the relation $V_{ij}^{n,1} = \Gamma V_{ij}^{n,2}$ holds. While this hypothesis lacks a physical basis, its impact is minimal due to the small number of pockets involved in each connected subgraph. Nevertheless, using an optimal transport method could potentially eliminate the need for this assumption.

Proposition 3.5 *Assume there are no cycles in the interaction graph* $(\mathbb{I}, \mathbb{O}, \mathbb{W}_\mathbb{I}, \mathbb{V}_\mathbb{O})$. *Hence the problem of pressure dynamics governed by the physical processes outlined in steps S1,*

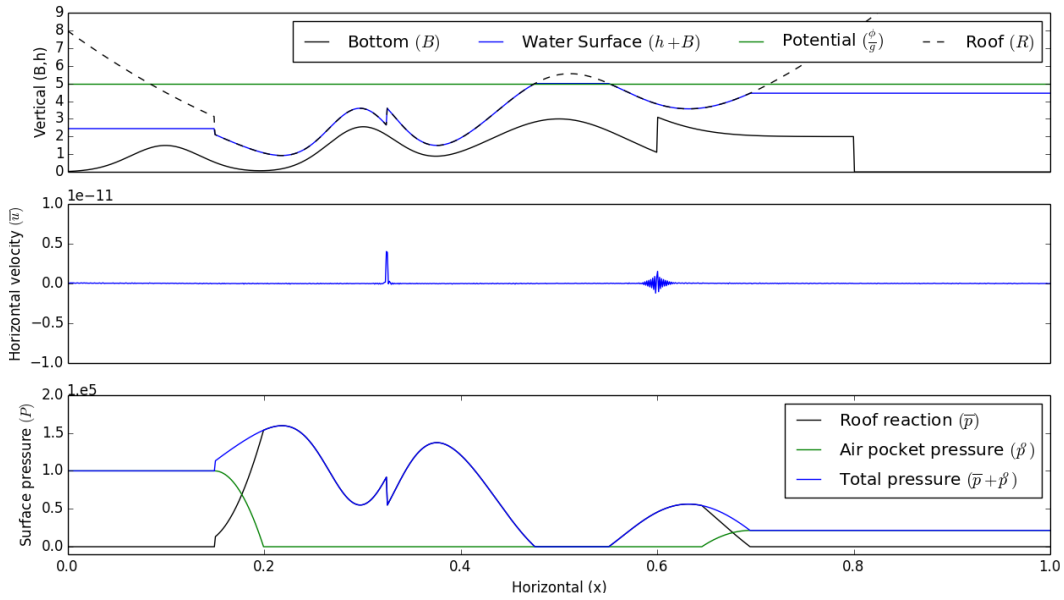

Figure 3.16: §3.1.3.2 | Steady state with several water level of the congested shallow water with air pockets model (3.16)-(3.2)-(3.18)-(3.19)-(3.20).

S2, and S3 has a unique solution. This solution is expressed as

$$P_j^{n+1} = \frac{\Gamma^{d-m}}{\left(V_j^{n+1}\right)^m}\left(\sum_{i\in\mathbb{V}_j}\left(P_i V_i^s \left(V_{ij}^{n,1}\right)^{m-s}\right)^{\frac{1}{m}}\right)^m \qquad \textit{with} \qquad \Gamma = \frac{\sum_{i\in\mathbb{I}} V_i^n}{\sum_{j\in\mathbb{O}} V_j^{n+1}} \tag{3.21}$$

and $V_{ij}^{n,1}$ is the solution to the well-posed linear system

$$\begin{aligned} &\textit{for any } i\in\mathbb{I}\,, && \sum_{j\in\mathbb{W}_i} V_{ij}^{n,1} = V_i^n \\ &\textit{for any } j\in\mathbb{O}\,, && \sum_{i\in\mathbb{V}_j} V_{ij}^{n,1} = \Gamma V_j^{n+1}. \end{aligned}$$

The existence of cycles in the connected subgraphs can be easily detected if the following algebraic condition is not satisfied

$$\operatorname{card}\mathbb{I} + \operatorname{card}\mathbb{O} - 1 = \sum_{i\in\mathbb{I}} \operatorname{card}\mathbb{W}_i. \tag{3.22}$$

In a one-dimensional framework, cycles cannot exist by definition of the connectivity of the pockets by their supports. Additionally, while the new pressures are well defined by equation (3.21), they are not necessarily guaranteed to be positive. Furthermore, it is possible for an old pocket with non-zero pressure to not be connected to any new pockets, i.e.

$$\operatorname{card}\mathbb{O} = 0 \quad \text{and} \quad P_{\mathbb{I}}^n \neq 0. \tag{3.23}$$

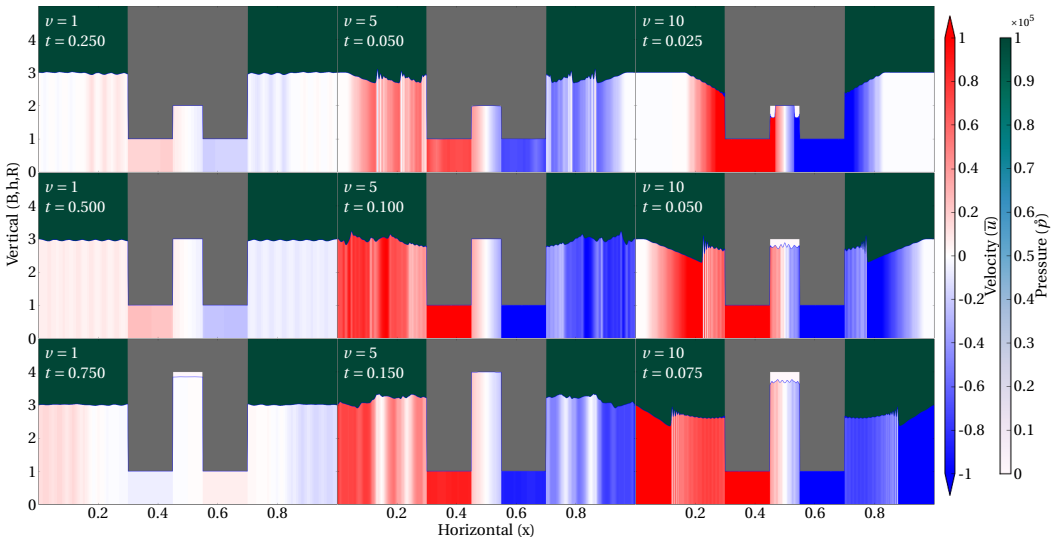

Figure 3.17: §3.1.3.2 | Numerical Torricelli's experiments with different velocity of the piston (left column $v = 1$, middle column $v = 5$, right column $v = 10$) at several times.

Both of these scenarios are non-physical. If they occur, which is very rare, the time step is reduced, and the free surface estimation step described in §3.1.1.1 is repeated, as illustrated in Figure 3.14.

In practice, the new pressure $\mathring{p}^{n+1}$ is not set to zero out of the supports of the pockets as defined by (3.17). Due to weak coupling and pressure discontinuities, the water surface struggles to detach from the roof. To address this issue, a regularization of the pressure $\mathring{p}^{n+1}$ is applied. This regularization adjusts $\mathring{p}^{n+1}$ without altering the total pressure, ensuring that $\mathring{p}^{n+1} + \overline{p}^{n+1}$ remains constant.

Figure 3.16 illustrates the potential complex steady states at rest that can exist. The numerical scheme defined by (3.4)-(3.6)-(3.21) is capable of reproducing these steady states. For the illustration, pressure regulation has been exaggerated, though in practice, it can be limited to just a few cells.

In Figure 3.17, we numerically reproduce Torricelli's experiment with varying velocities v of the roof at the center of the domain. With a low velocity of $v = 1$ (left column), the results align with the physical experiment: initially, the water level inside the chamber rises, and then a vacuum forms above a height of 73 cm. With a higher velocity of $v = 5$ (middle column), the water level inside the chamber exceeds 73 cm due to inertia effects. The system eventually returns to a steady state over time. At an even higher velocity of $v = 10$ (right column), a vacuum pocket forms immediately because the fluid is unable to keep up with the speed of the roof, again due to inertia. When examining the perturbation of the free surface, we can distinguish two frequencies. The first, most visible in the left column, is a high-frequency oscillation corresponding to the numerical time step. This perturbation results from weak coupling and diminishes with smaller time steps. The second frequency is slower and corresponds to a shockwave traveling from one part of the

congested domain to the other. This signal remains visible with finer mesh resolutions.

3.1.4 Perspectives

In this section, we present a model for floating body dynamics along with its numerical resolution. This model provides a foundation for understanding the interaction between fluid and floating structures, which has a range of practical applications.

From an applied perspective, a natural progression of this work would be to extend the model to account for more complex solid mechanics, such as deformable or articulated bodies. These bodies are more realistic representations of many physical systems, especially when considering the dynamic behavior of ships, floating platforms, or marine energy convertors. Additionally, the extension of the model to two horizontal dimensions would allow for more accurate simulations of real-world scenarios, where fully three-dimensional effects are significant. However, even though the physics governing deformable and articulated solids is well established, the primary challenge in advancing this model lies not in the fundamental understanding of these physical processes, but rather in the implementation and code coupling required to efficiently simulate them. Particularly, the distribution of computational resources becomes a critical factor when dealing with highly complex geometries and multi-body interactions. While this challenge is significant and certainly important for the practical execution of simulations, it is more a question of computational strategy than of new model development or numerical approximation theory. Nevertheless, overcoming these challenges is essential for conducting both physical and numerical experiments, which would enable the validation of the model and comparisons between simulated and real-world results.

One of the major modeling challenges that emerges in this context is the consideration of submerged objects within the fluid. Submerged (or partially submerged) bodies, such as some marine energy convertors or infrastructure below the water surface, introduce complex interactions between the object and the surrounding water. One potential approach to address this issue is through the use of multi-layer models §2.1.2.3, where, in certain regions, there are no exchanges between layers due to the presence of a submerged object, while in the rest of the domain, such exchanges are allowed. However, implementing such a model is far from straightforward, as the definition of these layers becomes intricately tied to the position and movement of the submerged object. The geometry of the object complicates the computational domain and requires dynamic adaptation of the layers, posing significant difficulties in practice.

Further exploration of other congested models could also be highly beneficial, as mentioned in §3.1.1. For example, in bio-mathematical models, the influence of congestion pressure on processes such as cell growth, death, or vascularization could be studied.

From a numerical standpoint, several important limitations remain. One significant issue is the inability of the ImEx scheme (3.4)-(3.6) to be used at dry fronts, where the water depth reaches zero. These dry fronts are regions where the fluid flow dynamics change drastically, such as in the case of coastal regions during low tide, where parts of the seabed become exposed. To address this, an alternative numerical scheme, such as

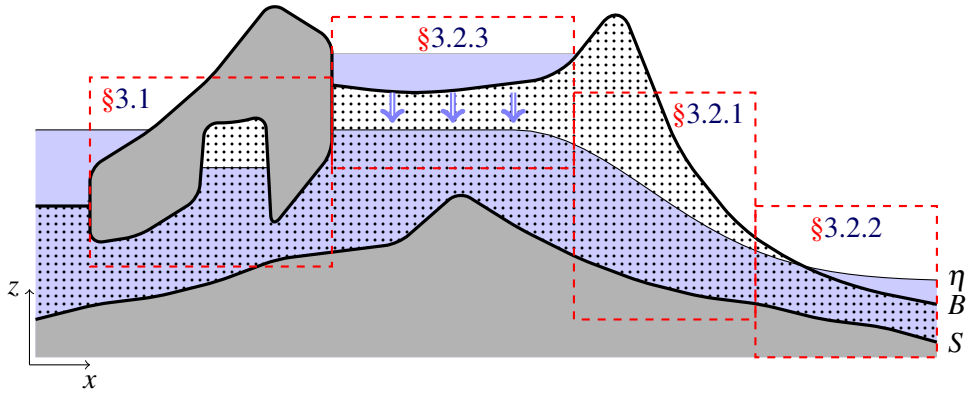

Figure 3.18: §3.2 | Illustration of a water drainage basin. Grey areas are impermeable soils, dotted areas are porous media and blue areas are saturated with water.

an approximate explicit Godunov scheme, can be employed in regions with small water depth. Still, in cases where a floating object comes into contact with the bottom, like a boat grounded during low tide, followed by a rising tide, there is no existing numerical scheme that can handle the situation satisfactorily.

Another major numerical difficulty involves the application of congestion constraints in (really) high-order numerical methods. High-order schemes are generally based on a representation of the solution with several degrees of freedom per cell. It is not clear how the congestion constraint affects the different degrees of freedom. Achieving a numerical method that can maintain both high accuracy and respect for congestion constraints remains a challenging and open area of research.

Finally, there are numerous unresolved questions in the mathematical analysis of congested models. In the specific case of the congested shallow water model (3.1), one notable issue is the presence of an indeterminate non-conservative product that occurs when the fluid meets the roof at the top of a hydraulic jump. This phenomenon, illustrated in Figure 3.6, represents a critical challenge in understanding how fluid behaves in constrained environments, particularly in pipes for hydraulic power stations.

3.2 Simulation of continental waters

This section focuses on modeling water flow at the drainage basin scale, over extended periods ranging from days to decades. Given these long time frames, groundwater flow becomes a key factor. The primary application considered here involves water resource management and risk assessment for infrastructure related to continental water bodies, such as bridges and dikes. Current models often rely on 3D simulations based on Darcy's law (3.24)-(3.27), which require substantial computational resources. These models are not well-suited for exploring various scenarios impacted by climate change or shifts in public policy. At the other end of the modeling spectrum is the Dupuit-Forchheimer model [Dup63], which simplifies the problem to a 2D diffusion equation, making it significantly

faster and easier to solve. However, while useful, the Dupuit-Forchheimer model has its limitations [Bou65, vS65], especially in situations where vertical velocities are critical, such as in infiltration or resurgence, or when the porous media morphology changes over time.

We begin by outlining the reference model firstly introduced by Boussinesq in 1904 [Bou04], which is considered to accurately capture the physical processes across an entire water drainage basin but is computationally prohibitive for large-scale applications. The model describes the flow of an incompressible fluid through a porous medium. Let $\Theta(x,z)$ represent the porosity of the medium, defined as the ratio of void space to total volume within a given element of the medium. Additionally, let $0 \leq \theta(t,x,z) \leq \Theta(x,z)$ represent the water content, i.e. the fraction of void space filled with fluid at any point in time and space. The water content $\theta(t,x,z)$ is governed by the conservation equation

$$\partial_t \theta + \nabla \cdot (\theta u) + \partial_z (\theta w) = 0 \tag{3.24}$$

where $u(t,x,z) \in \mathbb{R}^d$ denotes the horizontal fluid velocity, and $w(t,x,z) \in \mathbb{R}$ represents the vertical fluid velocity. The flow of both surface water and groundwater is modeled using the congested Euler equations, which include drag forces to account for the interaction with the porous medium

$$\begin{aligned} \partial_t u + u \cdot \nabla u + w \partial_z u &= -\nabla (p(\theta) + \overline{p}) - \frac{u}{\kappa} \\ \partial_t w + u \cdot \nabla w + w \partial_z w &= -\partial_z (p(\theta) + \overline{p}) - g - \frac{w}{\kappa}. \end{aligned} \tag{3.25}$$

Here, $\kappa(x,z) > 0$ denotes the hydraulic conductivity of the porous medium, $p(\theta) \geq 0$ represents the capillary pressure, which is a given function of the water content, and $\overline{p}(t,x,z)$ is the pore pressure, which enforces the congestion constraint $\min(\Theta - \theta, \overline{p}) = 0$, see §3.1.1.1. We also assume the existence of a surface elevation $S(x)$, referred to as the bedrock, where a non-penetration condition holds, as described in (2.3)

$$u_{|z=S} \cdot \nabla S - w_{|z=S} = 0. \tag{3.26}$$

One of the main challenges in modeling fluid flow through porous media is accurately characterizing the pressure field $p(\theta)$, which depends on complex local factors such as grain shape, connectivity, and fluid rheology. In large-scale simulations, these detailed effects are often simplified or neglected using homogenization techniques to reduce computational costs [Hor12].

A unique aspect of flow in a water drainage basin is that the flow regime varies significantly depending on the region being considered. Typically, a drainage basin is divided into three distinct regions, separated by three surfaces, assumed to be mono-valued: the substratum $S(x)$ at the bottom of the domain, the bathymetry $B(x)$ at the top of the porous medium, and the unknown water table $\eta(t,x)$, also referred to as the free surface, where the flow beneath this surface is fully saturated. The water table can intersect with the bathymetry, particularly in regions such as seas, lakes, and rivers, see Figure 3.18.

Above the surface $B(x) < z$: This region lies above the porous medium, where the flow is unimpeded by the medium. Here, the parameters are set as $\Theta = 1$ and $\kappa \to \infty$. The dynamics of this flow are the focus of §2.

The vadose zone $\eta(t,x) < z \leq B(x)$**:** This region consists of the unsaturated part of the porous medium, where $\theta < \Theta$ and thus $\pi = 0$. Flow in this zone is primarily infiltration, moving vertically from the surface to the water table.

The aquifer $S(x) < z \leq \eta(x)$**:** This region is the saturated part of the porous medium, where $\theta = \Theta$ and $\pi \neq 0$. The flow here is mostly horizontal, constrained by the substratum, and shares similarities with surface flow, see §3.2.1.

As illustrated in Figure 3.18, a water drainage basin may contain confined aquifers, where the surface is constrained by an impermeable layer. When such an aquifer fills, air pockets can become trapped beneath this layer. These situations are analogous to surface flows confined by a roof, and the solutions discussed in §3.1 can be applied to groundwater flows as well. The case of a perched water table or an underground river can also be modeled by overlapping surface zones, vadose zones, and aquifers. However, these composite cases remain perpectives at the moment. Additionally, we assume that the hydraulic conductivity κ is sufficiently low in the porous medium. As a result, by applying a classical Hilbert expansion, the Euler equations can be simplified to Darcy's law [Dar56] below the bathymetry

$$\begin{aligned} u &= -\kappa \nabla (p(\theta) + \overline{p}) \\ w &= -\kappa \partial_z (p(\theta) + \overline{p} + gz). \end{aligned} \tag{3.27}$$

Substituting these expressions into the continuity equation (3.24) leads to the Richards equation (3.39) [Ric31]. A numerical solution of Richards equation is proposed in [CZ10].

3.2.1 Approximate models of groundwater table

In this section, we focus on modeling the evolution of the water table, assuming it remains below the bathymetry, i.e. $\eta(t,x) < B(x)$. The case where the water table or free surface intersects the bathymetry will be addressed in §3.2.2. Consequently, it is concluded that the subsurface flow beneath the water table follows a divergence-free condition, expressed as

$$\nabla \cdot (\Theta u) + \partial_z (\Theta w) = 0. \tag{3.28}$$

The water table itself satisfies a kinematic equation (2.4), with a source term arising from the unsaturated flow above the water table, as discussed in §3.2.3. However, in this section, we neglect the unsaturated flow. The dynamics of the water table, governed by equations (2.4)-(3.26)-(3.27)-(3.28), are referred to in the literature as the groundwater waves problem. The similarities between this and the water waves problem discussed in §2.1.1 are well recognized, as noted in [NAFP97]. It is important to note that Darcy's law implies the velocity field, more precisely $\kappa^{-1}(u,w)^\intercal$ is curl-free, without requiring additional assumptions. This naturally leads to the question of deriving approximate models in the regime of small shallowness numbers, following the approach proposed in [Lan13] or discussed in §2.1. In groundwater flow literature, the regime of small shallowness number is referred to as the Dupuit-Forchheimer regime. Similar to the water waves problem, the accuracy of these approximate models can be evaluated by two key properties of the groundwater waves problem. First, the groundwater waves model satisfies an energy dissipation law

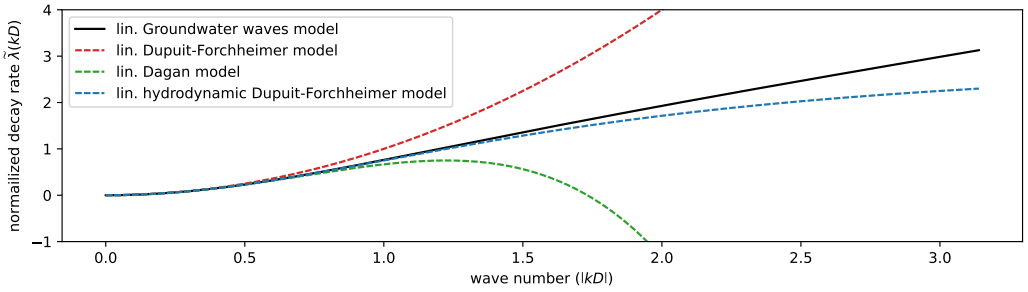

Figure 3.19: §3.2.1.1 | Comparison of the linear normalized decay rate of several models:
- Black solid line: the groundwater waves model (3.29),
- Red dashed line: the Dupuit-Forchheimer model (3.30),
- Green dashed line: the Dagan model (3.31),
- Blue dashed line: the hydrodynamic Dupuit-Forchheimer model (3.32),

Proposition 3.6 *For sufficiently regular solutions of the model* (2.4)-(3.26)-(3.27)-(3.28)*, the following potential energy dissipation law holds*

$$\partial_t \mathscr{P} + \nabla \cdot \left(\int_S^{S+h} (gz + \overline{p}) \Theta u \, \mathrm{d}z \right) = - \int_S^{S+h} \frac{\Theta}{\kappa} \left(|u|^2 + w^2 \right) \mathrm{d}z$$

where $\mathscr{P}(x,h) = g \int_S^{S+h} \Theta z \, \mathrm{d}z$ *is the potential energy.*

Second, it is possible to characterizes the time it takes for small perturbations in the groundwater table to dissipate. More specifically, by linearizing the groundwater waves problem around a steady state of rest $h(t,x) = D$ and $u = 0$, with constant coefficients $\Theta(t,x,z) = \overline{\Theta}$, $\kappa(t,x,z)\,\overline{\kappa}$, and $S(x) = 0$, we look for solutions under the form

$$h(t,x) = D + \hat{h} e^{ik \cdot x} e^{-\frac{g\overline{\kappa}\widetilde{\lambda}}{D} t}$$

where k is the wave number and $\widetilde{\lambda}$ is the linear normalized decay rate. The linear normalized decay rate of the groundwater waves problem is given by

$$\widetilde{\lambda}(kD) = kD \tanh(kD). \tag{3.29}$$

This type of analysis resembles the dispersion relation used in water wave problems [Air45]. Dispersion relations, such as the decay rate, are valuable for mathematical analysis, particularly in Fourier analysis, and for comparing and evaluating the accuracy of approximate models. The decay rate of the groundwater waves model is illustrated in Figure 3.19, where it is compared with other models.

3.2.1.1 Approximate models in the Dupuit-Forchheimer regime

In this section, we assume that hydraulic conductivity and porosity depend solely on the horizontal dimension, specifically $\Theta(x,z) = \overline{\Theta}(x)$ and $\kappa(x,z) = \overline{\kappa}(x)$. The simplest and

most well-known approximate model is the Dupuit-Forchheimer model [Dup63], expressed as

$$\partial_t V - \nabla \cdot \left(g \overline{\kappa} V \nabla \left(h + S \right) \right) = 0 \tag{3.30}$$

where $V(x,h) = \overline{\Theta}(x) h$ represents the volume of water per unit of horizontal space. This model is formally justified by assuming hydrostatic pressure, $\overline{p} = g(\eta - z)$, known in this context as the Forchheimer assumption. This assumption is valid when the shallowness number is sufficiently small, see §1.1. By integrating the groundwater model along the vertical, we obtain the Dupuit-Forchheimer regime, for which the parallel can be drawn with the shallow water regime for water waves, see §2.1.

Proposition 3.7 *For sufficiently regular solutions of the Dupuit-Forchheimer model* (3.30)*, the following potential energy dissipation law holds*

$$\partial_t \mathscr{P} - \nabla \cdot \left(\frac{g^2 \overline{\kappa} V}{2} \nabla \left| h + S \right|^2 \right) = -g^2 \overline{\kappa} V \left| \nabla \left(h + S \right) \right|^2$$

where the potential energy is given by $\mathscr{P}(x,h) = g \overline{\Theta}(x) \frac{h^2}{2}$.

The linear normalized decay rate of the Dupuit-Forchheimer model (3.30) is given by $\widetilde{\lambda}(kD) = |kD|^2$. This decay rate is illustrated in Figure 3.19, alongside other models. A key limitation of the Dupuit-Forchheimer model is evident: higher wave numbers are attenuated more rapidly compared to the groundwater waves model.

To enhance the modeling of the groundwater table, Dagan [Dag67] proposed a modified model that incorporates higher-order derivatives. This model is expressed as

$$\partial_t V - \nabla \cdot \left(g \overline{\kappa} \overline{\Theta} \left(h \nabla \left(h + S \right) + \nabla \left(\frac{\omega_h}{\overline{\kappa} \overline{\Theta}} \nabla \cdot \left(\overline{\kappa} \overline{\Theta} \nabla \left(h + S \right) \right) \right) \right) \right) = 0 \tag{3.31}$$

where $\omega_h = \frac{h^3}{3}$. The model arises from a Hilbert expansion of the pressure term in Darcy's equation (3.27) with respect to the shallowness number. Its linear normalized decay rate is given by $|kD|^2 - \frac{|kD|^4}{3}$, which represents a second-order Taylor expansion of the decay rate of the groundwater waves model. While the Dagan model aims to improve the decay rate, it sacrifices energy dissipation. Instead, it adheres to a balance law

$$\partial_t \mathscr{P} - \nabla \cdot \left(g^2 \overline{\kappa} \overline{\Theta} \left(h^2 \nabla h + \left(h \nabla \left(\omega_h \Delta h \right) - \omega_h \Delta h \nabla h \right) \right) \right) = -g^2 \overline{\kappa} \overline{\Theta} \left(h \left| \nabla h \right|^2 - \omega_h \left| \Delta h \right|^2 \right).$$

A Fourier analysis reveals that the linearized Dagan model is ill-posed unless specific assumptions are made regarding the spectrum of the initial conditions. As shown in Figure 3.19, the decay rate for sufficiently large wave numbers, where $|kD| > \sqrt{3}$, becomes negative. This indicates that wave amplitudes increase, which is clearly unphysical, and asymptotically, the very high frequencies blows-up instantaneously.

Following the derivation of the hydrodynamic models presented in §2.1, we propose an approximate hydrodynamic model for groundwater waves in [Par24a]. The model is formally justified using a Taylor expansion of the unknown function with respect to the shallowness number, see §1.1. The model is expressed as follows

$$\partial_t V - \nabla \cdot \left(g \overline{\Theta} h \left(\mathrm{I} + \mathscr{T}_{\overline{\kappa}, \overline{\Theta}} \left[h, S \right] \right)^{-1} \left(\overline{\kappa} \nabla \left(h + S \right) \right) \right) = 0 \tag{3.32}$$

where the operator $\mathscr{T}_{\overline{\kappa},\overline{\Theta}}[\mathbf{h},\mathbf{B}](U)$ is defined as

$$\mathscr{T}_{\overline{\kappa},\overline{\Theta}}[\mathbf{h},\mathbf{B}](U)=\alpha_{\mathbf{B}}U+\frac{\overline{\kappa}}{\mathbf{h}}\nabla\left(\frac{\gamma_{\mathbf{h},\mathbf{B}}}{\overline{\kappa}}\cdot U\right)-\frac{\gamma_{\mathbf{h},\mathbf{B}}}{\overline{\Theta}\mathbf{h}}\nabla\cdot\left(\overline{\Theta}U\right)-\frac{\overline{\kappa}}{\mathbf{h}}\nabla\left(\frac{\omega_{\mathbf{h}}}{\overline{\kappa}\overline{\Theta}}\nabla\cdot\left(\overline{\Theta}U\right)\right)$$

with the coefficients $\alpha_{\mathbf{B}}$, $\gamma_{\mathbf{h},\mathbf{B}}$ and $\omega_{\mathbf{h}}$ defined by (2.45). This operator $\mathscr{T}_{\overline{\kappa},\overline{\Theta}}[\mathbf{h},\mathbf{B}](U)$ generalizes the dispersive operator $\mathscr{T}[\mathbf{h},\mathbf{B}](U)$ defined in (2.45) and used in the dispersive model (2.13), accounting for the inhomogeneity of the porous medium. Specifically, when $\nabla\overline{\kappa}=\nabla\overline{\Theta}=0$, we recover $\mathscr{T}_{\overline{\kappa},\overline{\Theta}}[\mathbf{h},\mathbf{B}](U)=\mathscr{T}[\mathbf{h},\mathbf{B}](U)$. Weakly hydrodynamic weakly non-linear models can also be derived by assuming small variations in water depth $h=D+O(\varepsilon)$ as for (2.47). This leads to the model (3.32) with the operator $\mathscr{T}_{\overline{\kappa},\overline{\Theta}}[D,\mathbf{B}](U)$ instead of $\mathscr{T}_{\overline{\kappa},\overline{\Theta}}[\mathbf{h},\mathbf{B}](U)$. Similarly, models with small bathymetry variations can be obtained, resulting in the model (3.32) with the operators $\mathscr{T}_{\overline{\kappa},\overline{\Theta}}[h,0](U)$ or $\mathscr{T}_{\overline{\kappa},\overline{\Theta}}[D,0](U)$ instead of $\mathscr{T}_{\overline{\kappa},\overline{\Theta}}[\mathbf{h},\mathbf{B}](U)$ for the fully non-linear or weakly non linear hydrodynamic models, respectively.

Proposition 3.8 *For sufficiently regular solutions of the fully hydrodynamic Dupuit-Forchheimer model* (3.32)*, the following potential energy dissipation law holds*

$$\partial_t\mathscr{P}+\nabla\cdot\left(\left(g(h+S)+\overline{q}\right)\overline{\Theta}h\overline{u}\right)=-\frac{\overline{\Theta}h}{\overline{\kappa}}\left(|\overline{u}|^2+\overline{w}^2+\frac{\widetilde{w}^2}{12}\right)$$

where the potential energy is given by $\mathscr{P}(x,h)=g\overline{\Theta}(x)\frac{h^2}{2}$*, the horizontal velocity* $\overline{u}(x,h)=-g\left(1+\mathscr{T}_{h,S}\right)^{-1}\left(\overline{\kappa}\nabla(h+S)\right)$*, the vertical velocities are defined as*

$$\overline{w}=\overline{u}\cdot\nabla S-\frac{h}{2\overline{\Theta}}\nabla\cdot\left(\overline{\Theta}\overline{u}\right)\qquad\text{and}\qquad\widetilde{w}=-\frac{h}{\overline{\Theta}}\nabla\cdot\left(\overline{\Theta}\overline{u}\right)$$

and the hydrodynamic pressure is given by $\overline{q}=\frac{h(6\overline{w}+\widetilde{w})}{12\overline{\kappa}}$.

The weakly nonlinear model, using $\mathscr{T}_{\overline{\kappa},\overline{\Theta}}[D,\mathbf{B}]$, does not satisfy an entropy dissipation law. The linear normalized decay rate of the hydrodynamic Dupuit-Forchheimer models (3.32) is given by

$$\widetilde{\lambda}(kD)=\frac{|kD|^2}{1+\frac{1}{3}|kD|^2}$$

as illustrated in Figure 3.19 alongside other models. The decay rate of the hydrodynamic Dupuit-Forchheimer model closely approximates that of the groundwater waves model, more so than either the Dupuit-Forchheimer or Dagan models. However, it is important to note that as the wave number kD approaches infinity, the decay rate of the hydrodynamic Dupuit-Forchheimer model converges to $\lambda_\infty=3$, while the decay rate of the groundwater waves model tends toward infinity. This suggests that discontinuities are preserved, albeit with reduced amplitudes, in the Dupuit-Forchheimer hydrodynamic model (3.32), unlike in the traditional Dupuit-Forchheimer model (3.30) and the groundwater waves model, where instantaneous regularization can be demonstrated. It is crucial to emphasize that discontinuous solutions fall outside the intended scope of the model. Thus, the hydrodynamic model is applicable for scenarios where the water table is steep enough to render the hydrostatic model inadequate, yet still flat enough to ensure that the shallowness number remains sufficiently small.

3.2.1.2 Entropy-satisfying numerical scheme

From a mathematical point of view, the hydrodynamic Dupuit-Forchheimer model is a nonlinear, non-local diffusion equation [AV10, BV+16, Váz17]. These models share similarities with various existing frameworks in the scientific literature, including the Patlak-Keller-Segel equations [Pat53, KS71], the Schurtz-Nicolai model [SNB00, GP11], the Stokes-Brinkman model [Bri49, KLLS11], and the non-local Exner model [ABP21]. Numerical approximations of non-local diffusion equations present significant mathematical challenges. One of the primary applications of models developed for the Dupuit-Forchheimer regime is the estimation of the water table over long-term scenarios, ranging from days to even decades. To carry out such simulations, it is essential to employ an efficient numerical scheme that does not impose overly restrictive time-step conditions. This necessity explains the widespread use of implicit schemes to solve the hydrostatic Dupuit-Forchheimer model (3.30). We aim to develop a scheme that, in the limit of small shallowness number, recovers an implicit scheme for the hydrostatic Dupuit-Forchheimer model (3.30).

To solve the hydrodynamic Dupuit-Forchheimer model, we introduce the velocity $\overline{u} = -g\left(1+\mathscr{T}_{h,S}\right)^{-1}\left(\overline{\kappa}\nabla\left(h+S\right)\right)$. Following the projection strategy presented in §2.3, the following numerical scheme is proposed

$$\begin{aligned} h_k^{n+1} &= h_k^n - \frac{\delta_t}{\overline{\Theta}_k}\nabla_k^\delta\cdot\left(\overline{\Theta}_\star\left\{h_\star^{n+\theta}\right\}_\star \overline{u}_\star^{n+1-\theta}\right) \\ \overline{u}_f^{n+1-\theta} + \mathscr{T}^f_{\overline{\kappa}_\star,\overline{\Theta}_\star}\left[h_\star^{n+\theta},S_\star\right]\left(\overline{u}_\star^{n+1-\theta}\right) &= -g\overline{\kappa}_f\nabla_f^\delta\left(h_\star^{n+1-\theta}+S_\star\right). \end{aligned} \tag{3.33}$$

Here, the water depth at intermediate time is defined as $h_\star^{n+\theta} = \theta h_\star^{n+1} + (1-\theta)h_\star^n$ for a given $\theta\in[0,\frac{1}{2}]$. The discrete space differential operator is defined as

$$\begin{aligned} \mathscr{T}^f_{\mathbf{h}_\star,\mathbf{B}_\star}(U_\star) = {}& \frac{\overline{\kappa}_f}{\{\mathbf{h}_\star\}_f}\left\{\frac{\mathbf{h}_\star}{\overline{\kappa}_\star\overline{\Theta}_\star}\left\{\overline{\Theta}_\star U_\star\cdot\nabla_\star^\delta\mathbf{B}_\star\right\}_\star\right\}_f\nabla_f^\delta\mathbf{B}_\star \\ &+\frac{\overline{\kappa}_f}{\{\mathbf{h}_\star\}_f}\left(\nabla_f^\delta\left(\frac{|\mathbf{h}_\star|^2}{2\overline{\kappa}_\star\overline{\Theta}_\star}\left\{\overline{\Theta}_\star U_\star\cdot\nabla_\star^\delta\mathbf{B}_\star\right\}_\star\right)-\left\{\frac{|\mathbf{h}_\star|^2}{2\overline{\kappa}_\star\overline{\Theta}_\star}\nabla_\star^\delta\cdot\left(\overline{\Theta}_\star U_\star\right)\right\}_f\nabla_f^\delta\mathbf{B}_\star\right) \\ &-\frac{\overline{\kappa}_f}{\{\mathbf{h}_\star\}_f}\nabla_f^\delta\left(\frac{|\mathbf{h}_\star|^3}{3\overline{\kappa}_\star\overline{\Theta}_\star}\nabla_\star^\delta\cdot\left(\overline{\Theta}_\star U_\star\right)\right). \end{aligned}$$

The discrete divergence and gradient operators are defined as

$$\nabla_k^\delta\cdot U_\star = \frac{1}{\mathfrak{m}_k}\sum_{f\in\mathbb{F}_k}U_f\cdot\mathfrak{n}_k^{k_f}\mathfrak{m}_f \qquad\text{and}\qquad \nabla_f^\delta\phi_\star = \frac{\phi_{k_f}-\phi_k}{\delta_f}\mathfrak{n}_k^{k_f}.$$

The reconstructions in the cells and at the faces are given by

$$\{\psi_\star\}_k = \frac{1}{\mathfrak{m}_k}\sum_{f\in\mathbb{F}_k}\psi_f\frac{\delta_f\mathfrak{m}_f}{2} \qquad\text{and}\qquad \{\phi_\star\}_f = \frac{\phi_{k_f}+\phi_k}{2}.$$

It is important to note that only the normal component of the velocity $\overline{u}_f^{n+1}\cdot\mathfrak{n}_k^{k_f}$ is considered a degree of freedom in this numerical scheme. This type of staggered grid,

commonly referred to as a MAC grid for Cartesian grids, is widely utilized in fluid dynamics, especially in the diffusive or low-Mach regime [Wes09, HKL14, Pat18, BHL24]. The scheme achieves second-order accuracy in space using these differential operators. However, it is applicable only to sufficiently regular meshes, as discussed in [DO05, Her00]. The parameter $\theta \in \left[0, \frac{1}{2}\right]$ alters the characteristics of the time scheme. When $\theta = 0$, the scheme is implicit, linear, and first-order in time. Conversely, when $\theta = \frac{1}{2}$, the scheme is implicit, nonlinear, and is based on the Crank-Nicolson method, resulting in second-order accuracy in time. While the nonlinear scheme provides enhanced accuracy, it is known to lack monotonicity when applied to simple nonlinear diffusion equations.

To solve the implicit scheme (3.33) with separated unknowns, the water depth h_k^{n+1} in the second equation is substituted using the first equation. This substitution results in the following system:

$$\begin{aligned} &\overline{u}_f^{n+1-\theta} + \mathscr{T}^f_{\overline{\kappa}_\star, \overline{\Theta}_\star}\left[h_\star^{n+\theta}, S_\star\right]\left(\overline{u}_\star^{n+1-\theta}\right) \\ -g\overline{\kappa}_f \nabla_f^\delta &\left((1-\theta)\frac{\delta_t}{\overline{\Theta}_\star}\nabla_\star^\delta \cdot \left(\overline{\Theta}_\star \left\{h_\star^{n+\theta}\right\}_\star \overline{u}_\star^{n+1-\theta}\right)\right) = -g\overline{\kappa}_f \nabla_f^\delta \left(h_\star^n + S_\star\right) \end{aligned}$$

Once the velocity $\overline{u}_f^{n+1} \cdot \mathfrak{n}_k^{k_f}$ is determined, the water depth can be computed using the first equation of (3.33).

The scheme (3.33) preserves the steady state, characterized by a constant water table $h_\star^n + S_\star$. Furthermore, it satisfies the following entropy dissipation law

Proposition 3.9 *Let h_k^n be the solution of the numerical scheme (3.33). Then the following dissipation law holds*

$$\begin{aligned} &\mathscr{P}_k\left(h_k^{n+1}\right) + \delta_t \nabla_k \cdot \left(\mathscr{G}_\star^{n+1-\theta}\right) \le \mathscr{P}_k\left(h_k^n\right) \\ &-\delta_t\left(\left\{\frac{\overline{\Theta}_\star\left\{h_\star^{n+\theta}\right\}_\star}{\overline{\kappa}_\star}\left|\overline{u}_\star^{n+1-\theta}\right|^2\right\}_k + \frac{\overline{\Theta}_k h_k^{n+\theta}}{\overline{\kappa}_k}\left(\left|\overline{w}_k^{n+1-\theta}\right|^2 + \frac{\left|\widetilde{w}_k^{n+1-\theta}\right|^2}{12}\right)\right) \end{aligned}$$

where the discrete potential energy is given by $\mathscr{P}_k(h) = g\overline{\Theta}_k h\left(\frac{h}{2} + S_k\right)$. The numerical energy flux is defined as

$$\begin{aligned} \mathscr{G}_f^{n+1-\theta} = &\left(g\left\{h_\star^{n+\theta}\right\}_f\left\{h_\star^{n+1-\theta} + S_\star\right\}_f + \left\{h_\star^{n+\theta}\overline{q}_\star^{n+1-\theta}\right\}_f\right)\overline{\Theta}_f \overline{u}_f^{n+1-\theta} \\ &+\delta_f^2 \frac{\overline{\Theta}_f}{4}\overline{u}_f^{n+1-\theta} \cdot \nabla_f^\delta S_\star \nabla_f^\delta q_{S,\star}^{n+1-\theta}. \end{aligned}$$

The discrete vertical velocities are given by

$$\overline{w}_k^{n+1-\theta} = \frac{1}{\overline{\Theta}_k}\left(\left\{\overline{\Theta}_\star \overline{u}_\star^{n+1-\theta} \cdot \nabla_\star^\delta S_\star\right\}_k - \frac{h_k^{n+\theta}}{2}\nabla_k^\delta \cdot \left(\overline{\Theta}_\star \overline{u}_\star^{n+1-\theta}\right)\right)$$

and

$$\widetilde{w}_k^{n+1-\theta} = -\frac{h_k^{n+\theta}}{\overline{\Theta}_k}\nabla_k^\delta \cdot \left(\overline{\Theta}_\star \overline{u}_\star^{n+1-\theta}\right).$$

The discrete hydrodynamic pressures are defined as

$$q_{S,k}^{n+1-\theta} = \frac{h_k^{n+\theta}}{\overline{\kappa}_k}\overline{w}_k^{n+1-\theta} \qquad \text{and} \qquad \overline{q}_k^{n+1-\theta} = \frac{h_k^{n+\theta}\left(6\overline{w}_k^{n+1-\theta} + \widetilde{w}_k^{n+1-\theta}\right)}{12\overline{\kappa}_k}.$$

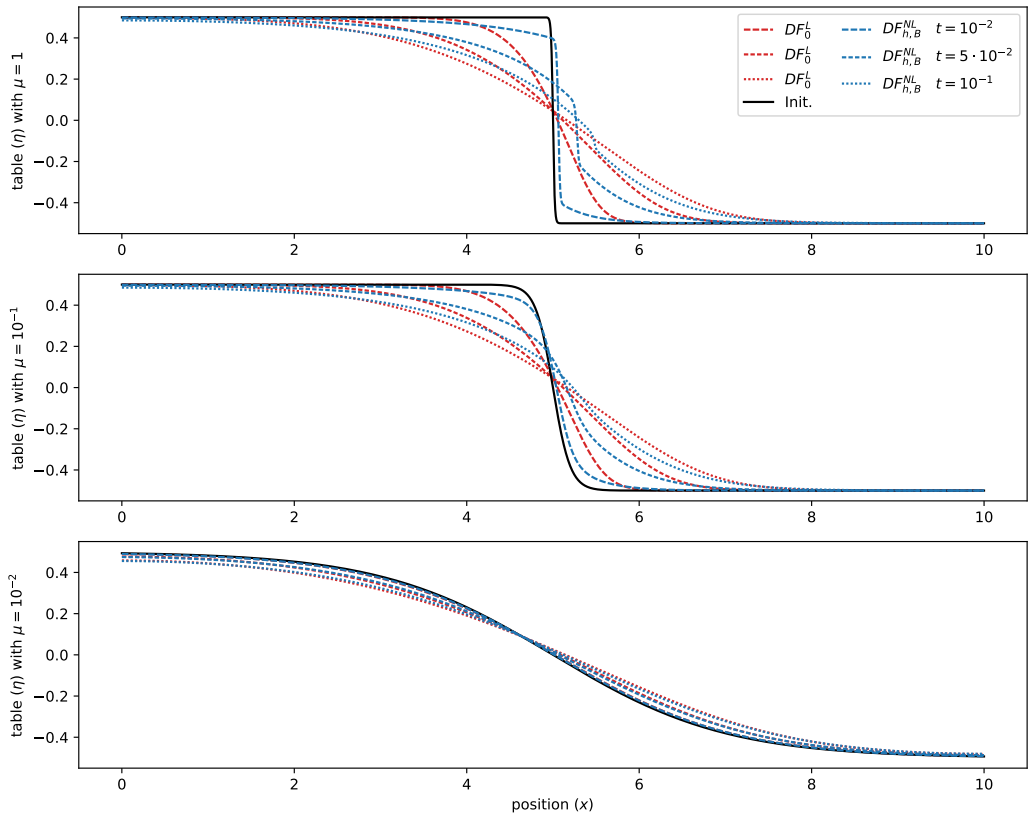

Figure 3.20: §3.2.1.2 | Water table elevations obtained by the hydrostatic model (3.30) (red lines) and the hydrodynamic model (3.32) (blue lines) for some initial conditions (black lines).

We also emphasize that when the shallowness number is sufficiently small, the solution of the numerical scheme (3.33) converges to the following scheme of the hydrostatic Dupuit-Forchheimer model (3.30)

$$h_k^{n+1} - \frac{\delta_t}{\overline{\Theta}_k} \nabla_k^\delta \cdot \left(g \overline{\kappa}_f \overline{\Theta}_\star \left\{ h_\star^{n+\theta} \right\}_\star \nabla_f^\delta \left(h_\star^{n+1-\theta} + S_\star \right) \right) = h_k^n. \tag{3.34}$$

Despite the unconditional stability result presented in Proposition 3.9, the numerical scheme (3.33) can exhibit instabilities when the time step is excessively large. The origins of these instabilities are not fully understood. To investigate their emergence, it would be necessary to explore alternative stability criteria, such as Total Variation Diminishing (TVD) norms, solution monotonicity, or maximum principles. However, these approaches present challenges at both the discrete and continuous levels. To mitigate these instabilities, we implement an adaptive time-stepping strategy. Specifically, the time step is reduced after several fixed-point iterations if convergence is not achieved. It seems that the time step should be of the same order as the spatial step. Although this strategy may not be optimal for practical applications, it offers a preliminary means to examine the behavior of

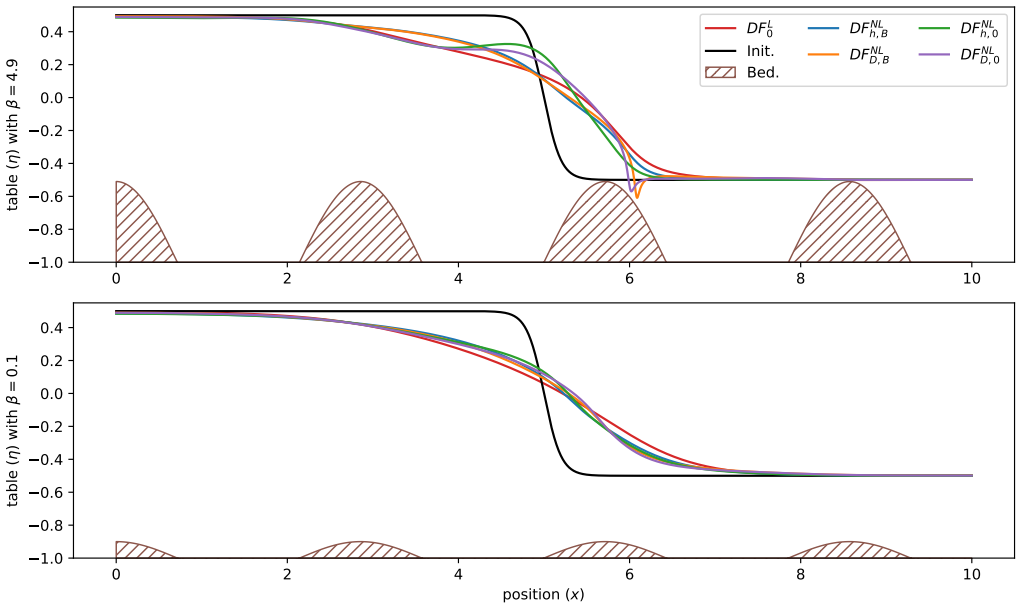

Figure 3.21: §3.2.1.2 | Water table elevations obtained by the hydrostatic model (3.30) (red line), the hydrodynamic model (3.32) fully non-linear and with large bathymetry variations $\mathscr{T}_{\overline{\kappa},\overline{\Theta}}[h,S]$ (blue line), fully non-linear and with small bathymetry variations $\mathscr{T}_{\overline{\kappa},\overline{\Theta}}[h,0]$ (green line), weakly non-linear and with large bathymetry variations $\mathscr{T}_{\overline{\kappa},\overline{\Theta}}[D,S]$ (orange line) and weakly non-linear and with small bathymetry variations $\mathscr{T}_{\overline{\kappa},\overline{\Theta}}[D,S]$ (purple line) over a bathymetry with large variations (top picture) and bathymetry with small variations (bottom picture).

the solutions.

In Figure 3.20, the solutions of the hydrostatic model (3.30) and the hydrodynamic model (3.32) are plotted for various initial conditions. When the initial condition is relatively flat (third line), the solutions from both models are identical. However, for very steep initial conditions, the solutions from the two models diverge significantly. These differences can be explained by decay rate analysis, which demonstrates that steep gradients are better preserved by the hydrodynamic model. Additionally, we observed that discontinuities tend to shift toward the direction of the lower water table, likely due to the nonlinearities inherent in the model.

In Figure 3.21, the solutions of the hydrostatic model (3.30) are compared with various hydrodynamic models (3.32), both fully and weakly nonlinear, considering small and large bathymetric variations. The results indicate that when bathymetric variations are significant, simplified hydrodynamic models can diverge considerably from the full hydrodynamic model. Specifically, models that neglect bathymetric variations in the hydrodynamic terms exhibit non-monotonic behavior upstream of a steep slope (for $x \in [4,5]$), even with a large water depth. Similarly, weakly nonlinear models also fail to maintain monotonicity, and do not adhere to the maximum principle, downstream of the steep slope (around $x = 6$),

where the water depth is shallow.

3.2.2 An approximate model of resurgence

As mentioned in §3.2, the water drainage basin consists of three regions: the surface, the vadose zone, and the aquifer. To perform simulations across the entire drainage basin, a numerical scheme capable of capturing the solution for all flow regimes is necessary. In particular, the scheme based on equations (3.24)-(3.25) have to recover the asymptotic diffusive regime described by (3.27). Asymptotic Preserving schemes in the diffusive regime are well-documented in the literature, see [Jin99, CGK13, DMTB15, BBCM16, BT16, BCT21].

When replacing the Euler equations with the asymptotic Richards equations (3.39) in porous media, the coupling between groundwater and surface water is typically achieved using the seepage boundary condition [SPPP17]. However, a scheme that discretizes the 3D equations (3.24)-(3.25) is not suitable for simulations at the scale of the water drainage basin. To conduct effective simulations across the entire catchment, coupling between the regions is essential. In this section, we focus on the scenario where the vadose zone can be neglected, allowing for direct connection between surface flow and the aquifer through a regular water table, see Figure 3.18. This situation is particularly relevant in coastal regions, where continental and ocean waters merge. It is important to note that exchanges can occur in both directions.

3.2.2.1 The Dupuit-Forchheimer/shallow water model

We propose to approximate the 3D model (3.24)-(3.25) using vertical integration methods based on the layerwise strategy outlined in §2.1.2.3, with imposed interface positions defined by vertical discontinuities in hydraulic conductivity and porosity. We present the simple case of two layers: the top layer represents the surface, while the bottom layer represents the porous media. The interface is defined as the minimum between the bathymetry and the water table, i.e. $\zeta_{3/2}(x,h) = \min(B(x), S(x)+h)$. For notation, we set $\zeta_{1/2}(x,h) = S(x)$ and $\zeta_{5/2}(x,h) = S(x)+h$. Next, we integrate the 3D model between the substratum and the interface to obtain the equations governing flow in the porous media, and similarly, we integrate the model between the interface and the water table to derive the equations governing flow in the surface. Additional assumptions are necessary to close the system, as discussed in §2.1 and §3.2.1. For simplicity, we present the results with hydrostatic models, although hydrodynamic models can also be derived. We obtain the bi-layer shallow water model with drag forces

$$\begin{aligned}
\partial_t V_1 + \nabla\cdot(V_1 u_1) &= G \\
\partial_t V_2 + \nabla\cdot(V_2 u_2) &= -G \\
\partial_t(V_1 u_1) + \nabla\cdot(V_1 u_1 \otimes u_1) &= -gV_1\nabla(h+S) - \frac{V_1 u_1}{\kappa_1} + u_{3/2} G \\
\partial_t(V_2 u_2) + \nabla\cdot(V_2 u_2 \otimes u_2) &= -gV_2\nabla(h+S) - \frac{V_2 u_2}{\kappa_2} - u_{3/2} G
\end{aligned} \tag{3.35}$$

Here, the volume of water and the effective conductivities in layer i are defined as

$$V_i(x,h) := \int_{\zeta_{i-1/2}(x,h)}^{\zeta_{i+1/2}(x,h)} \Theta(x,z)\,\mathrm{d}z \quad \text{and} \quad \kappa_i(x,h) := \left(\int_{\zeta_{i-1/2}(x,h)}^{\zeta_{i+1/2}(x,h)} \frac{\Theta(x,z)}{\kappa(x,z)}\,\mathrm{d}z\right)^{-1} V_i(x,h).$$

By the definition of the interface $\zeta_{3/2}(x,h)$, the volume V_1 is bounded by the free volume in the porous medium $\overline{V}_1(x) = \int_{S(x)}^{B(x)} \Theta(x,z)\,\mathrm{d}z$, and if it does not reach this bound, the volume of water at the surface vanishes. We conclude with the complementarity constraint

$$\min\left(\overline{V}_1 - V_1, V_2\right) = 0.$$

It is worth noting that while the complementarity constraint is written similarly to the congestion constraint (3.2), it acts differently because it is associated with the exchanged mass G, which influences the mass flux rather than acting as a force, as is the case with the roof reaction. The velocity at the interface $u_{3/2}$ is defined as in (2.1.2.3) by (2.10) to ensure energy dissipation.

Proposition 3.10 *If $\lambda \geq 0$ and for sufficiently smooth solutions of the model (3.35), the following mechanical energy dissipation law holds*

$$\partial_t\left(\mathscr{P} + \mathscr{K}_1 + \mathscr{K}_2\right) + \nabla\cdot\left(g(S+h)(V_1u_1 + V_2u_2) + \mathscr{K}_1u_1 + \mathscr{K}_2u_2\right) \leq -\left(\frac{V_1|u_1|^2}{\kappa_1} + \frac{V_2|u_2|^2}{\kappa_2}\right)$$

where $\mathscr{P}(x,h) = g\int_S^{S+h}\Theta(x,z)\,z\,\mathrm{d}z$ and $\mathscr{K}_i = \mathscr{K}(V_i,u_i)$ with $\mathscr{K}(V,u) = V\frac{|u|^2}{2}$. The equality holds when $\lambda = 0$.

Finally, the Dupuit-Forchheimer/shallow water model is obtained by considering $\kappa_1 \ll 1$ and $\kappa_2 \to \infty$. This allows us to recover the Dupuit-Forchheimer equation in the ground layer, with the mass exchange represented on the right-hand side. By summing the mass conservation equations of the two layers, we derive the Dupuit-Forchheimer/shallow water model

$$\begin{aligned} &\partial_t V + \nabla\cdot\left(V_2u_2 - g\kappa_1V_1\nabla(S+h)\right) = 0 \\ &\partial_t(V_2u_2) + \nabla\cdot(V_2u_2\otimes u_2) = -gV_2\nabla(S+h) + \left[\nabla\cdot\left(g\kappa_1V_1\nabla(S+h)\right)\mathbb{1}_{h\geq B}\right]_-^{\lambda}u_2 \end{aligned} \tag{3.36}$$

where $V(x,h) = V_1(x,h) + V_2(x,h)$ and $[\phi]_-^{\lambda} := \frac{\phi - \lambda|\phi|}{2}$. The last term in the momentum equation represents the exchange of momentum between the two layers. Since the velocity in the ground layer is negligible, this term appears as a friction term with a coefficient $[\nabla\cdot(g\kappa_1V_1\nabla(h+S))]_+^{\lambda}$. It is important to note that this coefficient is unsigned when $\lambda = 0$.

Proposition 3.11 *If $\lambda \geq 0$ and for sufficiently smooth solutions of the Dupuit-Forchheimer/shallow water model (3.36), the following mechanic energy dissipation law holds*

$$\partial_t\left(\mathscr{P} + \mathscr{K}_2\right) + \nabla\cdot\left(\left(g(S+h) + \frac{|u_2|^2}{2}\right)V_2u_2 - \frac{g^2\kappa_1V_1}{2}\nabla|S+h|^2\right) \leq -g^2\kappa_1V_1|\nabla(S+h)|^2$$

where $\mathscr{P}(x,h) = g\int_S^{S+h}\Theta(x,z)\,z\,\mathrm{d}z$ and $\mathscr{K}_2 = V_2\frac{|u_2|^2}{2}$. The equality holds when $\lambda = 0$.

3.2.2.2 Entropy-satisfying numerical scheme

The Dupuit-Forchheimer/shallow water model shares a similar formalism with the shallow water model with roof (3.3). Specifically, it is advantageous to use the potential of conservative forces, $\phi = g(S+h)$, alongside the velocity u_2 as numerical unknowns. This ensures the conservation of steady states at rest and energy dissipation at the discrete level. We propose to adapt the numerical scheme (3.4)-(3.6) as follows. The continuity equation is discretized in this manner

$$\mathscr{V}_k\left(\phi_k^{n+1}\right) = V_k^n - \frac{\delta_t^{n+1}}{\mathfrak{m}_k}\sum_{f\in\mathbb{F}_k}\left(\mathscr{F}_f^{n+1} - \mathscr{D}_f^{n+1}\right)\cdot \mathfrak{n}_f^k \mathfrak{m}_f \tag{3.37}$$

where $\mathscr{V}_k(\phi) = V\left(x_k, \frac{\phi}{g} - S_k\right)$ and $V_k^n = \mathscr{V}_k\left(\phi_k^n\right)$. The numerical mass flux of the surface flow is defined as

$$\mathscr{F}_f^{n+1} = \mathscr{F}_{CPR}\left(\delta_t^{n+1}, \begin{pmatrix}\mathfrak{d}_k\\ \mathscr{V}_{2,k}^{n+1}\left(\phi_k^{n+1}\right)\\ \phi_k^{n+1}\\ \overline{u}_{2,k}^n\end{pmatrix}, \begin{pmatrix}\mathfrak{d}_{k_f}\\ \mathscr{V}_{2,k_f}^{n+1}\left(\phi_{k_f}^{n+1}\right)\\ \phi_{k_f}^{n+1}\\ \overline{u}_{2,k_f}^n\end{pmatrix}\right)$$

with the numerical flux $\mathscr{F}_{CPR}$ defined by (3.5) and the diffusion in the porous media

$$\mathscr{D}_f^{n+1} = \mathscr{D}\left(\begin{pmatrix}\mathfrak{d}_k\\ \kappa_{1,k}\mathscr{V}_{1,k}^{n+1}\left(\phi_k^{n+1}\right)\\ \phi_k^{n+1}\end{pmatrix}, \begin{pmatrix}\mathfrak{d}_{k_f}\\ \kappa_{1,k_f}\mathscr{V}_{1,k_f}^{n+1}\left(\phi_{k_f}^{n+1}\right)\\ \phi_{k_f}^{n+1}\end{pmatrix}\right)$$

with the flux

$$\mathscr{D}\left(\begin{pmatrix}\mathfrak{d}_L\\ \mathscr{V}_{1,L}\\ \phi_L\end{pmatrix}, \begin{pmatrix}\mathfrak{d}_R\\ \mathscr{V}_{1,R}\\ \phi_R\end{pmatrix}\right) = \frac{1}{2}\left(\frac{\mathscr{V}_{1,L}}{\mathfrak{d}_L} + \frac{\mathscr{V}_{1,R}}{\mathfrak{d}_R}\right)\frac{\phi_R - \phi_L}{2}\mathfrak{n}_f^L$$

where $\mathscr{V}_{1,k}^n(\phi) = \min\left(\mathscr{V}_k^n(\phi), \overline{V}_1\right)$ is the volume of groundwater and $\mathscr{V}_{2,k}^n(\phi) = \left[\mathscr{V}_k^n(\phi) - \overline{V}_1\right]_+$ is the volume of surface water. Here, $\mathfrak{d}_k$ represents the compactness of the cell, see §1.2. Once the new potential is known, we compute the exchange of mass between the layers as follows

$$G_k^{n+1} = \frac{V_{2,k}^{n*} - V_{2,k}^{n+1}}{\delta_t^{n+1}}$$

where $V_{2,k}^{n+1} = \mathscr{V}_{2,k}^{n+1}\left(\phi_k^{n+1}\right)$ and $V_{2,k}^{n*}$ represents the volume of surface water without accounting for the mass exchange

$$V_{2,k}^{n*} = V_{2,k}^n - \frac{\delta_t^{n+1}}{\mathfrak{m}_k}\sum_{f\in\mathbb{F}_k}\mathscr{F}_f^{n+1}\cdot\mathfrak{n}_f^k\mathfrak{m}_f.$$

We could try to determine the exchanges using the flow in the porous medium, by $-\frac{1}{\mathfrak{m}_k}\sum_{f\in\mathbb{F}_k}\mathscr{D}_f^{n+1}\cdot\mathfrak{n}_f^k\mathfrak{m}_f\mathbb{1}_{h_k^{n+1}\geq B_k}$ which aligns more closely with the continuous formulation. However, this approach does not guarantee entropy stability, as shown in Proposition

3.12. When the flow is above the bathymetry at times t^n and t^{n+1}, both formulations become equivalent. Finally, the velocity is computed explicitly using an upwind scheme

$$\begin{aligned} V_{2,k}^{n+1}\overline{u}_k^{n+1} = \left(V_{2,k}^n - \delta_t^{n+1}\left[G_k^{n+1}\right]_+^\lambda\right)\overline{u}_k^n - \frac{\delta_t^{n+1}V_{2,k}^{n+1}}{\mathfrak{m}_k}\sum_{f\in\mathbb{F}_k}\frac{\phi_k^{n+1}+\phi_{k_f}^{n+1}}{2}\mathfrak{n}_f^k\mathfrak{m}_f \\ -\frac{\delta_t^{n+1}}{\mathfrak{m}_k}\sum_{f\in\mathbb{F}_k}\left(\overline{u}_k^n\left[\mathscr{F}_f^{n+1}\cdot\mathfrak{n}_f^k\right]_+ - \overline{u}_{k_f}^n\left[\mathscr{F}_f^{n+1}\cdot\mathfrak{n}_f^k\right]_-\right)\mathfrak{m}_f. \end{aligned} \tag{3.38}$$

Unlike the case of the layerwise shallow water model presented in §2.3.1.3, here the exchange are treated explicitly and potentially centered (when $\lambda = 0$). In §2.3.1.3, we opted for an upwind implicit scheme to ensure stability with an explicit Godunov-type scheme without requiring additional CFL conditions. However, thanks to the ImEx scheme (3.37)-(3.38), the overall scheme remains entropy-satisfying.

Proposition 3.12 *Under the same CFL condition as for the scheme* (3.4)-(3.6)*, i.e.*

$$\delta_t^{n+1} \leq \frac{\min\left(\mathfrak{d}_k,\mathfrak{d}_{k_f}\right)}{2\nu_f} \text{ with } \nu_f = \frac{\left|\frac{V_{2,k}^{n+1}\overline{u}_k^n + V_{2,k_f}^{n+1}\overline{u}_{k_f}^n}{2}\cdot\mathfrak{n}_f^k\right| + \frac{V_{2,k}^{n+1}+V_{2,k_f}^{n+1}}{2}\sqrt{\frac{\gamma}{4}\left|\phi_{k_f}^{n+1}-\phi_k^{n+1}\right|}}{\min\left(V_{2,k}^{n+1},V_{2,k_f}^{n+1}\right)}$$

for any $\lambda \geq 0$ and $\gamma \geq 1$, the numerical scheme (3.37)-(3.38) *is entropy-satisfying. That is, there exists a numerical flux $\mathscr{G}_f$ such that*

$$\mathscr{P}_k^{n+1} + \mathscr{K}_{2,k}^{n+1} + \frac{\delta_t}{\mathfrak{m}_k}\sum_{f\in\mathbb{F}_k}\mathscr{G}_f\cdot\mathfrak{n}_f^k\mathfrak{m}_f \leq \mathscr{P}_k^n + \mathscr{K}_{2,k}^n - \delta_t\kappa_{1,k}V_{1,k}^{n+1}\left|\frac{1}{m_k}\sum_{f\in\mathbb{F}_k}\frac{\phi_{k_f}^{n+1}-\phi_k^{n+1}}{2}\mathfrak{n}_f^k\mathfrak{m}_f\right|^2.$$

where $\mathscr{P}_k^n = \mathscr{P}\left(x_k,h_k^n\right)$ and $\mathscr{K}_{2,k}^n = \frac{V_{2,k}^n}{2}\left|u_{2,k}^n\right|^2$. Additionally, the numerical scheme is well-balanced for the steady states at rest. Specifically, if there is $\Phi\in\mathbb{R}$ such that $\phi_k^n = \Phi$ and $\overline{u}_k^n = 0$, then the numerical scheme remains steady, i.e., $\phi_k^{n+1} = \Phi$ and $\overline{u}_k^{n+1} = 0$.

Unfortunately, the CFL condition in Proposition 3.12 implies a zero time step when the water volume at the surface vanishes. While it is possible to remove a face f from the CFL condition if both surrounding cells are dry, the cells at the dry front still pose a challenge. Many of the intended applications, such as modeling resurgences, involve dry zones on the surface, and the model (3.36) was specifically designed to capture the water table as it intersects with the bathymetry. As a result, the current numerical strategy is not entirely satisfactory. In practice, however, resurgence cases, where groundwater emerges from the porous medium to the surface, seem to work with a reasonably small time step. In Figure 3.22, we illustrate a typical resurgence scenario. For reference, the minimum time step is set to 10^{-5} while the mesh size is 10^{-3}. The flow enters from the left side of the porous medium through the boundary condition. Initially, the flow diffuses within the porous medium (top right image), and after some time, the water reaches the surface. As the flow fills the porous medium, this stage is not well captured by the model, as the surface flow is limited and immediately infiltrates into the porous medium (bottom left image).

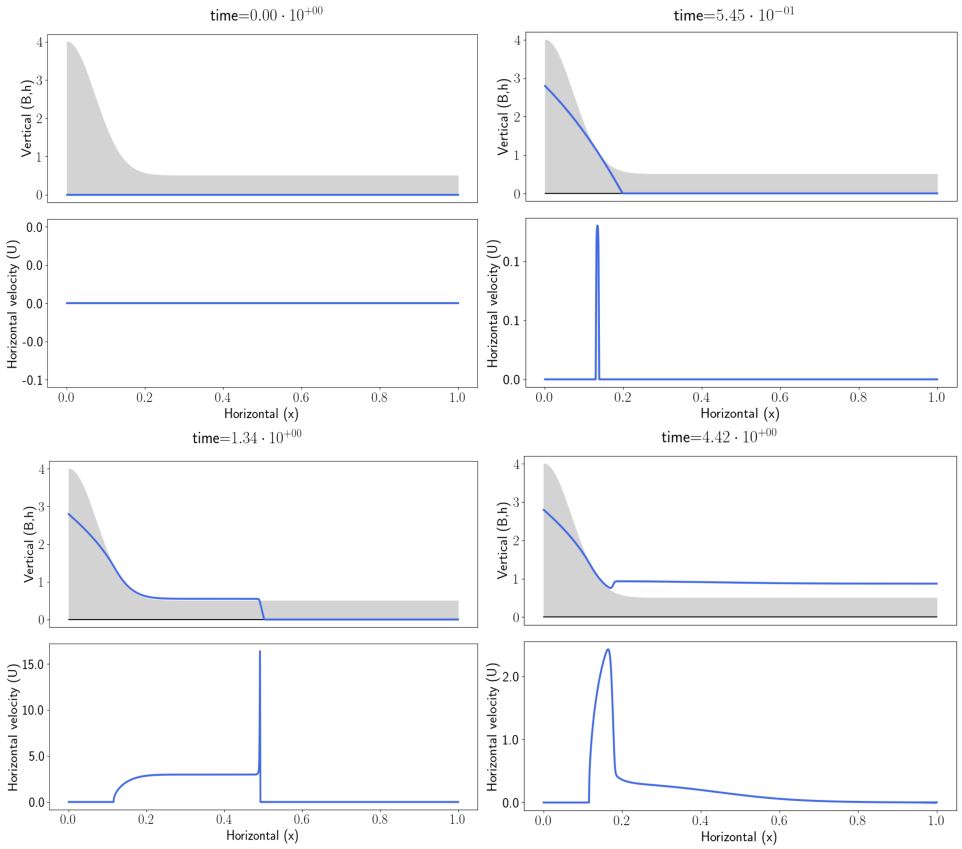

Figure 3.22: §3.2.2 | Simulation of a resurgence. (top left) Initial condition. (top right) Resurgence. (bottom left) Filling the porous media. (bottom right) Formation of an hydraulic jump.

This issue will be addressed in the next section §3.2.3. Eventually, the flow reaches the right boundary, which is modeled as a wall. Notably, a smooth hydraulic jump forms at the resurgence point (bottom right image). It is also worth mentioning that the congestion constraint can still be incorporated into the numerical scheme. Figure 3.23 demonstrates the ability to simulate seepage flooding under a dyke.

3.2.3 An approximate model of infiltration

This section focuses on modeling flow in porous media, accounting for both congested (aquifer) and non-congested (vadose) zones. Assuming low hydraulic conductivity, flow in porous media is typically described by the Richards equations (3.24)-(3.27), expressed as

$$\partial_t \theta - \nabla \cdot (\kappa \theta \nabla (p(\theta) + \overline{p})) - \partial_z (\kappa \theta \partial_z (p(\theta) + \overline{p} + gz)) = 0 \tag{3.39}$$

with the congestion constraint $\min(\Theta - \theta, \overline{p}) = 0$, as discussed in §3.1.1.1. Much of the literature focuses on modeling capillary pressure $p(\theta)$ [vG80, JMN11], along

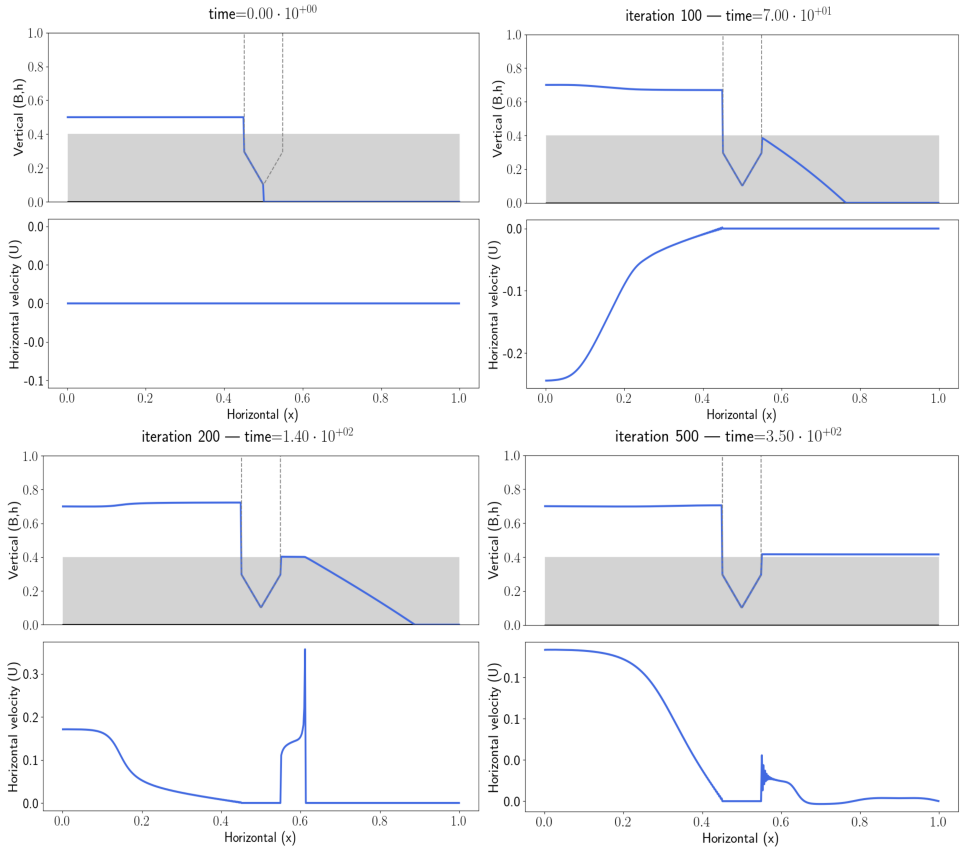

Figure 3.23: §3.2.2 | Simulation of a seepage flooding under a dyke. (top left) Initial condition. (top right) Filling the porous media. (bottom left) Resurgence (bottom right) Flooding

with its mathematical analysis [ADB85, CW99, Mik10, CP12]. Numerous numerical methods have been employed to discretize the Richards equation since the 1980s [MF04, DM05, SW05, FYL09, SK11, ORS+14, FO17, ZYZ+19, CGES21]. However, at the scale of the drainage basin scale, over extended periods ranging from days to decades, 3D simulations of the Richards equations are not feasible.

3.2.3.1 The Dupuit-Forchheimer/Richards model

In the vadose zone, it is evident that flow cannot be considered primarily horizontal. On the contrary, if the shallowness number, see §1.1 is sufficiently small, the flow is predominantly vertical, leading to a 1D vertical advection-reaction equation where horizontal flow is negligible. This equation is given by

$$\partial_t \theta - \partial_z \left(\kappa \theta \partial_z \left(p(\theta) + gz \right) \right) = -\gamma \tag{3.40}$$

with the boundary condition $\theta(t,x,B) = \theta_B(t,x)$. This simplification allows us to solve the vertical transport of water by column, which can be easily computed in parallel. One

challenge in solving (3.40) is that the model is only valid in a moving, unknown domain, specifically from the water table to the bathymetry $z \in [\eta(t,x), B(x)]$, where the water table η is determined by the groundwater wave model or an approximation of it, see §3.2.1. To address this, we propose extending (3.40) to the entire half-plane $z \in]-\infty, B(x)]$, adding the source term $\gamma(t,x,z)$, which represents the mass exchange from the vadose zone to the aquifer. This term ensures the complementarity constraint

$$\min(\Theta \mathbb{1}_{z \geq \eta} - \theta, \gamma) = 0 \qquad \text{with} \qquad \gamma(t,x,z > \eta(t,x)) = 0 \tag{3.41}$$

where the porosity Θ is assumed to be large enough not to be reached above the water table. The mass lost by the vadose zone is added to the aquifer. In this section, we assume that the hydrostatic Dupuit-Forchheimer model (3.30), with an additional source term for the vadose zone's contribution, is sufficiently accurate for the aquifer. However, more sophisticated models can be considered, see §3.2.1.1. The governing equation is

$$\partial_t V - \nabla \cdot (g\overline{\kappa} V \nabla (h + B)) = \int_{-\infty}^{B} \gamma \mathrm{d}z. \tag{3.42}$$

It is clear that the strategy preserve the total mass of water $\int_{\mathbb{R}} \left(V + \int_{-\infty}^{B} \theta \, \mathrm{d}z \right) \mathrm{d}x$. From a mathematical modeling point of view, in the previous model (3.39), the constraint was imposed by forces as in §3.1.1.1, while in this new model, it is imposed by mass exchange as in §3.2.2.

Proposition 3.13 *Assume the capillary pressure be a regular increasing function that vanishes with the water content, i.e.* $p(0) = 0$. *For sufficiently smooth solutions of the Dupuit-Forchheimer/Richards model* (3.40)-(3.42)*, the following mechanic energy dissipation law holds*

$$\begin{aligned} \partial_t \left(\mathscr{P} + \int_{-\infty}^{B} \mathscr{P}_v \mathrm{d}z \right) - \nabla \cdot \left(\frac{g^2 \overline{\kappa} V}{2} \nabla |S+h|^2 \right) = \left(\frac{\kappa\theta}{2} \partial_z |p(\theta) + gz|^2 \right)_{|z=B} \\ - g^2 \overline{\kappa} V |\nabla (S+h)|^2 - \int_{-\infty}^{B} \kappa\theta \, |\partial_z (p(\theta) + gz)|^2 \, \mathrm{d}z \end{aligned}$$

where $\mathscr{P}(x,h) = g \int_S^{S+h} \Theta(x,z) z \, \mathrm{d}z$ *and* $\mathscr{P}_v(x,z,\theta)$ *satisfies* $\partial_\theta \mathscr{P}_v = p(\theta) + gz$.

3.2.3.2 Entropy-satisfying numerical scheme

We now focus on the numerical solution of the Dupuit-Forchheimer/Richards model (3.40)-(3.42). We propose a numerical strategy based on operator splitting, where the fluxes are treated first without mass exchange, followed by a focus on the mass exchange in the second step. This approach allows the horizontal Dupuit-Forchheimer model and the vertical Richards equation to be solved in parallel, which significantly reduces computational costs. Any numerical method that approximates both the Dupuit-Forchheimer model and the Richards equation can be used. However, for efficiency, we employ a strategy that imposes no restriction on the time step. For example, let η_k^{n*} represent the solution of

the scheme (3.34), which approximates the Dupuit-Forchheimer model without mass exchange. Similarly, the vertical Richards equation is solved without mass exchange using a non-linear implicit centered scheme, i.e.

$$\theta_{k,j}^{n*} - \frac{\delta_t}{\delta_{k,j}^z}\left(\kappa_{k,j-1/2}\theta_{k,j-1/2}^{n*} \frac{p\left(\theta_{k,j-1}^{n*}\right) + g\delta_{k,j-1/2}^z - p\left(\theta_{k,j}^{n*}\right)}{\delta_{k,j-1/2}^z} - \kappa_{k,j+1/2}\theta_{k,j+1/2}^{n*} \frac{p\left(\theta_{k,j}^{n*}\right) - p\left(\theta_{k,j+1}^{n*}\right) - g\delta_{k,j+1/2}^z}{\delta_{k,j+1/2}^z} \right) = \theta_{k,j}^n \tag{3.43}$$

where the vertical face reconstructions are computed as $\psi_{j+1/2} = \frac{\psi_j + \psi_{j+1}}{2}$ for example. A variable vertical step $\delta_{k,j}^z > 0$ is used to adapt to the hydraulic conductivity, minimizing numerical diffusion. Specifically, the step size is chosen such that $\delta_{k,j}^z \kappa_{k,j}$ remains homogeneous across the domain. Note that the vertical index is numbered downward, i.e. $z_{k,j+1} = z_{k,j} - \delta_{k,j+1/2}^z$, with $z_{k,1} = B_k - \frac{\delta_{k,1}^z}{2}$. Finally, the unknowns at time t^{n+1}, including mass exchange, are computed as:

$$\Theta\left(x, \eta_k^{n+1}\right)\eta_k^{n+1} = \Theta\left(x, \eta_k^{n*}\right)\eta_k^{n*} + \sum_{j=J}^{\infty} \theta_{k,j}^{n*}\delta_{k,j}^z \qquad \text{and} \qquad \theta_{k,j}^{n+1} = \begin{cases} \theta_{k,j}^{n*} & \text{if } j < J \\ 0 & \text{else} \end{cases} \tag{3.44}$$

where the index J is defined such that some properties hold.

Let

$$J_c = \min_j \left\{ z_{k,j} \le \eta_k^{n+1} \right\} \quad \text{and} \quad J_e = \min_{j* \ge J_c} \left\{ \sum_{j=j*}^{\infty} \left(g\left(\eta_k^{n+1} - z_{k,j}\right) - p\left(\theta_{k,j}^{n+1}\right)\right)\theta_{k,j}^{n*} \le 0 \right\}.$$

If $J \le J_e$, then the discrete counterpart of the complementarity condition (3.41) holds. Specifically, for any cell where $z_{k,j} \le \eta_k^{n+1}$ we have $\theta_{k,j}^{n+1} = 0$, while $\theta_{k,J-1}^{n+1}$ may be non-zero. However, this condition alone is not sufficient to ensure entropy stability. The second index J_e addresses this limitation by ensuring that the center of mass of the exchanged water remains above the water table, thereby decreasing the potential energy during the exchange step.

Proposition 3.14 *Assume the capillary pressure is a regular increasing function, and neglect the inlet in the porous medium, i.e.* $\theta_B = 0$. *If* $J \le J_e$, *the numerical scheme* (3.34)-(3.43)-(3.44) *is entropy-satisfying, meaning the following energy dissipation law holds*

$$\begin{aligned} \mathscr{P}_k^{n+1} + \sum_{j=1}^{\infty} \mathscr{P}_{v,k,j}^{n+1}\delta_{k,j}^z - \delta_t \nabla_k \cdot \left(\frac{g^2 \overline{\kappa}_f \overline{\Theta}_f \left\{h_\star^n\right\}_f}{2} \nabla_f^\delta \left|S_\star + h_\star^{n*}\right|^2 \right) \\ \le \mathscr{P}_k^n + \sum_{j=1}^{\infty} \mathscr{P}_{v,k,j}^n \delta_{k,j}^z - \delta_t \left\{ g^2 \overline{\kappa}_\star \overline{\Theta}_\star \left\{h_\star^n\right\}_\star \left| \nabla_f^\delta \left(S_\star + h_\star^{n+1}\right)\right|^2 \right\}_k \\ - \delta_t \sum_{j=1}^{\infty} \kappa_{k,j-1/2}\theta_{k,j-1/2}^{n*} \left| \frac{p\left(\theta_{k,j-1}^{n*}\right) + g\delta_{k,j-1/2}^z - p\left(\theta_{k,j}^{n*}\right)}{\delta_{k,j-1/2}^z} \right|^2 \delta_{k,j-1/2}^z \end{aligned}$$

where $\mathscr{P}_k^n = \mathscr{P}\left(x_k, h_k^n\right)$ *and* $\mathscr{P}_{v,k,j}^n = \mathscr{P}_v\left(x_k, z_{k,j}, \theta_{k,j}^n\right)$.

It is important to note that the condition $J \leq J_e$ is not always achievable, particularly if there is insufficient water above the water table. Also if the vertical variation of water content is too stiff, this condition can imply that the vadose zone being emptied far from the water table. In practice, the condition can almost always be achieved with just a few cells above the surface. If it is not we simply set $J = J_c$. Additionally, it is worth noting that the definitions of the indices J_c and J_e may seem to conflict with the definitions of the unknowns at time t^{n+1} in (3.44). However, by calculating the exchanges from the bottom cell to the top cell and checking the conditions between each cell, it is relatively straightforward to determine the indices J_c and J_e. Finally, the infinite sums in the scheme are theoretically used to avoid imposing boundary conditions in the scheme (3.43). In practice, we implement a no-penetration condition few cells below the substratum, utilizing an exponential mesh size.

3.2.4 Perspectives

In this section, our aim is to advance continental water models, with a particular focus on improving predictions of water resources. The current work is preliminary, and several key aspects need refinement before these models can be applied to realistic configurations and scenarios.

The hydrodynamic models (3.32) we consider are non-local nonlinear diffusion equations [AV10]. In the linear case, with for flat substratum, the maximum principle can be demonstrated [GP11]. However, extending this analysis to more general, non-flat substratum, while also considering the full nonlinearity of the equations, remains highly challenging. This is despite the substantial body of literature on related models, see [Váz17]. Among the various non-local diffusion models, the hydrodynamic model (3.32) has a distinct structure, as it adheres to a projection framework. This structure can potentially facilitate the analysis of the model. From a numerical standpoint, constructing a scheme that preserves crucial stability properties, such as the maximum principle or TVD-stability, is far from straightforward, even in the linear case. Ensuring these additional stability conditions would prevent instabilities from emerging, particularly when large time steps are used.

One of the important objectives for improving these models is to better represent complex porous media, especially when addressing the presence of impermeable layers and perched groundwater systems. This challenge is analogous to the issue of submerged objects in shallow water models, as discussed in §3.1.4, and could similarly be approached through a layerwise vertical discretization method, as outlined in §2.1.2.3. However, in the context of porous media, if inertia is neglected, the problem is significantly simplified compared to shallow water dynamics.

The assumption of homogeneity in the vertical direction for porous media is another unrealistic simplification in many practical cases. In hydrostatic models, vertical variations in hydraulic conductivity and porosity typically lead to modifications in the effective hydraulic conductivity and porosity, which are then expressed as functions of the water head. However, in hydrodynamic models, incorporating vertical dependence becomes more com-

plex. A possible solution is the use of a layerwise approach, where hydraulic conductivity and porosity are treated as constants within each layer. This strategy aligns well with the reality that most porous media are naturally stratified due to successive sedimentary deposition. This layered structure of the media could, therefore, be effectively captured by such a model. Alternatively, a more sophisticated approach could be derived using a Zakharov/Craig-Sulem formulation [Zak68], adapted to address groundwater flow problems. In this approach, since $\kappa^{-1}(u,w)^{\intercal}$ forms a curl-free field, even with vertical variations in coefficients, it may provide a robust method considering asymptotic models in the Dupuit-Forchheimer regime even with vertical depend coefficients.

To generalize the treatment of the medium further, it is important to consider cases where certain materials, such as clay or fractured rock, introduce anisotropy in hydraulic conductivity. While accounting for anisotropy in the horizontal plane is relatively straightforward, doing so in the vertical direction presents additional complexities. One approach to address vertical anisotropy involves parameterizing the horizontal hydraulic conductivity by the vertical coordinate, as explored in [GDRB18]. This strategy would allow for a more accurate representation of the directional dependence of flow properties in materials that exhibit anisotropic behavior.

Looking forward, coupling the hydrodynamic models with the dynamics of the porous medium itself could represent a significant step forward. This could involve accounting for variations in porosity and hydraulic conductivity as the porous medium undergoes physical changes, such as settling or swelling, due to prolonged droughts or heavy rainfall. Such processes affect the hydrodynamic equilibrium, making the system far more complex to study. Numerical schemes that can capture these dynamic changes while conserving mass and energy are a substantial scientific challenge. Moreover, the geomorphological evolution of the porous medium could be explored using a dynamic mesh that evolves in response to forces generated by fluid flow. A dynamic Dupuit-Forchheimer/shallow water model (3.36) that incorporates such changes in the porous medium could serve as an alternative to the existing shallow water/Exner models [vWv07], offering a more refined framework for studying geomorphological processes coupled with water flow.

In summary, improving continental water models requires addressing several interrelated challenges: handling complex porous media, accounting for vertical heterogeneity and anisotropy, ensuring numerical stability in hydrodynamic models, and eventually coupling with the dynamic evolution of the porous medium. These advancements are crucial for developing more realistic and robust models capable of simulating water resource dynamics in various environments and under uncertain climate scenarios.

Bibliography

[AAGP18] N. Aguillon, E. Audusse, E. Godlewski, and M. Parisot, "Analysis of the Riemann Problem for a Shallow Water Model with Two Velocities," *SIAM Journal on Mathematical Analysis*, vol. 50, no. 5, pp. 4861–4888, 2018. [Online]. Available: https://doi.org/10.1137/17M1152887 (Cited on pages 2, 6, 7 and 37.)

[ABB+04] E. Audusse, F. Bouchut, M.-O. Bristeau, R. Klein, and B. Perthame, "A fast and stable well-balanced scheme with hydrostatic reconstruction for shallow water flows," *SIAM J. Sci. Comput.*, vol. 25, no. 6, pp. 2050–2065, 2004. (Cited on page 43.)

[ABD08] E. Audusse, M. O. Bristeau, and A. Decoene, "Numerical simulations of 3d free surface flows by a multilayer saint-venant model," *International Journal for Numerical Methods in Fluids*, vol. 56, no. 3, pp. 331–350, 2024/09/30 2008. [Online]. Available: https://doi.org/10.1002/fld.1534 (Cited on page 38.)

[ABD23] R. Abgrall, S. Busto, and M. Dumbser, "A simple and general framework for the construction of thermodynamically compatible schemes for computational fluid and solid mechanics," *Applied Mathematics and Computation*, vol. 440, p. 127629, 2023. (Cited on page 32.)

[Abg18] R. Abgrall, "A general framework to construct schemes satisfying additional conservation relations. application to entropy conservative and entropy dissipative schemes," *Journal of Computational Physics*, vol. 372, pp. 640–666, 2018. (Cited on page 32.)

[ABP21] E. Audusse, L. Boittin, and M. Parisot, "Asymptotic derivation and simulations of a non-local exner model in large viscosity regime," *ESAIM: M2AN*, vol. 55, no. 4, pp. 1635–1668, 2021. [Online]. Available: https://doi.org/10.1051/m2an/2021031 (Cited on pages 57 and 90.)

[ABPSM11] E. Audusse, M.-O. Bristeau, B. Perthame, and J. Sainte-Marie, "A multilayer Saint-Venant system with mass exchanges for shallow water flows. Derivation and numerical validation," *ESAIM: M2AN*, vol. 45, no. 1, pp. 169–200, 2011. (Cited on pages 7 and 8.)

[ACSE+21] E. Audusse, J. Caldas Steinstraesser, L. Emerald, P. Heinrich, A. Paris, and M. Parisot, "Comparison of models for the simulation of landslide generated tsunamis," *ESAIM: ProcS*, vol. 70, pp. 14–30, 2021. [Online]. Available: https://doi.org/10.1051/proc/202107002 (Cited on page 57.)

[ADB85] H. W. Alt and E. Di Benedetto, "Nonsteady flow of water and oil through inhomogeneous porous media," *Annali della Scuola Normale Superiore di Pisa - Classe di Scienze*, vol. Ser. 4, 12, no. 3, pp. 335–392, 1985. [Online]. Available: http://www.numdam.org/item/ASNSP_1985_4_12_3_335_0/ (Cited on page 99.)

[ADM09] D. Antonopoulos, V. Dougalis, and D. Mitsotakis, "Initial-boundary-value problems for the bona-smith family of boussinesq systems," *Advances in Differential Equations*, vol. 14, no. 1/2, Jan. 2009. [Online]. Available: http://dx.doi.org/10.57262/ade/1355867277 (Cited on page 27.)

[Air45] G. B. Airy, *Tides and waves*. B. Fellowes, 1845. (Cited on pages 5 and 87.)

[AK09] R. Abgrall and S. Karni, "Two-layer shallow water system: a relaxation approach," *SIAM J. Sci. Comput.*, vol. 31, pp. 1603–1627, 2009. (Cited on page 75.)

[AK10] ——, "A comment on the computation of non-conservative products," *Journal of Computational Physics*, vol. 229, no. 8, pp. 2759–2763, 2010. [Online]. Available: https://www.sciencedirect.com/science/article/pii/S0021999109006949 (Cited on page 37.)

[AKM89] S. N. Antontsev, A. Kazhiktov, and V. N. Monakhov, *Boundary value problems in mechanics of nonhomogeneous fluids*. Elsevier, 1989. (Cited on page 27.)

[And05] N. Andrianov, "Performance of numerical methods on the non-unique solution to the Riemann problem for the shallow water equations," *International Journal for Numerical Methods in Fluids*, vol. 47, no. 8-9, pp. 825–831, 2005. (Cited on page 45.)

[AÖR22] R. Abgrall, P. Öffner, and H. Ranocha, "Reinterpretation and extension of entropy correction terms for residual distribution and discontinuous galerkin schemes: application to structure preserving discretization," *Journal of Computational Physics*, vol. 453, p. 110955, 2022. (Cited on page 32.)

[AR00] A. Aw and M. Rascle, "Resurrection of 'second order' models of traffic flow," *SIAM Journal on Applied Mathematics*, vol. 60, no. 3, pp. 916–938, 2000. [Online]. Available: https://doi.org/10.1137/S0036139997332099 (Cited on page 62.)

[Aud05] E. Audusse, "A multilayer Saint-Venant model: derivation and numerical validation," *Discrete and continuous dynamical systems. Series B*, vol. 5, pp. 189–214, 2005. (Cited on page 7.)

[Aud12] C. Audiard, "Non-homogeneous boundary value problems for linear dispersive equations," *Communications in Partial Differential Equations*, vol. 37, no. 1, pp. 1–37, 2012. (Cited on page 27.)

[AV10] F. Andreu-Vaillo, *Nonlocal diffusion problems*. American Mathematical Soc., 2010, no. 165. (Cited on pages 90 and 102.)

[AV18] R. Asokan and D. Vinodh, "Soliton and exact solutions for the kdv–bbm type equations by tanh–coth and transformed rational function methods," *International Journal of Applied and Computational Mathematics*, vol. 4, no. 4, p. 100, 2018. [Online]. Available: https://doi.org/10.1007/s40819-018-0533-7 (Cited on page 21.)

[AWvJ08] E. Agamloh, A. Wallace, and A. von Jouanne, "Application of fluid-structure interaction simulation of an ocean wave energy extraction device," *Renewable Energy*, vol. 33, no. 4, pp. 748–757, 2008. (Cited on page 59.)

[Bar04] E. Barthélemy, "Nonlinear shallow water theories for coastal waves," *Surveys in Geophysics*, vol. 25, no. 3, pp. 315–337, 2004. (Cited on page 30.)

[Bar19] W. Barsukow, "Stationarity preserving schemes for multi-dimensional linear systems," *Mathematics of Computation*, vol. 88, no. 318, pp. 1621–1645, 2019. (Cited on page 43.)

[Bar21] ——, "Truly multi-dimensional all-speed schemes for the euler equations on cartesian grids," *Journal of Computational Physics*, vol. 435, p. 110216, 2021. [Online]. Available: https://www.sciencedirect.com/science/article/pii/S002199912100111X (Cited on page 63.)

[BB03] F. Berthelin and F. Bouchut, "Weak solutions for a hyperbolic system with unilateral constraint and mass loss," *Annales de l'Institut Henri Poincare (C) Non Linear Analysis*, vol. 20, no. 6, pp. 975–997, 2003. [Online]. Available: http://www.sciencedirect.com/science/article/pii/S029414490300012X (Cited on pages 60 and 62.)

[BB12] F. Berthelin and D. Broizat, "A model for the evolution of traffic jams in multi-lane," *Kinetic and Related Models*, vol. 5, no. 4, pp. 697–728, 2012. (Cited on page 62.)

[BBBBC21] S. Bulteau, M. Badsi, C. Berthon, and M. Bessemoulin-Chatard, "A fully well-balanced and asymptotic preserving scheme for the shallow-water equations with a generalized manning friction source term," *Calcolo*, vol. 58, no. 4, p. 41, Sep 2021. [Online]. Available: https://link.springer.com/content/pdf/10.1007/s10092-021-00432-7.pdf (Cited on page 43.)

[BBBD20] C. Bassi, L. Bonaventura, S. Busto, and M. Dumbser, "A hyperbolic reformulation of the serre-green-naghdi model for general bottom topographies," *Computers & Fluids*, vol. 212, p. 104716, 2020. [Online]. Available: https://www.sciencedirect.com/science/article/pii/S0045793020302863 (Cited on page 30.)

[BBCM16] C. Berthon, M. Bessemoulin-Chatard, and H. Mathis, "Numerical convergence rate for a diffusive limit of hyperbolic systems: p-system with damping," *The SMAI Journal of computational mathematics*, vol. 2, pp. 99–119, 2016. [Online]. Available: http://www.numdam.org/articles/10.5802/smai-jcm.10/ (Cited on page 94.)

[BBCR00] F. Bouchut, Y. Brenier, J. Cortes, and J.-F. Ripoll, "A hierarchy of models for two-phase flows," *Journal of Nonlinear Science*, vol. 10, no. 6, pp. 639–660, 2000. [Online]. Available: http://dx.doi.org/10.1007/s003320010006 (Cited on pages 60 and 62.)

[BBD20a] C. Bassi, S. Busto, and M. Dumbser, "High order ader-dg schemes for the simulation of linear seismic waves induced by nonlinear dispersive free-surface water waves," *Applied Numerical Mathematics*, vol. 158, pp. 236–263, 2020. [Online]. Available: https://www.sciencedirect.com/science/article/pii/S0168927420302300 (Cited on page 30.)

[BBD+20b] A. Bermúdez, S. Busto, M. Dumbser, J. L. Ferrín, L. Saavedra, and M. E. Vázquez-Cendón, "A staggered semi-implicit hybrid fv/fe projection method for weakly compressible flows," *Journal of Computational Physics*, vol. 421, p. 109743, 2020. [Online]. Available: https://www.sciencedirect.com/science/article/pii/S0021999120305179 (Cited on page 30.)

[BBF+22] C. Berthon, S. Bulteau, F. Foucher, M. M'baye, and V. Michel-Dansac, "A very easy high-order well-balanced reconstruction for hyperbolic systems with source terms," *SIAM Journal on Scientific Computing*, vol. 44, no. 4, pp. A2506–A2535, 2022. (Cited on page 43.)

[BBM97] T. B. Benjamin, J. L. Bona, and J. J. Mahony, "Model equations for long waves in nonlinear dispersive systems," *Philosophical Transactions of the Royal Society of London. Series A, Mathematical and Physical Sciences*, vol. 272, no. 1220, pp. 47–78, 2024/01/23 1997. [Online]. Available: https://doi.org/10.1098/rsta.1972.0032 (Cited on pages 19 and 20.)

[BBP] M. Bergmann, U. Bosi, and M. Parisot, "Novel Boussinesq/Navier-Stokes two way coupling for the simulation of wave-structure interaction," working paper or preprint. (Cited on page 58.)

[BC16] C. Berthon and C. Chalons, "A fully well-balanced, positive and entropy-satisfying godunov-type method for the shallow-water equations," *Mathe-*

matics of Computation, vol. 85, no. 299, pp. 1281–1307, 2016. (Cited on page 43.)

[BC17] K. Brenner and C. Cancès, "Improving Newton's Method Performance by Parametrization: The Case of the Richards Equation," *SIAM Journal on Numerical Analysis*, vol. 55, no. 4, pp. 1760–1785, 2017. [Online]. Available: https://doi.org/10.1137/16M1083414 (Cited on page 62.)

[BCDD+23] C. Berthon, M. J. Castro Díaz, A. Duran, T. Morales de Luna, and K. Saleh, "Artificial viscosity to get both robustness and discrete entropy inequalities," *Journal of Scientific Computing*, vol. 97, no. 3, p. 65, 2023. (Cited on page 32.)

[BCS02] Bona, Chen, and Saut, "Boussinesq equations and other systems for small-amplitude long waves in nonlinear dispersive media. i: Derivation and linear theory," *Journal of Nonlinear Science*, vol. 12, no. 4, pp. 283–318, Aug 2002. [Online]. Available: http://dx.doi.org/10.1007/s00332-002-0466-4 (Cited on page 22.)

[BCT21] F. Blachère, C. Chalons, and R. Turpault, "Very high-order asymptotic-preserving schemes for hyperbolic systems of conservation laws with parabolic degeneracy on unstructured meshes," *Computers & Mathematics with Applications*, vol. 87, pp. 41–49, 2021. [Online]. Available: https://www.sciencedirect.com/science/article/pii/S0898122121000390 (Cited on page 94.)

[BD15] A. Babarit and G. Delhommeau, "Theoretical and numerical aspects of the open source BEM solver NEMOH," in *11th European Wave and Tidal Energy Conference*, Nantes, France, 2015. [Online]. Available: https://hal.archives-ouvertes.fr/hal-01198800 (Cited on page 59.)

[BD22] S. Busto and M. Dumbser, "A staggered semi-implicit hybrid finite volume / finite element scheme for the shallow water equations at all froude numbers," *Applied Numerical Mathematics*, vol. 175, pp. 108–132, 2022. [Online]. Available: https://www.sciencedirect.com/science/article/pii/S0168927422000319 (Cited on page 63.)

[BD23] C. Brutto and M. Dumbser, "A semi-implicit finite volume scheme for a simplified hydrostatic model for fluid-structure interaction," *International Journal for Numerical Methods in Fluids*, vol. 95, no. 1, pp. 107–142, 2023. (Cited on page 63.)

[BDDR08] F. Berthelin, P. Degond, M. Delitala, and M. Rascle, "A model for the formation and evolution of traffic jams," *Archive for Rational Mechanics and Analysis*, vol. 187, no. 2, pp. 185–220, 2008. [Online]. Available: https://doi.org/10.1007/s00205-007-0061-9 (Cited on page 62.)

[BDE+21] S. Busto, M. Dumbser, C. Escalante, N. Favrie, and S. Gavrilyuk, "On high order ader discontinuous galerkin schemes for first order hyperbolic reformulations of nonlinear dispersive systems," *Journal of Scientific Computing*, vol. 87, no. 2, p. 48, 2021. [Online]. Available: https://doi.org/10.1007/s10915-021-01429-8 (Cited on page 30.)

[BDF+19] C. Berthon, A. Duran, F. Foucher, K. Saleh, and J. D. D. Zabsonré, "Improvement of the hydrostatic reconstruction scheme to get fully discrete entropy inequalities," *Journal of Scientific Computing*, vol. 80, no. 2, pp. 924–956, 2019. [Online]. Available: https://doi.org/10.1007/s10915-019-00961-y (Cited on pages 32 and 43.)

[BDL+20] W. Boscheri, G. Dimarco, R. Loubère, M. Tavelli, and M.-H. Vignal, "A second order all mach number imex finite volume solver for the three dimensional euler equations," *Journal of Computational Physics*, vol. 415, p. 109486, 2020. [Online]. Available: https://www.sciencedirect.com/science/article/pii/S0021999120302606 (Cited on page 67.)

[BDLB+08] F. Berthelin, P. Degond, V. Le Blanc, S. Moutari, M. Rascle, and J. Royer, "A traffic-flow model with constraints for the modeling of traffic jams," *Mathematical Models and Methods in Applied Sciences*, vol. 18, no. supp01, pp. 1269–1298, 2008. [Online]. Available: http://www.worldscientific.com/doi/abs/10.1142/S0218202508003030 (Cited on page 62.)

[BDS12] C. Berthon, B. Dubroca, and A. Sangam, "A local entropy minimum principle for deriving entropy preserving schemes," *SIAM Journal on Numerical Analysis*, vol. 50, no. 2, pp. 468–491, 2012. (Cited on page 32.)

[BEG12] C. Bourdarias, M. Ersoy, and S. Gerbi, "A mathematical model for unsteady mixed flows in closed water pipes," *Science China Mathematics*, vol. 55, no. 2, pp. 221–244, 2012. [Online]. Available: http://dx.doi.org/10.1007/s11425-011-4353-z (Cited on page 61.)

[BEG13] ——, "Air entrainment in transient flows in closed water pipes : A two-layer approach," *ESAIM: M2AN*, vol. 47, no. 2, pp. 507–538, 2013. [Online]. Available: https://doi.org/10.1051/m2an/2012036 (Cited on page 75.)

[BEG14] ——, "Unsteady mixed flows in non uniform closed water pipes: a full kinetic approach," *Numerische Mathematik*, vol. 128, no. 2, pp. 217–263, Oct 2014. [Online]. Available: https://link.springer.com/content/pdf/10.1007/s00211-014-0611-7.pdf (Cited on page 61.)

[BEK+17] W. Barsukow, P. V. F. Edelmann, C. Klingenberg, F. Miczek, and F. K. Röpke, "A numerical scheme for the compressible low-mach

number regime of ideal fluid dynamics," *Journal of Scientific Computing*, vol. 72, no. 2, pp. 623–646, Aug 2017. [Online]. Available: https://link.springer.com/content/pdf/10.1007/s10915-017-0372-4.pdf (Cited on page 63.)

[BEKER19] U. Bosi, A. P. Engsig-Karup, C. Eskilsson, and M. Ricchiuto, "A spectral/hp element depth-integrated model for nonlinear wave–body interaction," *Computer Methods in Applied Mechanics and Engineering*, vol. 348, pp. 222 – 249, 2019. [Online]. Available: http://www.sciencedirect.com/science/article/pii/S0045782519300416 (Cited on page 61.)

[BEKP11] S. Bryson, Y. Epshteyn, A. Kurganov, and G. Petrova, "Well-balanced positivity preserving central-upwind scheme on triangular grids for the saint-venant system," *ESAIM: Mathematical Modelling and Numerical Analysis*, vol. 45, no. 3, pp. 423–446, 2011. (Cited on page 43.)

[BELV16] C. Besse, M. Ehrhardt, and I. Lacroix-Violet, "Discrete artificial boundary conditions for the linearized korteweg–de vries equation," *Numerical Methods for Partial Differential Equations*, vol. 32, no. 5, pp. 1455–1484, 2024/09/30 2016. [Online]. Available: https://doi.org/10.1002/num.22058 (Cited on page 27.)

[Ber94] J.-P. Berenger, "A perfectly matched layer for the absorption of electromagnetic waves," *Journal of Computational Physics*, vol. 114, no. 2, pp. 185–200, 1994. [Online]. Available: https://www.sciencedirect.com/science/article/pii/S0021999184711594 (Cited on page 45.)

[Ber02] F. Berthelin, "Existence and weak stability for a pressureless model with unilateral constraint," *Mathematical Models and Methods in Applied Sciences*, vol. 12, no. 02, pp. 249–272, 2002. [Online]. Available: http://www.worldscientific.com/doi/abs/10.1142/S0218202502001635 (Cited on pages 60 and 62.)

[BG07] C. Bourdarias and S. Gerbi, "A finite volume scheme for a model coupling free surface and pressurised flows in pipes," *Journal of Computational and Applied Mathematics*, vol. 209, no. 1, pp. 109 – 131, 2007. [Online]. Available: //www.sciencedirect.com/science/article/pii/S0377042706006686 (Cited on page 61.)

[BG08] ——, "A conservative model for unsteady flows in deformable closed pipes and its implicit second-order finite volume discretisation," *Computers & Fluids*, vol. 37, no. 10, pp. 1225–1237, 2008. [Online]. Available: https://www.sciencedirect.com/science/article/pii/S0045793008000042 (Cited on page 61.)

[BGC03] S. Benzoni-Gavage and R. M. Colombo, "An-populations model for traffic flow," *European Journal of Applied Mathematics*, vol. 14, no. 5, pp. 587–612, 2003. (Cited on page 62.)

[BGDD07] S. Benzoni-Gavage, R. Danchin, and S. Descombes, "On the well-posedness for the euler-korteweg model in several space dimensions," *Indiana University Mathematics Journal*, vol. 56, no. 4, pp. 1499–1579, 2007. [Online]. Available: http://www.jstor.org/stable/24902741 (Cited on page 24.)

[BGKN22] C. Besse, S. Gavrilyuk, M. Kazakova, and P. Noble, "Perfectly Matched Layers Methods for Mixed Hyperbolic–Dispersive Equations," *Water Waves*, vol. 4, no. 3, pp. 313–343, oct 2022. [Online]. Available: https://link.springer.com/article/10.1007/s42286-022-00069-1 (Cited on page 45.)

[BGL17] C. Bourdarias, S. Gerbi, and R. Lteif, "A numerical scheme for an improved green–naghdi model in the camassa–holm regime for the propagation of internal waves," *Computers & Fluids*, vol. 156, pp. 283–304, 2017. [Online]. Available: https://www.sciencedirect.com/science/article/pii/S0045793017302505 (Cited on page 30.)

[BHI14] M. Bergmann, J. Hovnanian, and A. Iollo, "An accurate cartesian method for incompressible flows with moving boundaries," *Communications in Computational Physics*, vol. 15, no. 5, pp. 1266–1290, 2014. (Cited on pages 59 and 75.)

[BHL24] A. Brunel, R. Herbin, and J.-C. Latché, "A staggered scheme for the compressible euler equations on general 3d meshes," *Journal of Scientific Computing*, vol. 100, no. 2, p. 30, Jun 2024. [Online]. Available: https://link.springer.com/content/pdf/10.1007/s10915-024-02560-y.pdf (Cited on pages 63 and 91.)

[BI16] M. Bergmann and A. Iollo, "Bioinspired swimming simulations," *Journal of Computational Physics*, vol. 323, pp. 310 – 321, 2016. [Online]. Available: http://www.sciencedirect.com/science/article/pii/S0021999116303175 (Cited on page 59.)

[BLMP17] A. Beljadid, P. G. LeFloch, S. Mishra, and C. Parés, "Schemes with well-controlled dissipation. hyperbolic systems in nonconservative form," *Communications in Computational Physics*, vol. 21, no. 4, pp. 913–946, 2017. [Online]. Available: https://www.cambridge.org/core/product/16751185D7F4C5EC296D22933FA131A9 (Cited on page 32.)

[BMD24] C. Berthon and V. Michel-Dansac, "A fully well-balanced hydrodynamic reconstruction," *Journal of Numerical Mathematics*, no. 0, 2024. (Cited on page 43.)

[BMGN18] C. Besse, B. Mésognon-Gireau, and P. Noble, "Artificial boundary conditions for the linearized benjamin–bona–mahony equation," *Numerische Mathematik*, vol. 139, no. 2, pp. 281–314, 2018. [Online]. Available: https://doi.org/10.1007/s00211-017-0943-1 (Cited on page 27.)

[BN07] D. Bresch and P. Noble, "Mathematical justification of a shallow water model," *Methods and Applications of Analysis*, vol. 14, no. 2, pp. 87–118, 6 2007. (Cited on page 6.)

[BNS17] C. Besse, P. Noble, and D. Sanchez, "Discrete transparent boundary conditions for the mixed KDV–BBM equation," *Journal of Computational Physics*, vol. 345, no. Supplement C, pp. 484 – 509, 2017. [Online]. Available: http://www.sciencedirect.com/science/article/pii/S0021999117304060 (Cited on page 27.)

[Boc19] E. Bocchi, "On the return to equilibrium problem for axisymmetric floating structures in shallow water," 2019. (Cited on pages 61 and 74.)

[Boc20] ——, "Floating structures in shallow water: Local well-posedness in the axisymmetric case," *SIAM Journal on Mathematical Analysis*, vol. 52, no. 1, pp. 306–339, 2020. [Online]. Available: https://doi.org/10.1137/18M1174180 (Cited on page 61.)

[Bon23] P. Bonneton, "Energy and dissipation spectra of waves propagating in the inner surf zone," *Journal of Fluid Mechanics*, vol. 977, p. A48, 2023. (Cited on page 53.)

[Bou04] J. Boussinesq, "Recherches théoriques sur l'écoulement des nappes d'eau infiltrées dans le sol et sur le débit des sources," *Journal de Mathématiques Pures et Appliquées*, vol. 5e série, 10, pp. 5–78, 1904. [Online]. Available: http://www.numdam.org/item/JMPA_1904_5_10__5_0/ (Cited on page 85.)

[Bou65] H. Bouwer, "Limitation of the dupuit-forchheimer assumption in recharge and seepage," *Transactions of the ASAE*, vol. 8, no. 4, pp. 512–0515, 1965. [Online]. Available: https://elibrary.asabe.org/abstract.asp?aid=40565&t=3 (Cited on page 85.)

[Bou03] F. Bouchut, "Entropy satisfying flux vector splittings and kinetic bgk models," *Numerische Mathematik*, vol. 94, no. 4, pp. 623–672, 2003. [Online]. Available: http://dx.doi.org/10.1007/s00211-002-0426-9 (Cited on page 32.)

[Bou04] ——, *Nonlinear stability of finite volume methods for hyperbolic conservation laws, and well-balanced schemes for sources*. Springer Science & Business Media, 2004. (Cited on pages 17, 30, 39, 43 and 78.)

[Boy02] F. Boyer, "A theoretical and numerical model for the study of incompressible mixture flows," *Computers & Fluids*, vol. 31, no. 1, pp. 41–68, 2002. [Online]. Available: https://www.sciencedirect.com/science/article/pii/S0045793000000311 (Cited on page 75.)

[Bri49] H. C. Brinkman, "A calculation of the viscous force exerted by a flowing fluid on a dense swarm of particles," *Flow, Turbulence and Combustion*, vol. 1, no. 1, pp. 27–34, Dec 1949. [Online]. Available: https://link.springer.com/content/pdf/10.1007/BF02120313.pdf (Cited on page 90.)

[BRMVCD21] S. Busto, L. Río-Martín, M. E. Vázquez-Cendón, and M. Dumbser, "A semi-implicit hybrid finite volume/finite element scheme for all mach number flows on staggered unstructured meshes," *Applied Mathematics and Computation*, vol. 402, p. 126117, 2021. [Online]. Available: https://www.sciencedirect.com/science/article/pii/S009630032100165X (Cited on page 63.)

[BT16] F. Blachère and R. Turpault, "An admissibility and asymptotic-preserving scheme for systems of conservation laws with source term on 2d unstructured meshes," *Journal of Computational Physics*, vol. 315, pp. 98–123, 2016. [Online]. Available: https://www.sciencedirect.com/science/article/pii/S0021999116001972 (Cited on page 94.)

[Bur48] J. Burgers, "A mathematical model illustrating the theory of turbulence," ser. Advances in Applied Mechanics, R. Von Mises and T. Von Kármán, Eds. Elsevier, 1948, vol. 1, pp. 171–199. [Online]. Available: https://www.sciencedirect.com/science/article/pii/S0065215608701005 (Cited on page 47.)

[But21] J. C. Butcher, *B-series: algebraic analysis of numerical methods*. Springer, 2021, vol. 55. (Cited on page 42.)

[BV94] A. Bermudez and M. E. Vazquez, "Upwind methods for hyperbolic conservation laws with source terms," *Comput. & Fluids*, vol. 23, no. 8, pp. 1049–1071, 1994. (Cited on page 43.)

[BV+16] C. Bucur, E. Valdinoci *et al.*, *Nonlocal diffusion and applications*. Springer, 2016, vol. 20. (Cited on page 90.)

[Cas99] V. Casulli, "A semi-implicit finite difference method for non-hydrostatic, free-surface flows," *International Journal for Numerical Methods in Fluids*, vol. 30, no. 4, pp. 425–440, 1999. [Online]. Available: http://dx.doi.org/10.1002/(SICI)1097-0363(19990630)30:4<425::AID-FLD847>3..0.CO;2-D (Cited on pages 12 and 63.)

[Cas14] ——, "A semi-implicit numerical method for the free-surface navier–stokes equations," *International Journal for Numerical Methods in*

Fluids, vol. 74, no. 8, pp. 605–622, 2014. [Online]. Available: https://onlinelibrary.wiley.com/doi/abs/10.1002/fld.3867 (Cited on page 63.)

[CBB10] R. Cienfuegos, E. Barthélemy, and P. Bonneton, "Wave-breaking model for boussinesq-type equations including roller effects in the mass conservation equation," *Journal of Waterway, Port, Coastal, and Ocean Engineering*, vol. 136, no. 1, pp. 10–26, Jan. 2010. [Online]. Available: http://dx.doi.org/10.1061/(ASCE)WW.1943-5460.0000022 (Cited on page 53.)

[CBCC92] J. Clottes, A. Beltrán, J. Courtin, and H. Cosquer, "La grotte cosquer (cap morgiou, marseille)," *Bulletin de la Société préhistorique française*, vol. 89, no. 4, pp. 98–128, 1992. [Online]. Available: http://www.jstor.org/stable/27921039 (Cited on page 75.)

[CC92] V. Casulli and R. T. Cheng, "Semi-implicit finite difference methods for three-dimensional shallow water flow," *International Journal for Numerical Methods in Fluids*, vol. 15, no. 6, pp. 629–648, 1992. [Online]. Available: https://onlinelibrary.wiley.com/doi/abs/10.1002/fld.1650150602 (Cited on pages 7 and 63.)

[CCH+19] Y. Cheng, A. Chertock, M. Herty, A. Kurganov, and T. Wu, "A new approach for designing moving-water equilibria preserving schemes for the shallow water equations," *Journal of Scientific Computing*, vol. 80, pp. 538–554, 2019. (Cited on page 43.)

[CD13] D. Clamond and D. Dutykh, "Fast accurate computation of the fully nonlinear solitary surface gravity waves," *Computers and Fluids*, vol. 84, pp. 35–38, Sep. 2013, 8 pages, 4 figures, 22 references. Other authors papers can be downloaded at http://www.denys-dutykh.com/. [Online]. Available: https://hal.archives-ouvertes.fr/hal-00759812 (Cited on page 15.)

[CDCRFNP07] M. Castro Díaz, T. Chacón Rebollo, E. D. Fernández-Nieto, and C. Parés, "On well-balanced finite volume methods for nonconservative nonhomogeneous hyperbolic systems," *SIAM Journal on Scientific Computing*, vol. 29, no. 3, pp. 1093–1126, 2007. (Cited on page 37.)

[CDK12] F. Cordier, P. Degond, and A. Kumbaro, "An asymptotic-preserving all-speed scheme for the Euler and Navier–Stokes equations," *Journal of Computational Physics*, vol. 231, no. 17, pp. 5685–5704, 2012. [Online]. Available: https://www.sciencedirect.com/science/article/pii/S0021999112002069 (Cited on page 63.)

[CDV17] F. Couderc, A. Duran, and J.-P. Vila, "An explicit asymptotic preserving low froude scheme for the multilayer shallow water model with density stratification," *Journal of Computational Physics*, vol. 343, pp. 235 – 270,

2017. [Online]. Available: http://www.sciencedirect.com/science/article/pii/S0021999117302899 (Cited on page 63.)

[CFMP13] M. J. Castro, U. S. Fjordholm, S. Mishra, and C. Parés, "Entropy conservative and entropy stable schemes for nonconservative hyperbolic systems," *SIAM Journal on Numerical Analysis*, vol. 51, no. 3, pp. 1371–1391, 2013. (Cited on page 37.)

[CFRB19] R. Chassagne, A. G. Filippini, M. Ricchiuto, and P. Bonneton, "Dispersive and dispersive-like bores in channels with sloping banks," *Journal of Fluid Mechanics*, vol. 870, pp. 595–616, 2019. [Online]. Available: https://www.cambridge.org/core/product/010A9881C15122ACCD155023FD54585F (Cited on page 30.)

[CGES21] J.-B. Clément, F. Golay, M. Ersoy, and D. Sous, "An adaptive strategy for discontinuous galerkin simulations of richards' equation: Application to multi-materials dam wetting," *Advances in Water Resources*, vol. 151, p. 103897, 2021. [Online]. Available: https://www.sciencedirect.com/science/article/pii/S030917082100052X (Cited on page 99.)

[CGHS02] F. Coquel, T. Gallouët, J.-M. Hérard, and N. Seguin, "Closure laws for a two-fluid two-pressure model," *Comptes Rendus Mathematique*, vol. 334, no. 10, pp. 927–932, 2002. [Online]. Available: https://www.sciencedirect.com/science/article/pii/S1631073X0202366X (Cited on page 75.)

[CGK13] C. Chalons, M. Girardin, and S. Kokh, "Large time step and asymptotic preserving numerical schemes for the gas dynamics equations with source terms," *SIAM Journal on Scientific Computing*, vol. 35, no. 6, pp. A2874–A2902, Jan. 2013. [Online]. Available: http://dx.doi.org/10.1137/130908671 (Cited on pages 63 and 94.)

[CGLGP08] M. Castro, J. M. Gallardo, J. A. López-García, and C. Parés, "Well-balanced high order extensions of Godunov's method for semilinear balance laws," *SIAM J. Numer. Anal.*, vol. 46, no. 2, pp. 1012–1039, 2008. (Cited on page 43.)

[CH52] C. F. Curtiss and J. O. Hirschfelder, "Integration of stiff equations," *Proceedings of the national academy of sciences*, vol. 38, no. 3, pp. 235–243, 1952. (Cited on page 42.)

[CH93] R. Camassa and D. D. Holm, "An integrable shallow water equation with peaked solitons," *Phys. Rev. Lett.*, vol. 71, pp. 1661–1664, Sep 1993. [Online]. Available: https://link.aps.org/doi/10.1103/PhysRevLett.71.1661 (Cited on page 21.)

[Cha20] C. Chalons, "Path-conservative in-cell discontinuous reconstruction schemes for non conservative hyperbolic systems," *Communications in Mathematical Sciences*, vol. 18, no. 1, pp. 1–30, 2020. (Cited on page 37.)

[Cho68] A. J. Chorin, "Numerical solution of the Navier-Stokes equations," *Mathematics of Computation*, vol. 22, no. 104, pp. 745–762, 1968. [Online]. Available: http://www.jstor.org/stable/2004575 (Cited on pages 18 and 30.)

[CKS19] C. Chalons, S. Kokh, and M. Stauffert, "An all-regime and well-balanced Lagrange-projection type scheme for the shallow water equations on unstructured meshes," Feb. 2019, working paper or preprint. [Online]. Available: https://hal.archives-ouvertes.fr/hal-02004835 (Cited on page 63.)

[CL14] A. Castro and D. Lannes, "Fully nonlinear long-wave models in the presence of vorticity," *Journal of Fluid Mechanics*, vol. 759, pp. 642–675, 2014. (Cited on page 12.)

[CLM10] F. Chazel, D. Lannes, and F. Marche, "Numerical Simulation of Strongly Nonlinear and Dispersive Waves Using a Green–Naghdi Model," *Journal of Scientific Computing*, vol. 48, no. 1, pp. 105–116, 2010. (Cited on page 30.)

[CLR20] C. Courtès, F. Lagoutière, and F. Rousset, "Error estimates of finite difference schemes for the korteweg–de vries equation," *IMA Journal of Numerical Analysis*, vol. 40, no. 1, pp. 628–685, 9/29/2024 2020. [Online]. Available: https://doi.org/10.1093/imanum/dry082 (Cited on page 34.)

[CMP01] M. Castro, J. Macías, and C. Parés, "A q-scheme for a class of systems of coupled conservation laws with source term. application to a two-layer 1-d shallow water system," *ESAIM: Mathematical Modelling and Numerical Analysis*, vol. 35, no. 1, pp. 107–127, 2001. (Cited on page 37.)

[CN17] G. Chen and S. Noelle, "A new hydrostatic reconstruction scheme based on subcell reconstructions," *SIAM Journal on Numerical Analysis*, vol. 55, no. 2, pp. 758–784, 2017. (Cited on page 43.)

[CP] M. Carreau and M. Parisot, "A unified shallow water/dupuit-forchheimer model for surface and groundwater flow at drainage basin scale," working paper or preprint. (Cited on page 58.)

[CP05] Y. Chitour and B. Piccoli, "Traffic circles and timing of traffic lights for cars flow," *Discrete and Continuous Dynamical Systems Series B*, vol. 5, no. 3, p. 599, 2005. (Cited on page 62.)

[CP12] C. Cancès and M. Pierre, "An existence result for multidimensional immiscible two-phase flows with discontinuous capillary pressure field," *SIAM Journal on Mathematical Analysis*, vol. 44, no. 2, pp. 966–992, Jan. 2012. [Online]. Available: http://dx.doi.org/10.1137/11082943X (Cited on page 99.)

[CPP13] V. Chabannes, G. Pena, and C. Prud'homme, "High-order fluid–structure interaction in 2d and 3d application to blood flow in arteries," *Journal of Computational and Applied Mathematics*, vol. 246, pp. 1 – 9, 2013, fifth International Conference on Advanced COmputational Methods in ENgineering (ACOMEN 2011). [Online]. Available: http://www.sciencedirect.com/science/article/pii/S0377042712004256 (Cited on page 59.)

[CPT01] G. Cerne, S. Petelin, and I. Tiselj, "Coupling of the interface tracking and the two-fluid models for the simulation of incompressible two-phase flow," *Journal of Computational Physics*, vol. 171, no. 2, pp. 776–804, 2001. [Online]. Available: https://www.sciencedirect.com/science/article/pii/S002199910196810X (Cited on page 75.)

[CRT08] L. Cheng, G. Ribatski, and J. R. Thome, "Two-Phase Flow Patterns and Flow-Pattern Maps: Fundamentals and Applications," *Applied Mechanics Reviews*, vol. 61, no. 5, 07 2008, 050802. [Online]. Available: https://doi.org/10.1115/1.2955990 (Cited on page 75.)

[CSZ97] H. Capart, X. Sillen, and Y. Zech, "Numerical and experimental water transients in sewer pipes," *Journal of Hydraulic Research*, vol. 35, no. 5, pp. 659–672, 09 1997. [Online]. Available: http://dx.doi.org/10.1080/00221689709498400 (Cited on page 75.)

[CTR23] M. Ciallella, D. Torlo, and M. Ricchiuto, "Arbitrary high order weno finite volume scheme with flux globalization for moving equilibria preservation," *Journal of Scientific Computing*, vol. 96, no. 2, p. 53, 2023. (Cited on page 43.)

[CW99] J. Carrillo and P. Wittbold, "Uniqueness of renormalized solutions of degenerate elliptic–parabolic problems," *Journal of Differential Equations*, vol. 156, no. 1, pp. 93–121, 1999. [Online]. Available: https://www.sciencedirect.com/science/article/pii/S0022039698935975 (Cited on page 99.)

[CZ10] V. Casulli and P. Zanolli, "A nested newton-type algorithm for finite volume methods solving richards' equation in mixed form," *SIAM Journal on Scientific Computing*, vol. 32, no. 4, pp. 2255–2273, Jan. 2010. [Online]. Available: http://dx.doi.org/10.1137/100786320 (Cited on page 86.)

[Dag67] G. Dagan, "Second order linearized theory of free-surface flow in porous media," *The Quarterly Journal of Mechanics and Applied Mathematics*, vol. 20, no. 4, pp. 517–526, January 1967. [Online]. Available: https://doi.org/10.1093/qjmam/20.4.517 (Cited on page 88.)

[Dar56] H. P. G. Darcy, *Détermination des lois d'èoulement de l'eau à travers le sable*, 1856. (Cited on page 86.)

[DBdM+19] C. Demay, C. Bourdarias, B. d. L. de Meux, S. Gerbi, and J.-M. Hérard, "A splitting method adapted to the simulation of mixed flows in pipes with a compressible two-layer model," *ESAIM: Mathematical Modelling and Numerical Analysis*, vol. 53, no. 2, pp. 405–442, 2019. (Cited on page 75.)

[DD22] F. Dhaouadi and M. Dumbser, "A first order hyperbolic reformulation of the navier-stokes-korteweg system based on the gpr model and an augmented lagrangian approach," *Journal of Computational Physics*, vol. 470, p. 111544, 2022. [Online]. Available: https://www.sciencedirect.com/science/article/pii/S0021999122006064 (Cited on page 30.)

[Del10] S. Dellacherie, "Analysis of godunov type schemes applied to the compressible euler system at low mach number," *J. Computational Phys.*, vol. 229, pp. 978–1016, 2010. (Cited on pages 63 and 64.)

[DH17] C. Demay and J.-M. Hérard, "A compressible two-layer model for transient gas–liquid flows in pipes," *Continuum Mechanics and Thermodynamics*, vol. 29, no. 2, pp. 385–410, Mar 2017. [Online]. Available: https://doi.org/10.1007/s00161-016-0531-0 (Cited on page 75.)

[DIT16] V. Duchêne, S. Israwi, and R. Talhouk, "A new class of two-layer green-naghdi systems with improved frequency dispersion," *Studies in Applied Mathematics*, vol. 137, no. 3, pp. 356–415, 2016. [Online]. Available: https://doi.org/10.1111/sapm.12125 (Cited on page 51.)

[DJOR16] S. Dellacherie, J. Jung, P. Omnes, and P.-A. Raviart, "Construction of modified godunov-type schemes accurate at any mach number for the compressible euler system," *Mathematical Models and Methods in Applied Sciences*, vol. 26, no. 13, pp. 2525–2615, 2016. [Online]. Available: https://doi.org/10.1142/S0218202516500603 (Cited on page 63.)

[DK22] V. Duchêne and C. Klein, "Numerical study of the serre-green-naghdi equations and a fully dispersive counterpart," *Discrete and Continuous Dynamical Systems - B*, vol. 27, no. 10, pp. 5905–5933 EP –, 2022. [Online]. Available: https://www.aimsciences.org/article/doi/10.3934/dcdsb.2021300 (Cited on page 51.)

[DLDP13] T. M. De Luna, M. C. Diaz, and C. Parés, "Reliability of first order numerical schemes for solving shallow water system over abrupt topography,"

Applied Mathematics and computation, vol. 219, no. 17, pp. 9012–9032, 2013. (Cited on page 45.)

[DLGP13] M. C. Díaz, J. A. López-García, and C. Parés, "High order exactly well-balanced numerical methods for shallow water systems," *Journal of Computational Physics*, vol. 246, pp. 242–264, 2013. (Cited on page 43.)

[DLMDV18] G. Dimarco, R. Loubère, V. Michel-Dansac, and M.-H. Vignal, "Second-order implicit-explicit total variation diminishing schemes for the euler system in the low mach regime," *Journal of Computational Physics*, vol. 372, pp. 178–201, 2018. [Online]. Available: https://www.sciencedirect.com/science/article/pii/S0021999118304005 (Cited on page 67.)

[DLV17] G. Dimarco, R. Loubère, and M.-H. Vignal, "Study of a new asymptotic preserving scheme for the euler system in the low mach number limit," *SIAM Journal on Scientific Computing*, vol. 39, no. 5, pp. A2099–A2128, 2017. [Online]. Available: https://doi.org/10.1137/16M1069274 (Cited on page 63.)

[DM05] A. Dogan and L. Motz, "Saturated-unsaturated 3d groundwater model. ii: Verification and application," *Journal of Hydrologic Engineering*, vol. 10, no. 6, pp. 505–515, 2024/09/17 2005. [Online]. Available: https://doi.org/10.1061/(ASCE)1084-0699(2005)10:6(505) (Cited on page 99.)

[DMC20] S. Di Marino and L. Chizat, "A tumor growth model of hele-shaw type as a gradient flow," *ESAIM: Control, Optimisation and Calculus of Variations*, vol. 26, p. 103, 2020. [Online]. Available: http://dx.doi.org/10.1051/cocv/2020019 (Cited on page 62.)

[DMLM95] G. Dal Maso, P. G. LeFloch, and F. Murat, "Definition and weak stability of nonconservative products," *Journal de mathématiques pures et appliquées*, vol. 74, no. 6, pp. 483–548, 1995. (Cited on page 37.)

[DMTB15] A. Duran, F. Marche, R. Turpault, and C. Berthon, "Asymptotic preserving scheme for the shallow water equations with source terms on unstructured meshes," *Journal of Computational Physics*, vol. 287, pp. 184–206, 2015. [Online]. Available: https://www.sciencedirect.com/science/article/pii/S0021999115000686 (Cited on page 94.)

[DNBS10] P. Degond, L. Navoret, R. Bon, and D. Sanchez, "Congestion in a macroscopic model of self-driven particles modeling gregariousness," *Journal of Statistical Physics*, vol. 138, pp. 85–125, 2010. (Cited on page 62.)

[DO05] K. Domelevo and P. Omnes, "A finite volume method for the laplace equation on almost arbitrary two-dimensional grids," *ESAIM: Mathematical Modelling and Numerical Analysis*, vol. 39, no. 6, pp.

1203–1249, Nov. 2005. [Online]. Available: http://dx.doi.org/10.1051/m2an:2005047 (Cited on page 91.)

[dOF10] A. F. de O. Falcão, "Wave energy utilization: A review of the technologies," *Renewable and Sustainable Energy Reviews*, vol. 14, no. 3, pp. 899–918, 2010. [Online]. Available: https://www.sciencedirect.com/science/article/pii/S1364032109002652 (Cited on page 75.)

[DR24] A. Duran and G. L. Richard, "Discretization of a new model of dispersive waves with improved dispersive properties and exact conservation of energy," Apr. 2024, working paper or preprint. [Online]. Available: https://hal.science/hal-04552250 (Cited on page 30.)

[dSV71] A.-J.-C. B. de Saint-Venant, "Théorie du mouvement non permanent des eaux, avec application aux crues des rivières et à l'introduction des marées dans leurs lits," *C.R. Acad. Sci. Paris*, vol. 73, pp. 147–154, 1871. (Cited on page 5.)

[Duc16] V. Duchêne, "The multilayer shallow water system in the limit of small density contrast," *Asymptotic Analysis*, vol. 98, no. 3, pp. 189–235, Jun. 2016. [Online]. Available: http://dx.doi.org/10.3233/ASY-161366 (Cited on page 7.)

[Duc21] ——, "Many Models for Water Waves," Habilitation à diriger des recherches, Université de Rennes 1, Jul. 2021. [Online]. Available: https://tel.archives-ouvertes.fr/tel-03282212 (Cited on page 4.)

[Dup63] J. É. J. Dupuit, *Études théoriques et pratiques sur le mouvement des eaux dans les canaux découverts et à travers les terrains perméables: avec des considérations relatives au régime des grandes eaux, au débouché à leur donner, et à la marche des alluvions dans les rivières à fond mobile*. Dunod, 1863. (Cited on pages 84 and 88.)

[DZBK16] V. Desveaux, M. Zenk, C. Berthon, and C. Klingenberg, "A well-balanced scheme to capture non-explicit steady states in the euler equations with gravity," *International Journal for Numerical Methods in Fluids*, vol. 81, no. 2, pp. 104–127, 2016. (Cited on page 43.)

[EDC19] C. Escalante, M. Dumbser, and M. J. Castro, "An efficient hyperbolic relaxation system for dispersive non-hydrostatic water waves and its solution with high order discontinuous galerkin schemes," *Journal of Computational Physics*, vol. 394, pp. 385–416, 2019. [Online]. Available: https://www.sciencedirect.com/science/article/pii/S0021999119303730 (Cited on page 30.)

[EFNGD+23] C. Escalante, E. D. Fernández-Nieto, J. Garres-Díaz, T. Morales de Luna, and Y. Penel, "Non-hydrostatic layer-averaged approximation of euler

system with enhanced dispersion properties," *Computational and Applied Mathematics*, vol. 42, no. 4, p. 177, May 2023. [Online]. Available: https://link.springer.com/content/pdf/10.1007/s40314-023-02309-7.pdf (Cited on pages 11 and 15.)

[EGH00] R. Eymard, T. Gallouët, and R. Herbin, "Finite volume methods," in *Solution of Equation in Rn (Part 3), Techniques of Scientific Computing (Part 3)*, ser. Handbook of Numerical Analysis. Elsevier, 2000, vol. 7, pp. 713–1018. [Online]. Available: https://www.sciencedirect.com/science/article/pii/S1570865900070058 (Cited on page 69.)

[EH16] G. El and M. Hoefer, "Dispersive shock waves and modulation theory," *Physica D: Nonlinear Phenomena*, vol. 333, pp. 11 – 65, 2016, dispersive Hydrodynamics. [Online]. Available: http://www.sciencedirect.com/science/article/pii/S0167278916301580 (Cited on page 21.)

[Eme21] L. Emerald, "Rigorous derivation from the water waves equations of some full dispersion shallow water models," *SIAM Journal on Mathematical Analysis*, vol. 53, no. 4, pp. 3772–3800, 2021. [Online]. Available: https://doi.org/10.1137/20M1332049 (Cited on page 51.)

[FG17] N. Favrie and S. Gavrilyuk, "A rapid numerical method for solving Serre–Green–Naghdi equations describing long free surface gravity waves," *Nonlinearity*, vol. 30, no. 7, p. 2718, 2017. [Online]. Available: http://stacks.iop.org/0951-7715/30/i=7/a=2718 (Cited on page 30.)

[FNPPSM18] E. D. Fernández-Nieto, M. Parisot, Y. Penel, and J. Sainte-Marie, "A hierarchy of dispersive layer-averaged approximations of Euler equations for free surface flows," *Communications in Mathematical Sciences*, vol. 16, no. 5, pp. 1169–1202, 2018. [Online]. Available: http://dx.doi.org/10.4310/CMS.2018.v16.n5.a1 (Cited on pages 2 and 12.)

[FO17] M. W. Farthing and F. L. Ogden, "Numerical solution of richards' equation: A review of advances and challenges," *Soil Science Society of America Journal*, vol. 81, no. 6, pp. 1257–1269, 2017. [Online]. Available: https://acsess.onlinelibrary.wiley.com/doi/abs/10.2136/sssaj2017.02.0058 (Cited on page 99.)

[Fua02] M. Fuamba, "Contribution on transient flow modelling in storm sewers," *Journal of Hydraulic Research*, vol. 40, no. 6, pp. 685–693, Nov. 2002. [Online]. Available: http://dx.doi.org/10.1080/00221680209499915 (Cited on page 61.)

[FYL09] M. Fahs, A. Younes, and F. Lehmann, "An easy and efficient combination of the mixed finite element method and the method of lines for the resolution of richards' equation," *Environmental Modelling & Software*,

vol. 24, no. 9, pp. 1122–1126, 2009. [Online]. Available: https://www.sciencedirect.com/science/article/pii/S1364815209000425 (Cited on page 99.)

[GBCP21] I. Gómez-Bueno, M. J. Castro, and C. Parés, "High-order well-balanced methods for systems of balance laws: a control-based approach," *Applied Mathematics and Computation*, vol. 394, p. 125820, 2021. (Cited on page 43.)

[GCDM21] E. Guerrero Fernández, M. J. Castro Díaz, M. Dumbser, and T. Morales de Luna, "An arbitrary high order well-balanced ader-dg numerical scheme for the multilayer shallow-water model with variable density," *Journal of Scientific Computing*, vol. 90, no. 1, p. 52, 2021. [Online]. Available: https://doi.org/10.1007/s10915-021-01734-2 (Cited on page 37.)

[GdLP+18] J.-L. Guermond, M. Q. de Luna, B. Popov, C. E. Kees, and M. W. Farthing, "Well-balanced second-order finite element approximation of the shallow water equations with friction," *SIAM Journal on Scientific Computing*, vol. 40, no. 6, pp. A3873–A3901, 2018. (Cited on page 43.)

[GDRB18] V. Guinot, C. Delenne, A. Rousseau, and O. Boutron, "Flux closures and source term models for shallow water models with depth-dependent integral porosity," *Advances in Water Resources*, vol. 122, pp. 1 – 26, 2018. [Online]. Available: http://www.sciencedirect.com/science/article/pii/S0309170818300484 (Cited on page 103.)

[GHR12] G. P. Galdi, J. G. Heywood, and R. Rannacher, *Fundamental directions in mathematical fluid mechanics*. Birkhäuser, 2012. (Cited on page 27.)

[GK96] M. F. Gobbi and J. T. Kirby, "A fourth order boussinesq-type wave model," in *Coastal Engineering 1996*, 1996, pp. 1116–1129. (Cited on page 27.)

[GKPT22] J.-L. Guermond, C. Kees, B. Popov, and E. Tovar, "Hyperbolic relaxation technique for solving the dispersive serre–green–naghdi equations with topography," *Journal of Computational Physics*, vol. 450, p. 110809, 2022. [Online]. Available: https://www.sciencedirect.com/science/article/pii/S002199912100704X (Cited on page 30.)

[GLM20] T. Goudon, J. Llobell, and S. Minjeaud, "An asymptotic preserving scheme on staggered grids for the barotropic euler system in low mach regimes," *Numerical Methods for Partial Differential Equations*, vol. 36, no. 5, pp. 1098–1128, 2024/09/30 2020. [Online]. Available: https://doi.org/10.1002/num.22466 (Cited on page 63.)

[GM98] M. F. Göz and C.-D. Munz, *Approximate Riemann Solvers for Fluid Flow with Material Interfaces*. Dordrecht: Springer Netherlands, 1998, pp. 211–235. [Online]. Available: https://doi.org/10.1007/978-94-015-9137-9_9 (Cited on page 46.)

[GM24] T. Goudon and S. Minjeaud, "An explicit well-balanced scheme on staggered grids for barotropic euler equations," *ESAIM: M2AN*, vol. 58, no. 4, pp. 1263–1299, 2024. [Online]. Available: https://doi.org/10.1051/m2an/2024035 (Cited on page 43.)

[GMCC13] C. Gopal, M. Mohanraj, P. Chandramohan, and P. Chandrasekar, "Renewable energy source water pumping systems—a literature review," *Renewable and Sustainable Energy Reviews*, vol. 25, pp. 351–370, 2013. [Online]. Available: https://www.sciencedirect.com/science/article/pii/S1364032113002633 (Cited on page 75.)

[GMS06] J. Guermond, P. Minev, and J. Shen, "An overview of projection methods for incompressible flows," *Computer Methods in Applied Mechanics and Engineering*, vol. 195, no. 44, pp. 6011 – 6045, 2006. [Online]. Available: http://www.sciencedirect.com/science/article/pii/S0045782505004640 (Cited on page 30.)

[GN76] A. E. Green and P. M. Naghdi, "A derivation of equations for wave propagation in water of variable depth," *Journal of Fluid Mechanics*, vol. 78, no. 2, pp. 237–246, 1976. (Cited on pages 10 and 24.)

[God59] S. K. Godunov, "A difference method for numerical calculation of discontinuous solutions of the equations of hydrodynamics," *Mat. Sb. (N.S.)*, vol. 47(89), no. 3, pp. 271–306, 1959. (Cited on page 31.)

[God79] K. Goda, "A multistep technique with implicit difference schemes for calculating two-or three-dimensional cavity flows," *Journal of computational physics*, vol. 30, no. 1, pp. 76–95, 1979. (Cited on page 40.)

[Gos00] L. Gosse, "A well-balanced flux-vector splitting scheme designed for hyperbolic systems of conservation laws with source terms," *Comput. Math. Appl.*, vol. 39, no. 9, pp. 135–159, 2000. (Cited on page 43.)

[GP01] J.-F. Gerbeau and B. Perthame, "Derivation of viscous Saint-Venant system for laminar shallow water; Numerical validation," *Discrete and Continuous Dynamical Systems - Series B*, vol. 1, no. 1, pp. 89–102, 2001. (Cited on page 6.)

[GP11] T. Goudon and M. Parisot, "On the spitzer–härm regime and nonlocal approximations: Modeling, analysis, and numerical simulations," *Multiscale Modeling & Simulation*, vol. 9, no. 2, pp. 568–600, 2011. [Online]. Available: https://doi.org/10.1137/100800269 (Cited on pages 90 and 102.)

[GPC07] J. M. Gallardo, C. Parés, and M. Castro, "On a well-balanced high-order finite volume scheme for shallow water equations with topography and dry areas," *Journal of Computational Physics*, vol. 227, no. 1, pp. 574–601, 2007. (Cited on page 43.)

[GPSMW18] E. Godlewski, M. Parisot, J. Sainte-Marie, and F. Wahl, "Congested shallow water model: roof modeling in free surface flow," *ESAIM: Mathematical Modelling and Numerical Analysis*, vol. 52, no. 5, pp. 1679–1707, Sep 2018. [Online]. Available: http://dx.doi.org/10.1051/m2an/2018032 (Cited on pages 56, 61, 63, 67 and 68.)

[GPSMW20] ——, "Congested shallow water model: on floating body," *The SMAI journal of computational mathematics*, vol. 6, pp. 227–251, 2020. [Online]. Available: https://smai-jcm.centre-mersenne.org/item/SMAI-JCM_2020__6__227_0/ (Cited on pages 56 and 70.)

[GPZ14] N. Goutal, M. Parisot, and F. Zaoui, "A 2d reconstruction for the transverse coupling of shallow water models," *International Journal for Numerical Methods in Fluids*, vol. 75, no. 11, pp. 775–799, 2014. [Online]. Available: http://dx.doi.org/10.1002/fld.3913 (Cited on page 56.)

[GQ98] J.-L. Guermond and L. Quartapelle, "On stability and convergence of projection methods based on pressure poisson equation," *International Journal for Numerical Methods in Fluids*, vol. 26, no. 9, pp. 1039–1053, 1998. (Cited on page 31.)

[GR96] E. Godlewski and P.-A. Raviart, *Numerical approximation of hyperbolic systems of conservation laws*, ser. Applied Mathematical Sciences. Springer-Verlag, New York, 1996, vol. 118. (Cited on pages 6, 30 and 45.)

[GR04] ——, "The numerical interface coupling of nonlinear hyperbolic systems of conservation laws. I: The scalar case," *Numer. Math.*, vol. 97, no. 1, pp. 81–130, 2004. (Cited on pages 36 and 46.)

[GS03] J.-L. Guermond and J. Shen, "Velocity-correction projection methods for incompressible flows," *SIAM Journal on Numerical Analysis*, vol. 41, no. 1, pp. 112–134, 2003. (Cited on page 31.)

[GS22] S. Gavrilyuk and K.-M. Shyue, "Singular solutions of the bbm equation: analytical and numerical study," *Nonlinearity*, vol. 35, no. 1, p. 388, 2022. [Online]. Available: https://dx.doi.org/10.1088/1361-6544/ac3921 (Cited on page 52.)

[GTR05] E. Godlewski, K.-C. L. Thanh, and P.-A. Raviart, "The numerical interface coupling of nonlinear hyperbolic systems of conservation laws : II. The case of systems," *ESAIM: Mathematical Modelling and Numerical Analysis*, vol. 39, no. 4, pp. 649–692, 2005. [Online]. Available: http://www.numdam.org/articles/10.1051/m2an:2005029/ (Cited on page 46.)

[Gue94] J.-L. Guermond, "Sur l'approximation des équations de navier-stokes par une méthode de projection," *Comptes rendus de l'Académie des sciences.*

Série 1, Mathématique, vol. 319, no. 8, pp. 887–892, 1994. (Cited on page 30.)

[Gue99] ——, "Un résultat de convergence d'ordre deux en temps pour l'approximation des équations de navier–stokes par une technique de projection incrémentale," *ESAIM: Mathematical Modelling and Numerical Analysis*, vol. 33, no. 1, pp. 169–189, 1999. (Cited on page 40.)

[GVV13] N. Grenier, J.-P. Vila, and P. Villedieu, "An accurate low-mach scheme for a compressible two-fluid model applied to free-surface flows," *J. Computational Phys.*, vol. 252, pp. 1–19, 2013. (Cited on page 63.)

[GWK16] G. J. Gassner, A. R. Winters, and D. A. Kopriva, "A well balanced and entropy conservative discontinuous galerkin spectral element method for the shallow water equations," *Applied Mathematics and Computation*, vol. 272, pp. 291–308, 2016. (Cited on page 42.)

[Hel58] H. Helmholtz, "Über integrale der hydrodynamischen gleichungen, welche den wirbelbewegungen entsprechen," *Journal für die reine und angewandte Mathematik*, vol. 1858, no. 55, pp. 25–55, 1858. [Online]. Available: https://doi.org/10.1515/crll.1858.55.25 (Cited on page 18.)

[Her00] F. Hermeline, "A finite volume method for the approximation of diffusion operators on distorted meshes," *Journal of Computational Physics*, vol. 160, no. 2, pp. 481–499, 2000. [Online]. Available: https://www.sciencedirect.com/science/article/pii/S0021999100964660 (Cited on page 91.)

[HHMM10] P. Helluy, J.-M. Hérard, H. Mathis, and S. Müller, "A simple parameter-free entropy correction for approximate riemann solvers," *Comptes rendus. Mécanique*, vol. 338, no. 9, pp. 493–498, 2010. (Cited on page 37.)

[HJL12] J. Haack, S. Jin, and J. Liu, "An all-speed asymptotic-preserving method for the isentropic euler and navier-stokes equations," *Communications in Computational Physics*, vol. 12, no. 4, pp. 955–980, 2012. (Cited on page 63.)

[HKL14] Herbin, R., Kheriji, W., and Latché, J.-C., "On some implicit and semi-implicit staggered schemes for the shallow water and euler equations," *ESAIM: M2AN*, vol. 48, no. 6, pp. 1807–1857, 2014. [Online]. Available: http://dx.doi.org/10.1051/m2an/2014021 (Cited on pages 63 and 91.)

[HKP+17] J. Harris, K. Kuznetsov, C. Peyrard, S. Saviot, A. Mivehchi, S. T. Grilli, and M. Benoit, "Simulation of wave forces on a gravity based foundation by a BEM based on fully nonlinear potential flow," in *27th Offshore and Polar Engineering Conference*, San Francsico, USA, 2017. (Cited on page 59.)

[HLL83] A. Harten, P. D. Lax, and B. v. Leer, "On upstream differencing and godunov-type schemes for hyperbolic conservation laws," *SIAM Review*, vol. 25, no. 1, pp. 35–61, 1983. [Online]. Available: https://doi.org/10.1137/1025002 (Cited on pages 31 and 32.)

[Hor12] U. Hornung, *Homogenization and porous media*. Springer Science & Business Media, 2012, vol. 6. (Cited on page 85.)

[Isr11] S. Israwi, "Large time existence for 1D Green-Naghdi equations," *Nonlinear Analysis: Theory, Methods & Applications*, vol. 74, no. 1, pp. 81–93, 1 2011. (Cited on page 10.)

[Jin99] S. Jin, "Efficient asymptotic-preserving (ap) schemes for some multiscale kinetic equations," *SIAM Journal on Scientific Computing*, vol. 21, no. 2, pp. 441–454, 1999. (Cited on page 94.)

[JMN11] M. A. C. Jan M. Nordbotten, *Large-Scale Models*. John Wiley & Sons, Ltd, 2011, ch. 4, pp. 115–152. [Online]. Available: https://onlinelibrary.wiley.com/doi/abs/10.1002/9781118137086.ch4 (Cited on page 98.)

[Joh49] F. John, "On the motion of floating bodies. I," *Communications on Pure and Applied Mathematics*, vol. 2, no. 1, pp. 13–57, 1949. [Online]. Available: http://dx.doi.org/10.1002/cpa.3160020102 (Cited on page 59.)

[Joh50] ——, "On the motion of floating bodies ii. simple harmonic motions," *Communications on Pure and Applied Mathematics*, vol. 3, no. 1, pp. 45–101, 1950. [Online]. Available: https://onlinelibrary.wiley.com/doi/abs/10.1002/cpa.3160030106 (Cited on page 59.)

[Kas00] M. Kashiwagi, "Non-linear simulations of wave-induced motions of a floating body by means of the mixed eulerian-lagrangian method," *Proceedings of the Institution of Mechanical Engineers, Part C: Journal of Mechanical Engineering Science*, vol. 214, no. 6, pp. 841–855, 2000. [Online]. Available: http://dx.doi.org/10.1243/0954406001523821 (Cited on pages 59 and 60.)

[KCKD00] A. B. Kennedy, Q. Chen, J. T. Kirby, and R. A. Dalrymple, "Boussinesq modeling of wave transformation, breaking, and runup. i: 1d," *Journal of Waterway, Port, Coastal, and Ocean Engineering*, vol. 126, no. 1, pp. 39–47, Jan. 2000. [Online]. Available: http://dx.doi.org/10.1061/(ASCE)0733-950X(2000)126:1(39) (Cited on page 53.)

[KDS14] M. Kazolea, A. Delis, and C. Synolakis, "Numerical treatment of wave breaking on unstructured finite volume approximations for extended Boussinesq-type equations," *Journal of Computational Physics*, vol. 271, pp. 281–305, 2014, frontiers in Computational Physics.

[Online]. Available: https://www.sciencedirect.com/science/article/pii/S0021999114000576 (Cited on pages 49 and 53.)

[KH12] J. Knudsen and P. Hjorth, *Elements of Newtonian Mechanics*. Springer Berlin Heidelberg, 2012. [Online]. Available: https://books.google.fr/books?id=rkP1CAAAQBAJ (Cited on page 71.)

[KK92] T. Karambas and C. Koutitas, "A breaking wave propagation model based on the boussinesq equations," *Coastal Engineering*, vol. 18, no. 1, pp. 1–19, 1992. [Online]. Available: https://www.sciencedirect.com/science/article/pii/037838399290002C (Cited on page 53.)

[KKKP04] S. Karni, E. Kirr, A. Kurganov, and G. Petrova, "Compressible two-phase flows by central and upwind schemes," *ESAIM: Mathematical Modelling and Numerical Analysis*, vol. 38, no. 3, pp. 477–493, 2004. (Cited on page 75.)

[KLLS11] M. Krotkiewski, I. S. Ligaarden, K.-A. Lie, and D. W. Schmid, "On the importance of the stokes-brinkman equations for computing effective permeability in karst reservoirs," *Communications in Computational Physics*, vol. 10, no. 5, pp. 1315–1332, 2011. (Cited on page 90.)

[KLP] M. Kazolea, R. Lteif, and M. Parisot, "A second order ImEx scheme for low-Mach regime," working paper or preprint. (Cited on page 58.)

[KN20] M. Kazakova and P. Noble, "Discrete Transparent Boundary Conditions for the Linearized Green–Naghdi System of Equations," *SIAM Journal on Numerical Analysis*, vol. 58, no. 1, pp. 657–683, 2020. [Online]. Available: https://doi.org/10.1137/18M1220248 (Cited on page 27.)

[KOS23] I. Kukavica, W. Ożański, and M. Sammartino, "The inviscid inflow-outflow problem via analyticity," *arXiv preprint arXiv:2310.20439*, 2023. (Cited on page 27.)

[KR18] M. Kazolea and M. Ricchiuto, "On wave breaking for Boussinesq-type models," *Ocean Modelling*, vol. 123, pp. 16 – 39, 2018. [Online]. Available: http://www.sciencedirect.com/science/article/pii/S1463500318300131 (Cited on page 53.)

[KR19a] M. Kazakova and G. L. Richard, "A new model of shoaling and breaking waves: one-dimensional solitary wave on a mild sloping beach," *Journal of Fluid Mechanics*, vol. 862, pp. 552–591, Jan 2019. [Online]. Available: http://dx.doi.org/10.1017/jfm.2018.947 (Cited on page 12.)

[KR19b] ——, "A new model of shoaling and breaking waves: one-dimensional solitary wave on a mild sloping beach," *Journal of Fluid Mechanics*, vol. 862, pp. 552–591, 2019. (Cited on page 53.)

[KR24] M. Kazolea and M. Ricchiuto, "Full Nonlinearity in Weakly Dispersive Boussinesq Models: Luxury or Necessity," *Journal of Hydraulic Engineering*, vol. 150, no. 1, Jan. 2024. [Online]. Available: http://dx.doi.org/10.1061/JHEND8.HYENG-13718 (Cited on page 30.)

[KS71] E. F. Keller and L. A. Segel, "Traveling bands of chemotactic bacteria: A theoretical analysis," *Journal of Theoretical Biology*, vol. 30, no. 2, pp. 235–248, 1971. [Online]. Available: https://www.sciencedirect.com/science/article/pii/0022519371900518 (Cited on page 90.)

[KZI18] B. Khorbatly, I. Zaiter, and S. Isrwai, "Derivation and well-posedness of the extended green-naghdi equations for flat bottoms with surface tension," *Journal of Mathematical Physics*, vol. 59, no. 7, Jul. 2018. [Online]. Available: http://dx.doi.org/10.1063/1.5020601 (Cited on page 27.)

[Lan13] D. Lannes, *The water waves problem: mathematical analysis and asymptotics*, M. Surveys and Monographs, Eds. Mathematical Surveys and Monographs, 2013, vol. 188. (Cited on pages vii, 4, 6, 10, 18, 25, 45 and 86.)

[Lan17] ——, "On the dynamics of floating structures," *Annals of PDE*, vol. 3, no. 1, p. 11, 2017. [Online]. Available: http://dx.doi.org/10.1007/s40818-017-0029-5 (Cited on pages 60, 74 and 75.)

[LB09] D. Lannes and P. Bonneton, "Derivation of asymptotic two-dimensional time-dependent equations for surface water wave propagation," *Physics of Fluids*, vol. 21, no. 1, 2009. (Cited on page 75.)

[LeV02] R. J. LeVeque, *Finite volume methods for hyperbolic problems*. Cambridge university press, 2002, vol. 31. (Cited on page 30.)

[LG08] X. Li and C. Gu, "An all-speed roe-type scheme and its asymptotic analysis of low mach number behaviour," *Journal of Computational Physics*, vol. 227, no. 10, pp. 5144–5159, 2008. [Online]. Available: https://www.sciencedirect.com/science/article/pii/S0021999108000697 (Cited on page 63.)

[LG13] ——, "Mechanism of roe-type schemes for all-speed flows and its application," *Computers & Fluids*, vol. 86, pp. 56–70, 2013. [Online]. Available: https://www.sciencedirect.com/science/article/pii/S0045793013002752 (Cited on page 63.)

[Lio13] P. Lions, *Mathematical Topics in Fluid Mechanics: Volume 1: Incompressible Models*. OUP Oxford, 2013. [Online]. Available: https://books.google.fr/books?id=5iRQNQEACAAJ (Cited on pages 18 and 51.)

[LM18] D. Lannes and G. Métivier, "The shoreline problem for the one-dimensional shallow water and Green-Naghdi equations," *Journal de l'École polytechnique — Mathématiques*, vol. 5, pp. 455–518, 2018. [Online]. Available: https://jep.centre-mersenne.org/articles/10.5802/jep.76/ (Cited on page 27.)

[LSJ93] M.-S. Liou and C. J. Steffen Jr, "A new flux splitting scheme," *J. Comput. Phys.*, vol. 107, no. 1, pp. 23–39, 1993. (Cited on page 63.)

[LW20] D. Lannes and L. Weynans, "Generating boundary conditions for a Boussinesq system," *Nonlinearity*, vol. 33, no. 12, pp. 6868–6889, oct 2020. [Online]. Available: https://doi.org/10.1088/1361-6544/abaa9e (Cited on page 27.)

[LZ07] F. Lugli and F. Zerbetto, "An introduction to bubble dynamics," *Phys. Chem. Chem. Phys.*, vol. 9, pp. 2447–2456, 2007. [Online]. Available: http://dx.doi.org/10.1039/B700766C (Cited on page 75.)

[Mar07] F. Marche, "Derivation of a new two-dimensional viscous shallow water model with varying topography, bottom friction and capillary effects," *European Journal of Mechanics - B/Fluids*, vol. 26, no. 1, pp. 49–63, 2007/2// 2007. (Cited on page 6.)

[Mat15] Y. Matsuno, "Hamiltonian formulation of the extended Green–Naghdi equations," *Physica D: Nonlinear Phenomena*, vol. 301-302, pp. 1–7, 2015. [Online]. Available: https://www.sciencedirect.com/science/article/pii/S0167278915000354 (Cited on page 27.)

[MBB+12] F. Matt, A. Babarit, C. Ben, F. David, O. Louise, S. Katie, S. Johannes, and P. Troch, "A review of numerical modelling of wave energy converter arrays," in *ASME 2012 International Conference on Ocean, Offshore and Artic Engineering*, Rio de Janeiro, Brazil, 2012. [Online]. Available: https://hal.archives-ouvertes.fr/hal-01202077 (Cited on page 59.)

[MDBCF17] V. Michel-Dansac, C. Berthon, S. Clain, and F. Foucher, "A well-balanced scheme for the shallow-water equations with topography or manning friction," *Journal of Computational Physics*, vol. 335, pp. 115–154, 4 2017. [Online]. Available: http://www.sciencedirect.com/science/article/pii/S0021999117300190 (Cited on page 43.)

[MDT21] V. Michel-Dansac and A. Thomann, *On High-Precision*

$$L^\infty$$

-stable IMEX Schemes for Scalar Hyperbolic Multi-scale Equations. Springer International Publishing, 2021, pp. 79–94. [Online]. Available: http://dx.doi.org/10.1007/978-3-030-72850-2_4 (Cited on page 67.)

[MF04] G. Manzini and S. Ferraris, "Mass-conservative finite volume methods on 2-d unstructured grids for the richards' equation," *Advances in Water Resources*, vol. 27, no. 12, pp. 1199–1215, 2004. [Online]. Available: https://www.sciencedirect.com/science/article/pii/S0309170804001204 (Cited on page 99.)

[Mik10] A. Mikelić, "A global existence result for the equations describing unsaturated flow in porous media with dynamic capillary pressure," *Journal of Differential Equations*, vol. 248, no. 6, pp. 1561–1577, 2010. [Online]. Available: https://www.sciencedirect.com/science/article/pii/S0022039609004446 (Cited on page 99.)

[MN08] B. Maurizio and D. Nicholas, "Nonlinear shallow water equation modeling for coastal engineering," *Journal of Waterway, Port, Coastal, and Ocean Engineering*, vol. 134, no. 2, pp. 104–120, 2024/09/30 2008. [Online]. Available: https://doi.org/10.1061/(ASCE)0733-950X(2008)134:2(104) (Cited on page 30.)

[Mon14] R. Monjarret, "Local well-posedness of the multi-layer shallow-water model with free surface," 2014. (Cited on page 7.)

[Mon15] ——, "Local well-posedness of the two-layer shallow water model with free surface," *SIAM Journal on Applied Mathematics*, vol. 75, no. 5, pp. 2311–2332, 2016/04/11 2015. (Cited on page 7.)

[MÖR24] Y. Mantri, P. Öffner, and M. Ricchiuto, "Fully well-balanced entropy controlled discontinuous galerkin spectral element method for shallow water flows: global flux quadrature and cell entropy correction," *Journal of Computational Physics*, vol. 498, p. 112673, 2024. (Cited on page 42.)

[MP17] B. Maury and A. Preux, "Pressureless euler equations with maximal density constraint: a time-splitting scheme," *Topological Optimization and Optimal Transport: In the Applied Sciences*, vol. 17, p. 333, 2017. (Cited on page 63.)

[MRCS10] B. Maury, A. Roudneff-Chupin, and F. Santambrogio, "A macroscopic crowd motion model of gradient flow type," *Mathematical Models and Methods in Applied Sciences*, vol. 20, no. 10, pp. 1787–1821, 2010. (Cited on pages 62 and 63.)

[MRN16] A. Mazaheri, M. Ricchiuto, and H. Nishikawa, "A first-order hyperbolic system approach for dispersion," *Journal of Computational Physics*, vol. 321, pp. 593 – 605, 2016. [Online]. Available: http://www.sciencedirect.com/science/article/pii/S0021999116302261 (Cited on page 30.)

[MS98] P. A. Madsen and H. A. Schäffer, "Higher–order boussinesq–type equations for surface gravity waves: derivation and analysis,"

Philosophical Transactions of the Royal Society of London. Series A: Mathematical, Physical and Engineering Sciences, vol. 356, no. 1749, pp. 3123–3181, 2022/03/16 1998. [Online]. Available: https://doi.org/10.1098/rsta.1998.0309 (Cited on page 27.)

[MSS97a] P. Madsen, O. Sørensen, and H. Schäffer, "Surf zone dynamics simulated by a boussinesq type model. part i. model description and cross-shore motion of regular waves," *Coastal Engineering*, vol. 32, no. 4, pp. 255–287, 1997. [Online]. Available: https://www.sciencedirect.com/science/article/pii/S0378383997000288 (Cited on page 53.)

[MSS97b] ——, "Surf zone dynamics simulated by a boussinesq type model. part ii: surf beat and swash oscillations for wave groups and irregular waves," *Coastal Engineering*, vol. 32, no. 4, pp. 289–319, 1997. [Online]. Available: https://www.sciencedirect.com/science/article/pii/S037838399700029X (Cited on page 53.)

[NAFP97] P. Nielsen, R. Aseervatham, J. D. Fenton, and P. Perrochet, "Groundwater waves in aquifers of intermediate depths," *Advances in Water Resources*, vol. 20, no. 1, pp. 37–43, 1997. [Online]. Available: https://www.sciencedirect.com/science/article/pii/S0309170896000152 (Cited on page 86.)

[NPT22] S. Noelle, M. Parisot, and T. Tscherpel, "A class of boundary conditions for time-discrete Green-Naghdi equations with bathymetry," *SIAM Journal on Numerical Analysis*, 2022. [Online]. Available: https://hal.archives-ouvertes.fr/hal-03256700 (Cited on pages 3, 29, 35, 36, 37 and 38.)

[NV14] P. Noble and J.-P. Vila, "Stability theory for difference approximations of euler–korteweg equations and application to thin film flows," *SIAM Journal on Numerical Analysis*, vol. 52, no. 6, pp. 2770–2791, 2024/09/30 2014. [Online]. Available: https://doi.org/10.1137/130918009 (Cited on page 24.)

[NXS07] S. Noelle, Y. Xing, and C.-W. Shu, "High-order well-balanced finite volume WENO schemes for shallow water equation with moving water," *J. Comput. Phys.*, vol. 226, no. 1, pp. 29–58, 2007. (Cited on page 43.)

[Oke93] N. Okey, "Alternative form of boussinesq equations for nearshore wave propagation," *Journal of Waterway, Port, Coastal, and Ocean Engineering*, vol. 119, no. 6, pp. 618–638, 2024/09/30 1993. [Online]. Available: https://doi.org/10.1061/(ASCE)0733-950X(1993)119:6(618) (Cited on page 24.)

[ORS+14] L. Orgogozo, N. Renon, C. Soulaine, F. Hénon, S. Tomer, D. Labat, O. Pokrovsky, M. Sekhar, R. Ababou, and M. Quintard, "An open source massively parallel solver for richards equation: Mechanistic modelling of water fluxes at the watershed scale," *Computer Physics Communications*, vol. 185, no. 12, pp. 3358–3371, 2014. [Online]. Available: https://www.sciencedirect.com/science/article/pii/S0010465514002719 (Cited on page 99.)

[Par] M. Parisot, "A well-balanced scheme for steady solution of dispersive shallow water models," working paper or preprint. (Cited on page 3.)

[Par06] C. Parés, "Numerical methods for nonconservative hyperbolic systems: a theoretical framework." *SIAM Journal on Numerical Analysis*, vol. 44, no. 1, pp. 300–321, 2006. [Online]. Available: https://doi.org/10.1137/050628052 (Cited on page 37.)

[Par19] M. Parisot, "Entropy-satisfying scheme for a hierarchy of dispersive reduced models of free surface flow," *International Journal for Numerical Methods in Fluids*, vol. 91, no. 10, pp. 509–531, 2019. [Online]. Available: https://onlinelibrary.wiley.com/doi/abs/10.1002/fld.4766 (Cited on pages 2, 33, 36 and 41.)

[Par23] ——, "Congested shallow water model: Trapped air pockets modeling," *SIAM Journal on Scientific Computing*, vol. 45, no. 6, pp. B828–B852, 2023. [Online]. Available: https://doi.org/10.1137/22M1514908 (Cited on pages 57 and 76.)

[Par24a] ——, "Derivation of weakly hydrodynamic models in the Dupuit-Forchheimer regime," Apr. 2024, working paper or preprint. [Online]. Available: https://hal.science/hal-04532765 (Cited on pages 57 and 88.)

[Par24b] ——, "Thick interface coupling technique for weakly dispersive models of waves," *ESAIM: M2AN*, vol. 58, no. 4, pp. 1497–1522, 2024. [Online]. Available: https://doi.org/10.1051/m2an/2024048 (Cited on pages 3, 47, 48 and 49.)

[Pat53] C. S. Patlak, "Random walk with persistence and external bias," *The bulletin of mathematical biophysics*, vol. 15, no. 3, pp. 311–338, Sep 1953. [Online]. Available: https://link.springer.com/content/pdf/10.1007/BF02476407.pdf (Cited on page 90.)

[Pat18] S. Patankar, *Numerical heat transfer and fluid flow*. CRC press, 2018. (Cited on page 91.)

[PC04] C. Parés and M. Castro, "On the well-balance property of roe's method for nonconservative hyperbolic systems. applications to shallow-water systems," *ESAIM: mathematical modelling and numerical analysis*, vol. 38, no. 5, pp. 821–852, 2004. (Cited on page 43.)

[PC18] G. Peyré and M. Cuturi, "Computational optimal transport," *Foundations and Trends in Machine Learning, vol. 11, no. 5-6, pp. 355-607, 2019*, 03 2018. [Online]. Available: https://arxiv.org/pdf/1803.00567 (Cited on page 78.)

[PCC88] A. Prosperetti, L. A. Crum, and K. W. Commander, "Nonlinear bubble dynamics," *The Journal of the Acoustical Society of America*, vol. 83, no. 2, pp. 502–514, 1988. [Online]. Available: https://doi.org/10.1121/1.396145 (Cited on page 76.)

[PE12] D. A. D. Pietro and A. Ern, *Mathematical Aspects of Discontinuous Galerkin Methods*. Springer Berlin Heidelberg, 2012. [Online]. Available: https://link.springer.com/book/10.1007/978-3-642-22980-0 (Cited on page 42.)

[PEMPB13] J. Palm, C. Eskilsson, G. Moura Paredes, and L. Bergdahl, "CFD simulation of a moored floating wave energy converter," in *Proceedings of the 10th European Wave and Tidal Energy Conference*, Aalborg, Denmark, 2013. (Cited on page 59.)

[Per67] D. H. Peregrine, "Long waves on a beach," *Journal of Fluid Mechanics*, vol. 27, no. 04, pp. 815–827, 1967. (Cited on page 26.)

[Per04] B. Perthame, "Pde models for chemotactic movements: Parabolic, hyperbolic and kinetic," *Applications of Mathematics*, vol. 49, no. 6, pp. 539–564, 2004. [Online]. Available: http://dx.doi.org/10.1007/s10492-004-6431-9 (Cited on page 62.)

[Per18] C. Perrin, "An overview on congestion phenomena in fluid equations," *Journées équations aux dérivées partielles*, pp. 1–34, 2018, talk:6. [Online]. Available: http://www.numdam.org/articles/10.5802/jedp.666/ (Cited on page 62.)

[PQ05] N. Parolini and A. Quarteroni, "Mathematical models and numerical simulations for the America's cup," *Computer Methods in Applied Mechanics and Engineering*, vol. 194, no. 9, pp. 1001–1026, 2005. [Online]. Available: http://www.sciencedirect.com/science/article/pii/S004578250400310X (Cited on page 59.)

[PS01] B. Perthame and C. Simeoni, "A kinetic scheme for the saint-venant system with a source term," *Calcolo*, vol. 38, no. 4, pp. 201–231, 2001. (Cited on page 31.)

[PV14] M. Parisot and J.-P. Vila, "Numerical scheme for multilayer shallow-water model in the low-froude number regime," *C.R. Acad. Sci. Paris, Ser. I*, vol. 352, pp. 953–957, 2014. (Cited on page 63.)

[PV16] ——, "Centered-potential regularization for the advection upstream splitting method," *SIAM Journal on Numerical Analysis*, vol. 54, no. 5, pp. 3083–3104, 2016. [Online]. Available: https://doi.org/10.1137/15M1021817 (Cited on pages 56, 63, 64, 65 and 66.)

[PZ15] C. Perrin and E. Zatorska, "Free/congested two-phase model from weak solutions to multi-dimensional compressible navier-stokes equations," *Communications in Partial Differential Equations*, vol. 40, no. 8, pp. 1558–1589, 2015. [Online]. Available: http://dx.doi.org/10.1080/03605302.2015.1014560 (Cited on pages 60 and 62.)

[QTV00] A. Quarteroni, M. Tuveri, and A. Veneziani, "Computational vascular fluid dynamics: problems, models and methods," *Computing and Visualization in Science*, vol. 2, no. 4, pp. 163–197, 2000. [Online]. Available: http://dx.doi.org/10.1007/s007910050039 (Cited on page 59.)

[Ram11] A. Rambaud, "Modélisation, analyse mathématique et simulations numériques de quelques problèmes aux dérivées partielles multi-échelles," Theses, Université Claude Bernard - Lyon I, Dec. 2011. [Online]. Available: https://theses.hal.science/tel-00656013 (Cited on page 7.)

[RB09] M. Ricchiuto and A. Bollermann, "Stabilized residual distribution for shallow water simulations," *Journal of Computational Physics*, vol. 228, no. 4, pp. 1071–1115, 2009. [Online]. Available: https://www.sciencedirect.com/science/article/pii/S0021999108005391 (Cited on page 69.)

[RCK10] V. Roeber, K. F. Cheung, and M. H. Kobayashi, "Shock-capturing boussinesq-type model for nearshore wave processes," *Coastal Engineering*, vol. 57, no. 4, pp. 407–423, 2010. [Online]. Available: https://www.sciencedirect.com/science/article/pii/S0378383909001860 (Cited on page 53.)

[RDF18] G. L. Richard, A. Duran, and B. Fabrèges, "A new model of shoaling and breaking waves. Part II. Run-up and two-dimensional waves," Aug. 2018, working paper or preprint. [Online]. Available: https://hal.archives-ouvertes.fr/hal-01861821 (Cited on page 53.)

[Red93] J. N. Reddy, "An introduction to the finite element method," *New York*, vol. 27, p. 14, 1993. (Cited on page 42.)

[RG12] G. L. Richard and S. L. Gavrilyuk, "A new model of roll waves: comparison with brock's experiments," *Journal of Fluid Mechanics*, vol. 698, pp. 374–405, 005 2012. [Online]. Available: https://www.cambridge.org/core/article/

div-class-title-a-new-model-of-roll-waves-comparison-with-brock-s-experiments-div/8A4C4FAC5A31F116AA767C38C9B9F1B1 (Cited on page 6.)

[RG15] ——, "Modelling turbulence generation in solitary waves on shear shallow water flows," *Journal of Fluid Mechanics*, vol. 773, pp. 49–74, 2015. (Cited on page 53.)

[Ric31] L. A. Richards, "Capillary conduction of liquids through porous mediums," *Physics*, vol. 1, no. 5, pp. 318–333, 1931. [Online]. Available: https://doi.org/10.1063/1.1745010 (Cited on page 86.)

[Rie11] F. Rieper, "A low-mach number fix for roe's approximate riemann solver," *Journal of Computational Physics*, vol. 230, no. 13, pp. 5263–5287, 2011. [Online]. Available: https://www.sciencedirect.com/science/article/pii/S0021999111001689 (Cited on page 63.)

[RM00] S. Roller and C.-D. Munz, "A low mach number scheme based on multi-scale asymptotics," *Computing and Visualization in Science*, vol. 3, no. 1, pp. 85–91, 2000. [Online]. Available: https://doi.org/10.1007/s007910050055 (Cited on page 63.)

[RT06] P.-A. Raviart and J.-M. Thomas, "A mixed finite element method for 2-nd order elliptic problems," in *Mathematical Aspects of Finite Element Methods: Proceedings of the Conference Held in Rome, December 10–12, 1975*. Springer, 2006, pp. 292–315. (Cited on pages 18 and 29.)

[Run95] C. Runge, "Ueber die numerische auflösung von differentialgleichungen," *Mathematische Annalen*, vol. 46, no. 2, pp. 167–178, 1895. [Online]. Available: https://doi.org/10.1007/BF01446807 (Cited on page 42.)

[SK11] P. Solin and M. Kuraz, "Solving the nonstationary richards equation with adaptive hp-FEM," *Advances in Water Resources*, vol. 34, no. 9, pp. 1062–1081, 2011, new Computational Methods and Software Tools. [Online]. Available: https://www.sciencedirect.com/science/article/pii/S0309170811000844 (Cited on page 99.)

[SKH+12] F. Shi, J. T. Kirby, J. C. Harris, J. D. Geiman, and S. T. Grilli, "A high-order adaptive time-stepping tvd solver for boussinesq modeling of breaking waves and coastal inundation," *Ocean Modelling*, vol. 43-44, pp. 36–51, 2012. [Online]. Available: https://www.sciencedirect.com/science/article/pii/S1463500311002010 (Cited on page 53.)

[SM11] J. Sainte-Marie, "Vertically averaged models for the free surface non-hydrostatic euler system: derivation and kinetic interpretation," *Mathematical Models and Methods in Applied Sciences*, vol. 21, no. 03, pp. 459–490, 2015/08/21 2011. (Cited on pages 13, 15 and 33.)

[SMM13] B. Samba, D. Mathurin, and F. Musandji, "Numerical modeling of mixed flows in storm water systems: Critical review of literature," *Journal of Hydraulic Engineering*, vol. 139, no. 4, pp. 385–396, 2022/08/06 2013. [Online]. Available: https://doi.org/10.1061/(ASCE)HY.1943-7900.0000680 (Cited on page 75.)

[SNB00] G. P. Schurtz, P. D. Nicolaï, and M. Busquet, "A nonlocal electron conduction model for multidimensional radiation hydrodynamics codes," *Physics of Plasmas*, vol. 7, no. 10, pp. 4238–4249, 9/29/2024 2000. [Online]. Available: https://doi.org/10.1063/1.1289512 (Cited on page 90.)

[SPPP17] C. Scudeler, C. Paniconi, D. Pasetto, and M. Putti, "Examination of the seepage face boundary condition in subsurface and coupled surface/subsurface hydrological models," *Water Resources Research*, vol. 53, no. 3, pp. 1799–1819, 2017. [Online]. Available: https://agupubs.onlinelibrary.wiley.com/doi/abs/10.1002/2016WR019277 (Cited on page 94.)

[SSM98] O. Sørensen, H. Schäffer, and P. Madsen, "Surf zone dynamics simulated by a boussinesq type model. iii. wave-induced horizontal nearshore circulations," *Coastal Engineering*, vol. 33, no. 2, pp. 155–176, 1998. [Online]. Available: https://www.sciencedirect.com/science/article/pii/S0378383998000076 (Cited on page 53.)

[Sul90] I. Suliciu, "On modelling phase transitions by means of rate-type constitutive equations. shock wave structure," *International Journal of Engineering Science*, vol. 28, no. 8, pp. 829–841, 1990. [Online]. Available: http://www.sciencedirect.com/science/article/pii/002072259090028H (Cited on page 31.)

[SW05] S. Sun and M. F. Wheeler, "Symmetric and nonsymmetric discontinuous galerkin methods for reactive transport in porous media," *SIAM Journal on Numerical Analysis*, vol. 43, no. 1, pp. 195–219, Jan. 2005. [Online]. Available: http://dx.doi.org/10.1137/S003614290241708X (Cited on page 99.)

[SYC93] P. M. Steffler and J. Yee-Chung, "Depth averaged and moment equations for moderately shallow free surface flow," *Journal of Hydraulic Research*, vol. 31, no. 1, pp. 5–17, Jan. 1993. [Online]. Available: http://dx.doi.org/10.1080/00221689309498856 (Cited on page 6.)

[TD90] N. Trieu Dong, "Sur une méthode numérique de calcul des écoulements non permanents soit à surface libre, soit en charge, soit partiellement à surface libre et partiellement en charge," *La Houille Blanche*, vol. 76, no. 2, pp. 149–158, Apr. 1990. [Online]. Available: http://dx.doi.org/10.1051/lhb/1990008 (Cited on page 61.)

[Tem68] R. Temam, "Une méthode d'approximation de la solution des équations de navier-stokes," *Bulletin de la Société Mathématique de France*, vol. 96, pp. 115–152, 1968. (Cited on pages 18 and 30.)

[Tes07] V. M. Teshukov, "Gas-dynamic analogy for vortex free-boundary flows," *Journal of Applied Mechanics and Technical Physics*, vol. 48, no. 3, pp. 303–309, 2007. [Online]. Available: http://dx.doi.org/10.1007/s10808-007-0039-2 (Cited on page 6.)

[TGM23] S. Tkachenko, S. Gavrilyuk, and J. Massoni, "Extended lagrangian approach for the numerical study of multidimensional dispersive waves: Applications to the serre-green-naghdi equations," *Journal of Computational Physics*, vol. 477, p. 111901, 2023. [Online]. Available: https://www.sciencedirect.com/science/article/pii/S0021999122009640 (Cited on page 30.)

[Tor99] E. F. Toro, *Riemann solvers and numerical methods for fluid dynamics: a practical introduction*. Springer Science & Business Media, 1999. (Cited on page 30.)

[Váz17] J. L. Vázquez, *The Mathematical Theories of Diffusion: Nonlinear and Fractional Diffusion*. Cham: Springer International Publishing, 2017, pp. 205–278. [Online]. Available: https://doi.org/10.1007/978-3-319-61494-6_5 (Cited on pages 90 and 102.)

[vG80] M. T. van Genuchten, "A closed-form equation for predicting the hydraulic conductivity of unsaturated soils," *Soil Science Society of America Journal*, vol. 44, no. 5, pp. 892–898, 1980. [Online]. Available: https://acsess.onlinelibrary.wiley.com/doi/abs/10.2136/sssaj1980.03615995004400050002x (Cited on page 98.)

[vK86] J. van Kan, "A second-order accurate pressure-correction scheme for viscous incompressible flow," *SIAM Journal on Scientific and Statistical Computing*, vol. 7, no. 3, pp. 870–891, 1986. [Online]. Available: https://doi.org/10.1137/0907059 (Cited on page 42.)

[vL79] B. van Leer, "Towards the ultimate conservative difference scheme. v. a second-order sequel to godunov's method," *Journal of Computational Physics*, vol. 32, no. 1, pp. 101 – 136, 1979. [Online]. Available: http://www.sciencedirect.com/science/article/pii/0021999179901451 (Cited on page 66.)

[vS65] J. van Schilfgaarde, "Limitations of dupuit-forchheimer theory in drainage," *Transactions of the ASAE*, vol. 8, no. 4, pp. 515–0516, 1965. [Online]. Available: https://elibrary.asabe.org/abstract.asp?aid=40566&t=3 (Cited on page 85.)

[vWv07] L. C. van Rijn, D.-J. R. Walstra, and M. van Ormondt, "Unified view of sediment transport by currents and waves. iv: Application of morphodynamic model," *Journal of Hydraulic Engineering*, vol. 133, no. 7, pp. 776–793, 2024/09/24 2007. [Online]. Available: https://doi.org/10.1061/(ASCE)0733-9429(2007)133:7(776) (Cited on page 103.)

[Wes09] P. Wesseling, *Principles of computational fluid dynamics*. Springer Science & Business Media, 2009, vol. 29. (Cited on page 91.)

[WKS99] G. Wei, J. T. Kirby, and A. Sinha, "Generation of waves in Boussinesq models using a source function method," *Coastal Engineering*, vol. 36, no. 4, pp. 271–299, 1999. [Online]. Available: https://www.sciencedirect.com/science/article/pii/S0378383999000095 (Cited on page 45.)

[WT03] G. Wu and R. Taylor, "The coupled finite element and boundary element analysis of nonlinear interactions between waves and bodies," *Ocean Engineering*, vol. 30, no. 3, pp. 387–400, 2003. [Online]. Available: http://www.sciencedirect.com/science/article/pii/S0029801802000379 (Cited on page 59.)

[WWGK17] N. Wintermeyer, A. R. Winters, G. J. Gassner, and D. A. Kopriva, "An entropy stable nodal discontinuous galerkin method for the two dimensional shallow water equations on unstructured curvilinear meshes with discontinuous bathymetry," *Journal of Computational Physics*, vol. 340, pp. 200–242, 2017. (Cited on page 42.)

[Xin14] Y. Xing, "Exactly well-balanced discontinuous galerkin methods for the shallow water equations with moving water equilibrium," *Journal of Computational Physics*, vol. 257, pp. 536–553, 2014. (Cited on page 43.)

[XS06] Y. Xing and C.-W. Shu, "High-order well-balanced finite difference weno schemes for a class of hyperbolic systems with source terms," *J. Sci. Comput.*, vol. 27, no. 1-3, pp. 477–494, 2006. (Cited on page 43.)

[XSN11] Y. Xing, C.-W. Shu, and S. Noelle, "On the advantage of well-balanced schemes for moving-water equilibria of the shallow water equations," *Journal of scientific computing*, vol. 48, no. 1, pp. 339–349, 2011. (Cited on page 43.)

[Xue08] R. Xue, "The initial–boundary value problem for the "good" boussinesq equation on the bounded domain," *Journal of Mathematical Analysis and applications*, vol. 343, no. 2, pp. 975–995, 2008. (Cited on page 27.)

[Yin04] Z. Yin, "Global weak solutions for a new periodic integrable equation with peakon solutions," *Journal of Functional Analysis*, vol. 212, no. 1, pp. 182–194, 2004. (Cited on page 52.)

[YKC09] Y. Yamazaki, Z. Kowalik, and K. F. Cheung, "Depth-integrated, non-hydrostatic model for wave breaking and run-up," *International Journal for Numerical Methods in Fluids*, vol. 61, no. 5, pp. 473–497, 2009. [Online]. Available: http://dx.doi.org/10.1002/fld.1952 (Cited on page 26.)

[YL13] Y.-H. Yu and Y. Li, "Reynolds-averaged Navier–Stokes simulation of the heave performance of a two-body floating-point absorber wave energy system," *Computers & Fluids*, vol. 73, pp. 104–114, 2013. [Online]. Available: http://www.sciencedirect.com/science/article/pii/S0045793012003878 (Cited on page 59.)

[Zak68] V. E. Zakharov, "Stability of periodic waves of finite amplitude on the surface of a deep fluid," *Journal of Applied Mechanics and Technical Physics*, vol. 9, no. 2, pp. 190–194, Mar 1968. [Online]. Available: https://link.springer.com/content/pdf/10.1007/BF00913182.pdf (Cited on page 103.)

[Zel91] J. Zelt, "The run-up of nonbreaking and breaking solitary waves," *Coastal Engineering*, vol. 15, no. 3, pp. 205–246, 1991. [Online]. Available: https://www.sciencedirect.com/science/article/pii/037838399190003Y (Cited on page 53.)

[ZYZ+19] Y. Zha, J. Yang, J. Zeng, C.-H. M. Tso, W. Zeng, and L. Shi, "Review of numerical solution of richardson–richards equation for variably saturated flow in soils," *WIREs Water*, vol. 6, no. 5, p. e1364, 2019. [Online]. Available: https://wires.onlinelibrary.wiley.com/doi/abs/10.1002/wat2.1364 (Cited on page 99.)

Some modeling and computational aspects of water waves action

Abstract: This manuscript provides an overview of my research into wave propagation, fluid-structure interactions, and groundwater flows, over large time and spatial scales with an emphasis on the development of new models and numerical methods. The dynamics of free-surface flows play a central role in many natural and engineering processes, and understanding these flows requires approximate models that capture both large-scale behavior and the subtle interactions between waves and physical structures.

Free-surface flows are widely model using the shallow water-type models. Where dispersive effects are significant, there are a number of scientific challenges to be overcome in order to make full use of these models. The first chapter of this manuscript, I introduce a framework for dispersive models, inspired by the classical framework for incompressible flows. I believe that this framework presents a promising foundation for tackling a number of scientific challenges, many of which are only briefly touched upon in this manuscript but represent exciting avenues for future research.

The second chapter delves deeper into the interaction of waves with their surrounding environment, specifically examining two key applications, renewable marine energy and water ressources. In the case of floating bodies, such as those used in marine renewable energy, the presence of a structure above the fluid flow introduces a unilateral constraint, commonly referred to as a congestion constraint. Additionally, the dynamics of potential air pockets trapped beneath the floating object must be accounted for, as they significantly influence the stability and behavior of the system. In the context of groundwater flows, a critical issue is modeling the exchange of water between surface flows and subsurface flows, which is essential for understanding processes such as aquifer recharge, river-groundwater interaction.

Across all the scientific challenges addressed in this manuscript, the role of constraints is fundamental for the modeling interest. However, these constraints introduce significant complexity into both the analytical and numerical treatment of the problems. Analyzing constrained problems is inherently difficult due to the mathematical intricacies involved. For this reason, my work has primarily focused on the development of numerical solutions for hyperbolic problems that involve a variety of constraints. These numerical methods are designed to handle the specific challenges posed by the constraints while ensuring that the solutions remain stable, accurate, and physically realistic.

Keywords: Free surface flows, Dispersive equations, Congested models, Waves/structure interactions, Unified models, Layerwise models, Asymptotic preserving schemes, Entropy-satisfying schemes, Coupling and adaptive schemes